INVESTIGATIONS ON THE RADIATION CHARACTERISTICS OF NEW HOLLOW DIELECTRIC HORN ANTENNAS

A THESIS SUBMITTED BY

V.P.JOSEPH

IN PARTIAL FULFILMENT OF THE REQUIREMENTS
FOR THE DEGREE OF

DOCTOR OF PHILOSOPHY

DEPARTMENT OF ELECTRONICS
FACULTY OF TECHNOLOGY
COCHIN UNIVERSITY OF SCIENCE AND TECHNOLOGY
KOCHI 682 022
INDIA

JULY 1999

dedicated to
my parents

CERTIFICATE

This is to certify that the thesis entitled "**Investigations on the Radiation Characteristics of New Hollow Dielectric Horn Antennas**" is a bona fide record of the research work carried out by Mr. V.P. Joseph under my supervision in the Department of Electronics, Cochin University of Science and Technology. The results embodied in this thesis or part of it have not been presented for any other degree.

Dr. K.T. Mathew
(Supervising Teacher)
Professor
Dept. of Electronics
Cochin University of Sci. & Tech.

KOCHI – 682 022

07 – 07 – 1999.

DECLARATION

I hereby declare that the work presented in this thesis entitled "**Investigations on the Radiation Characteristics of New Hollow Dielectric Horn Antennas**" is based on the original work done by me under the supervision of Dr. K.T. Mathew, in the Department of Electronics, Cochin University of Science and Technology, and no part thereof has been presented for the award of any other degree.

KOCHI – 682 022

07 – 07 – 1999.

V.P. JOSEPH

ACKNOWLEDGEMENT

At the very outset, my deep sense of gratitude to my research guide, Dr. K.T. Mathew, Professor, Department of Electronics, Cochin University of Science and Technology, for his able guidance, continuous encouragement and unreserved support.

I am grateful to Dr. P.R.S. Pillai, Professor and head of the Department of Electronics, for the keen interest and constant inspiration he has shown in the progress of my research.

I am deeply indebted to Prof. K.G. Nair and Prof. C.S. Sridhar, former Heads of the Dept. of Electronics, for their kind suggestions and motivation.

I would like to express my gratitude to Dr. K. Vasudevan, Dr. P. Mohanan, Dr. C.K. Anandan and Dr. Tessamma Thomas for their valuable suggestions during the course of my research.

It is with immense pleasure that I wish to place on record my gratitude to Fr. C.A. Thomas, Principal and all the faculty members of the Department of Physics, Christ College, Irinjalakuda for their constant and continuous encouragement. I take this opportunity to place on record, the cooperation, help and encouragement I received from my friends Dr. John K. Thomas and Dr. V.S. Joskumar, Department of Zoology, Christ College, Irinjalakuda.

I express my deep sense of gratitude to my colleagues, Dr. Joe Jacob (Lecturer, Newman College, Thodupuzha), Mr. Sebastian Mathew (Lecturer, K. E. College, Mannanam), Dr. U. Ravindranath (Lecturer, Dept. of Electronics, Cochin University of Sci. & Tech.), Dr. Jacob George, Mr. S. Bijukumar, Mr. Binoy, Mr. V. Anand (Lecturer, N.S.S. College, Nenmara) and Mr. Sunny Joseph (Lecturer, M. A. College of Engineering, Kothamangalam) for their help in various ways.

I am grateful to my former colleagues of microwave lab, Dr. K.K. Narayanan (Lecturer, S. D. College, Alleppy) and Dr. Thomaskutty Mathew (Lecturer, M. G. University, Kottayam) for their help and suggestions. Thanks are also due to Mr. Paul V John, Mr. G. Girish and Mr. M. Cyriac for their help and valuable suggestions.

Finally I take this opportunity to place on record my sincere thanks to all members of faculty and non-teaching staff of Dept. of Electronics, Cochin University of Science and Technology.

V.P. JOSEPH

INVESTIGATIONS ON THE RADIATION CHARACTERISTICS OF NEW HOLLOW DIELECTRIC HORN ANTENNAS

CONTENTS

Chapter 1

INTRODUCTION

This chapter serves to discuss the importance of antennas in communication systems and to introduce the topic of this research work. The different types of antennas used for various applications and the details of metallic horn antennas are presented in the initial section of the chapter. The second section gives a brief account of the dielectric rod antennas, dielectric loaded metallic horn antennas and hollow and solid dielectric horn antennas. The final section briefly discusses the scope of the present work and the motivation behind it.

James Clerk Maxwell's prediction of the existence of electromagnetic waves in 1873 and Heinrich Hertz's experimental verification of Maxwell's prediction in 1888 have laid the foundation stones for modern microwave and millimeter wave communication engineering. Sir Oliver Lodge's experiments on reflection and refraction of electromagnetic waves and his demonstration of electromagnetic energy radiation from hollow pipes in 1894 and Professor J.C.Bose's experiment with a pyramidal horn as a receiver in his spectrometer in 1897 initiated the study of antenna theory. An antenna forms the most important constituent of any communication set-up and without it no communication over long distance is possible. With the recent advancements in the field of communication facilities, the antenna engineering also achieved great importance.

An antenna or aerial is defined as a means for radiating or receiving radio waves. Basically it is a structure associated with the region of transmission between a guided wave and a free space wave, or vice versa. In other wards, the antenna acts as an impedance transformer between the hardware of the communication set-up and the free space. The antenna is derived from a transmission line or waveguide, for effectively transferring energy from the source to free space without any loss or reflection. The antenna used for transmitting energy is called transmitting antenna and the one used for receiving energy is called the receiving antenna. Apart from their different functions, transmitting and receiving antennas behave identically. That is, their behavior is reciprocal. In additions to the transmitting or receiving functions, an antenna acts as a directional device.

1.1 DIFFERENT TYPES OF ANTENNAS

Innumerable types of antennas have been designed to be used at different frequencies for various applications. Different communication systems like radio, television , radar, satellite systems etc. are operated in separate frequency bands. The power requirements for different applications are also different. These functions necessitates the design and development of separate antennas for separate applications. For low frequency applications wires, grids, rods, dipole arrays etc. are frequently used. In the microwave and millimeter wave ranges dipole antennas, slot antennas and their arrays, reflector antennas like corner reflectors, parabolic reflectors, cylindrical reflectors

etc., aperture antennas like horn antennas, helical antennas etc., lens antennas, dielectric and dielectric loaded metal antennas etc, are commonly used. In the millimeter range, microstrips and dielectric rod arrays are very important.

1.2 METALLIC HORN ANTENNAS

The horn antennas are the result of flaring of the open end of the waveguide structure. It is one of the simplest and most widely used microwave antenna. The horn provides a gradual transition of the electromagnetic energy from the waveguide to free space conditions and thus prevents the reflection of energy back to the source.

Horn antennas are the widely used transmitting and receiving antennas in the laboratory. Due to its attractive features like simplicity of structure, ease of fabrication, high gain and good radiation characteristics, it is also used for lot of other applications. Horn antennas are commonly used in radio astronomy, satellite tracking, as a primary feed in communication dishes etc. It is also used as a standard gain antenna for comparing the gain of other antennas.

Horn antennas are classified into three basic types in accordance with their structure. They are the pyramidal horns, E and H-plane sectoral horns and conical horns. Fig. 1.I. shows a schematic representation of these basic types. Pyramidal and sectoral horns are the extension of rectangular waveguide. If the flaring is only in one dimension, the resultant structure is a sectoral horn. If the flaring is in both dimensions, the structure is called a pyramidal horn. The beam width is narrow in the flared plane and broad in the other. For E-plane sectoral horns the radiation pattern is narrow in the E-plane and broad in the H-plane. For H-plane sectoral horns the pattern is broad in the E-plane and narrow in the H-plane. A conical horn is constructed by flaring the open end of a circular waveguide. For all the three types the directivity is a function of flare angle and length. As length of the horn increases, the directivity also increases.

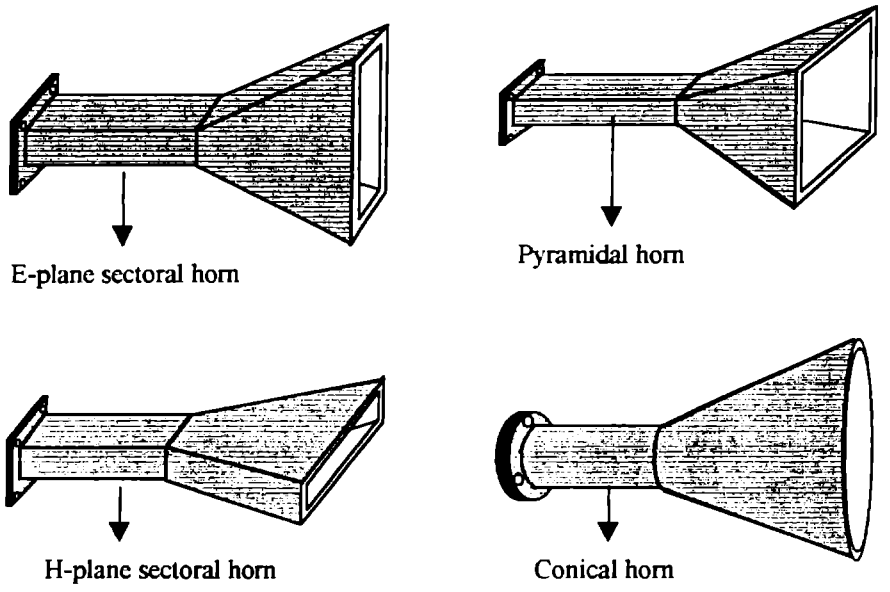

Fig. 1.1 Schematic representation of the basic types of Horn antennas.

Along with these basic types of horn antennas, other modified structures such as, corrugated horns, multimode horns, aperture matched horns, dielectric loaded horns etc. are also used for various applications.

1.3 DIELECTRIC ROD AND HORN ANTENNAS

Out of the different types of antennas designed for microwave and millimeter wave frequencies, the dielectric and dielectric loaded antennas form a very important group. These antennas are relatively recent additions to the numerous types of antennas and they exhibit a lot of attractive characteristics. The main members of this group are the dielectric rods, dielectric tubes and dielectric horns. These antennas are notable for of their low loss, high gain, light weight, the feasibility of obtaining shaped beams, ease of fabrication etc.

1.3.1 Dielectric Rod Antennas

Basic types of tapered and uniform dielectric rods of rectangular and circular cross-section are shown in Fig.1.2. Other rod antennas like corrugated rod antennas, leaky wave antennas etc. also are used for some specialised applications.

Dielectric rod antennas behaves as a dielectric waveguide. Radiation from the rod occurs only from the discontinuities, probably from the feed-end, from the free-end and from any other abrupt structural discontinuities. For a uniform rod the feed-end and free-end are to be taken into consideration and the radiated power will be the sum of the radiation from these discontinuities. Low gain ,high side lobe levels and deep minima due to interference from feed-end and free-end are the main characteristics of these antennas. For tapered rods the free-end discontinuity is reduced but power leaks through the taper profile and the radiated power is the sum of the radiation from the leaky wave structure, feed-end and free-end.

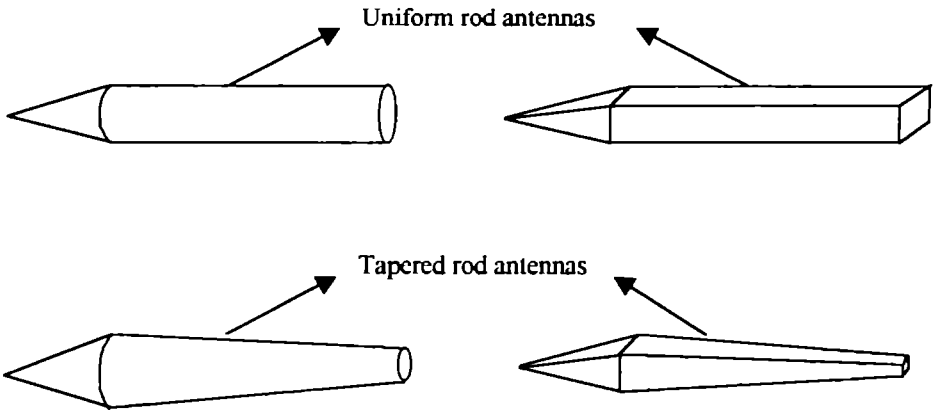

Fig.1.2 Schematic representation of basic types of dielectric rod Antennas

Different theoretical approaches based on 'two aperture theory', 'scattering theory', 'Schelkunoff's equivalence principle', 'Marcatili's theory' etc. are used to explain the performance of these antennas.

1.3.2 Dielectric Loaded Metallic Horn Antennas

Loading of metallic horn antennas with dielectric materials is found to be effective in increasing the gain of the antenna, reduction in cross-polar levels and modification of the radiation patterns with considerable reduction in side lobe levels. Conical and rectangular horn antennas with complete dielectric filling and dielectric lining inside also had been studied by different researchers. Here we make use of the guiding action of the dielectric material.

1.3.3 Hollow and Solid Dielectric Horn Antennas

Only a few attempts were made to explore the possibilities of this class of antennas. The solid dielectric horn antenna is an extension of dielectric rod antenna. The rod is flared out into a large aperture so that the launching discontinuity is reduced. In this case the radiation is from the feed-end and free-end only. So 'two aperture theory' can be used to calculate the radiation pattern.

Circular hollow dielectric horn antennas are good substitutes for tapered rod antennas. These antennas have very good radiation pattern in the E-plane and poor pattern in the H-plane. Whenever a narrow beam with a low side lobe level is required in the E-plane, these antennas can be used more effectively than metallic horn antennas.

The available rectangular hollow dielectric horn antennas are constructed by replacing the walls of a metallic horn by low loss dielectric sheets. For this horn, the discontinuity at the feed-end is greater and so the side lobe levels are very high. Fig.1.3. shows the schematic representation of different hollow and solid dielectric horn antennas.

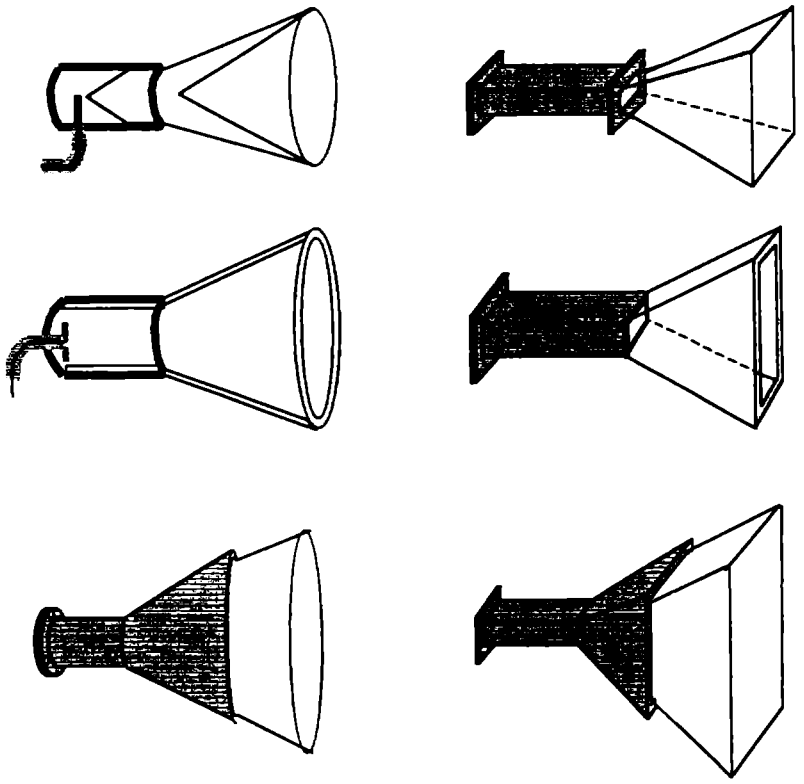

Fig. 1.3 Schematic representation of different hollow and solid dielectric Horn antennas.

1.4 SCOPE OF THE PRESENT WORK

Investigations on the design and development of certain new hollow dielectric horn antennas of rectangular cross section have been carried out. The main shortcoming of the existing ordinary hollow dielectric horn antenna (HDH) is the abrupt discontinuity at the feed-end. A new launching technique using a dielectric rod is introduced to overcome this limitation. Also a strip loading technique is employed for further modification of the antenna. Radiation parameters of new HDH antennas of E-plane sectoral, H-plane sectoral and pyramidal types were studied and are found to be very attractive.

Theoretical approach based on Marcatili's principle and two aperture theory along with diffraction theory and image theory is used to support the experimental findings. The HDH is considered as solid horn of effective dielectric constant and the aperture field is evaluated. The antenna is excited by the open waveguide in the dominant TE_{10} mode and so the existence of any hybrid mode is ruled-out. The theoretical results are observed to be in good agreement with the experimental results.

1.5 MOTIVATION BEHIND THE WORK

The E-plane radiation patterns of conical hollow dielectric horn antennas are narrow with low side lobe levels and the H-plane radiation patterns are broad with high side lobes. The radiation patterns of rectangular hollow dielectric horn antennas suffers from high side lobe levels in both planes. The main motivation behind this work was to get good E and H-plane patterns from the rectangular HDH antennas, so that it may be used to replace small metallic horns. The poor characteristics of HDH are due to its feed-end discontinuity. The first preference of the study was to overcome this discrepancy using a good launching method. The ultimate aim behind this research work was to develop a new dielectric feed horn having all the advantages of a metallic horn along with the additional merits of dielectric antennas.

Chapter 2

REVIEW OF THE PAST WORK

A detailed account of the previous work done in the field of dielectric rod and horn antennas are given in this chapter. It is difficult to start with a review of dielectric horn antennas without considering its metallic counterpart. So some important developments in the field of metallic horn antennas are presented in the initial part of the chapter. A survey of the scientific literature related to the theoretical methods adopted for the dielectric rod and horn antennas are also included.

2.1 METALLIC HORN ANTENNAS

The forerunner of the horn, namely, the hollow pipe radiator have been first used by Sir Oliver Lodge in 1894 for radiating and receiving microwaves. In 1897 Professor J.C.Bose used a pyramidal horn as the receiver in his spectrometer. After that several researchers analyzed and modified the radiation characteristics of metallic horn antennas.

A review paper by Ramsay [1] comprises all works in this field before 1900. The first experimental and theoretical analysis of waveguide radiators was reported by Barrow et al.[2]. The radiation properties of sectoral horn antennas are theoretically analyzed and experimentally verified by Barrow et al.[3,4]. They have also reported [5] the design principles of electromagnetic horn antennas for obtaining the required beam width and gain.

Southworth et al.[6] have presented the experimental results of directive properties of metal pipes and conical horns. Chu [7] has analyzed the radiation properties of hollow pipes and horns using Vector Kirchoff's formula. Woonton et al.[8] have studied the radiation patterns of horn antennas and compared the experimental results with the corrected formula by Chu et. al. and with Kirchoff's formula. Rhodes [9] has discussed the effect of radiation pattern on flare angle and length for sectoral horn antennas. Some experimental curves useful for designing sectoral horns has been presented by Bennet [10]. Horton [11] has utilized a simple integral method for computing the radiation pattern of horn antennas.

King [12] has presented some optimum design data for conical horns. Schorr et al.[13] have analyzed the propagation constants and aperture fields of conical horns. With appropriate modifications these equations can be used for pyramidal horns also. Jakes [14] and Braun [15] have published the details regarding the gain of horn antennas.

There are a lot of research publications related to metallic horn antennas. A few works, which deals with the basic developments in the field have been discussed here. Many other works of relevance, related to the fundamental theory, operating principles and design of various horn antennas are brought together by Love [16] in a collection of reprinted papers.

2.2 DIELECTRIC ROD ANTENNAS

Uniform and tapered dielectric rod antennas of circular and rectangular cross section have been studied by several workers. A detailed survey of developments in this field up to 1985 is presented by Chatterjee [17].

Electromagnetic wave propagation through dielectric cylinders was suggested and investigated quiet early in this century by Hondros et al. [18] in 1910, Zahn [19] in 1916 and Schriever [20] in 1920. Later Southworth [21], Carson [22] and Elsasser [23] analyzed the attenuation and transmission losses in dielectric waveguide.

The first advance treatment of the problem of radiation from dielectric rod antennas has been considered by Watson et al.[24,25], Halliday [26] and Horton [27]. They have computed the far field radiation pattern of dielectric rod starting from the surface currents using Schelkunoff's equivalence principle [28]. A detailed summary of these works has been given by Kiely [29] in 1953.

The dielectric cylindrical antenna belongs to the group of surface wave antennas while rod antennas can support surface or guided modes [30,31].Theoretical analysis of the radiation of electromagnetic energy from dielectric cylinders and rods based on different approaches has been published by several researchers. Halliday et al.[26]considered the cylindrical dielectric rod antenna as two end fire arrays of Huyghen's secondary radiators distributed on the surface of the rod (Scalar Huyghen's theory). The revised concept of Huyghen's radiators was formulated for a closed surface by different workers [32,33,34] and finally revised by Schelkunoff [28]

(Schelkunoff's equivalence principle). Vector Kirchhoff's formula used along with Schelkunoff's equivalence principle involving electric and magnetic field vector potentials was formalized by Stratton [35], which is also described by Silver [36]. In another approach it is assumed that the radiation takes place only from two apertures at the feed end and free end of the rod (Two aperture theory). Workers like James [37,38], Dilli [39,40], Narayanan [41] and Anderson [42] followed this approach. Blakey [43] treated the dielectric rod antenna as a scattering problem (Scattering theory) and Wilkers [44] has considered the dielectric rod as a lens having cross sectional dimensions of the order of a wavelength (Wavelength lens approach).

Chatterjee et al.[45,46,47] have considered that the radiation takes place from the distribution of fields or of surface currents from the whole surface of the antenna. They have also given a detailed account of the radiation properties of dielectric rod aerials [48,49,50].

The analysis of field distributions in and around the rectangular dielectric guide has been presented by several workers. The most important one was the approximate boundary value analysis put forward by Marcatili [51] to obtain closed form solutions of the transverse propagation constants. It is assumed that the fields are propagating along the dielectric guide in the form of surface waves tightly bound to the guide. The field variations inside the cross section of the guide are assumed to be sinusoidal and outside the guide it becomes an exponentially decaying field. Schlosser et al.[52] suggested a method with rigorous computational steps, theoretically valid over a wider range than Marcatili,s method. The limitations of Marcatili,s approximate formula have been studied by Schweig et al.[53] in comparison with a finite difference method for high dielectric constant rectangular dielectric waveguide.

Goell [54] suggested a circular harmonic computer analysis of the propagating modes of a rectangular dielectric waveguide based on a representation of the radial variation of longitudinal electric and magnetic fields of the modes by a sum of Bessel functions inside the core and by a sum of modified Bessel functions outside.

Cullen et al.[55] modified Goell's method further using a point matching technique. Variational methods have been suggested by Pergla [56], Mittra [57] and Shaw et al.[58]. They have assumed a test solution with two or three variable parameters in the core. From the test solution, the fields outside the core are derived and the parameters are adjusted to achieve a constant solution. Ogusu [59,60] published a numerical analysis of the rectangular dielectric guide using the generalized telegraphist's and verified the results experimentally. Pitale [61] used a Green's function method to explain the propagation through a dielectric waveguide. Huen et. al. [62] have suggested a rigorous formulation for solving the scattering of plane waves by a composite wedge of metal and lossless dielectric. This employs the Kirchhoff's integral in the physical region and the extinction theorem in their mathematical complementary regions to make the correction of the primary approximated solution.

Malherbe [63] has analyzed the radiation properties of an open-ended non radiative dielectric waveguide and compared the calculated values, with the use of a simple theory of radiation that is based on the field distributions in the guide. He has also presented [64] the development of a corporate feed for application to antennas fed from a non radiative dielectric waveguide.

Radiation characteristics of tapered dielectric rods has been analyzed by different researchers. Kiely [29] and Zuker [65] have discussed the problem of tapering of a dielectric cylindrical rod and derived some design formula. James [66] presented an engineering approach to the design of tapered dielectric rod antennas and compared its performance with hollow dielectric horn antennas. He treated this antenna as a system of 'm' planar radiating apertures. The radiated field is the sum of the radiation from each aperture. Marcuse [67] also has used a similar step synthesis method to evaluate the radiated power from a cylindrical dielectric rod. Kubo [68] has numerically analyzed the leakage characteristics of a cylindrical dielectric waveguide with a periodically varying radius.

Radiation from tapered dielectric rod antennas has also been studied both experimentally and theoretically by Kumar [69,70,71]. Felsen [72] has done an approximate analysis of the radiation properties of a two-dimensional tapered surface wave antenna having a linear susceptance variation.

The radiation characteristics of rectangular dielectric rod antennas have been demonstrated by workers like Shiau [73], Kobayashi et al.[74,75] and Yao et al.[76]. Sen et al.[77,78] have predicted theoretically and verified experimentally, the radiation characteristics of untapered rectangular dielectric rod antennas.

Paulit et al.[79,80]have done extensive work on the theoretical analysis of the radiation patterns and gain of linearly tapered rectangular dielectric rod antenna using Schelkunoff's equivalence principle and verified the numerical results experimentally. They found that, the mismatch at the feed end for the tapered rod is much less than that for an untapered rod.

Kiely [81,29] has done theoretical and experimental work on dielectric tube antennas and studied the influence of tube length, diameter and wall thickness on radiation patterns. Gallet [82] and Narasimhan et al.[83] have also studied the performance of dielectric tube antennas and showed that these antennas are more directive than dielectric rod antennas.

For dielectric rod and tube antennas, several launching methods are proposed by different researchers to enhance the launching efficiency. James [84] used a circular waveguide launcher and the launcher radiation was about 10% of the incident guide power. Brown [85] concluded that the side lobe levels can be improved by launching from a larger aperture or alternatively using a ring source launcher. Potak et al.[86] suggested another method of placing a flange or choke around the metal waveguide aperture for increasing the launching efficiency. Sen et al.[77,78] have theoretically derived and experimentally verified the launching efficiency for a rectangular dielectric rod antenna exited by a metallic rectangular waveguide carrying the dominant TE_{10} mode. Booker et al.[87] and Blakey [88] have used the unperturbed fields

tangential to the feed aperture to calculate the power radiated from the launcher to free space. Deschamps [89] suggested a method for experimental measurement of the aperture efficiency. Trinh et al.[90] have developed a launching horn for the rectangular dielectric rod at millimeter wave frequencies, which suppresses the side lobe levels.

2.3 DIELECTRIC LOADED METALLIC HORN ANTENNAS

Dielectric loading in metallic horns of conical and rectangular type, proposed by several researchers, were found to enhance the aperture efficiency, reduce the beam widths, increase the gain, reduce the cross polar levels and lower the side lobe levels.

This type of modifications were initiated by Bartlet et. al.[91], who proposed the use of a dielectric cone of low relative permittivity to improve the efficiency of microwave reflector antennas.

Tsandowlas et al.[92] have studied theoretically and experimentally the effect of symmetrical loading of horn apertures with E-plane dielectric slabs. They have found that this method increases the flatness of the aperture electric field distribution and hence enhances the aperture efficiency.

The effect of loading dielectric slabs centrally along the H-planes have theoretically analyzed for rectangular horn antennas by Ashton et al.[93]. Baldwin et al.[94] have studied the effect of loading dielectric slabs in the E-walls of rectangular horns. A rectangular radiating aperture centrally loaded with a dielectric slab in the H-plane presented by Sabnani et al.[95] gives identical principal plane patterns. They have also given theoretical support for their findings.

Hamid et al.[96] have reported the use of a dielectric plug at the end of a round waveguide for getting narrow radiation patterns with gain enhancement. They have also studied the effect of depth of penetration of the rod into the waveguide.

For getting rotationally symmetric radiation patterns with low side lobe levels from conical horn antenna Satoh [97] has used a dielectric band inside the aperture of the horn. Vokurka [98] has designed a simple feed with high polarization purity, by partially loading the grooves of the corrugated surface of the horn with dielectric material.

The radiation characteristics of a conical horn loaded with a dielectric sphere has been reported by Martin [99]. Gain enhancement and beam symmetry can be achieved by this method.

For getting identical symmetric radiation patterns in both E and H-planes with very low cross polarization over two desirable frequency bands Kumar [100] presented a new type of dual-band waveguide feed, loaded with a dielectric ring and a corrugated choke. In another work [101] he has theoretically predicted and experimentally verified the radiation patterns of a dielectric lined cylindrical waveguide feed.

Balling et al.[102] have studied the radiation properties of a dielectric-lined dual-mode horn and achieved high aperture efficiency and low cross polarization simultaneously over a wide band. Nair et al.[103] have presented a high gain multi-mode dielectric coated rectangular horn antenna and a dielectric coated conical horn [104] for beam modifications. They have also presented the radiation properties of a double-flare multi-mode dielectric loaded horn antenna [105] and a dielectric loaded biconical horn [106]

Aly et al.[107] have showed that for a longitudinally slotted horn, the slot depth required for achieving low cross polarization can be considerably reduced by filling the slots with a dielectric material. Lier [108] has studied both theoretically and experimentally the radiation characteristics of a conical metal horn loaded with a dielectric core inside and separated from the metal walls by another dielectric layer having lower permitivity than the core. Considerable reduction in side lobe levels and cross polarization levels over wide frequency range can be achieved using this technique.

He has also reported [109] a broad-band elliptical beam-shape horn with low cross polarization levels using dielectric core approach.

Narasimhan et al.[110] have reported a dielectric loaded corrugated dual-frequency circular waveguide horn feed having radiation patterns with good symmetry and low side lobe levels. Raghavan et al.[111] have reported the analysis of a dielectric ring-loaded dual mode conical horn using numerical modal matching technique.

Knop et al.[112] have analyzed using asymptotic techniques, the radiation properties of dielectric loaded horn and corrugated horn. Knop [113] has also analyzed the HE_{11} mode fields that can exist inside and across the aperture of a metallic wall conical horn, centrally loaded with a concentric dielectric material. The experimental results are found to agree well with the theoretical predictions.

Lier et al.[114] have reported a hybrid mode conical dielectric horn with metalized outer surface and inner surface with circular conducting strip structure. The cross polar levels can be minimized for selected frequencies using this method.

Olver et al.[115] have reported a conical horn loaded with dielectric cone. This method is very effective for getting low cross polarization over a wide band of frequencies.

Lee et al.[116] have described a circular waveguide horn with a lossy magnetic coating in the interior walls for getting good circularly polarized waves. Wang et al. [117] have presented a magnetically coated horn having performance similar to corrugated horns. By coating the inner walls of a pyramidal horn using dissipative materials, Ghobrial et al.[118] achieved a reduction of 7dB in cross polarization level.

Nair et al.[119] reported gain enhancement of a circular aperture plural mode H-plane sectoral horn by symmetric dielectric loading on the walls of the horn. They have also studied the performance of the horn with a dielectric core inside the horn,

with air gap between the dielectric and horn metal walls. This technique increases the directivity and reduces the side lobe levels and cross polarization levels.

Joe et al.[120] have reported the possibility of axial beam tilt using an assymetric hollow dielectric E-plane sectoral horn constructed by replacing one side of a rectangular hollow dielectric E-plane sectoral horn by a metal sheet. They found that the tilted power can be shifted between two angles using a narrow metallic strip of optimum length arranged on the dielectric side of the horn.

A practical design for supporting the inner core of a millimeter wave dielectric loaded horn has reported by Cabill [121]. He has obtained good input impedance match, excellent radiation characteristics and high mechanical strength using this technique.

Stephen et al.[122] have reported a technique for the reduction of side lobe levels of a simulated corrugated horn antenna by loading the outer surface of the E-walls of the horn with a strip loaded dielectric substrate. They have also reported [123,124] the development of a new rectangular feed horn using strip attached dielectric loading technique.

2.4 DIELECTRIC HORN ANTENNAS

Solid and hollow dielectric horn antennas come under this category. These antennas are relatively recent additions to the dielectric group of antennas. Only few attempts were made to explore the possibilities of this new class.

Solid dielectric horns of different shapes can be constructed by giving modifications to the rod antenna. A detailed treatment of solid conical dielectric horn excited using a conical metallic horn (launcher) have been presented by Clarricoats et al.[125,126] in two parts. In part one they have developed the theory of propagation and radiation by dielectric cones. In part two, the radiation characteristics of Cassegrain

reflectors employing dielectric cone feeds are presented. They emphasized the similarity between the hybrid modes that propagate on a dielectric cone and those in a corrugated horn. Kiely [29] in 1953, after certain experiments, concluded that cylindrical dielectric horn antennas had a higher gain than a metal horn of the same dimension.

Brooking et al.[127] have theoretically predicted and experimentally verified the radiation patterns of pyramidal dielectric waveguide (solid dielectric horn) excited by a pyramidal horn antenna. To find the propagation constants and the aperture field, they have used the approximate method proposed by Marcatili [51]. The pyramidal dielectric horn inserted into the pyramidal metallic horn is found to be capable of modifying the radiation pattern of the horn with considerable reduction in 'Half Power Beam Width' and gain enhancement.

A detailed study of the radiation characteristics of the solid rectangular dielectric horn of pyramidal shapes with small E-plane and H-plane flaring , excited by an open metallic waveguide, was theoretically and experimentally studied by Narayanan[41].

A very important work in the field of hollow dielectric horn to be cited here is the work done by James[66]. He has used a semi empirical method to design a conical hollow dielectric horn antenna with variable wall thickness. A stepped tube model for the conical hollow dielectric horn was followed, considering only the launcher radiation and the radiation from the mouth of the horn. He had showed that the radiation patterns of this antennas are superior in the E-plane and inferior in the H-plane. He also suggested that this antenna can be used to replace small metallic horns, if E-plane patterns are of importance. When the flare angle is reduced to zero, this horn exhibited similar patterns to that of the tapered rod antennas. A study of some rectangular shaped horns with variable wall thickness based on the same principle, had also been carried out.

A rectangular hollow dielectric horn having uniform wall thickness have been studied by few researchers recently. Singh et al.[128] have investigated both theoretically and experimentally, the amplitude of the aperture field of an E-plane sectoral hollow dielectric horn antenna. The horn was constructed by replacing the walls of a metallic horn using dielectric sheets and is excited using open metallic waveguide. They have obtained a reasonable agreement between the theoretical and experimental results. Singh et al.[129] have also studied the aperture field distribution and far field radiation of a H-plane sectoral hollow dielectric horn antenna in a similar manner. Recently the author has reported a strip loading technique for modifying the E-plane pattern of an E-plane sectoral hollow dielectric horn [130].

Chapter 3

METHODOLOGY

The methodology adopted and the facilities used for the study of radiation characteristics of the new hollow dielectric horn antenna are discussed in this chapter. The details regarding the different sophisticated equipments used to analyse the performance of the antenna are presented. A detailed description of the fabrication of the test antenna is also given. The chapter includes the methods and experimental set-up used to study the important characteristics of the antenna such as the radiation pattern, gain, VSWR, impedance and other associated parameters.

3.1 EXPERIMENTAL FACILITIES USED

The major facilities used for the experimental study of the antenna characteristics are

1. Network Analyzer (HP 8410 C/HP 8510B).
2. Antenna positioner and controller and
3. The Anechoic chamber.

3.1.1 The Network Analyzer Setup

Microwave Network Analyzer is a sophisticated equipment which provides a modern approach to microwave measurements. This equipment combines a sweep oscillator, a transducer, a harmonic frequency converter and display unit as shown in Fig. 3.1. For the present study HP 8410C and HP 8510B network analyzers are used.

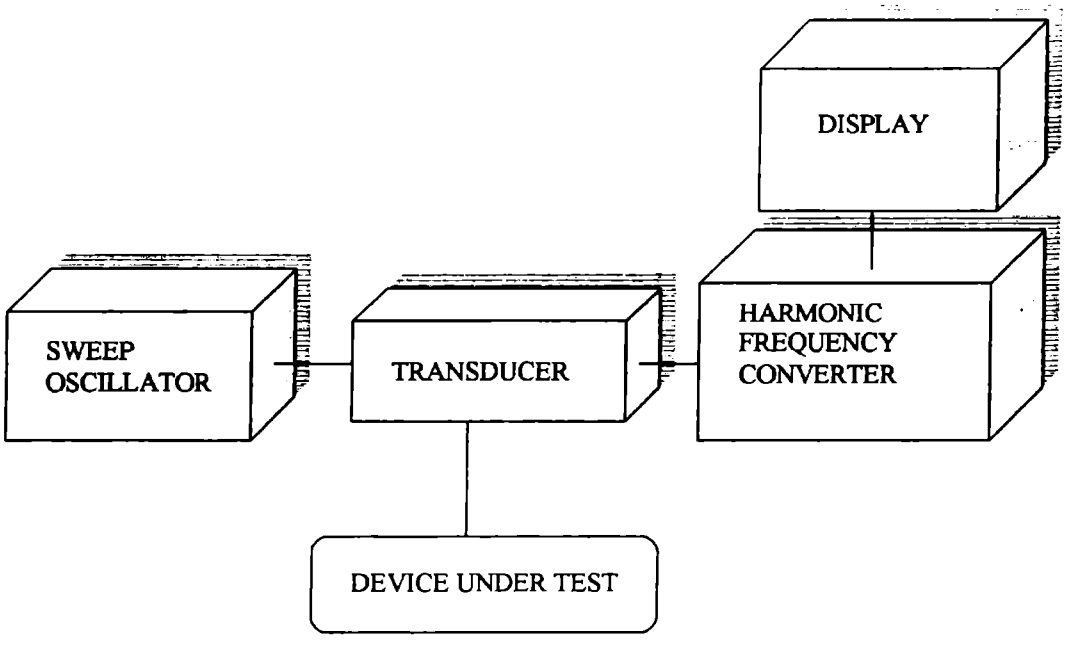

Fig. 3.1 Network Analyzer setup.

The sweep oscillator is a completely solid state self-contained multi-band sweep signal source which provides a sine wave signal to stimulate the device under test. The model HP 8350B can be used along with HP 8410C network analyzer and HP 8341B can be used with HP 8510 B analyzer.

The transducer, which is the reflection transmission test set, is connected between the signal source and the harmonic frequency converter. This unit provides three functions. Initially, it splits the incoming signal into the reference and the test signals. Secondly, it provides an extension capability for the electrical length of the reference channel, so that the distance traveled by the test and reference signals are equal. Lastly it connects the system properly for transmission or reflection measurements.

The harmonic frequency converter mixes the R.F signal with the output of a local oscillator and the resulting IF signal is given to the display unit through the network analyzer.

For the present study, HP 8510B and HP 8410C network analyzers are used. The system HP 8510B is used for impedance and VSWR measurements while HP 8410C is used for gain measurements. The radiation pattern measurements are performed using both HP 8510B and HP 8410C systems.

8410C, a manually operated model, can be used for the continuous simultaneous phase and magnitude ratio measurements of RF voltages. It measures phase angles from 0 to 360 degrees and magnitude ratios in decibels over a dynamic range of 60dB. Measurements can be made on single frequencies and on swept frequencies from 110MHz to 12.4GHz.

8510B is fully automatic computer controlled system. This system can be operated in the frequency range from 0.045GHz to 26.5GHz for measuring transmission and reflection characteristics of active and passive networks in the form of gain, reflection coefficient, S-parameters and normalized impedance over a dynamic range of

110dB. Five independent markers and two independent channels are provided for highlighting and displaying the results. The displayed results can be in the logarithmic/linear magnitude, phase or group delay format on polar or rectangular co-ordinates. For the direct measurement of the impedance, smith chart format also is provided. The measurements can be done either in Ramp mode or in Step mode. In step mode measurements can be performed in 801 data points with a maximum averaging of 4K. One important capability of this system is its ability of time domain measurements, which gives more accuracy in measurements.

3.1.2 Antenna Positioner and Controller

The antenna positioner with a remote control is used to rotate the test antenna to any desired angle so that the radiation pattern in the receiver mode can be plotted. The antenna positioner or turn-table consists of an a.c. motor with gear system for rotating the platform and a mechanism for mounting the antenna on the platform. The height of the mounting mechanism can be adjusted for aligning the axes of the receiver along that of the transmitter.

The receiving antenna (AUT) arranged on the turn-table, is placed in the quiet zone of the anechoic chamber. The rotation of the turn table is controlled by a remote control placed outside the chamber. To avoid the rotation of the platform beyond the required span, limit switches are provided with the positioner. The output from the receiving antenna is connected to the transmission return port of the test set-up using a cable.

3.1.3 Anechoic Chamber

Antenna measurements should be performed in a perfectly free space environment to avoid electromagnetic interference from the surrounding instruments and walls. The anechoic chamber is constructed to artificially simulate the free space environment in the laboratory. Fig. 3.2 shows a schematic representation of the

microwave anechoic chamber. Pyramidal shaped structures with microwave absorbing materials embedded in it is fixed all over the inner walls of the chamber. The position of the turn table and the receiver is in the quiet zone of the chamber as shown in the figure.

3.2 FABRICATION OF THE TEST ANTENNA

The test antenna called the New Hollow Dielectric Horn Antenna (AUT) is fabricated from ordinary hollow dielectric horn antenna (HDH) by modifying it using two techniques. It is observed that these modifications are capable of producing drastic changes in the performance of the antenna. The first technique is a new launching technique, which involves the introduction of a properly tapered dielectric rod at the throat of the horn and the second one is a strip loading technique. E-plane sectoral horns, H-plane sectoral horns and Pyramidal horns of different flare angles were fabricated to suit the experimental frequency band. i.e., the X-band. Table 3.1. shows the list of experimental horn antennas fabricated.

Table 3.1 List of experimental horn antennas fabricated.

E-plane sectoral horn		**H-plane sectoral horn**		**Pyramidal horn**		
Flare angle (Degree) α_E	**Axial Length (cm)**	**Flare angle (Degree)** α_H	**Axial Length (cm)**	**Flare angle (Degree)** α_E	α_H	**Axial Length (cm)**
10	15	10	12	20	10	15
20	15	20	12	20	20	15
30	15	30	12	20	30	15
40	15	45	12	10	20	15
50	15	60	12	30	20	15
20	12	20	15	20	20	12
20	9	20	9	20	20	9
20	6					
20	21					

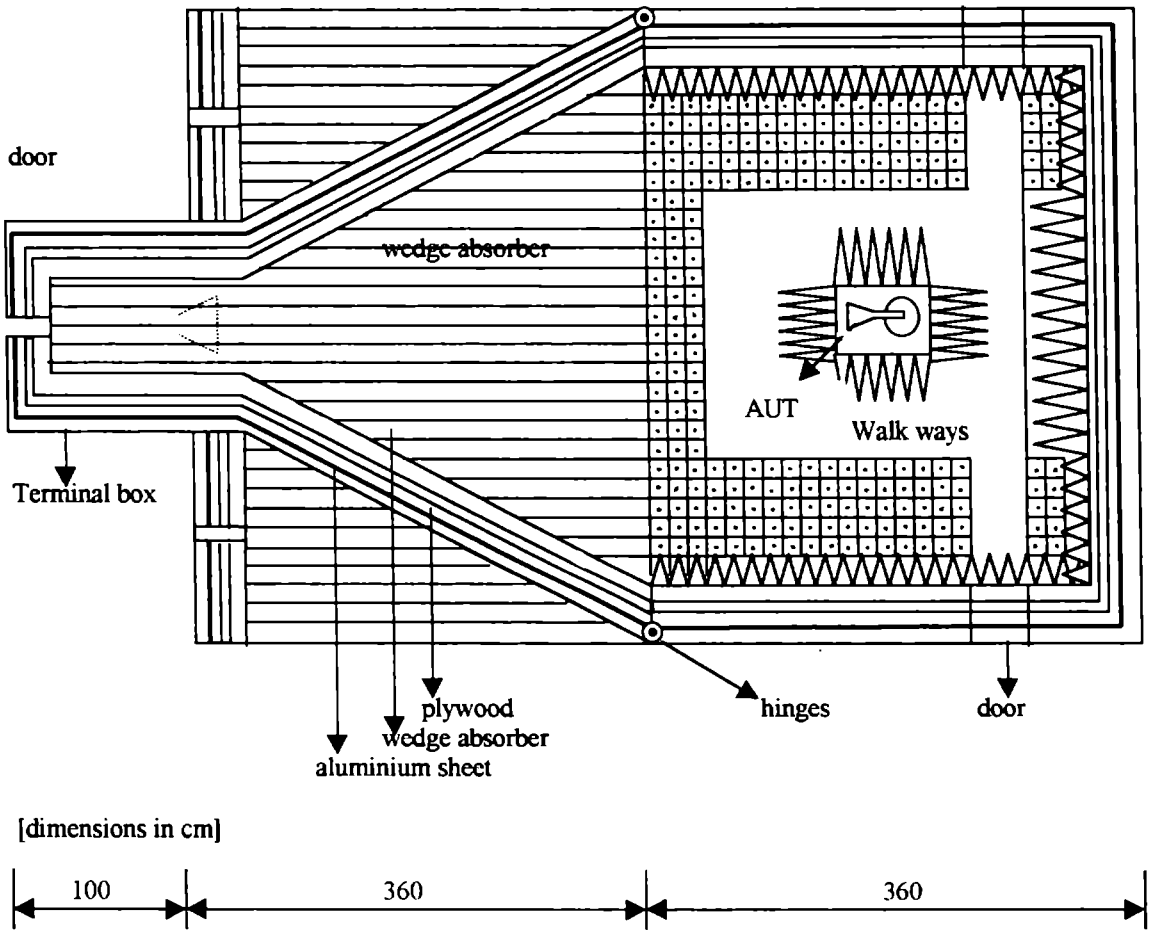

Fig. 3.2 Schematic representation of the microwave anechoic chamber [top view].

3.2.1. Fabrication of ordinary Hollow Dielectric Horn (HDH)

The HDH is constructed by replacing the walls of a metallic horn by low-loss dielectric sheet (polystyrene of dielectric constant ε_r= 2.56) of thickness 2 or 3 mm. For the HDH the thickness of the dielectric sheet also is a parameter for adjusting the performance of the antenna. In the present study the variation of this parameter is not taken into consideration because, the study concentrates on the newly introduced modifying techniques.

The HDH is a dielectric horn structure joined at the end of an open metallic waveguide. So there is a discontinuity at the throat of the horn (feed-end) as far as the power flow is concerned. The schematic diagram of the HDH is shown in fig. 3.3. It is difficult to join the dielectric horn structure at the end of the metallic waveguide. Use of good adhesive materials solves this problem to some extend. The new launching technique adopted here, not only provides good launching action, but also solves this problem.

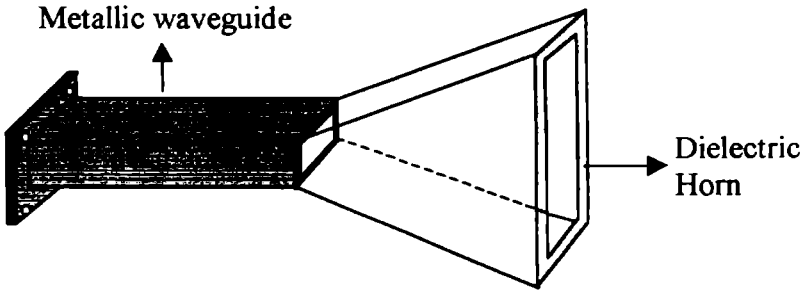

Fig. 3.3 Schematic representation of Ordinary Hollow Dielectric Horn (E-Plane Sectoral) Antenna.

3.2.2 Launcher technique

3.2.2.1 Launcher design and optimization

Fig. 3.4. shows a schematic representation of the new launcher. It is fabricated using the same dielectric material (polystyrene) used for fabricating the test antenna. The breadth b_0 and thickness a_0 are equal to the inner dimensions of the waveguide. The tapered side is introduced into the waveguide with suitable length for seating. The length projecting outside the waveguide is well inside the horn structure. The total length 'l' of the launcher, length of projection 'p', depth of penetration 'd' and tapering length 't' are optimized for getting good results.

3.2.2.1.1 Length of projection 'p'

The length of projection 'p' of the launcher inside the horn is optimized for effectively transferring the electromagnetic energy from the waveguide to the horn. When 'p' is large, ($>>\lambda_0$), the protruding part of the launcher itself acts as a rod antenna. If 'p' is small compared to λ_0 , the situation is somewhat similar to the open

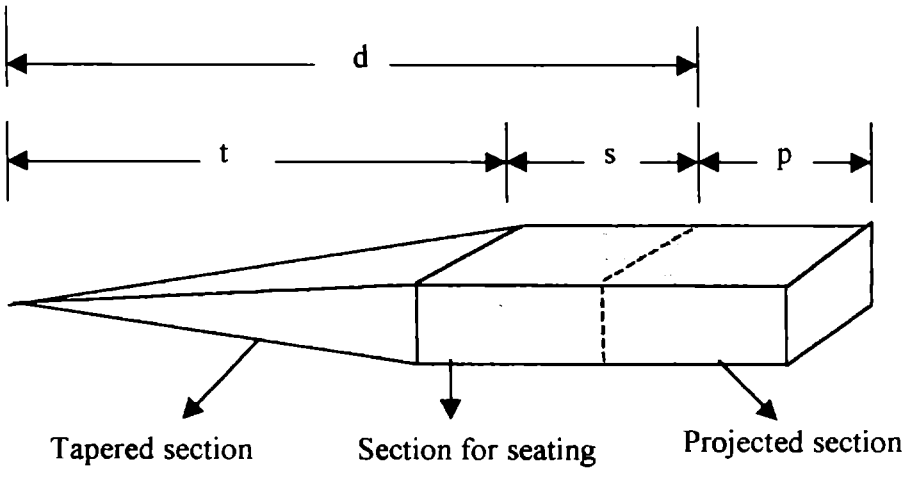

Fig. 3.4 Schematic representation of the optimized launcher.

waveguide. These effects can be verified by plotting the radiation patterns of the launcher for different 'p' values. The length for 'p' equal to λ_0 is found to be sufficient for good launching. So for the present study, the wavelength corresponding to the mid-frequency of the experimental band (3 cm) is taken as the optimized value for 'p'.

In order to optimize the profile of the projected section, radiation patterns of horns with launchers of different shapes for the projected section were studied (Fig. 3.5). Experiments using launchers with projected section profiles other than the uniform shape, give no substantial improvement for the radiation pattern. So the shape of the projected section of the launcher is optimized to be uniform.

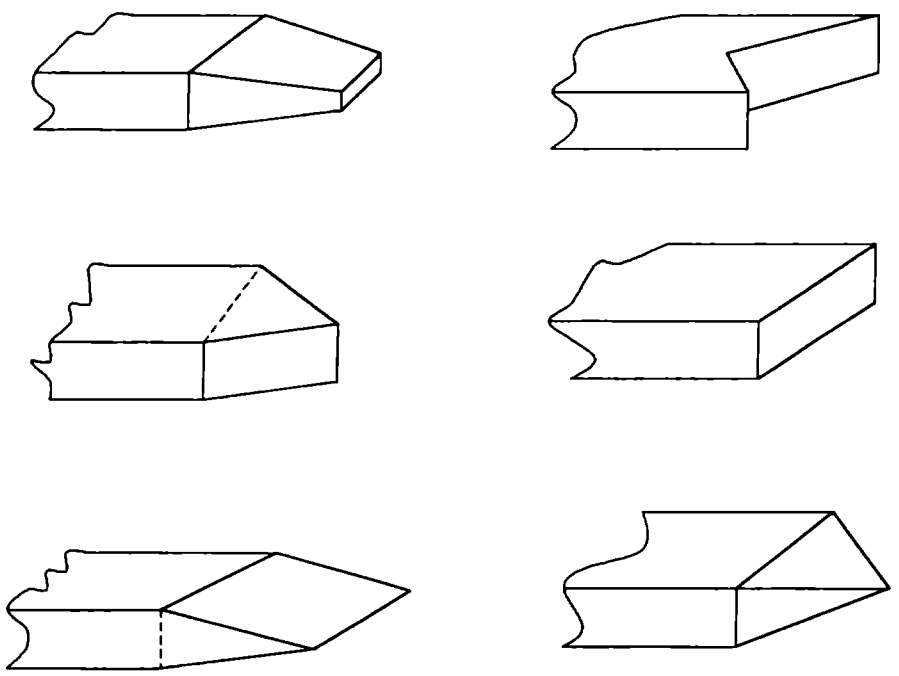

Fig.3.5 Different shapes for the projected section of the launcher.

3.2.2.1.2 Tapering length 't'

The tapering length 't' of the launcher is optimized for minimum VSWR. It is observed that the introduction of the launcher inside the waveguide increases the VSWR of the antenna. By giving a proper tapering to the launcher the reflected power can be minimize to negligible values. The VSWR of the launcher is studied for different tapering lengths and its value is found to be less than 1.75 for the entire X-band for tapering lengths greater than 8cm. So for the present study, the tapering length 't' is empirically optimized to be 8cm.

3.2.2.1.3 Depth of penetration 'd'

The depth of penetration 'd' includes the tapering length 't' and length 's' for seating. 't' is already optimized and so the value of 's' decides the penetration depth 'd'. The VSWR of the launcher is found to vary almost sinusoidally with 'd' for all frequencies. However, the maximum value of VSWR is below 1.75. So 's' can have any value, sufficient for good seating. In the present study the value of 's' is taken as 3cm.

3.2.2.2 New HDH with the optimized launcher (HDHL)

The details of the optimized launcher is given in Fig. 3.4. The total length of the launcher is 14cm (d+p). The launcher and HDH are fabricated into a single unit as shown in Fig. 3.6. The schematic representation of both sectoral and pyramidal HDHL are shown in the figure. Now it is enough to introduce the tapered section of the launcher into the open waveguide for getting the new HDH (HDHL), as illustrated for an E-plane sectoral horn in Fig. 3.7.

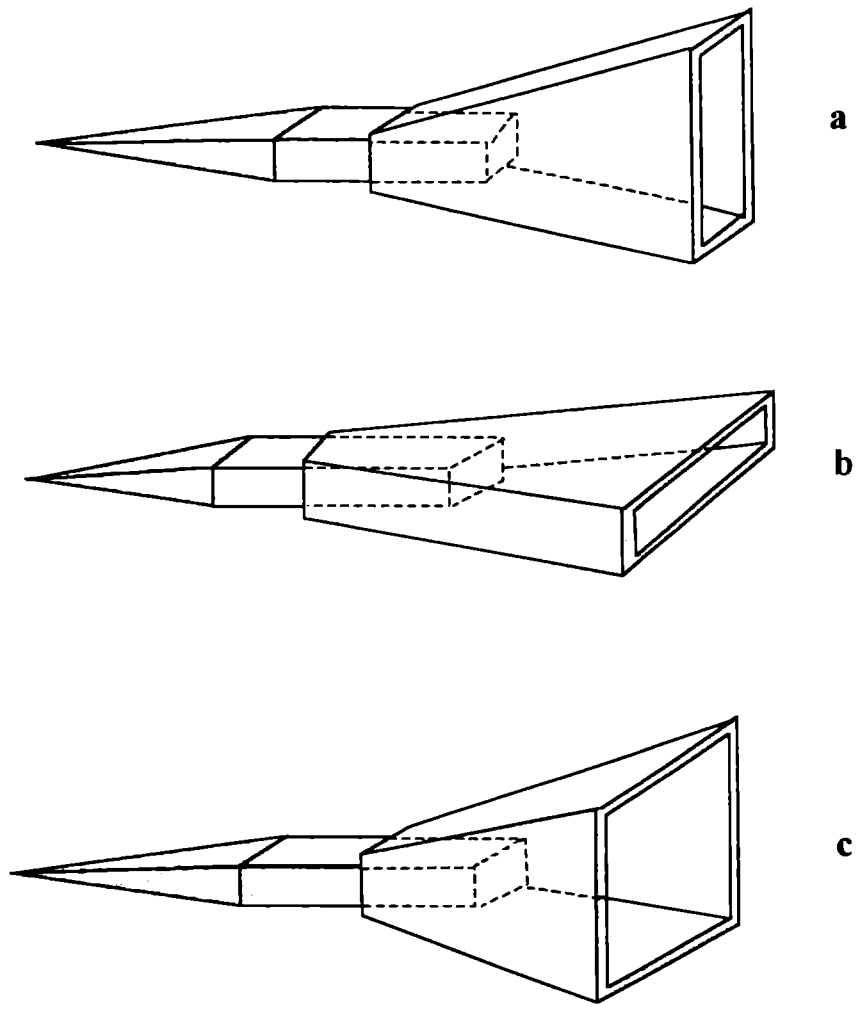

Fig.3.6 Schematic representation of the hollow dielectric horn with the launcher (HDHL), [a] E-plane sectoral horn, [b] H-plane sectoral horn, [c] pyramidal horn

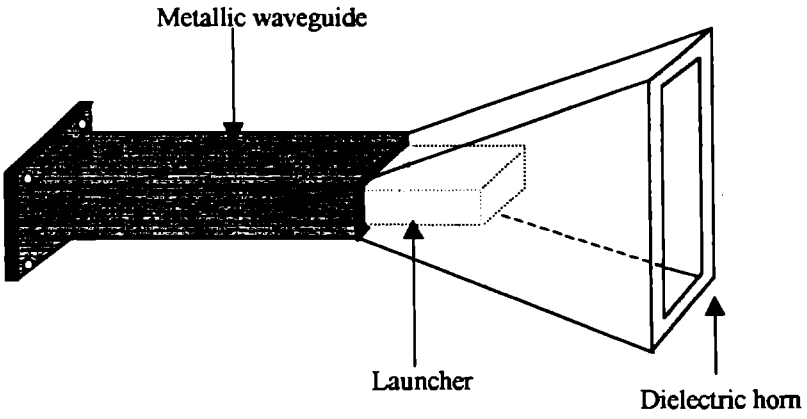

Fig.3.7 Schematic diagram of the HDHL introduced into the open Waveguide (E-plane sectoral HDHL)

3.2.3 Strip loading technique.

The second technique introduced for further modification of HDHL is the strip loading technique. In this method good conducting metallic strips of optimum dimensions are loaded on the walls of the HDHL. Aluminum or copper strips can be used for this purpose. The strip loading is carried out in different ways for sectoral and pyramidal horns as detailed below.

3.2.3.1 Strip loaded HDHL

3.2.3.1.1 E-plane sectoral horn.

For E-plane sectoral horns, the strip loading is done on the E-walls (walls perpendicular to the E vector) of the horn as shown in Fig.3.8. The width 'w' of the strips are equal to the inner broader dimension a_0 of the waveguide. The length of the strip 'l' is a parameter to be varied. So strips having different lengths (multiples of $\lambda/2$) are fabricated.

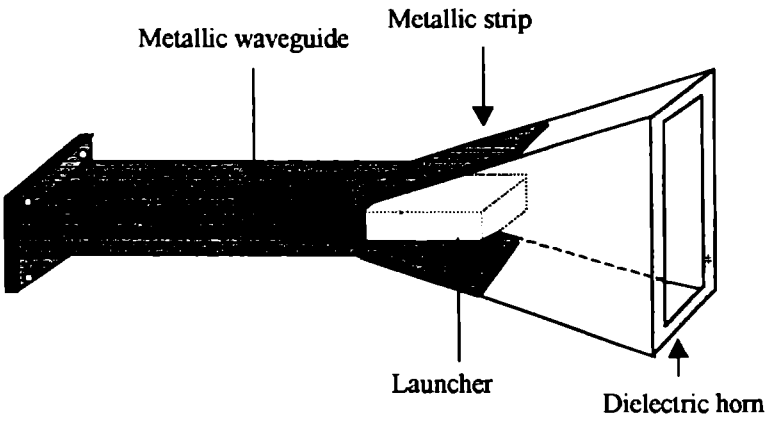

Fig.3.8. Schematic representation of the strip loaded E-plane sectoral horn antenna with the launcher.

Loading of strips on the parallel walls (H-walls) is not advisable due to many reasons. Initially, it adversely affect the radiation pattern of the antenna. In the H-plane it behaves similar to a metallic sectoral horn. Secondly, it needs large metallic sheets, only slightly less than that required to construct a metallic sectoral horn. Another possibility is loading of metallic strips on both walls simultaneously (E and H walls). The resultant structure is nothing but a small metallic horn with a dielectric lining inside. So there is no meaning in trying this type of strip loading also.

3.2.3.1.2 H-plane sectoral horn

For H-plane sectoral horns, the strip loading is done on the H-walls (perpendicular to the H vector) of the horn as shown in Fig.3.9. Here the width 'w' is equal to the inner smaller dimensions of the waveguide b_0. In this case also strips having different lengths are constructed to study its effect on radiation patterns. The strip loading on the parallel sides is not practiced because of reasons mentioned for the case of E-plane sectoral horn antennas.

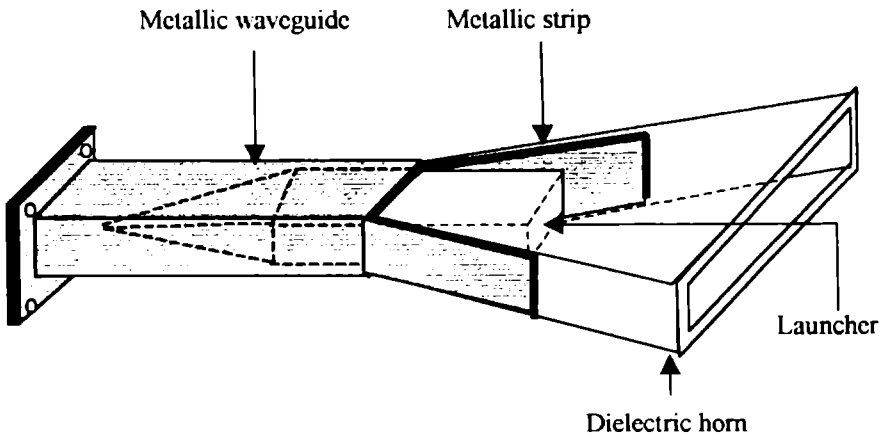

Fig.3.9 Schematic representation of the strip loaded hollow dielectric H-plane sectoral horn antenna(SHDHL)

3.2.3.1.3 Pyramidal horns

Strip loading in pyramidal horns can be done on the E walls or H walls. But unlike sectoral horns, we need metallic strips of angular dimensions for pyramidal horns. This in turn will increase the area of the metallisation region. Also, it is observed that this type of strip loading on E or H walls does not produce any good results.

Another strip loading method, which has proved to be effective for pyramidal horns is illustrated in Fig.3.10. Horns loaded with strips having width equal to a_0, are loaded on the E walls as shown in the figure is found to show some good results. Experiments are performed with strip-loaded horns of different strip lengths.

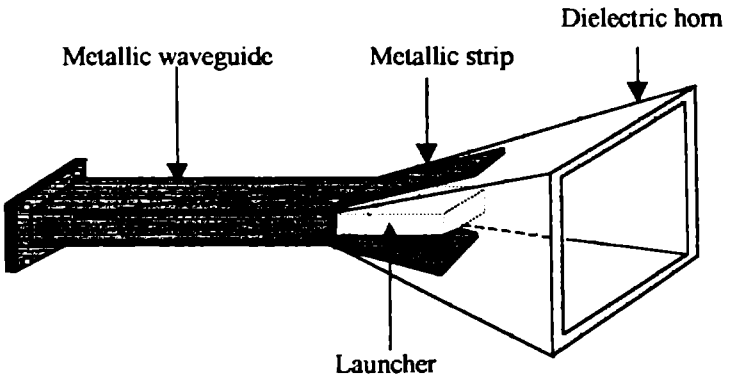

Fig.3.10 Schematic diagram of the strip loaded pyramidal hollow dielectric horn antenna(SHDHL)

3.3 PARAMETERS STUDIED

The performance of an antenna is characterized in terms of different antenna parameters. The various parameters studied are [1] Radiation pattern,[2] Directive gain and [3] Impedance and VSWR.

3.3.1 Radiation pattern

Radiation pattern is a graphical representation of the radiation properties of the antenna as a function of space co-ordinates. Actually we need a three dimensional radiation pattern for completely specifying the radiation properties of the antenna. But in almost all practical cases we are satisfied with the two principal plane patterns. For a linearly polarized antenna these planes are the E and H-planes. H-plane is the plane parallel to the magnetic vector H and E-plane is the plane parallel to the electric vector E, both planes passing through the axis of the antenna. Though it is significant to plot the radiation pattern for the near field, in most cases the radiation pattern in the far field is

much important. If the magnitudes of the electric or magnetic field intensity is plotted , we get the field pattern and a plot of power intensity gives the power pattern.

The radiation patterns can be drawn in rectangular or polar form. From these patterns, it is easy to find out the direction of maximum radiation, HPBW, -10dB beam width, side lobe levels, cross-polar levels, axial gain etc.

3.3.2 Directive Gain and Directivity

Almost all antennas radiate more power in certain directions. Directive gain of an antenna in a given direction is defined as the ratio of the radiation intensity in that direction to the radiation intensity of a reference antenna. The reference is usually taken as an isotropic source, a hypothetical antenna having equal radiation in all directions. The directivity of an antenna is the value of the directive gain in the direction of its maximum value. The directivity D of an antenna is given by the expression,

$D\ (dB) = 10 \log \{P_{(test)} / P_{(iso)}\}$; P is the power density.

If θ and ϕ are the HPBW in the two principal planes, the directivity can be approximately written as

$$D = 41\ 000\ (deg^2)/\ \theta\ (deg) \times \phi(deg)$$

3.3.3 Impedance and VSWR

Antenna impedance and VSWR are very important parameters as far as the performance of the antenna is concerned. Antenna impedance Z is a complex quantity given by

$Z = R + j\ X$; where R is the antenna resistance and X is the antenna reactance. The impedance of the antenna is a measure of the efficiency with which it acts as a transducer between the transmission line and propagation medium.

A part of the energy transmitted may be reflected from the input side of the antenna and giving rise to a standing wave voltage distribution in the transmission

line or waveguide. The reflection coefficient, a measure of the reflected component is defined as the ratio of the reflected energy to the incident energy. The voltage standing wave ratio VSWR is the ratio of the maximum to minimum standing wave voltages present at the input side of the antenna.

$$VSWR = V_{max} / V_{mim}$$

The VSWR expressed in decibels is called the standing wave ratio SWR.

$$SWR\ (dB) = 20 \log_{10} VSWR$$

In terms of the magnitude of the reflection co- efficient ρ,

$$VSWR = \sigma = (1+\rho) / (1-\rho).$$

$\sigma = 1$ is an ideal case, for which $\rho = 0$, For good practical antennas the value of σ is slightly greater, but close to 1.

3.4 EXPERIMENTAL SETUP

The experimental setup and the procedure used to study the important antenna characteristics are discussed in the following sections.

3.4.1 Radiation pattern

The experimental setup employed to plot the far field radiation pattern of the test antenna is given in Fig.3.11. The setup consists of the antenna under test (AUT) arranged inside the anechoic chamber and HP 8510B/(HP 8410C) network analyzer system as shown.

The antenna used as the transmitter is a standard pyramidal horn in the X-band connected to the reference port of the reflection transmission test set. The AUT is used as the receiver and is mounted on the turn-table, provided with a remote control. It is placed in the quiet zone of the acechoic chamber. To satisfy the far field condition, the distance between the transmitter and receiver is adjusted to be greater than $2D^2 / \lambda$, D is the largest aperture dimension of the antenna and λ is the wavelength used. The output

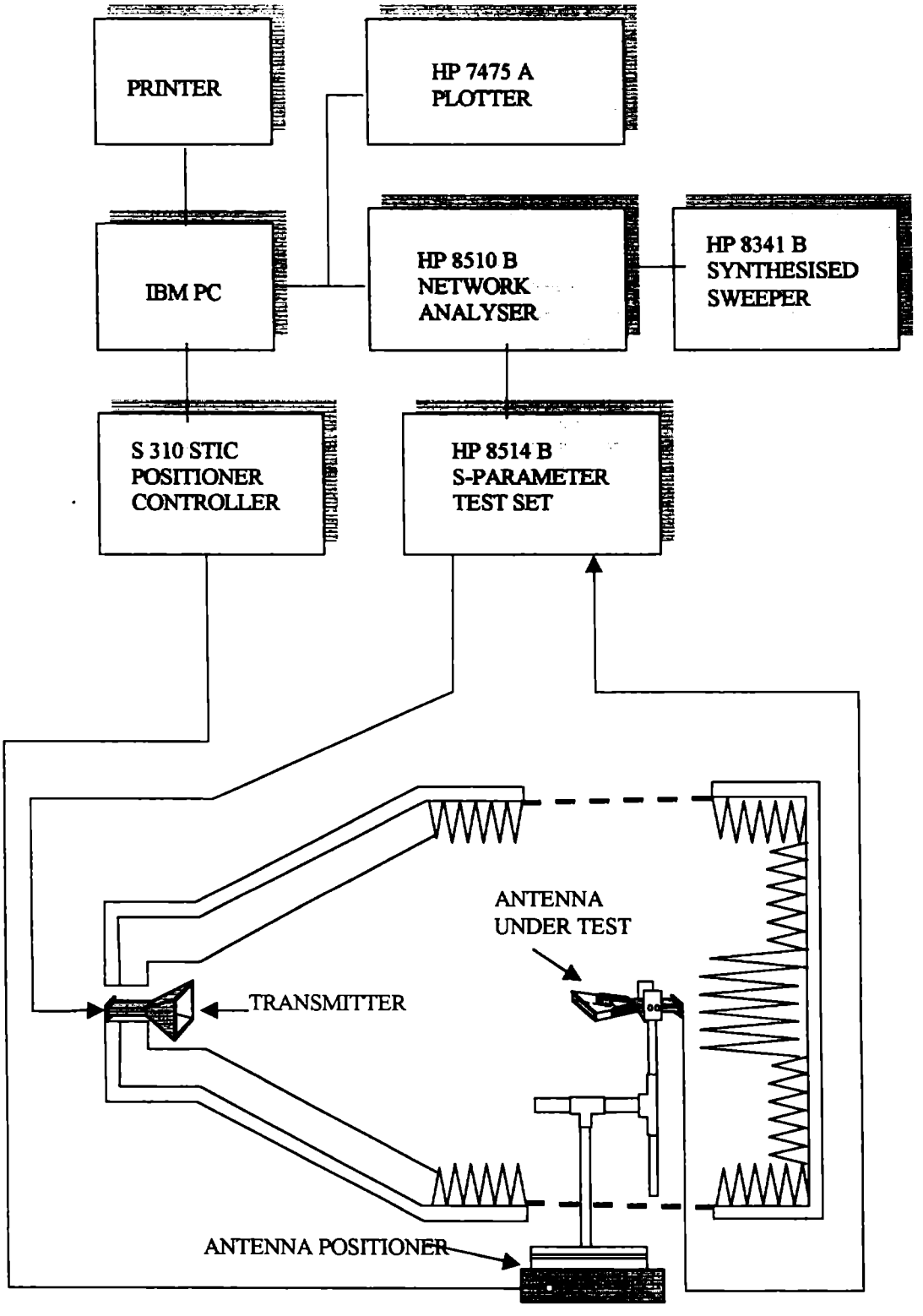

Fig.3.11 Experimental setup to study the radiation pattern of the test Antenna

from the receiving antenna is connected to the transmission return port of the test setup using cables. Before starting measurements, the axes of the transmitting and receiving antennas are adjusted to coincide each other.

In the first part of the measurements, the radiation patterns of the hollow dielectric horn with the launcher (HDHL) at different frequencies in the X-band are plotted for E-plane sectoral horn, H-plane sectoral horn and pyramidal horns. Radiation patterns of ordinary HDH also are taken for comparison. In the second part, effect of strip loading on radiation pattern is studied. For E-plane sectoral horns and pyramidal horns, strips of width a_0 with different lengths $\lambda/2$, 2 $\lambda/2$, $3\lambda/2$ etc. are loaded on the E walls and radiation patterns are taken. For H-plane sectoral horns, strips of width b_0 with different lengths are loaded on the H walls of the horn and radiation patterns are plotted. Finally radiation patterns for equivalent metallic horns are also plotted for comparison.

Different parameters like HPBW, relative gain, cross-polar levels, side lobe levels etc. can be easily found out from these radiation patterns.

3.4.2 Directive Gain

Gain of HDH and HDHL are measured at different frequencies for all experimental horns. For SHDHL gain variation with frequency and strip length are also analyzed.

Gain measurements were done by comparing the gain of different horns with that of a standard horn. Initially the standard horn is placed at a fixed position in the far field region of the anechoic chamber and the received power corresponding to its gain, at different frequencies are noted. Now the standard horn is replaced by the test horn and the received power is compared with that of the standard horn. For HDHL, gain variation with frequency and for SHDHL gain variation with frequency and strip length are analyzed.

3.4.3 Impedance and VSWR

The experimental setup for measuring the impedance and VSWR is shown in Fig. 3.12. HP 8510B network analyzer system is used for the purpose. The AUT is connected to the port 1 of the test set. The start and stop frequencies are selected by the 'stimulus' menu to 8 and 12GHz. and the analyzer is adjusted to the reflection mode using the 'parametric' menu. The display on the screen gives the VSWR with frequency. Along with VSWR plot, using the smith chart option, the impedance of the test antenna can be displayed and can be plotted.

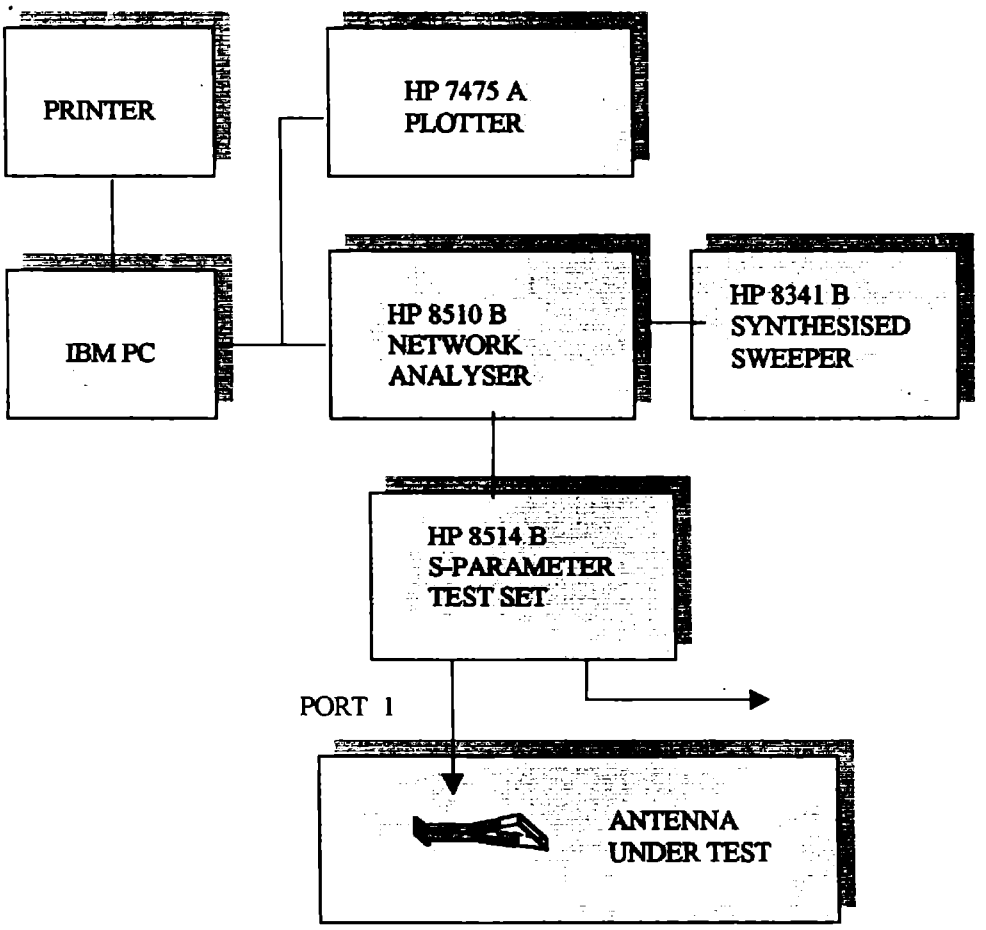

Fig. 3.12 Experimental setup to study the VSWR of the test antenna.

Chapter 4

EXPERIMENTAL RESULTS

The results of the experimental studies on the radiation characteristics of the new hollow dielectric horn antennas are discussed in this chapter. The experiments are conducted in the X-band. The important radiation characteristics such as radiation pattern, HPBW, side-lobe level, cross-polar level, VSWR, gain etc., for E and H-plane sectoral horns and pyramidal horns are presented under various sections. Results related to the optmisation of length of projection, depth of penetration and tapering of the launcher are sketched in the initial part. The radiation characteristics of the new HDH are discussed in the following sections. In the first section, the results of the new launching technique leading to the design of HDHL (Hollow Dielectric Horn with Launcher) are presented. The next section gives a detailed picture of the radiation properties of strip loaded hollow dielectric horn antennas (SHDHL). A comparative study of the new HDH antennas and equivalent metallic horn antennas form the final section.

4.1 LAUNCHER OPTIMIZATION

Fig. 4.1. gives the schematic representation of the optimized launcher. The methods used to optimize the launcher were discussed in section 3.2.2 of chapter 3. The results obtained for the optimized conditions are discussed in the following sections.

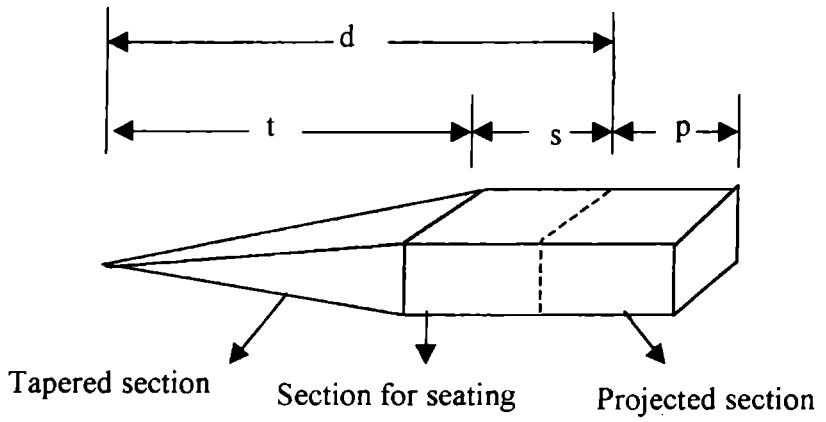

Fig.4.1 Schematic representation of the optimized launcher

4.1.1 Tapering length 't'

The section of the launcher inside the waveguide is properly tapered to minimize the backward reflection. The Voltage Standing Wave Ratio (VSWR) of the waveguide or horn varies in a sinusoidal manner with frequency for all tapering lengths. For tapering lengths of 8 cm or above, the maximum value of VSWR is found to be less than 1.75 for the entire X-band. So for the present study the value of 't' is selected (optimized) as 8 cm.

4.1.2 Depth of penetration 'd'

The depth of penetration 'd' is the sum of the tapering length 't' and the length for seating 's'. 't' is optimized as 8 cm and so we need only to discuss 's'. Keeping 't' constant, VSWR of the horn is studied for various values of 'd'. It is observed that the VSWR varies sinusoidally with 'd', but within the limit, for all frequencies as shown in Fig.4.2. So the value of 's' is not very important. Therefore it is enough to select a minimum suitable length for proper seating of the antenna at the end of the waveguide. For the present case 's' is taken as 3 cm, so that 'd' =11 cm.

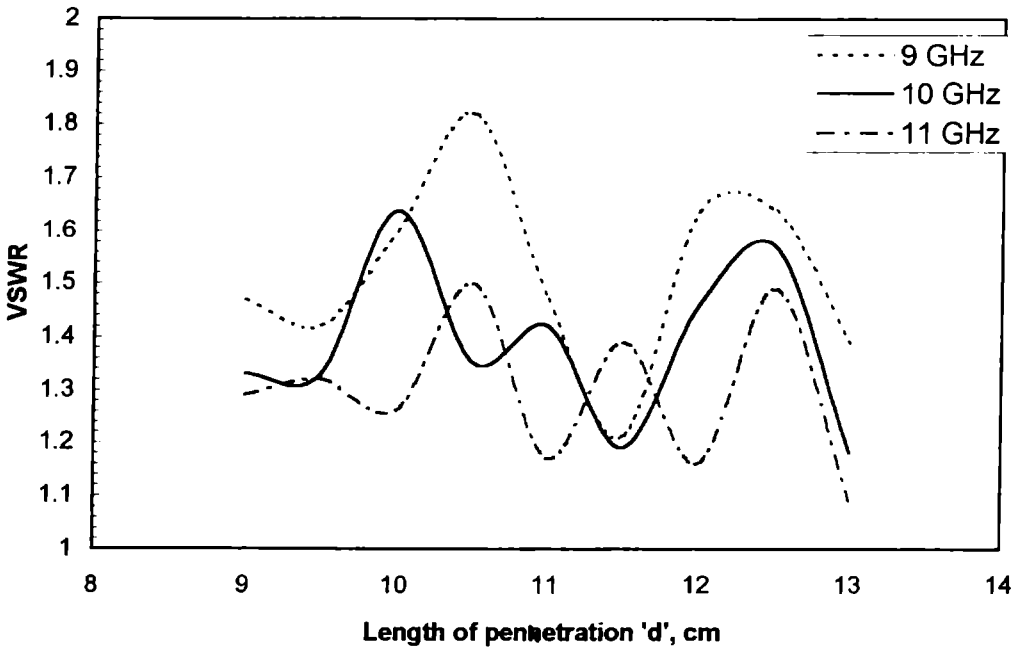

Fig.4.2 VSWR variation with launcher penetration depth 'd' at different Frequencies

4.1.3 Length of projection 'p'

As discussed in the previous chapter, the length of projection 'p', for effectively transferring the power from the waveguide to the antenna is selected. In that case the leakage due to discontinuity at the end of the waveguide becomes small. This length is selected by studying the radiation patterns of the waveguide with the launcher. If 'p' is very small (say 1 cm) the radiation pattern is somewhat similar to that of the open waveguide. If 'p' is large (say 5cm) the rod itself acts as an antenna, which increases the side lobe levels. Therefore a moderate length (3cm) equal to the free space wavelength corresponding to the mid frequency of the experimental X-band is selected as the

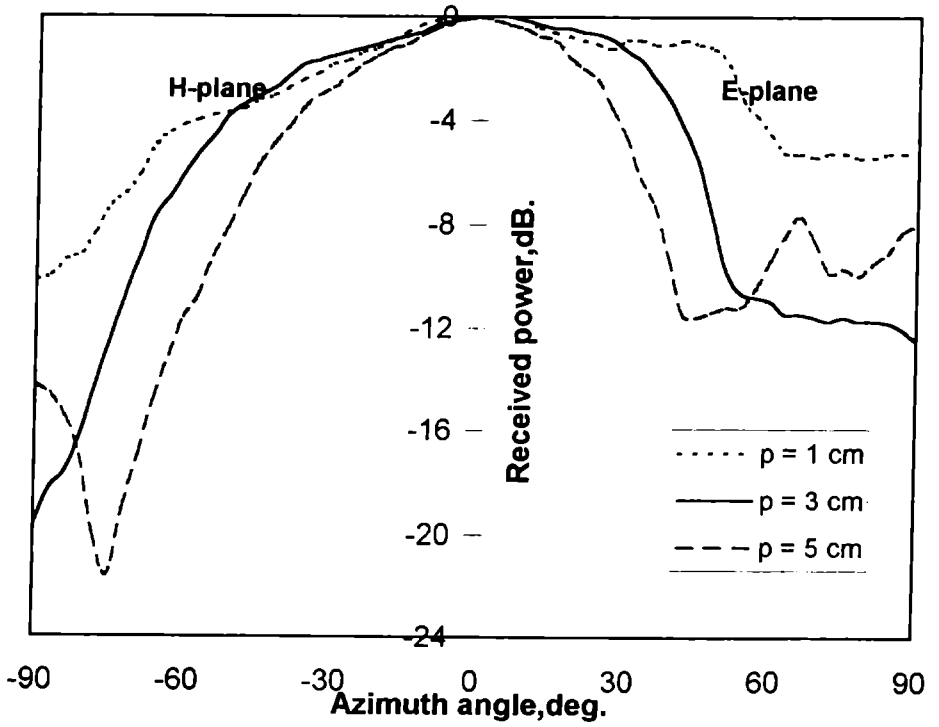

Fig.4.3 Radiation pattern of the launcher for different values of 'p' at 8GHz.

optimized value for 'p'. The E and H-plane radiation patterns of the open waveguide with the launcher for different 'p' values are shown in Fig.4.3. The VSWR variation with frequency for the open waveguide with the optimized launcher is shown in Fig.4.4.

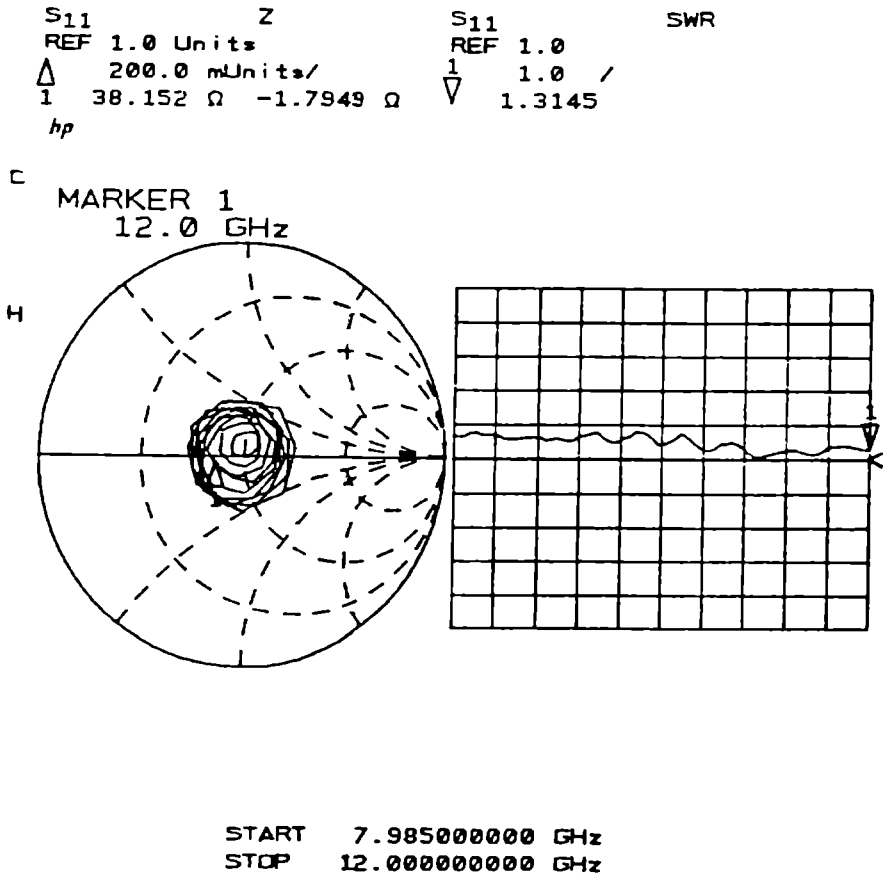

Fig.4.4 VSWR variation with frequency for the optimized launcher.

4.2 EFFECTS OF THE NEW LAUNCHING TECHNIQUE

The ordinary hollow dielectric horn (HDH) with the optimised launcher placed at the throat of the horn forms the HDHL antenna. The effects of this new launching technique are presented for both E-plane and H-plane sectoral and pyramidal horn antennas.

4.2.1 E-plane sectoral HDHL

The schematic diagram of the E-plane sectoral HDHL is shown in Fig.4.5. The merits of the radiation properties of this antenna over ordinary HDH are discussed in the following sections.

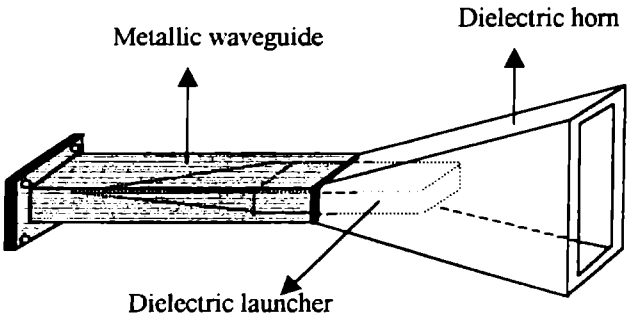

Fig. 4.5 Schematic representation of the E-plane sectoral HDHL

4.2.1.1 Radiation pattern

Fig.4.6. shows the E and H-plane radiation patterns of HDH and HDHL antennas of flare angle $\alpha_E = 30°$. It is evident from the patterns that the new launching technique reduces the side lobe levels to a considerable extent. The side lobe levels of both E and H-plane patterns are high for ordinary HDH. For HDHL the E-plane side lobe

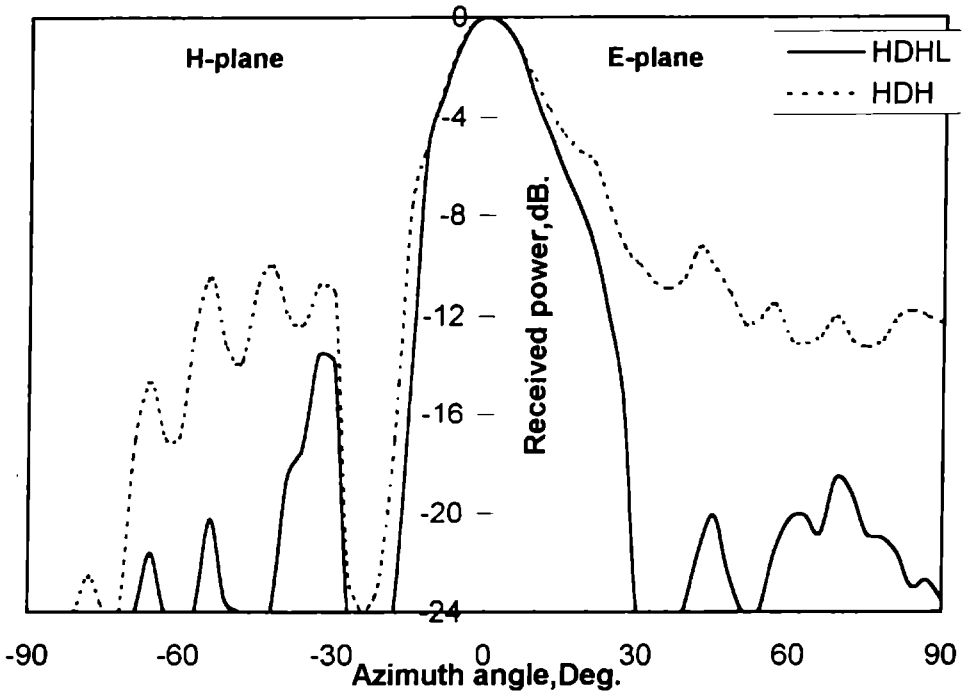

Fig.4.6 E and H-plane radiation patterns of E-plane sectoral HDH and HDHL at 8.5 GHz. $\alpha_E = 30°$.

levels are very low for almost all cases, but the H-plane side lobe levels are comparably high (around −14dB). One noticeable feature of the radiation patterns is that, in many cases, the E and H-plane 'Half Power Beam Widths' (HPBW) are almost equal. Fig.4.7. shows the E and H-plane radiation patterns for 20° horn at 10 GHz. It is clear that both E and H-plane patterns are narrow and almost identical, with HPBW around 25°. This is a clear deviation from the behavior of E-plane metallic sectoral horns. The basic property of the metallic sectoral horn is to produce a narrow pattern in the flared plane (E-plane pattern of E-plane sectoral horn) and a broad pattern in the other plane (H-plane pattern of E-plane sectoral horn).

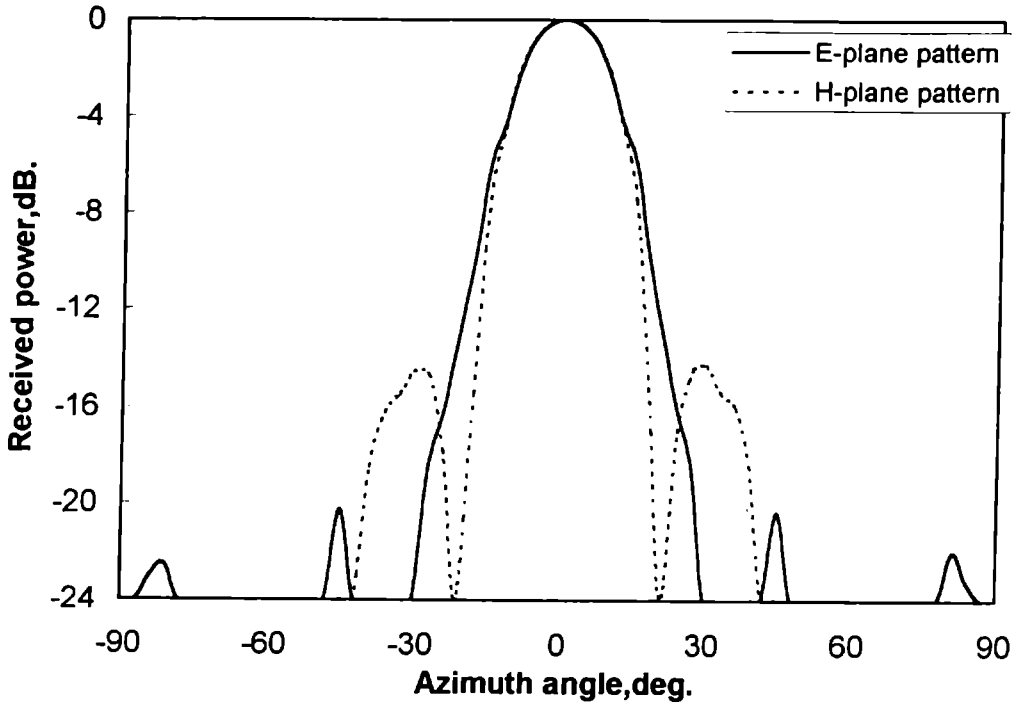

Fig.4.7 E and H-plane radiation patterns of E-plane sectoral HDHL at 10GHz. $\alpha_E = 20°$.

The HPBW variation with frequency in the H-plane and E-plane for E-plane HDHL of flare angle 10° and 20° are shown in fig.4.8.a and 4.8.b respectively. It is evident from the graph that the HPBW decreases with frequency as in the case of metallic horns. The HPBW variations for HDH are also shown for comparison.

Fig. 4.9. shows the variation of the first side lobe levels of the E and H-plane patterns with frequency for the HDH and HDHL antennas of flare angles 20° and 30°. The side lobe levels of E-plane patterns are found to be very low for all frequencies.

Table 4.I. shows the 3dB and 10dB beam width and side lobe levels for different E-plane HDHL antennas at different frequencies.

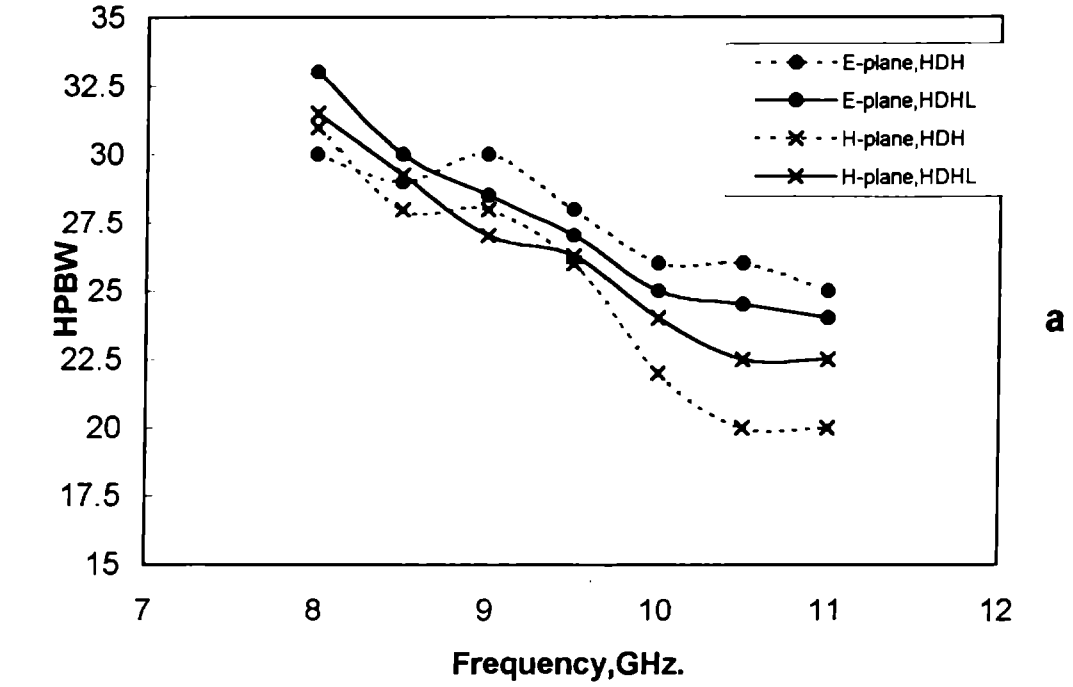

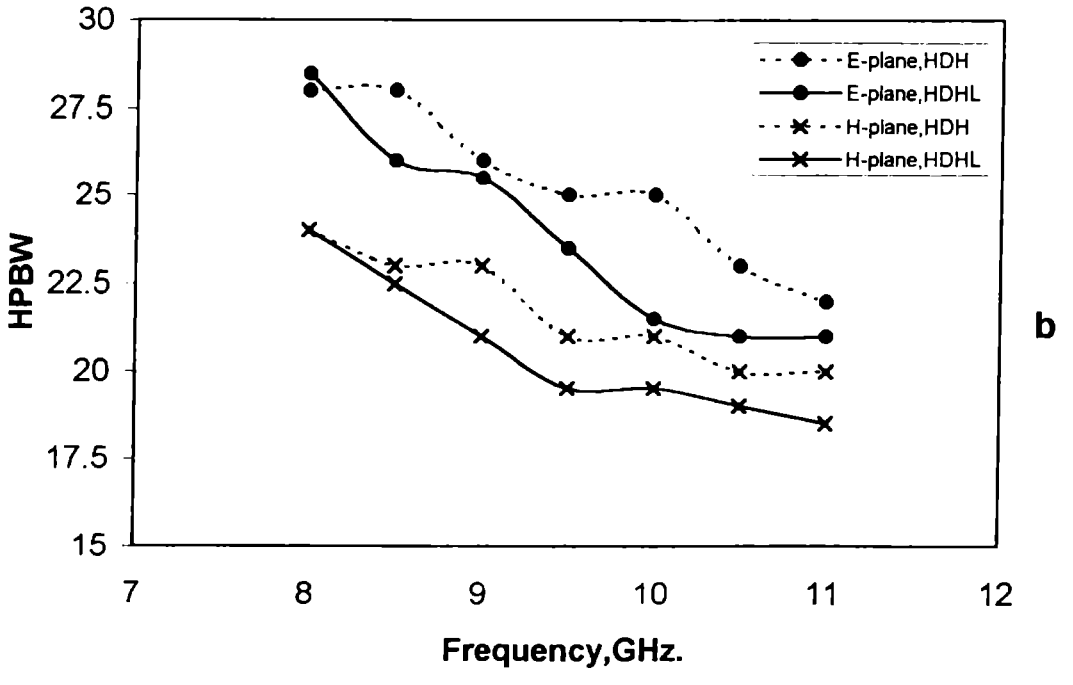

Fig.4.8 E and H-plane HPBW variation with frequency for E-plane sectoral HDH and HDHL. (a) $\alpha_E = 10°$, (b) $\alpha_E = 20°$.

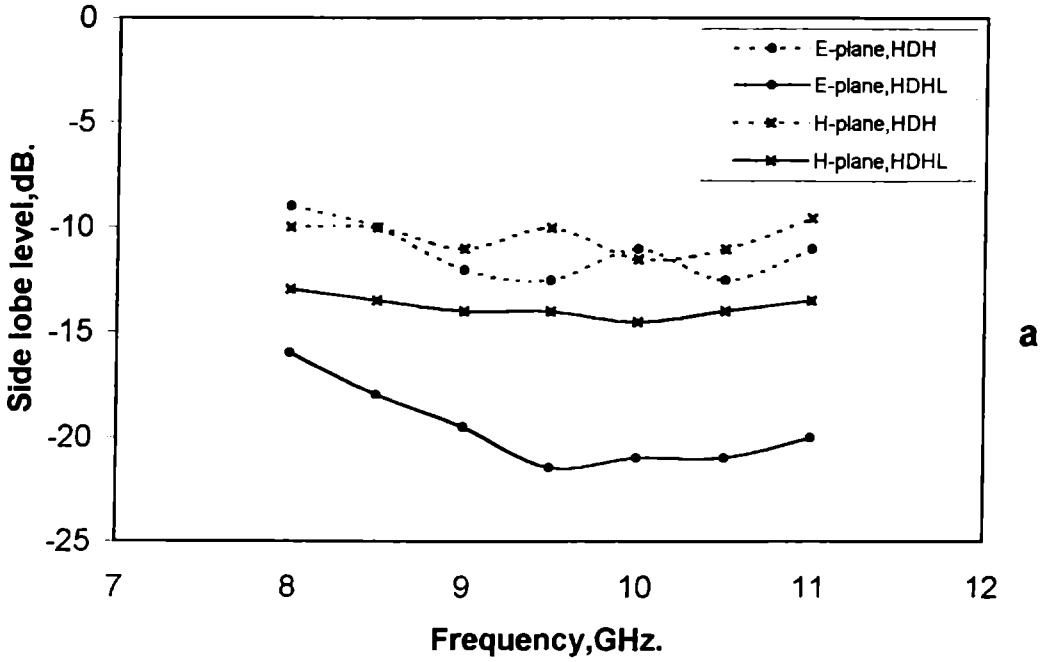

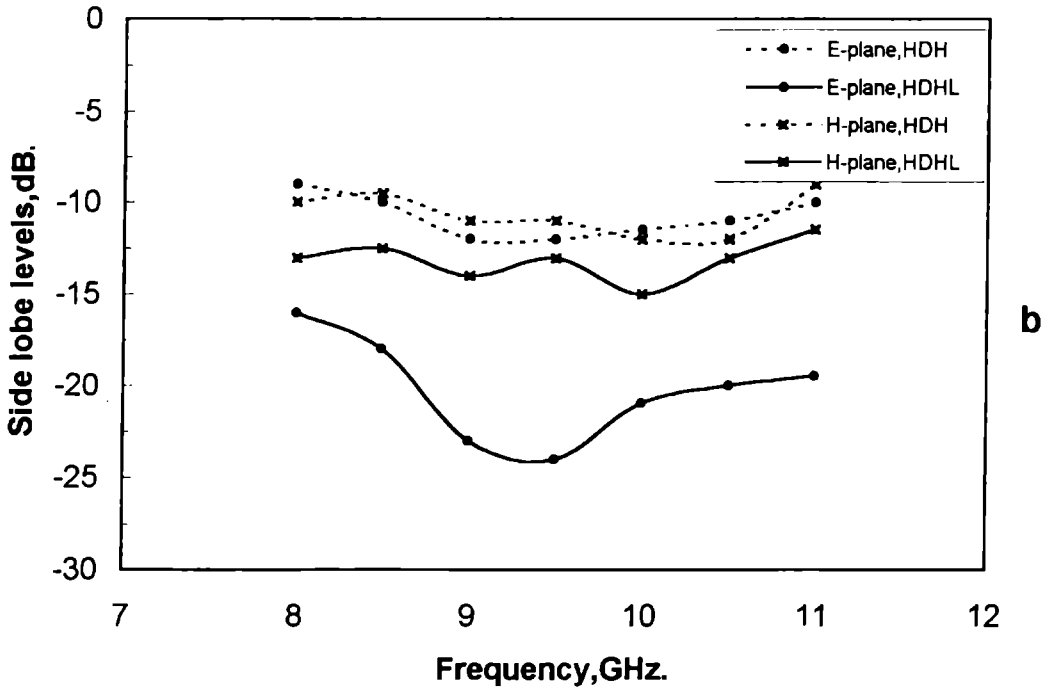

Fig.4.9 Side lobe level variation with frequency for E-plane sectoral HDH and HDHL. (a) $\alpha_E = 20°$, (b) $\alpha_E = 30°$.

Table 4.1 3dB beam width, 10dB beam width and first side lobe levels for different E-plane sectoral HDHL horn antennas at different frequencies.

Flare angle (Degree)	Frequency (GHz)	3dB beam width (Degree)		10dB beam width (Degree)		First side lobe level (dB)	
		H	E	H	E	H	E
10	8.0	31.5	33.0	51.0	55.5	-13.2	-14.0
	8.5	29.5	30.0	49.5	51.0	-13.75	-15.5
	9.0	27.0	28.5	45.0	48.0	-15.25	-18.0
	9.5	26.25	27.0	42.0	45.0	-14.5	-19.0
	10.0	24.0	25.0	39.0	42.0	-20.0	-20.0
	10.5	22.5	24.5	37.5	42.0	-15.0	-18.0
	11.0	22.5	24.0	38.0	39.0	-13.0	-16.0
20	8.0	24.0	28.5	39.0	54.0	-13.0	-16.0
	8.5	22.5	26.0	36.0	49.0	-13.5	-18.0
	9.0	21.0	25.5	34.5	45.0	-14.0	-19.5
	9.5	19.5	23.5	32.5	43.5	-14.0	-21.5
	10.0	19.5	21.5	32.0	40.0	-14.5	-21.0
	10.5	18.0	21.0	30.0	39.0	-14.0	-21.0
	11.0	21.0	19.5	36.0	36.0	-13.5	-20.0
30	8.0	27.5	28.0	45.0	67.5	-13.0	-16.0
	8.5	25.5	25.5	43.5	63.0	-13.5	-18.5
	9.0	24.0	24.5	40.5	55.0	-13.5	-22.5
	9.5	24.5	22.5	39.0	53.0	-13.0	-24.0
	10.0	20.0	22.5	34.5	49.0	-15.0	-21.0
	10.5	21.0	24.0	36.0	54.0	-13.0	-20.0
	11.0	21.0	20.0	37.5	53.0	-11.5	-19.5
40	8.0	27.0	34.0	42.0	72.0	-13.0	-17.0
	8.5	24.0	37.5	40.5	70.0	-12.5	-18.0
	9.0	24.5	36.0	40.5	66.0	-12.5	-19.0
	9.5	22.5	39.0	37.5	68.0	-11.0	-20.0
	10.0	21.0	37.5	36.0	61.0	-12.0	-20.0
	10.5	19.5	45.0	33.0	66.0	-11.5	-17.0
	11.0	19.5	45.0	67.5	68.0	-7.0	-15.5
50	8.0	22.5	63.0	40.0	88.5	-9.5	-15.0
	8.5	24.0	53.0	39.0	84.0	-10.5	-17.0
	9.0	22.5	50.0	37.5	80.0	-11.5	-17.0
	9.5	21.0	53.0	34.5	77.0	-11.5	-17.5
	10.0	22.5	48.0	37.5	70.0	-10.0	-17.0
	10.5	19.0	53.0	33.0	72.0	-9.5	-15.0
	11.0	19.5	56.0	37.5	75.0	-9.0	-13.5

4.2.1.2 Cross-polar levels

The cross-polar levels of different horns are measured at different frequencies. Its value is found to be very low around –40dB for all cases. Fig. 4.10. shows a typical plot of the co-polar and cross-polar patterns for E-plane sectoral HDHL of flare angle 20° at 10GHz.

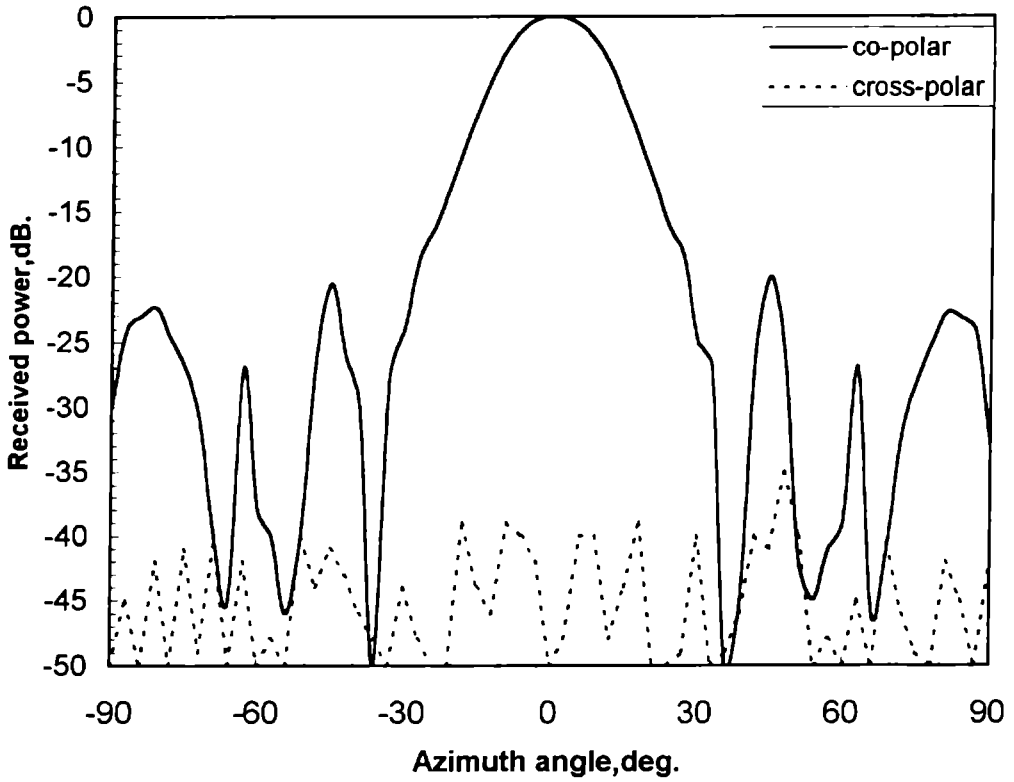

Fig. 4.10 Co-polar and cross-polar radiation patterns of E-plane sectoral HDHL at 10GHz, α_E=20°.

4.2.1.3 VSWR and Impedance

Fig. 4.11. shows the variation of VSWR and impedance with frequency for HDH and HDHL (α_E =20°).The VSWR of HDHL is less than that of HDH and open waveguide with launcher, for all frequencies. Table 4.2. shows the maximum and minimum values of VSWR for different E-plane HDHL in the X-band.

Table 4.2 Maximum and minimum values of VSWR for different E-plane sectoral HDHL antennas in the X-band.

Horn angle (Deg.)	Maximum value	Minimum value
10	1.32	1.05
20	1.55	1.10
30	1.66	1.04
40	1.40	1.03
50	1.75	1.13

4.2.1.4 Directive Gain

The axial gain of the E-plane sectoral HDHL antennas are high because of narrow patterns in both E and H-planes, low side lobe levels and low VSWR. Gain enhancements up to 3dB are observed over HDH for different cases. Fig. 4.12. shows the variation of axial gain with frequency for HDH and HDHL for flare angles 10° and 20°.Axial gains of other HDHL antennas for different frequencies are given in table 4.3.

Table 4.3 Axial gain of different E-plane sectoral HDHL antennas.

Frequency (GHz)	Axial Gain (dB)				
	α_E = 10°	α_E = 20°	α_E = 30°	α_E = 40°	α_E = 50°
8.0	15.25	15.25	15.65	14.85	13.25
8.5	16.20	16.0	16.8	16.0	15.2
9.0	16.23	16.13	17.5	15.93	12.33
9.5	17.55	17.93	18.55	16.35	15.35
10.0	18.53	19.13	19.13	16.75	16.33
10.5	18.68	19.48	19.7	16.65	16.08
11.0	19.0	17.8	19.4	15.60	15.8

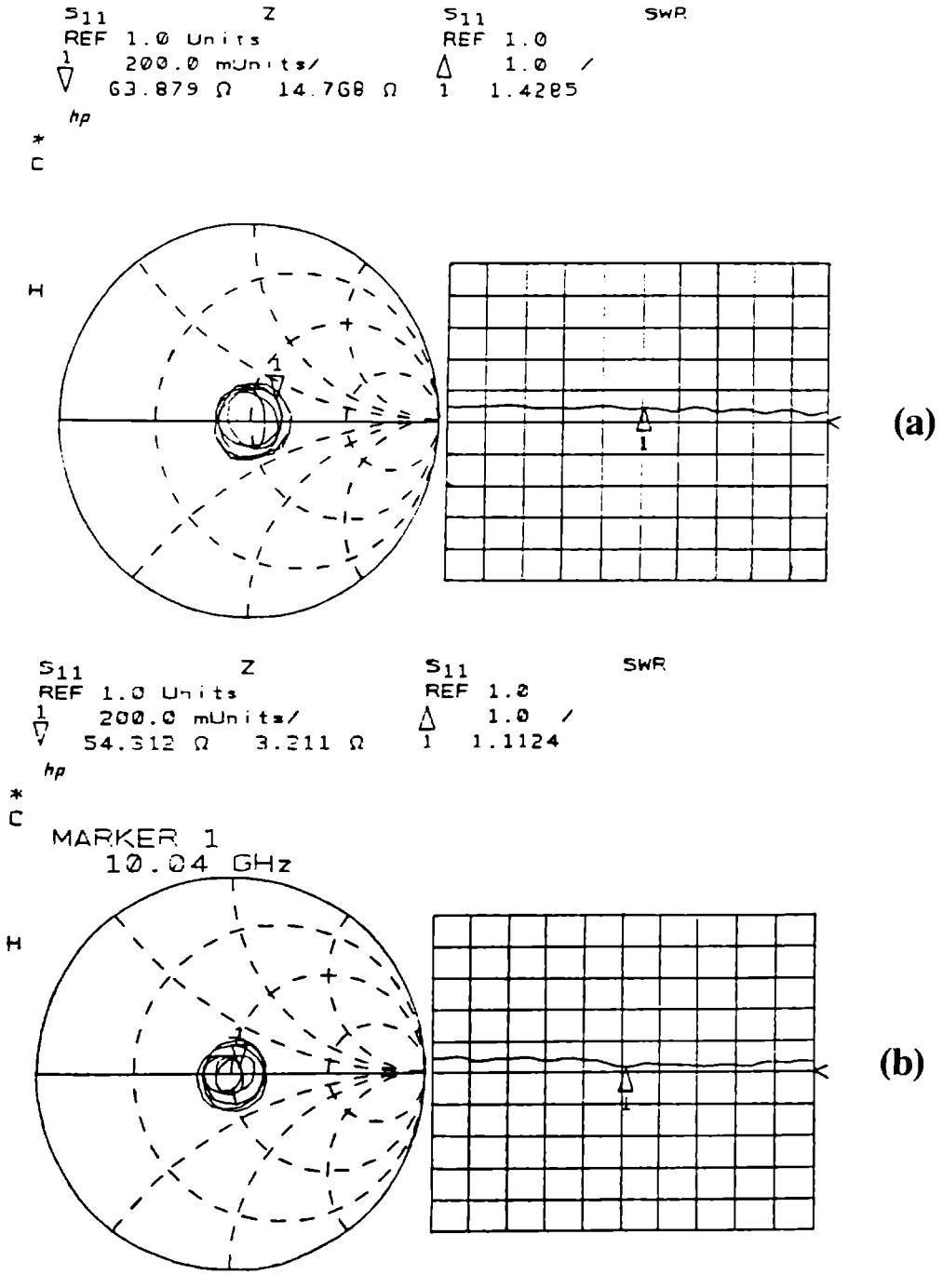

Fig.4.11 VSWR variation with frequency for E-plane sectoral horn. $\alpha_E = 20°$, (a) HDH, (b) HDHL.

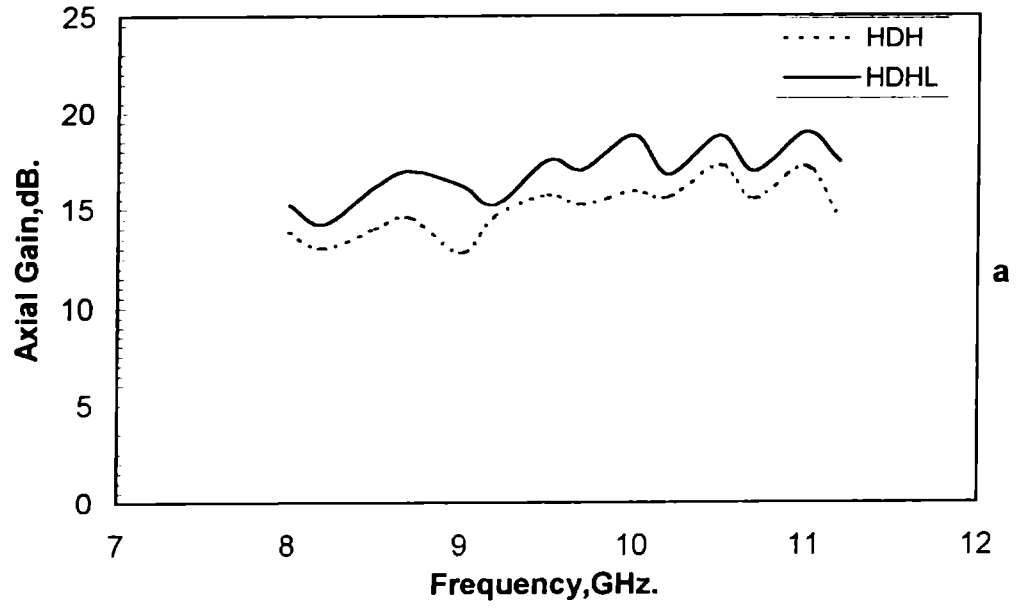

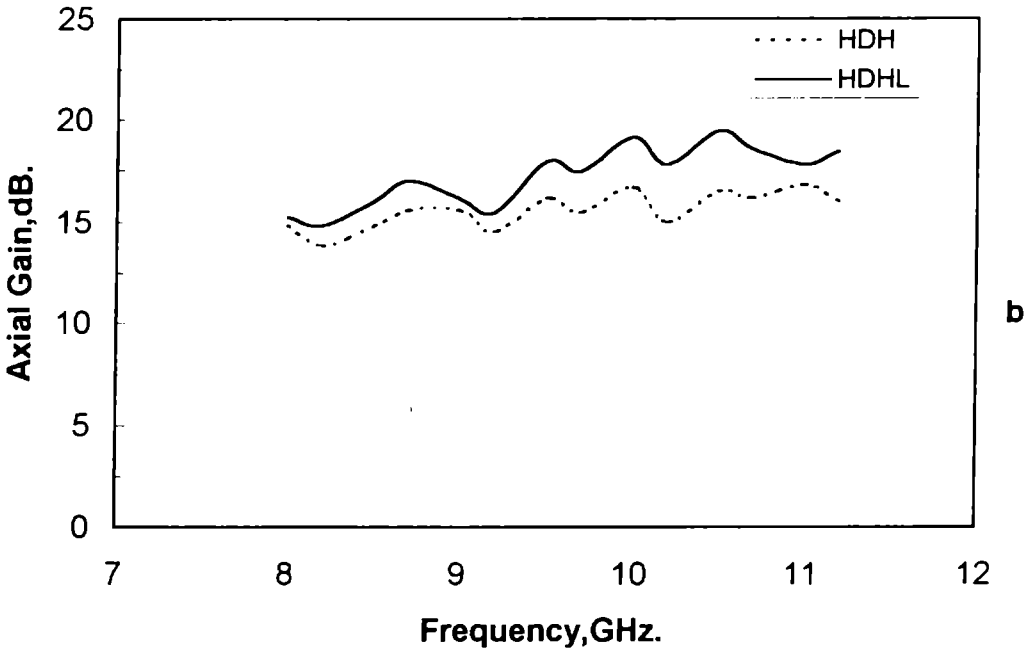

Fig.4.12 Variation of axial gain with frequency for E-plane sectoral HDH and HDHL. (a) $\alpha_E = 10°$, (b) $\alpha_E = 20°$.

4.2.2 H-plane sectoral HDHL

The schematic representation of H-plane sectoral HDHL is shown in Fig. 4.13. The behavior of this antenna is different from that of E-plane sectoral HDHL in many respects.

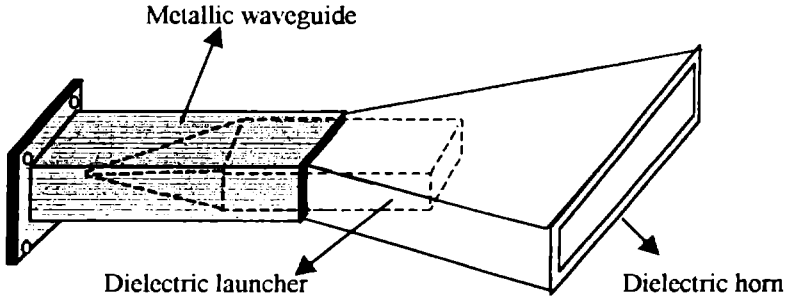

Fig. 4.13 Schematic representation of the H-plane HDH with Launcher (HDHL)

4.2.2.1 Radiation pattern

Unlike the E-plane sectoral HDHL the radiation pattern of the H-plane HDHL is narrow in one plane and broad in the other. The radiation pattern of a metallic H-plane sectoral horn antenna is narrow in the H-plane (flared plane) and broad in the E-plane. But for the new dielectric H-plane sectoral horn, the H-plane pattern is broad and the E-plane pattern is narrow. However, for small flared horns the H-plane patterns are also narrow. The H-plane patterns of ordinary HDH itself are broad. The introduction of the launcher reduces the broadness of the H-plane pattern. Fig. 4.14. shows the radiation patterns of H-plane sectoral HDH and HDHL for flare angle 60 degree at 9 GHz. Fig. 4.15. shows the E and H-plane patterns of H-plane sectoral HDHL of flare angle 10 degree at 9.5 GHz. As is evident from the radiation pattern, the side lobe levels of both E and H-plane patterns are reduced considerably by this launching technique.

The HPBW variation with frequency in the H-plane and E-plane for H-plane sectoral HDHL along with that of HDH are shown in Fig. 4.16. for flare angles 30 and 20 degrees.

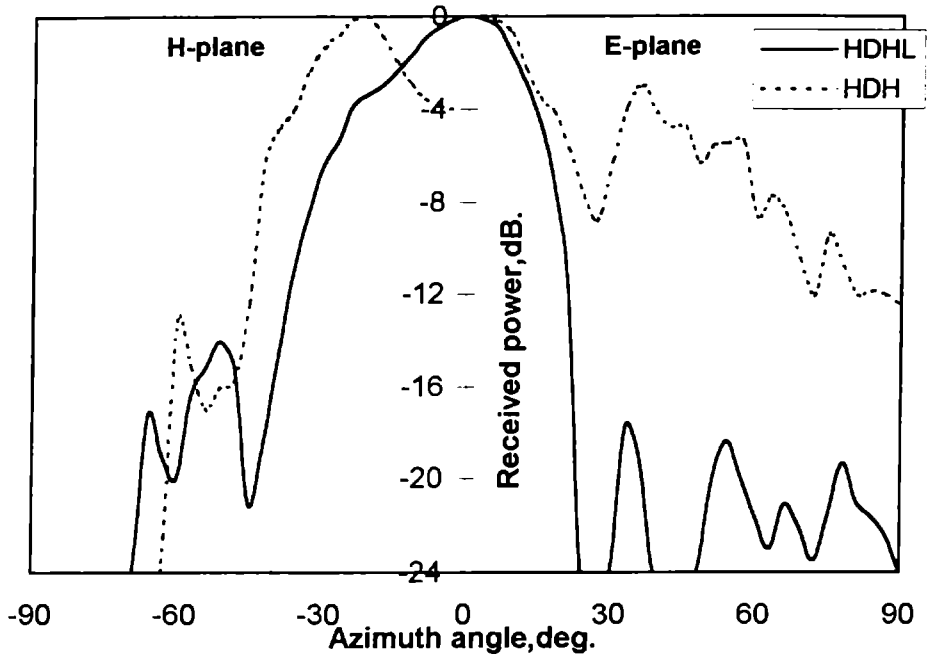

Fig.4.14 E and H-plane radiation patterns of H-plane sectoral HDH and HDHL at 9GHz. $\alpha_H = 60°$

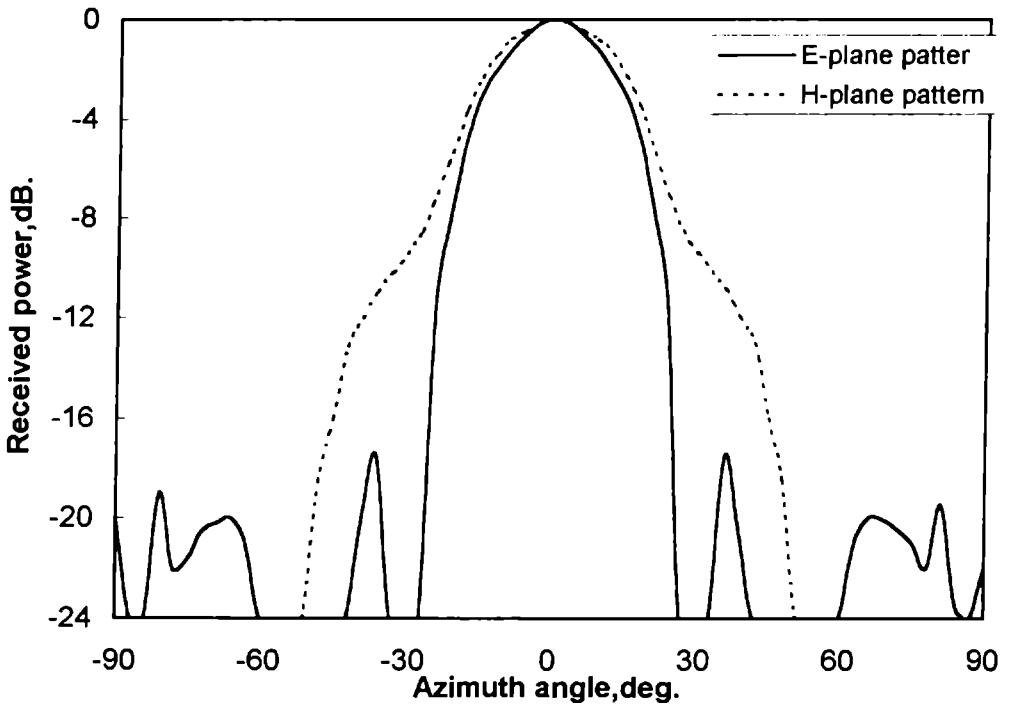

Fig.4.15 E and H-plane radiation patterns of H-plane sectoral HDHL at 9.5GHz. $\alpha_H = 10°$

The first side lobe level variation with frequency for E and H-plane patters of horns of flare angle 20 and 10 degree are given in Fig. 4.17. The corresponding side lobe levels for HDH are also given for comparison. The graph shows that the side lobe levels in the H-plane are very low for almost all cases.

Table 4.4. shows the 3dB beam width, 10dB beam width and first side lobe levels for different H-plane sectoral HDHL antennas at different frequencies.

Table 4.4 3dB beam width, 10dB beam width and first side lobe levels for different H-plane sectoral HDHL horn antennas at different frequencies.

Flare angle (Degree)	Frequency (GHz)	3dB beam width (Degree)		10dB beam width (Degree)		First side lobe level (dB)	
		H	E	H	E	H	E
10	8.0	42.0	33.0	88.5	54.0	-24.0	-16.0
	8.5	37.5	31.0	75.0	51.0	-28.0	-16.0
	9.0	34.5	30.0	70.5	46.0	-27.0	-18.5
	9.5	33.0	28.5	66.0	45.0	-26.0	-17.5
	10.0	31.0	25.5	60.0	42.0	-22.0	-16.0
	10.5	30.0	24.0	75.0	40.0	-18.5	-16.0
20	8.0	28.0	28.5	70.0	49.0	-30.0	-15.0
	8.5	30.0	27.0	69.0	45.0	-30.0	-15.0
	9.0	25.0	28.5	66.0	45.0	-31.0	-18.0
	9.5	24.0	25.0	65.0	40.5	-30.0	-17.0
	10.0	25.0	24.0	65.0	37.5	-32.0	-24.0
	10.5	27.0	25.5	60.0	37.5	-22.0	-20.0
30	8.0	54.0	26.0	87.0	42.0	-32.0	-13.0
	8.5	51.0	22.5	78.0	42.0	-35.0	-11.5
	9.0	51.0	22.5	75.0	37.5	-32.0	-14.5
	9.5	50.0	21.0	76.0	36.0	-32.0	-12.5
	10.0	48.0	21.0	69.0	33.0	-32.0	-14.5
	10.5	48.0	19.0	66.0	31.0	-26.0	-11.0
45	8.0	78.0	27.0	108.0	50.0	-24.0	-15.5
	8.5	63.0	25.0	102.0	53.0	-31.0	-17.0
	9.0	61.0	27.0	96.0	43.5	-28.0	-26.0
	9.5	27.0	24.0	87.0	45.0	-21.0	-21.0
	10.0	56.0	24.0	84.0	41.0	-20.0	-24.0
	10.5	56.0	25.0	82.0	39.0	-14.0	-20.0
60	8.0	75.0	26.0	112.0	45.0	-24.0	-14.0
	8.5	61.0	25.5	102.0	43.0	-26.0	-15.0
	9.0	50.0	24.0	99.0	39.0	-14.5	-17.0
	9.5	44.0	21.0	84.0	36.0	-18.5	-20.0
	10.0	62.0	20.0	80.0	31.5	-18.0	-20.0
	10.5	61.0	19.5	84.0	33.0	-15.5	-17.0

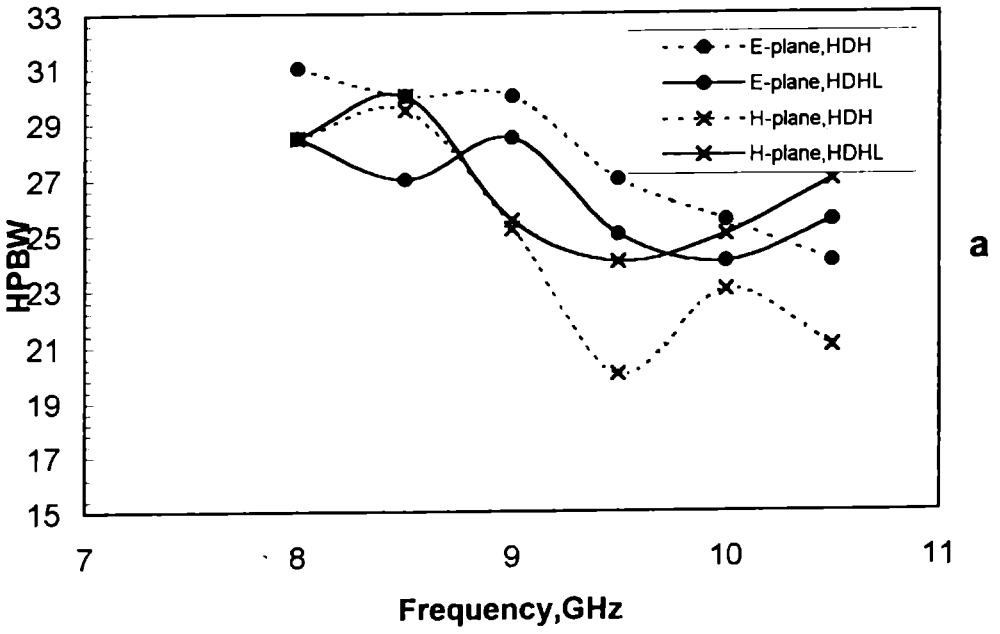

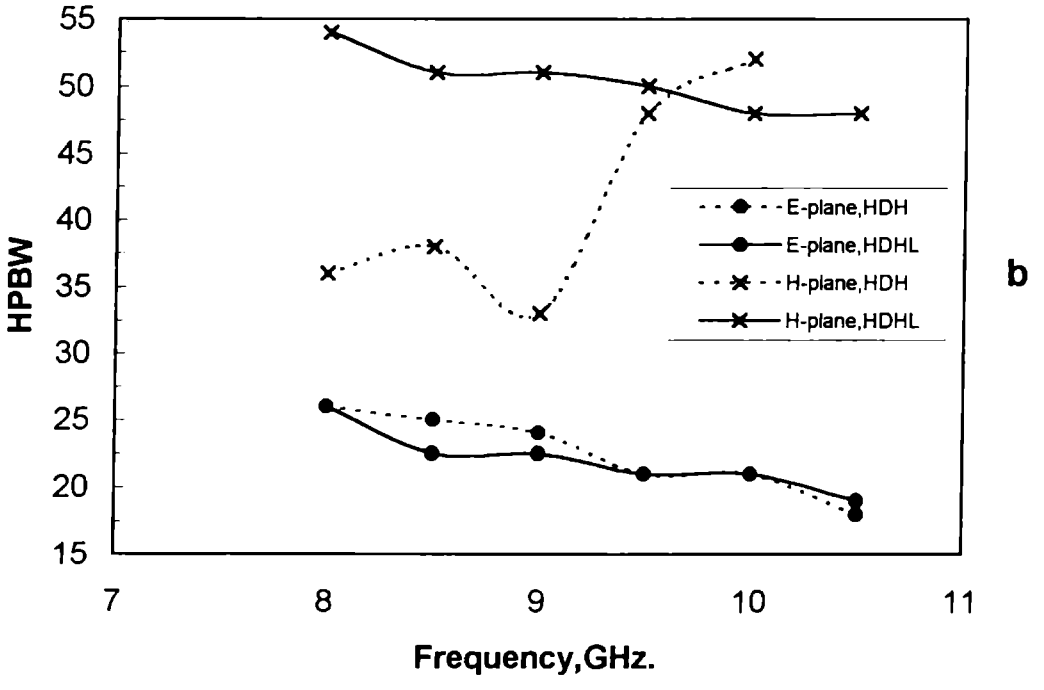

Fig. 4.16 E and H-plane HPBW variation with frequency for H -plane sectoral HDH and HDHL . (a) $\alpha_H = 20°$,(b) $\alpha_H = 30°$.

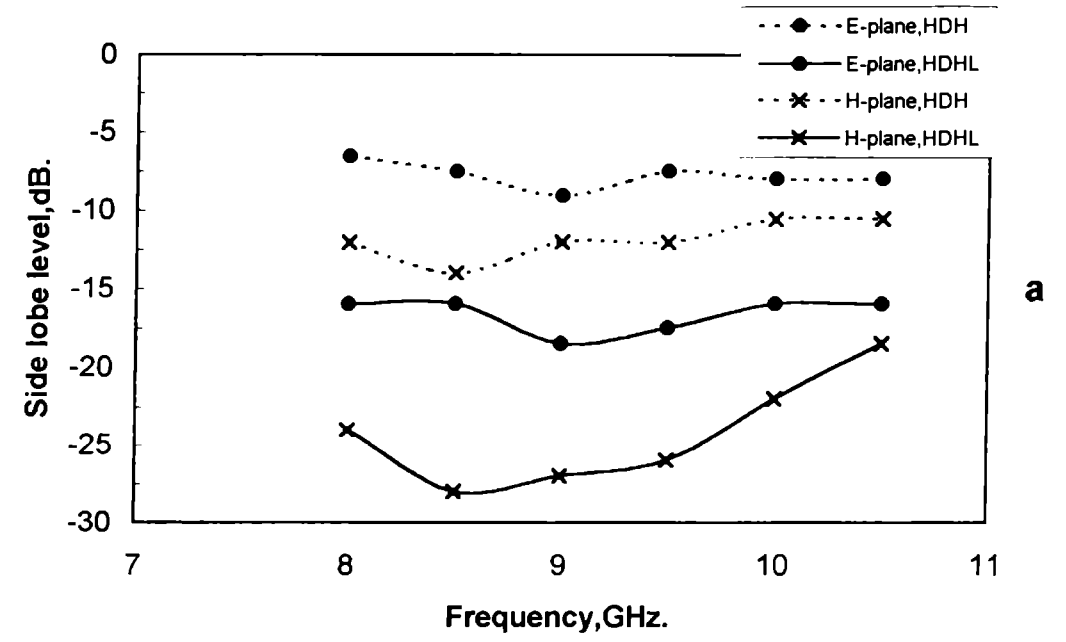

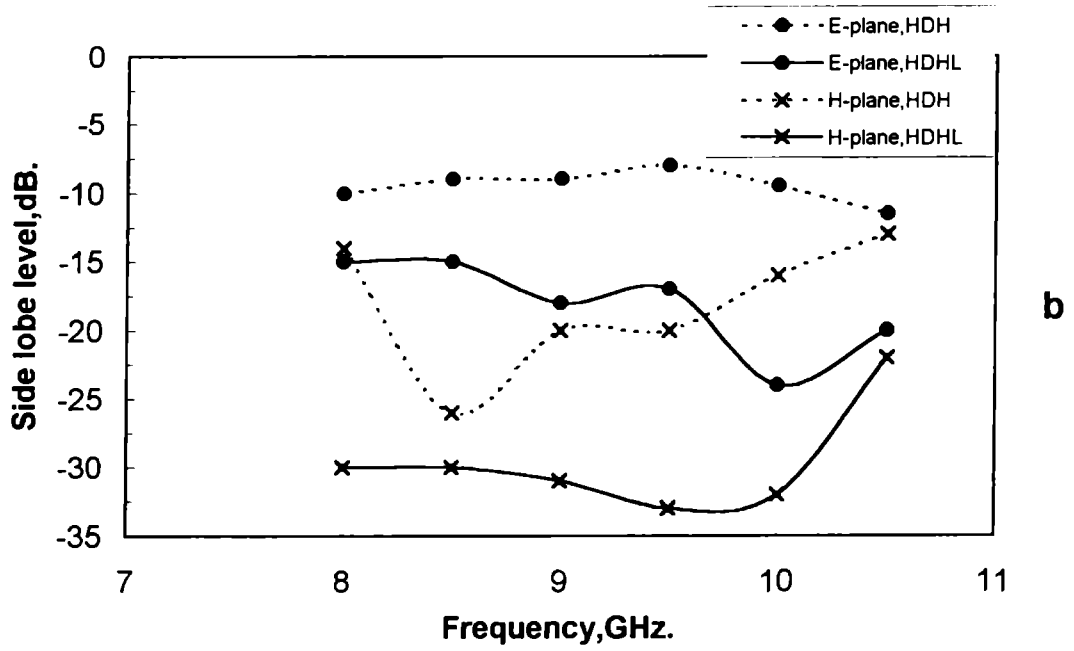

Fig.4.17 Side lobe level variation with frequency for H-plane sectoral HDH and HDHL . (a) $\alpha_H = 10°$, (b) $\alpha_H = 20°$.

4.2.2.2 Cross-polar levels

Cross-polar levels for H-plane sectoral HDHL antennas are also very low, around –40dB, irrespective of the flare angle and frequency. Fig. 4.18. shows a typical plot of co-polar and cross-polar patterns for horn of flare angle 20° at 10GHz.

4.2.2.3 VSWR and Impedance

The variation of impedance and VSWR with frequency for H-plane sectoral HDH and HDHL (α_H = 20°) antenna are shown in Fig. 4.19. For this type of antennas also the VSWR reduces to very low values with the new launching technique. Table 4.5. shows the maximum and minimum values of VSWR for different H-plane horns.

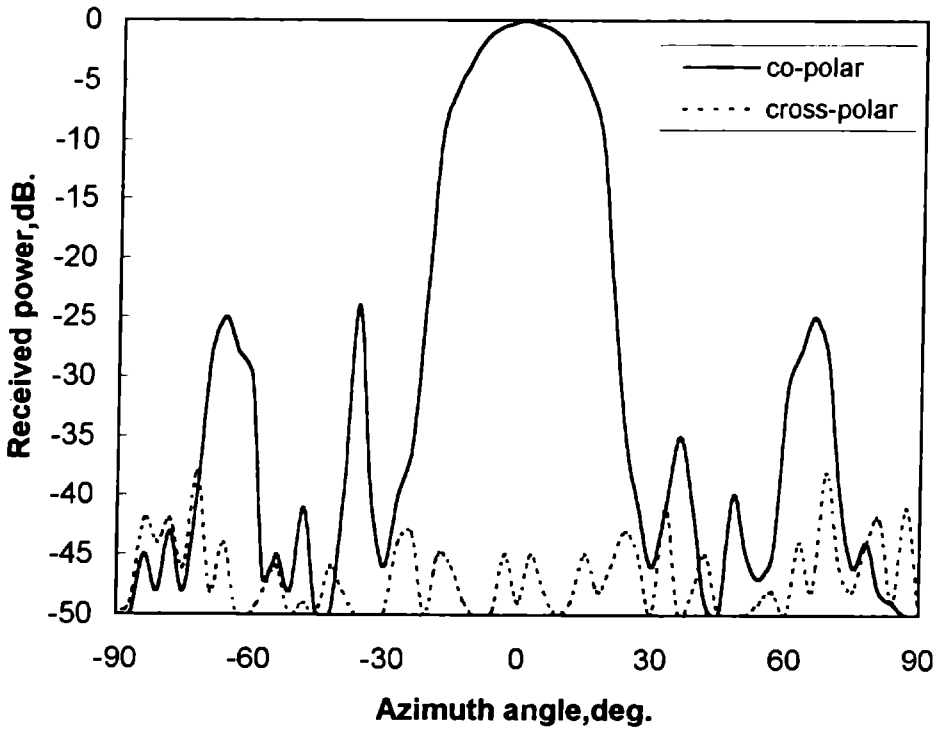

Fig. 4.18 Co-polar and cross-polar radiation patterns of H-plane sectoral HDHL at 10GHz, α_H=20°.

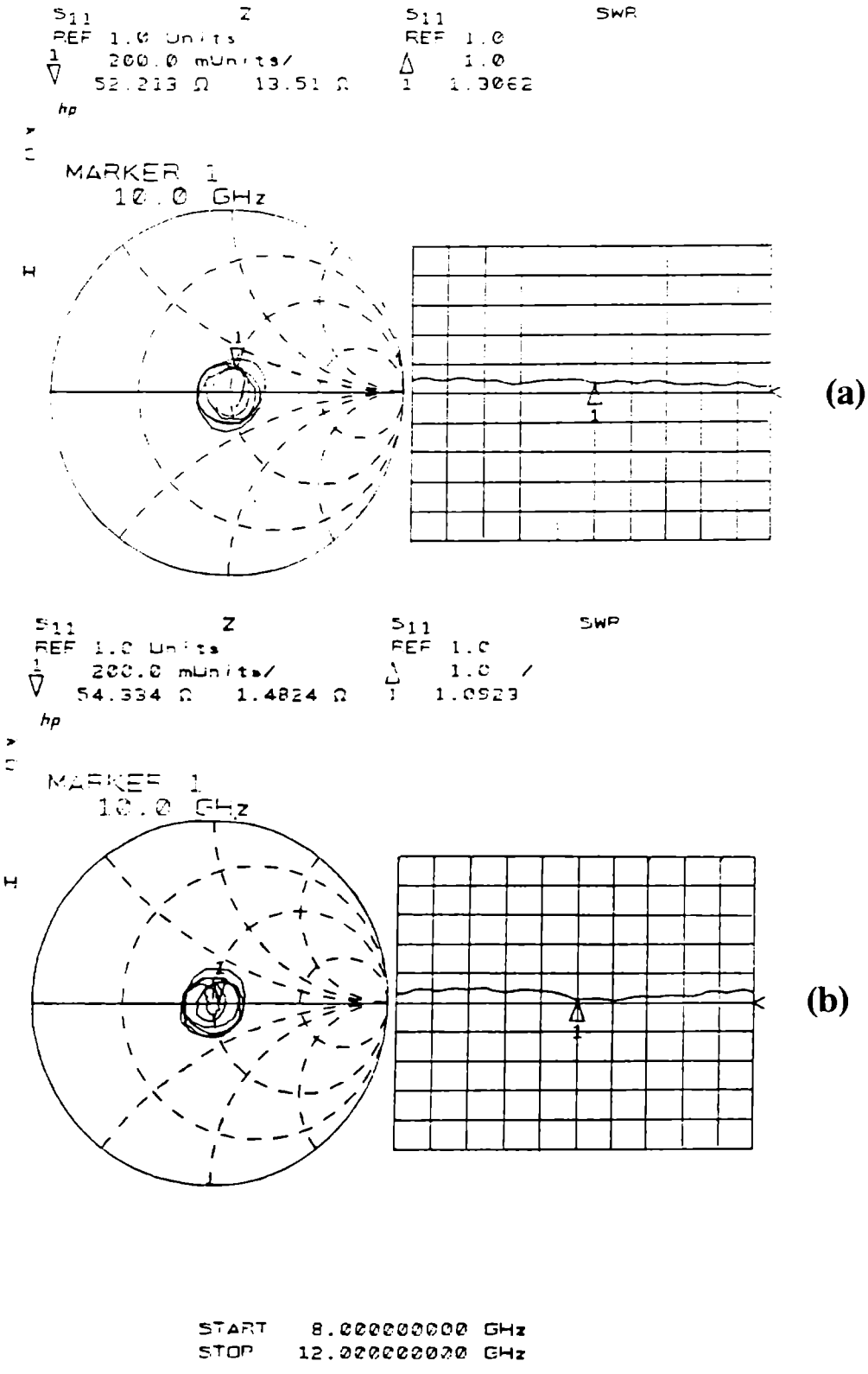

Fig.4.19 VSWR variation with frequency for H-plane sectoral horn. $\alpha_H = 20°$, (a) HDH, (b) HDHL.

Table 4.5 Maximum and minimum values of VSWR for different H-plane sectoral HDHL antennas in the X-band.

Horn angle (Deg.)	Maximum value	Minimum value
10	1.42	1.05
20	1.53	1.08
30	1.55	1.05
40	1.56	1.02
50	1.76	1.07

4.2.2.4 Directive Gain

Axial gain enhancement up to 4dB can be achieved using this launching method in H-plane sectoral HDHL antennas. But the axial gain of H-plane HDHL is less than that of E-plane HDHL because of its broad H-plane patterns. Fig. 4.20. shows the variation of axial gain with frequency for H-plane sectoral HDH and HDHL of flare angle 10 and 20 degrees. Axial gain of other experimental H-plane sectoral HDHL antennas for different frequencies are given in Table.4.6.

Table 4.6 Axial gain of different H-plane sectoral HDHL antennas.

Frequency (GHz)	Axial Gain (dB)				
	$\alpha_H = 10°$	$\alpha_H = 20°$	$\alpha_H = 30°$	$\alpha_H = 45°$	$\alpha_H = 60°$
8.0	12.85	12.45	12.05	10.05	11.65
8.5	14.4	14.00	13.20	11.40	13.20
9.0	11.93	11.93	6.65	7.93	11.13
9.5	14.95	14.95	12.95	11.75	14.15
10.0	16.33	15.13	13.53	13.53	15.13
10.5	17.28	16.06	14.48	14.08	15.68
11.0	17.60	17.00	14.20	15.40	17.00

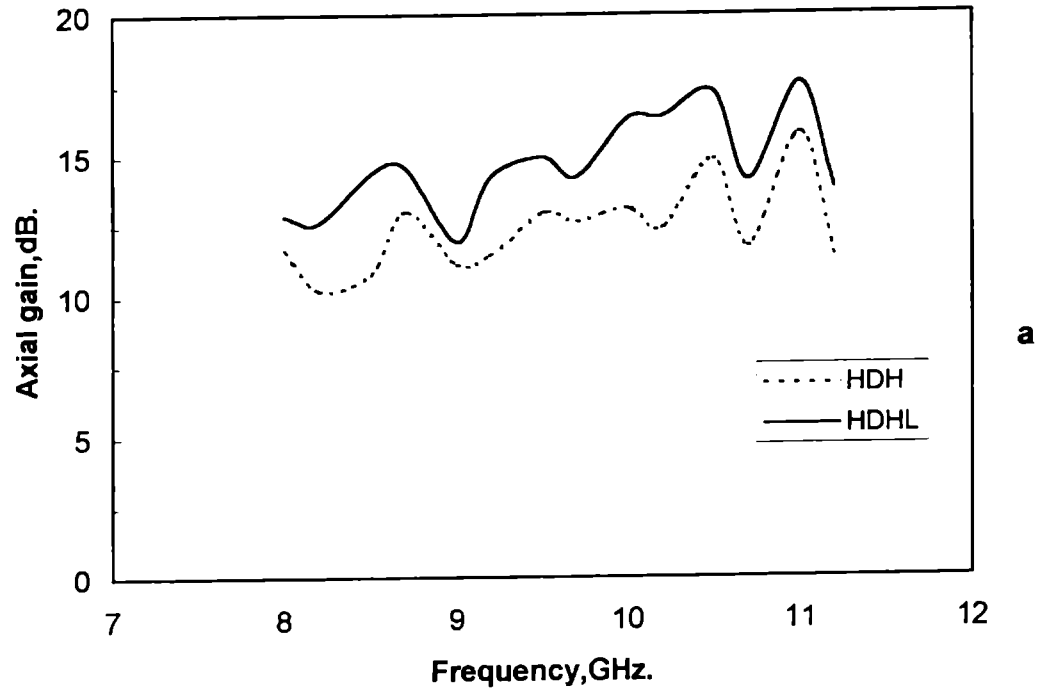

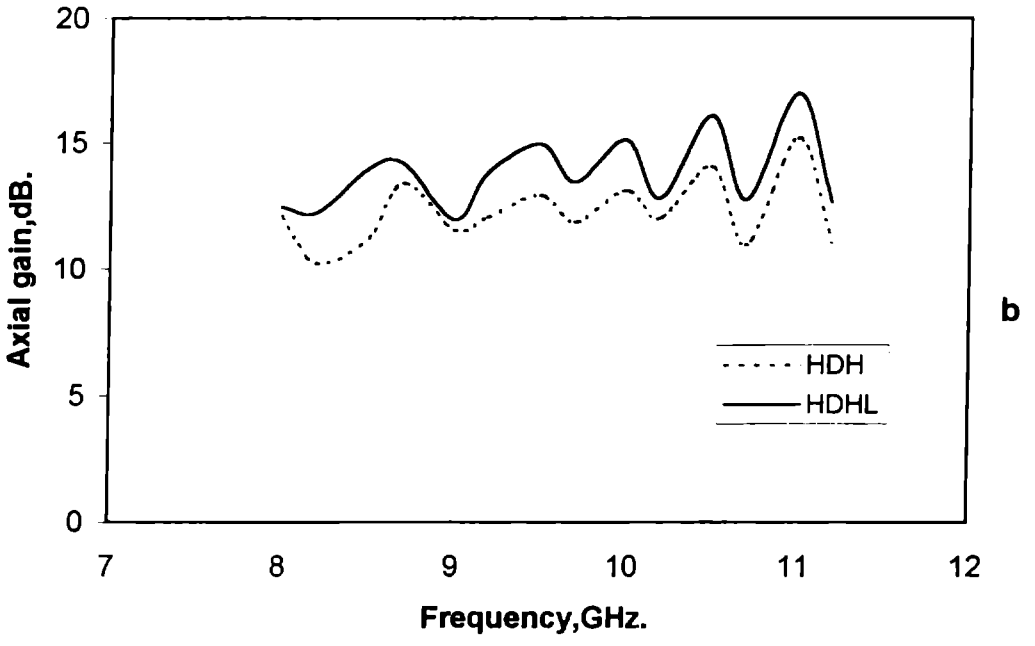

Fig.4.20 Variation of axial gain with frequency for H-plane sectoral HDH and HDHL. (a) $\alpha_H = 10°$, (b) $\alpha_H = 20°$.

4.2.3 Pyramidal HDHL

Fig. 4.21. shows a schematic diagram of the pyramidal HDHL.

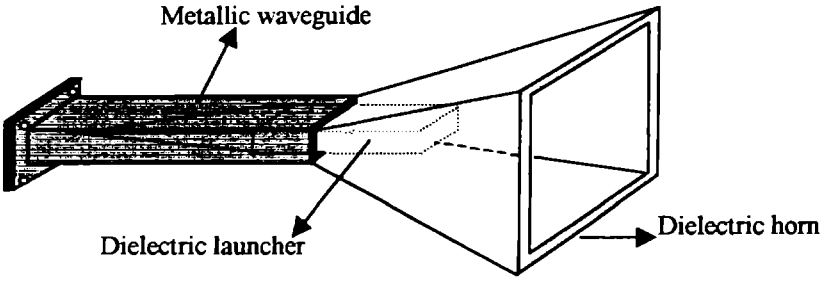

Fig. 4.21 Schematic representation of the Pyramidal HDH with Launcher (HDHL)

4.2.3.1 Radiation pattern

The radiation patterns of small flared pyramidal HDHL antennas in the E-plane are almost identical to that of E-plane sectoral HDHL and in the H-plane is somewhat similar to that of H-plane sectoral horns. For horns with small flaring in the H-plane, the H-plane patterns are narrow. As the flare angle in the H-plane increases, the H-plane pattern changes to a split or rippled broad pattern. The E-plane patterns of horns with small flaring in the H-plane are very good with low side lobe levels. Fig. 4.22. shows the E and H-plane patterns for a pyramidal HDHL at 9GHz. The corresponding patterns for pyramidal HDH are also given for comparison. Fig. 4.23. shows a typical plot of E and H-plane patters for a pyramidal HDHL of flare angle (α_H=20°, α_E=20°) at 9.5GHz.

The variation of half power beam width with frequency in the E and H-planes for HDH and HDHL for horns of flare angle (α_H=10°, α_E=20°)and (α_H=20°, α_E=20°) are shown in fig. 4.24. For horns with small α_H values, these results are similar to that of E-plane sectoral HDHL.

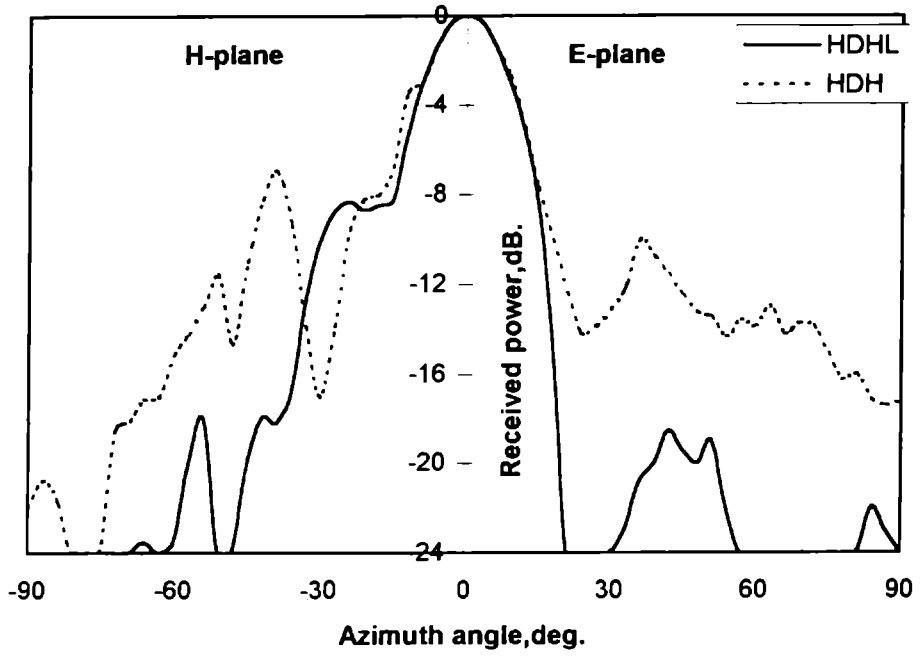

Fig. 4.22 E and H-plane radiation patterns of pyramidal HDH and HDHL at 9GHz. $\alpha_E = 20°$, $\alpha_H = 10°$.

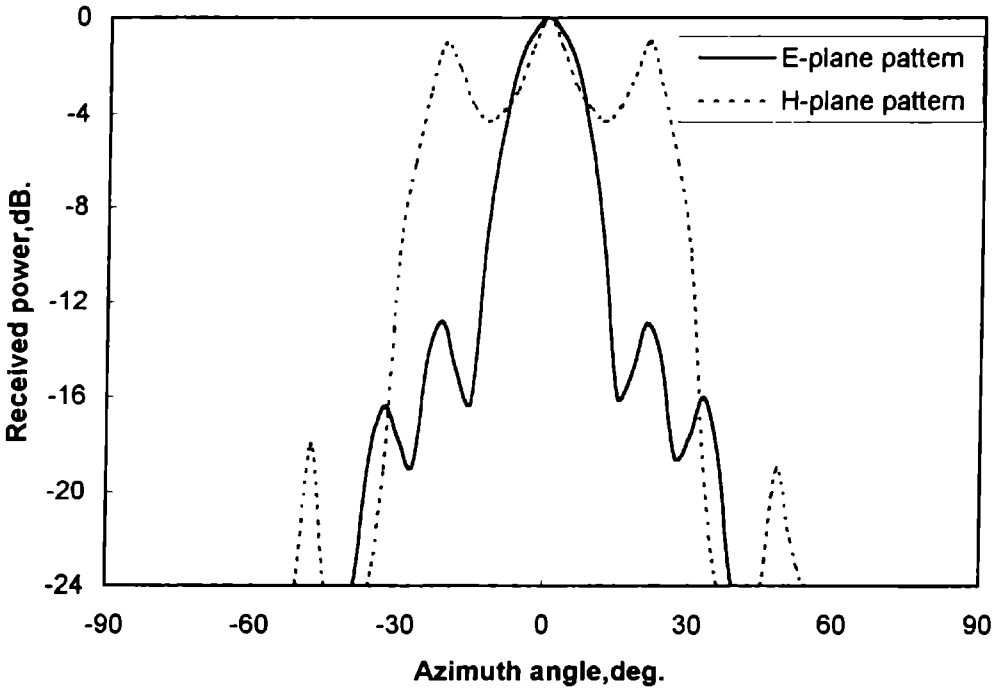

Fig. 4.23 E and H-plane radiation patterns of pyramidal HDHL at 9.5GHz. $\alpha_E = 20°$, $\alpha_H = 20°$.

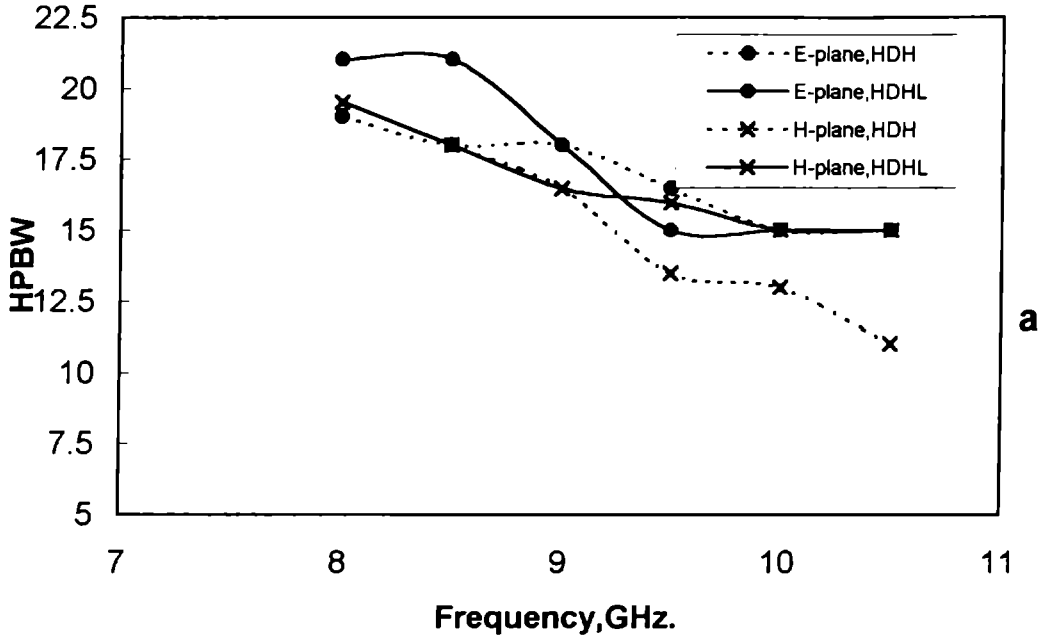

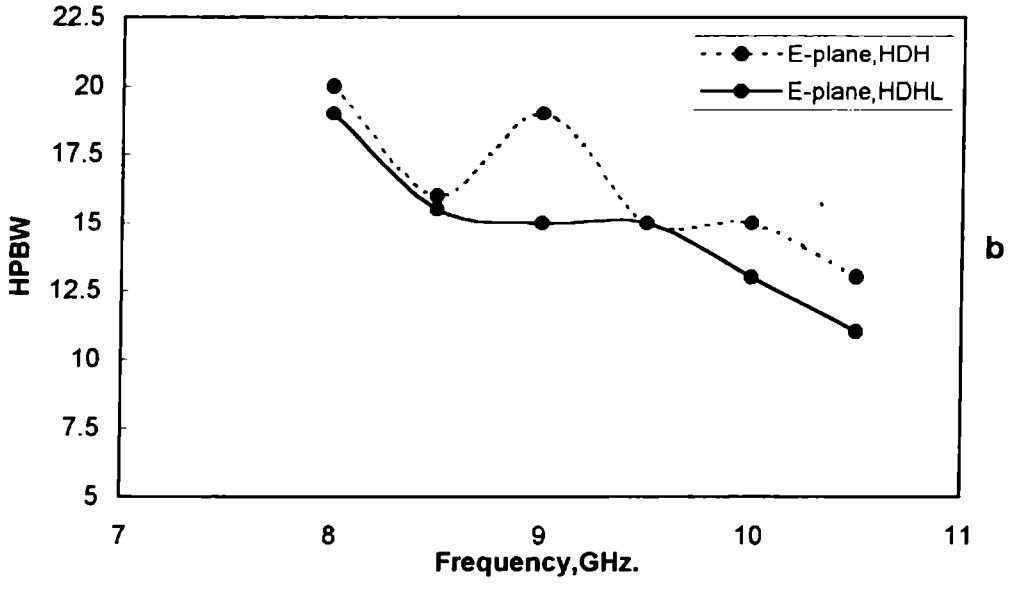

Fig.4. 24 E and H-plane HPBW variation with frequency for pyramidal HDH and HDHL.(a) $\alpha_E = 20°, \alpha_H = 10°$,(b) $\alpha_E = 20°$, $\alpha_H = 20°$.

The side lobe levels are very low for E-plane patterns and high for H-plane patterns. For a given value of α_E, as α_H increases, the side lobe level increase and finally becomes ripples on the top of the main beam. Fig. 4.25. shows side lobe level variation with frequency for two horns along with those for their HDH counterparts.

Table. 4.7. gives the 3dB beam width, 10dB beam width and side lobe levels for different pyramidal HDHL at different frequencies.

Table 4.7 3dB beam width, 10dB beam width and first side lobe levels for different pyramidal HDHL horn antennas at different frequencies.

Flare angle (Degree) α_E α_H	Frequency (GHz)	3dB beam width (Degree)		10dB beam width (Degree)		First side lobe level (dB)	
		H	E	H	E	H	E
20 10	8.0	19.5	21.0	48.0	37.5	-16.0	-16.0
	8.5	18.0	21.0	53.0	34.5	-24.0	-20.0
	9.0	16.5	18.0	61.0	33.0	-17.0	-18.5
	9.5	16.0	15.0	30.0	30.0	-16.0	-21.0
	10.0	15.0	15.0	25.0	28.0	-18.0	-25.0-
	10.5	15.0	15.0	24.0	27.0	-16.0	30.0
20 20	8.0	18.0	19.0	68.0	38.0	-18.5	-13.5
	8.5	*	15.5	--	33.0	--	-16.5
	9.0	*	15.0	--	28.0	--	-16.5
	9.5	*	15.0	--	27.0	--	-13.0
	10.0	*	13.0	--	24.0	--	-18.0
	10.5	*	11.0	--	18.0	--	-17.0
20 30	8.0	**	--	--	--	--	--
	8.5	**	--	--	--	--	--
	9.0	**	--	--	--	--	--
	9.5	**	--	--	--	--	--
	10.0	**	--	--	--	--	--
	10.5	**	--	--	--	--	--
			--	--	--	--	--
10 20	8.0	20.0	21.0	--	37.5	--	-13.0
	8.5	*	19.2	--	31.5	--	-13.0
	9.0	*	16.5	--	27.0	--	-13.0
	9.5	*	15.0	--	24.0	--	-12.0
	10.0	*	13.5	--	24.0	--	-10.5
	10.5	*	12.5	--	22.5	--	-8.0
30 20	8.0	*	20.0	--	45.0	--	-17.0
	8.5	*	14.0	--	37.0	--	-17.0
	9.0	*	12.0	--	29.0	--	-22.5
	9.5	*	12.0	--	22.0	--	-18.0
	10.0	*	11.0	--	28.0	--	-20.0
	10.5	*	12.0	--	21.0	--	-19.5

* ripple pattern ** split pattern

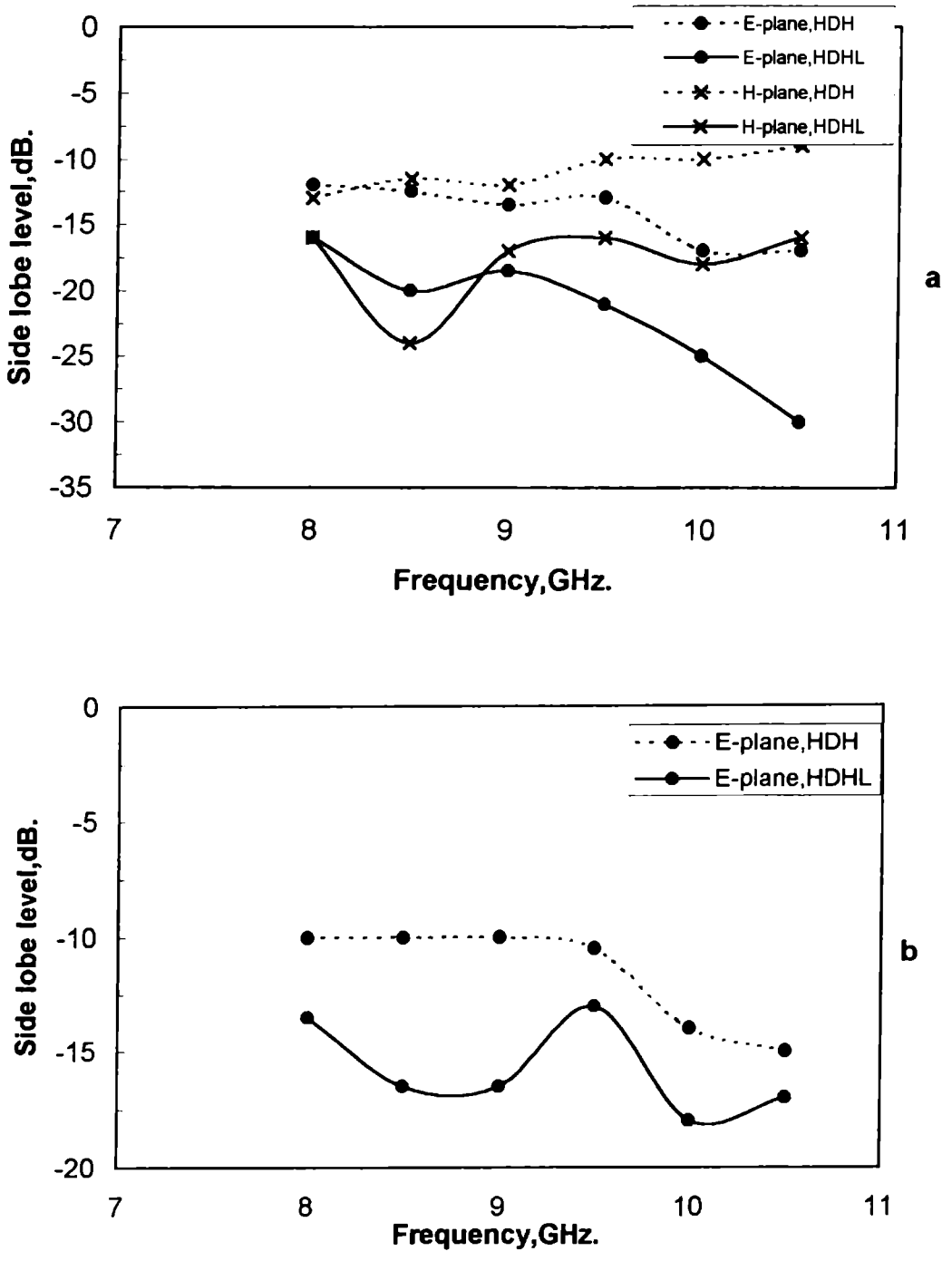

Fig.4. 25 Side lobe level variation with frequency for pyramidal HDH and HDHL .(a) $\alpha_E = 20°, \alpha_H = 10°$,(b) $\alpha_E = 20°$, $\alpha_H = 20°$.

4.2.3.2 Cross-polar levels

For pyramidal HDHL antennas the cross-polar levels are slightly greater, compared to that of sectoral HDHL. It is found to be around –30dB for all cases. One typical cross-polar and co-polar patterns for pyramidal HDHL (α_H=10°, α_E=20°) is shown in Fig.4.26.

4.2.3.3 VSWR and Impedance

A typical plot of impedance and VSWR with frequency for a pyramidal HDH and HDHL antennas (α_H=10°, α_E=20°) are shown in Fig. 4.27. In this case also, as for the sectoral horns , the VSWR is less for HDHL for the entire experimental band. Table. 4.8. shows the maximum and minimum values of VSWR for different horns in the X-band.

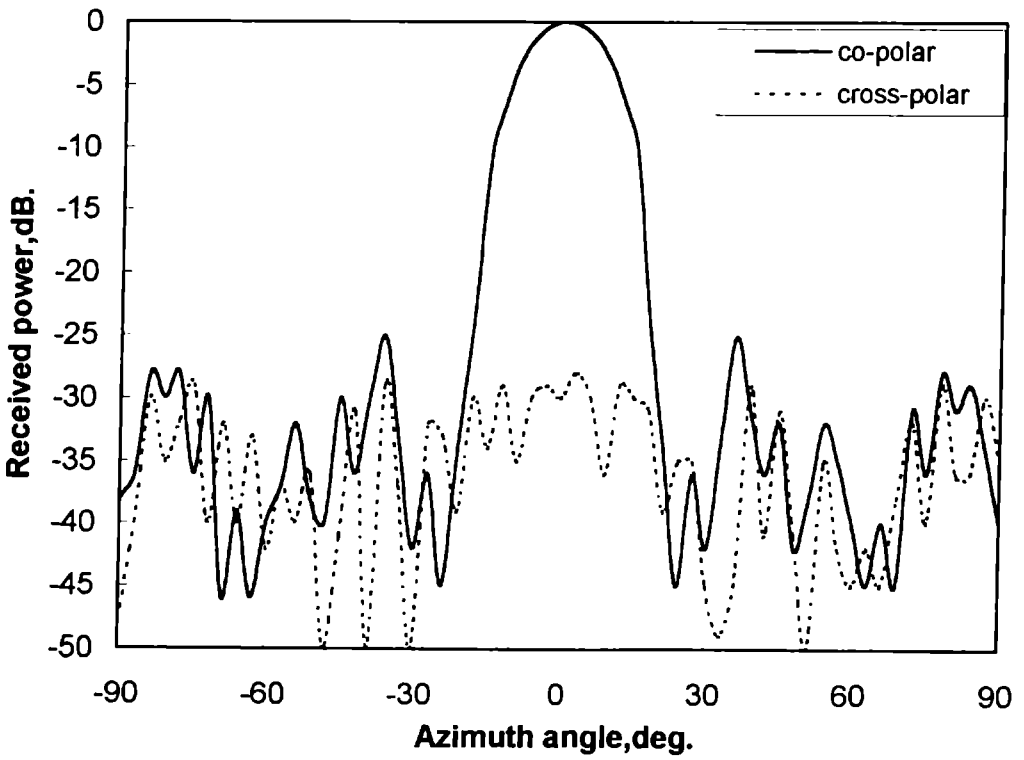

Fig.4.26 Co-polar and cross-polar radiation patterns of pyramidal HDHL at 10GHz, α_E = 20°, α_H = 10°.

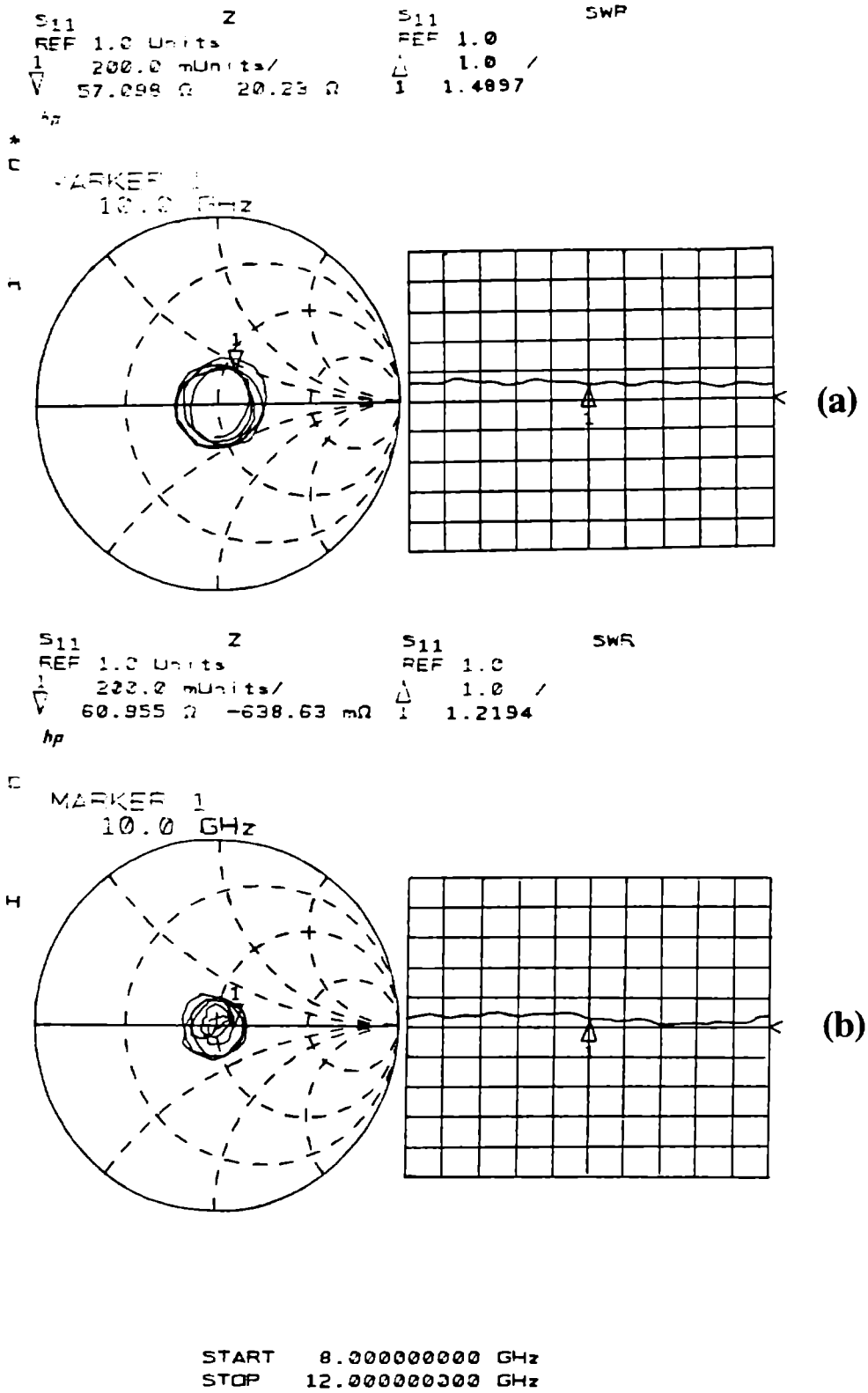

Fig. 4.27 VSWR variation with frequency for pyramidal horn. $\alpha_E = 20°$, $\alpha_H = 10°$. (a) HDH, (b) HDHL.

Table 4.8 Maximum and minimum values of VSWR for different pyramidal HDHL antennas in the X-band.

Horn angle (Deg.)		Maximum value	Minimum value
α_E	α_H		
10	20	1.40	1.10
20	20	1.50	1.12
30	20	1.60	1.15
20	10	1.46	1.08
20	30	1.55	1.09

4.2.3.4 Directive Gain

The axial gain of pyramidal HDHL antennas are greater than that of HDHL. As α_H increases, irrespective of the value of α_E, the gain decreases. Fig. 4.28. gives the variation of axial gain with frequency for two pyramidal HDH and HDHL antennas. Axial gains of some other pyramidal horns at different frequencies are available from Table. 4.9.

Table 4.9 Axial gain of different H-plane sectoral HDHL antennas.

Frequency (GHz)	Axial Gain (dB)				
	α_E α_H	α_E α_H	α_E α_H	α_E α_H	α_E α_H
	10 20	20 20	30 20	20 10	20 30
8.0	13.05	12.85	12.25	14.85	9.05
8.5	14.40	14.00	14.00	16.6	9.20
9.0	11.53	12.00	11.53	14.93	**
9.5	14.35	14.55	13.35	17.55	6.10
10.0	14.33	14.73	13.93	18.73	5.50
10.5	15.28	15.68	15.68	19.68	5.60
11.0	15.30	15.80	15.00	20.40	**

** split pattern

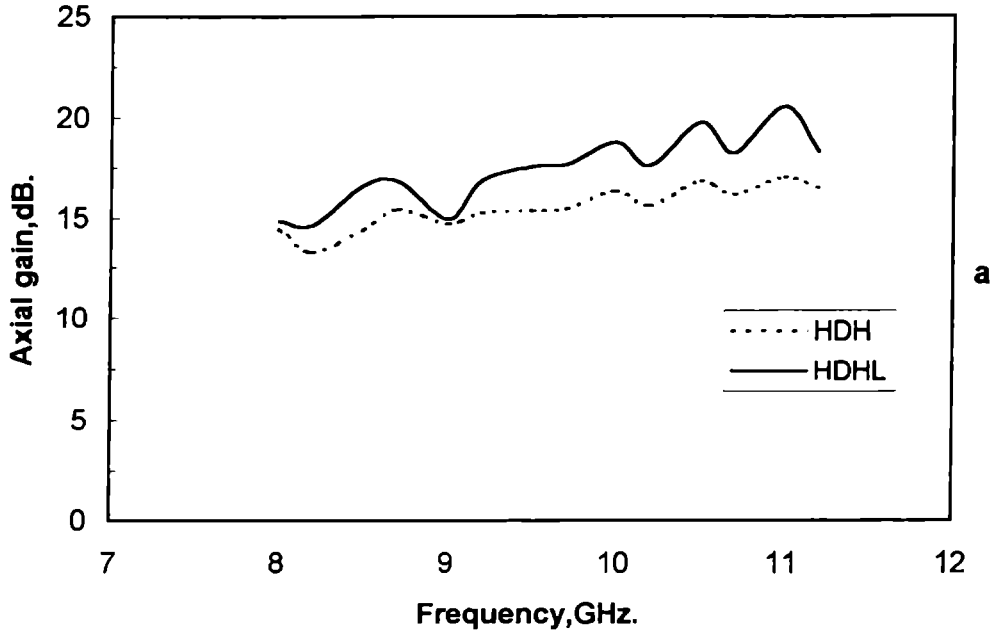

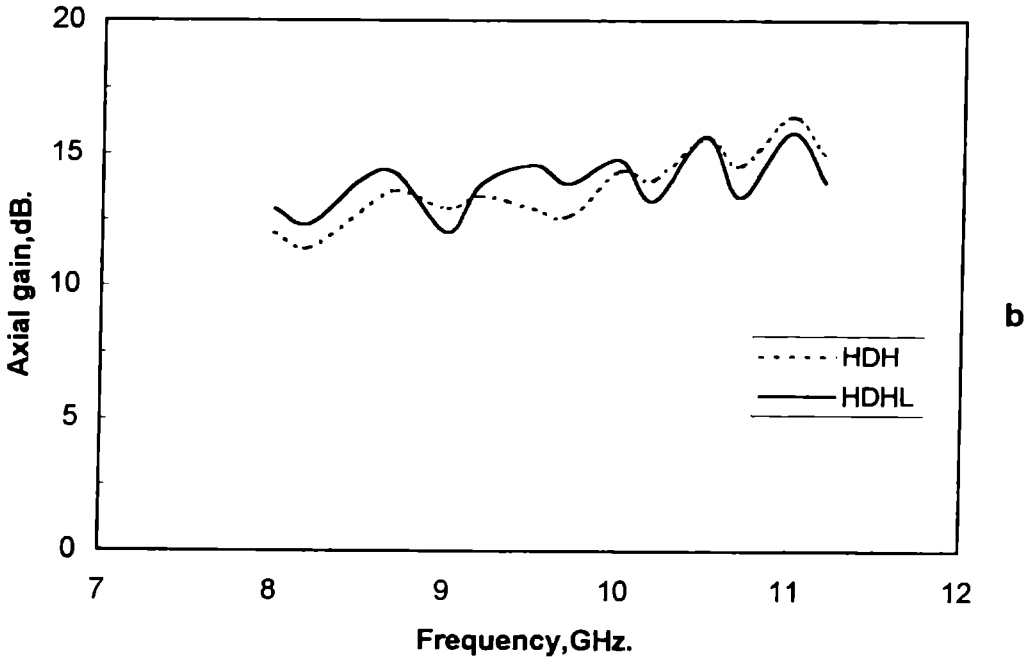

Fig.4.28 Variation of axial gain with frequency for pyramidal HDH and HDHL.(a) $\alpha_E = 20°, \alpha_H = 10°$,(b) $\alpha_E = 20°$, $\alpha_H = 20°$.

4.3 EFFECT OF STRIP LOADING

The launching technique converts the HDH to a new antenna (HDHL),with many attractive features. The second technique, namely the strip loading technique, modifies the performance of the antenna further. The new strip loaded antennas (SHDHL) were elaborately discussed in sections 3.2.4 and 3.2.5. of chapter 3. In this section the results of the strip loading on E and H-plane sectoral horns and pyramidal horns are discussed separately.

4.3.1 E-plane sectoral SHDHL

The schematic diagram of the strip loaded E-plane sectoral hollow dielectric horn antenna (SHDHL) is shown in Fig. 4.29. Strips of width a_0 are loaded on the E-walls of the horn. Strip length 'l' can be varied. As 'l' changes the characteristics of the antenna will change.

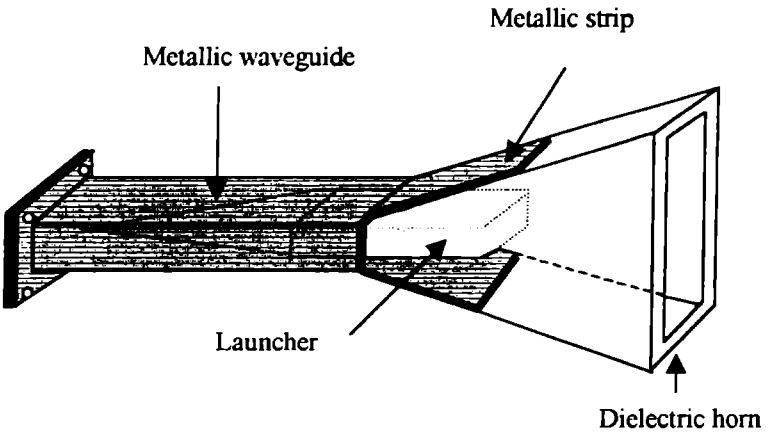

Fig.4.29 Schematic representation of the strip loaded E-plane HDH with Launcher (SHDHL)

4.3.1.1 Radiation pattern

The radiation pattern of E-plane HDHL is further modified by strip loading The strip loading provides an easy method for adjusting the HPBW of the SHDHL in the E-plane, while the HPBW in the H-plane remains almost same. Fig. 4.30. shows the E and H-plane radiation patterns of SHDHL of flare angle 20° with strip length $2\lambda_0$ at 9 GHz. The radiation patterns of the corresponding HDHL are also given for comparison. By adjusting the strip length identical radiation patterns in both principal planes can be obtained. This result is very significant because it is not possible to attain such a result with any conventional sectoral horns. Thus the radiation pattern of E-plane sectoral SHDHL is almost similar to that of a metallic pyramidal horn (narrow beams in both E and H-planes). Fig. 4.31. is a typical case of identical radiation patterns in both planes.

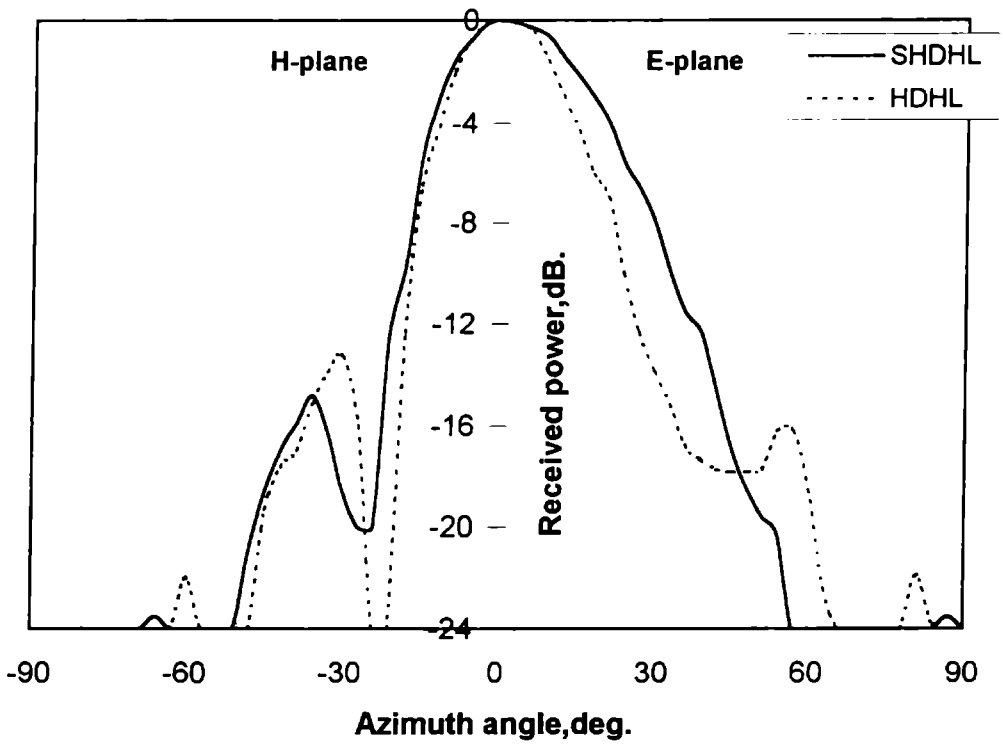

Fig.4.30 E and H-plane radiation patterns of E-plane sectoral HDHL and SHDHL at 9GHz. $\alpha_E = 30°$, $l = 2\lambda_0$.

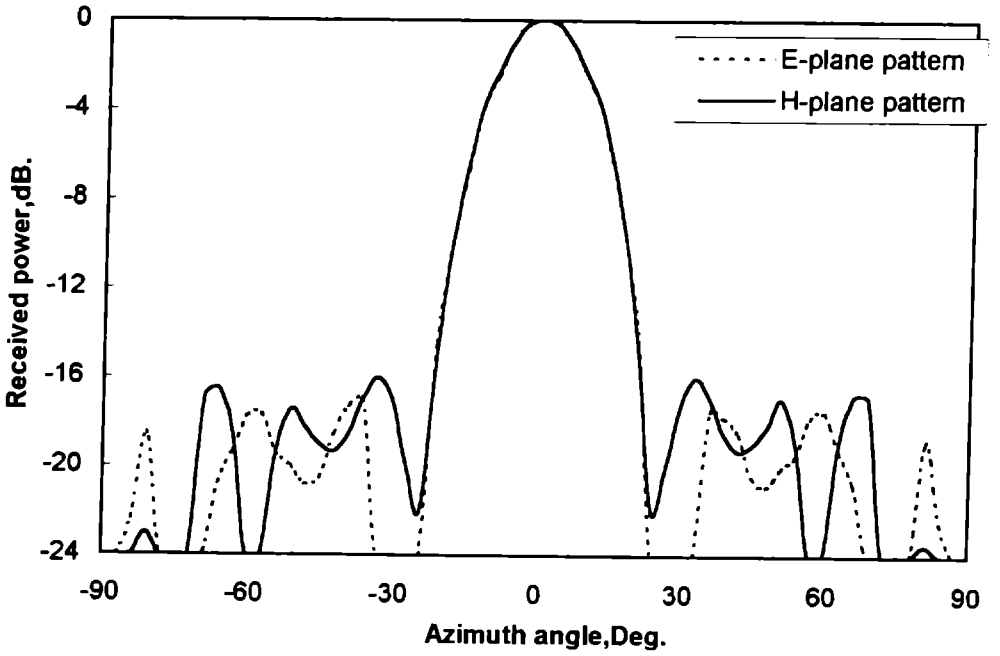

Fig.4.31 E and H-plane radiation patterns of E-plane sectoral SHDHL at 10.5GHz.(identical E and H patterns). $\alpha_E = 10°, l = 1\lambda_0$.

The variation of HPBW with frequency and strip length for two typical horns are shown in Fig. 4.32.

The strip loading also provides a method for adjusting the side lobe levels. The ends of the strips act as diffraction points and that in turn will change the side lobes of the HDHL. The variation of first side lobe levels for horns of flare angle 20° and 30° for E and H-plane patterns with strip length and frequency are shown in Fig. 4. 33.

Table. 4.10. shows the values of 3dB beam width, 10dB beam width and side lobe levels for various E-plane sectoral SHDHL antennas at different frequencies.

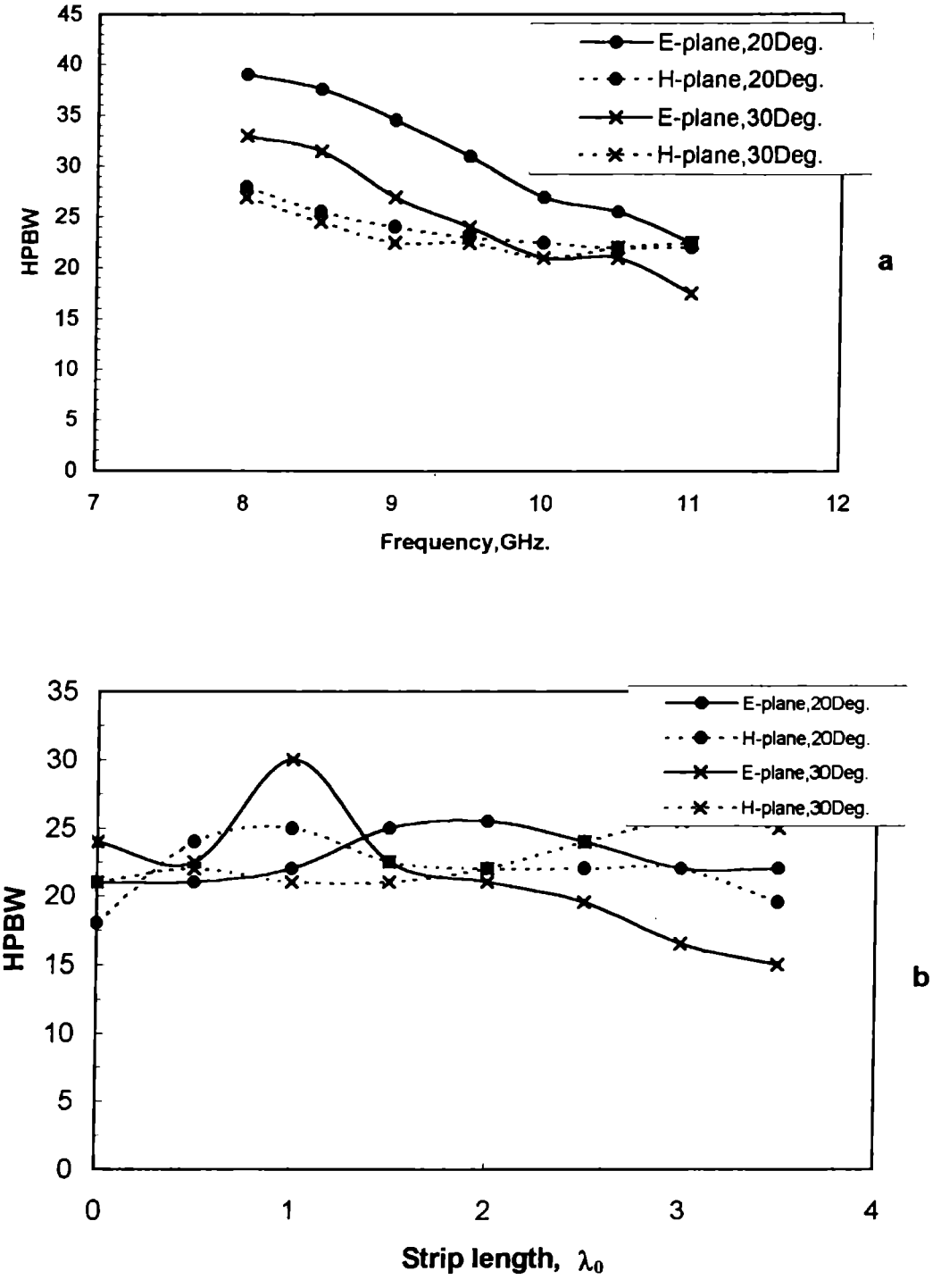

Fig.4.32 E and H-plane HPBW variation with (a) frequency ($l = 2\lambda_0$) and (b) strip length (f = 10.5GHz), for E-plane sectoral SHDHL, $\alpha_E = 20°$ and $30°$.

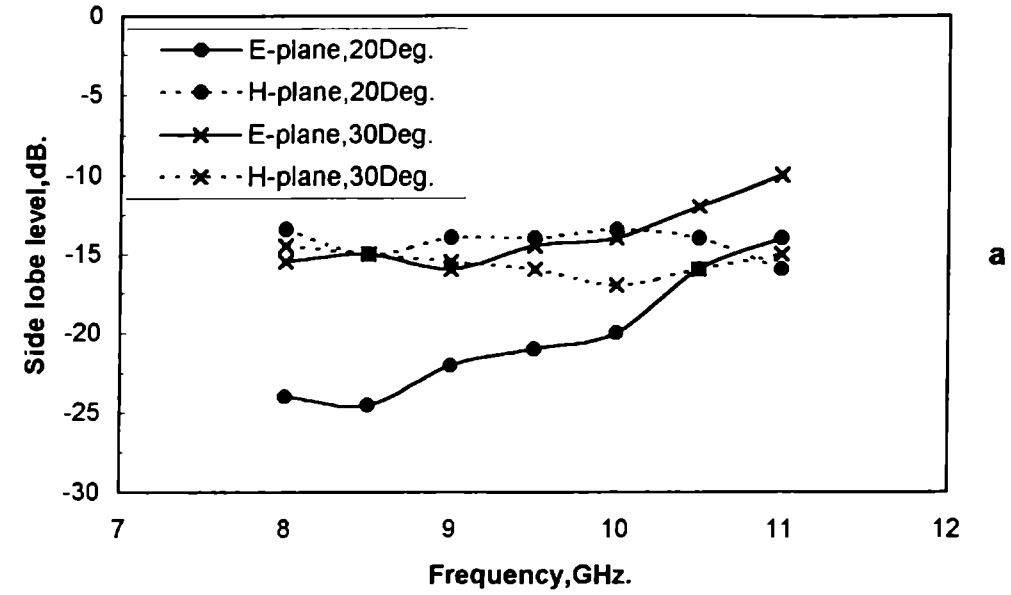

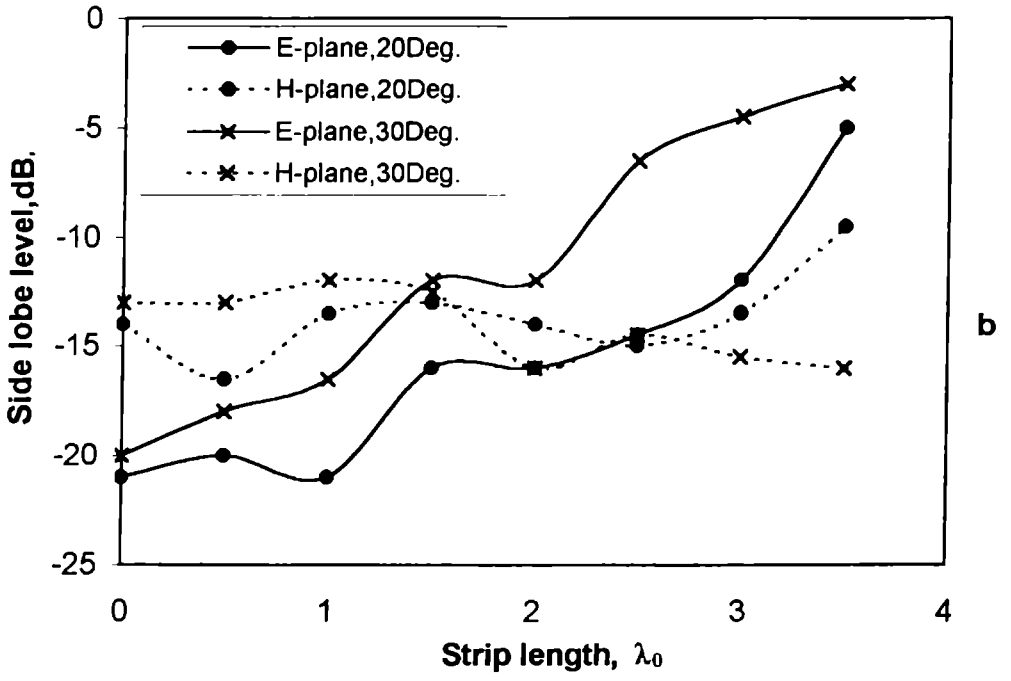

Fig.4.33 Side lobe level variation with (a) frequency ($l = 2\lambda_0$) and (b) strip length (f = 10.5GHz), for E-plane sectoral SHDHL, $\alpha_E = 20°$ and $30°$.

Table 4.10 3dB beam width, 10dB beam width and first side lobe levels for different E-plane sectoral SHDHL horn antennas at different frequencies.

Flare angle (Degree)	Frequency (GHz)	Strip Length λ_0	3dB beam width (Degree)		10dB beam width (Degree)		First side lobe level (dB)	
			H	E	H	E	H	E
10	8.5	1	28.5	30.0	46.5	54.0	-17.0	-13.0
		2	27.0	36.0	44.2	67.5	-19.0	-12.0
		3	29.2	48.0	40.5	102.0	-13.5	-16.5
	9.5	1	25.0	25.0	40.5	49.0	-16.7	-14.5
		2	24.5	31.5	40.5	61.5	-16.0	-16.0
		3	22.5	48.0	41.0	89.0	-12.0	-22.0
	10.5	1	22.5	22.5	39.0	37.5	-16.0	-17.0
		2	22.5	30.0	40.5	52.5	-15.0	-19.0
		3	22.5	36.0	42.0	77.0	-12.0	-13.5
20	8.5	1	28.5	28.5	45.0	67.5	-14.0	-21.0
		2	25.5	37.5	42.0	69.0	-15.0	-24.5
		3	25.5	33.0	43.0	60.0	-15.5	-15.0
	9.5	1	24.5	24.0	40.5	51.0	-14.0	-17.5
		2	23.0	31.0	39.0	61.5	-14.0	-21.0
		3	23.0	27.0	40.0	52.0	-15.0	-13.0
	10.5	1	25.0	22.0	39.0	42.0	-13.5	-21.0
		2	22.0	25.5	37.0	46.5	-14.0	-16.0
		3	22.0	22.0	37.0	39.5	-13.5	-12.0
30	8.5	1	24.0	36.0	40.5	75.0	-12.0	-24.0
		2	24.5	31.5	40.0	60.0	-15.0	-15.0
		3	25.0	25.0	41.0	44.0	-14.5	-11.5
	9.5	1	22.5	27.0	38.0	64.5	-13.5	-20.0
		2	22.5	24.0	40.0	48.0	-16.0	-14.5
		3	25.5	21.0	45.0	37.5	-14.5	-9.5
	10.5	1	21.0	30.0	37.5	61.0	-12.0	-16.5
		2	22.0	21.0	40.5	57.0	-16.0	-12.0
		3	25.5	16.5	58.0	96.0	-15.5	-4.5
40	8.5	1	19.5	48.0	31.5	75.0	-11.5	-22.0
		2	18.0	31.5	34.0	75.0	-15.0	-17.0
		3	19.5	23.0	36.0	105.0	-13.0	-30.0
	9.5	1	18.0	48.0	30.0	74.0	-12.0	-21.5
		2	16.5	39.0	30.0	102.0	-12.5	-24.0
		3	19.5	81.0	37.5	103.0	-9.0	-14.5
	10.5	1	15.0	48.0	27.0	74.0	-10.0	-21.0
		2	13.0	59.0	27.0	93.0	-12.0	-17.5
		3	15.0	--	--	--	-10.0	--
50	8.5	1	25.5	54.0	42.0	81.0	-9.0	-31.0
		2	23.0	48.0	39.0	108.0	-12.0	-16.5
		3	22.5	--	37.0	--	-10.5	--
	9.5	1	22.5	54.0	36.0	84.0	-10.5	-27.0
		2	21.0	72.0	36.0	107.0	-12.5	-18.0
		3	19.5	--	34.5	--	-8.0	--
	10.5	1	16.5	56.0	30.0	82.0	-9.0	-23.0
		2	16.5	50.0	30.0	90.0	-8.0	-14.5
		3	13.5	**	27.0	--	-5.5	--

** split patterns

4.3.1.2 Cross-polar levels

The maximum cross-polar levels of E-plane sectoral SHDHL are slightly greater than that for the corresponding HDHL. It is around –35dB for this case. One typical co-polar and cross-polar patterns for SHDHL of flare angle 20deg. ($l=2\lambda_0$) at 10GHz is shown in Fig. 4.34.

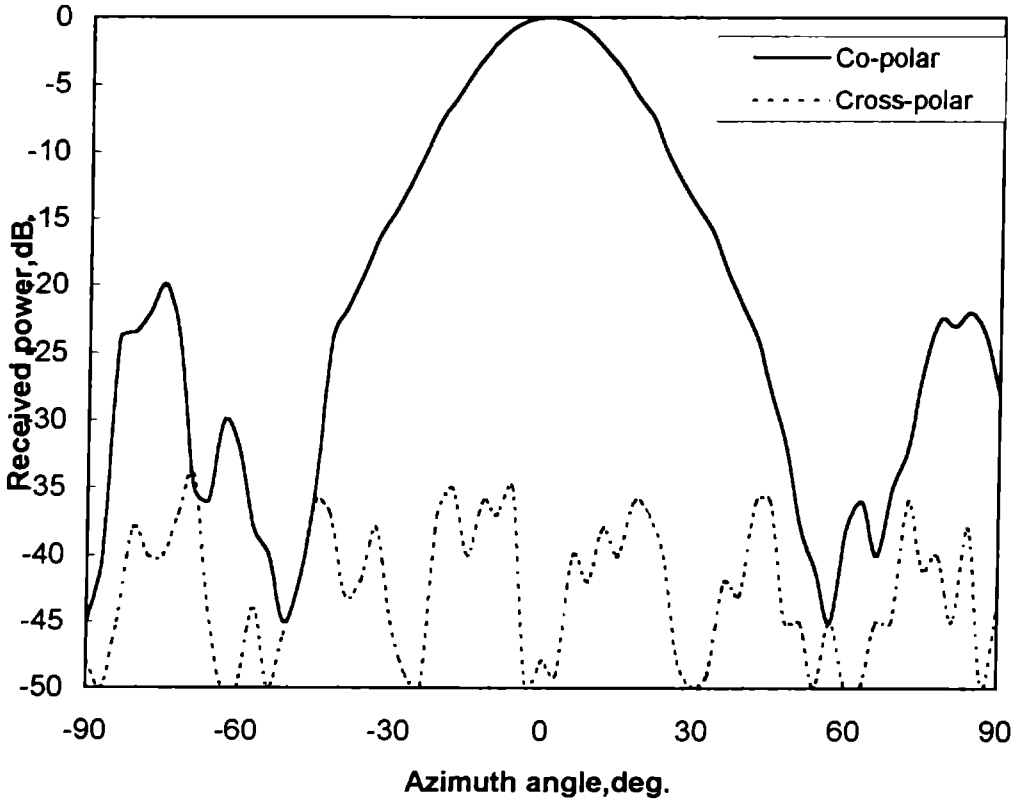

Fig.4.34 Co-polar and cross-polar radiation patterns of E-plane sectoral SHDHL at 10GHz, $\alpha_E=20°, l = 2\lambda_0$.

4.3.1.3 VSWR and Impedance

A plot of impedance and VSWR with frequency for SHDHL ($\alpha_E=20°$., $l=2\lambda_0$) is shown in Fig. 4.35. The corresponding plot for HDHL also is given. The strip loading increases the VSWR of HDHL at certain frequencies. The variation of strip length also changes the VSWR as evident from Fig. 4.36.

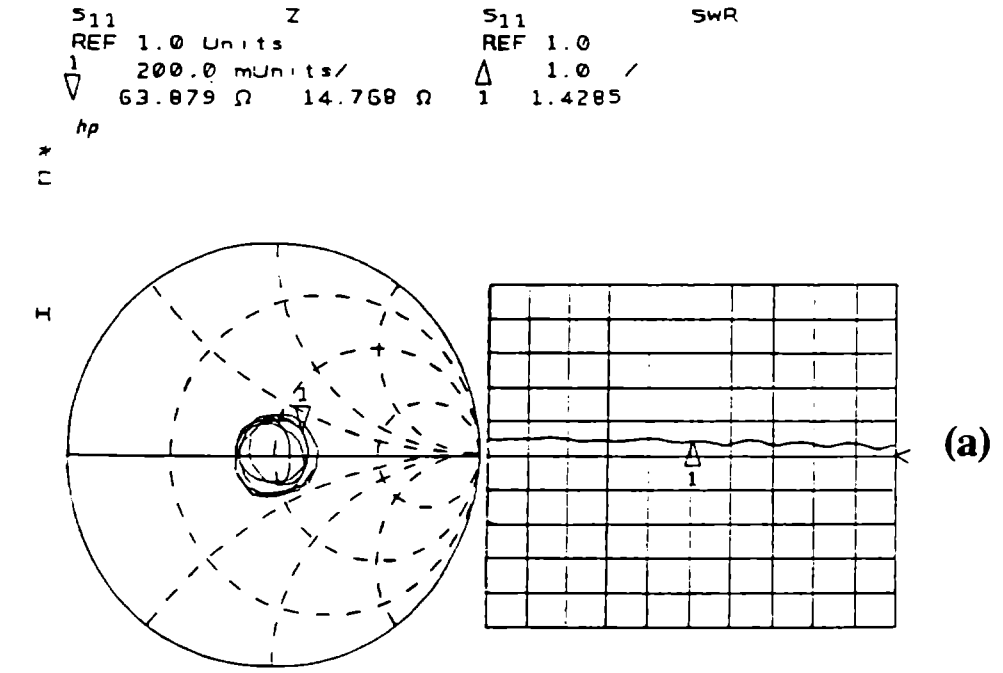

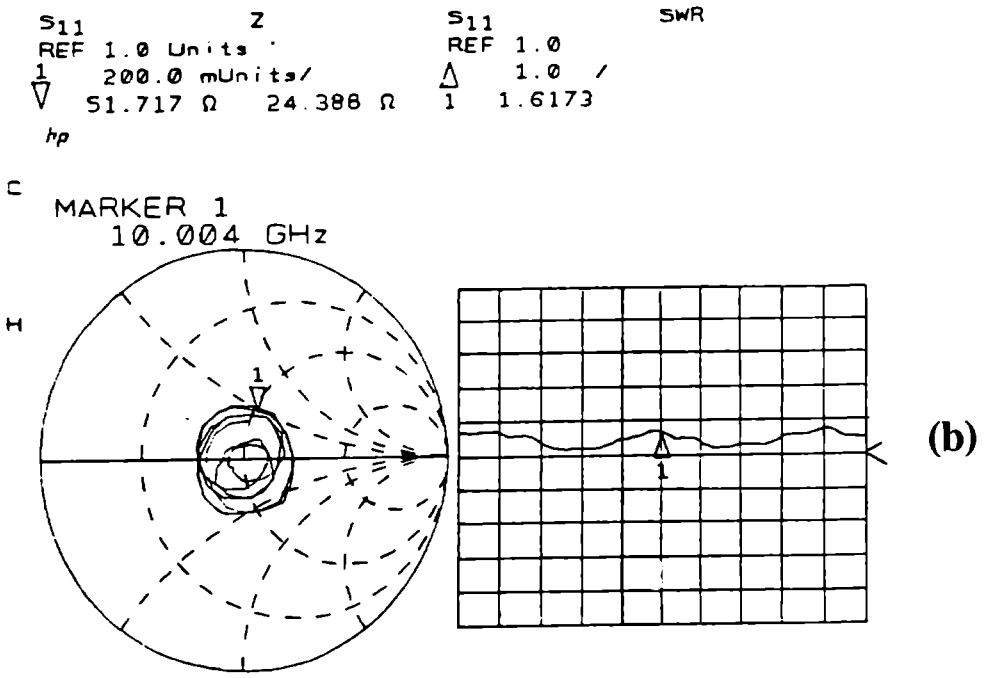

Fig.4.35 VSWR variation with frequency for E-plane sectoral horn. $\alpha_E = 20°$ l = $2\lambda_0$, (a) HDHL, (b) SHDHL.

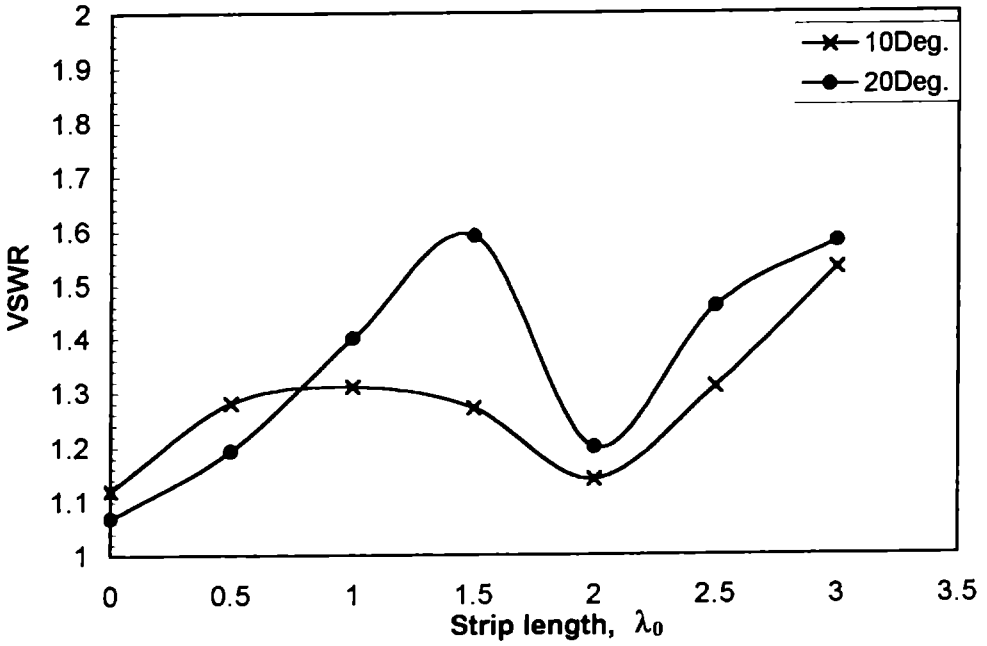

Fig.4.36 VSWR variation with strip length for E-plane sectoral SHDHL at 10.5GHz. for $\alpha_E = 10°$ and 20°.

4.3.1.4 Directive Gain

The axial gain of HDHL decreases slightly for almost all frequencies with strip loading. But still the gain of SHDHL is greater than the corresponding ordinary HDH in most of the cases. Fig. 4.37. shows the gain variation with frequency for E-plane sectoral SHDHL. Also, the gain slightly decreases with increase in strip length as shown in Fig. 4.38. The axial gain variation with frequency and strip length for different E-plane sectoral SHDHL are available in Table. 4.11.

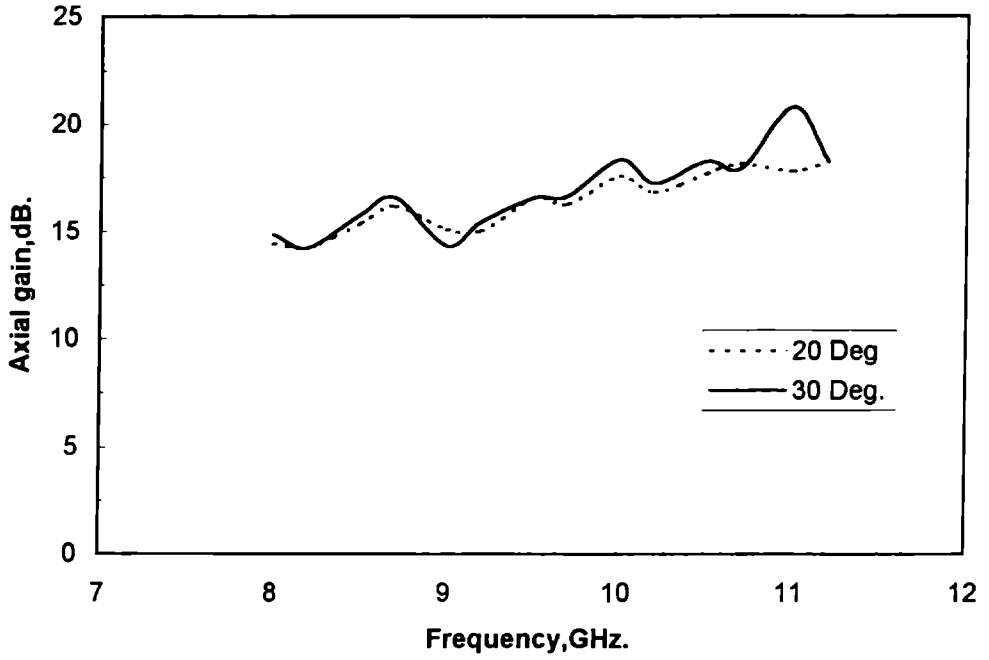

Fig.4.37 Axial gain variation with frequency for E-plane sectoral SHDHL $\alpha_E = 20°$ and $30°$, $l = 1\lambda_0$.

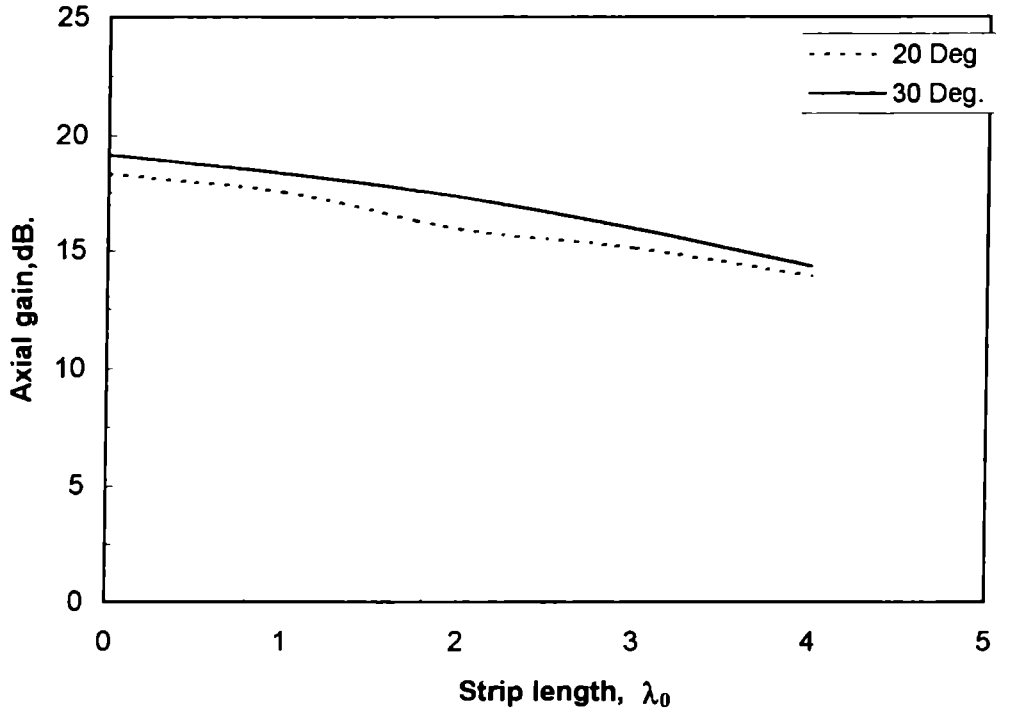

Fig.4.38 Axial gain variation with strip length for E-plane sectoral SHDHL at 10GHz. $\alpha_E = 20°$ and $30°$.

Table 4.11 Axial gain of different E-plane sectoral SHDHL antennas.

Frequency (GHz)	Axial Gain (dB)							
	$\alpha_E = 10°$				$\alpha_E = 20°$			
	Strip length(λ)				Strip length(λ)			
	0	1	2	3	0	1	2	3
8.00	15.2	13.6	13.2	11.6	15.2	14.4	13.6	13.2
8.25	14.2	13.4	12.8	11.0	14.6	14.2	13.0	11.8
8.50	16.2	15.2	14.4	13.2	16.0	15.4	14.4	13.2
8.75	17.0	15.8	15.0	13.4	16.8	16.2	15.0	14.2
9.00	14.7	13.9	13.1	11.9	15.7	15.1	13.9	14.5
9.25	15.4	15.0	13.4	11.4	15.2	15.0	13.4	12.5
9.50	17.5	16.5	14.1	12.1	17.3	16.5	14.5	13.7
9.75	17.0	16.2	14.2	12.2	16.6	16.2	14.2	13.8
10.00	18.5	16.7	15.1	12.3	18.3	17.5	15.9	15.1
10.25	16.8	16.0	14.4	11.6	17.0	16.8	15.2	13.6
10.50	18.6	17.6	15.2	11.6	18.4	17.6	15.2	14.0
10.75	16.9	16.5	16.1	13.3	18.3	18.1	16.5	15.3
11.00	19.0	18.2	15.8	12.2	18.0	17.8	15.0	13.0
	$\alpha_E = 30°$				$\alpha_E = 40°$			
8.00	15.6	14.8	14.0	14.4	14.8	14.0	13.5	13.4
8.25	15.0	14.2	13.8	13.8	14.2	13.5	13.0	13.0
8.50	16.8	15.8	15.6	15.4	16.0	15.2	14.6	14.2
8.75	17.6	16.6	15.8	15.8	16.6	15.6	14.6	14.2
9.00	15.9	14.3	14.3	14.7	15.9	15.0	14.1	13.8
9.25	16.8	15.4	15.2	14.6	14.6	14.2	13.2	13.0
9.50	18.5	16.5	16.5	14.9	16.3	15.6	14.8	14.0
9.75	17.8	16.6	16.2	15.0	16.2	15.2	14.7	14.1
10.00	19.1	18.3	17.3	15.9	16.7	15.6	14.8	14.2
10.25	18.2	17.2	16.0	14.8	16.0	15.0	14.5	13.5
10.50	19.4	18.2	17.2	14.6	16.6	15.6	14.5	13.6
10.75	17.9	17.9	17.3	15.3	14.6	14.0	13.5	13.1
11.00	19.2	20.8	17.8	14.2	15.6	14.3	13.8	13.2

4.3.2 H-plane sectoral SHSHL

Fig. 4.39. shows the schematic representation of H-plane sectoral SHDHL. Conducting strips of width b_0 are loaded on H-walls of the horn as shown in the figure. This horn shows some interesting characteristics as detailed in the following sections.

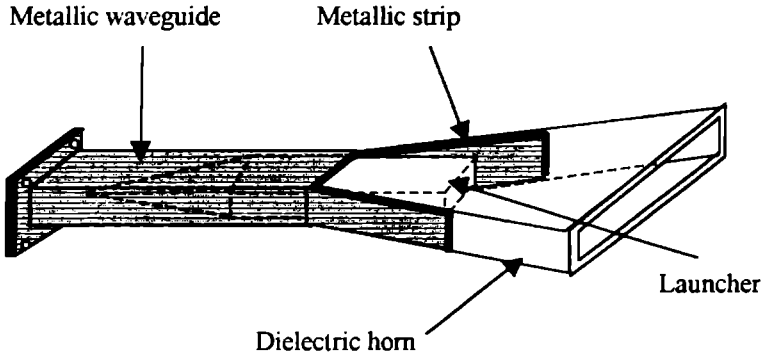

Fig.4.39 Schematic representation of the H-plane sectoral SHDHL

4.3.2.1 Radiation pattern

The H-plane radiation pattern of H-plane sectoral HDHL can be drastically modified using the strip loading method. It is mentioned earlier that the H-plane patterns of HDHL are broad. It is possible to have a rippled or square (flat-topped) or split radiation pattern from SHDHL by adjusting the strip length and frequency. Change of frequency or strip length may cause the ripples, giving way to splitting of the main beam into two. The square radiation pattern is one with a flat-top and large HPBW. Also, the radiated power suddenly decreases to very low values beyond the 3dB points. Fig. 4.40. shows the E and H-plane patterns of H-plane sectoral SHDHL horn of flare angle 20° at 10GHz.The corresponding cases for equivalent HDHL are also shown. Fig. 4.41. shows example for broad and split H-plane pattern obtained from H-plane sectoral SHDHL antenna. Fig. 4.42. shows a typical example of flat-topped radiation pattern obtained for SHDHL of horn angle 20° with strip length $2\lambda_0$ at 10.4GHz.

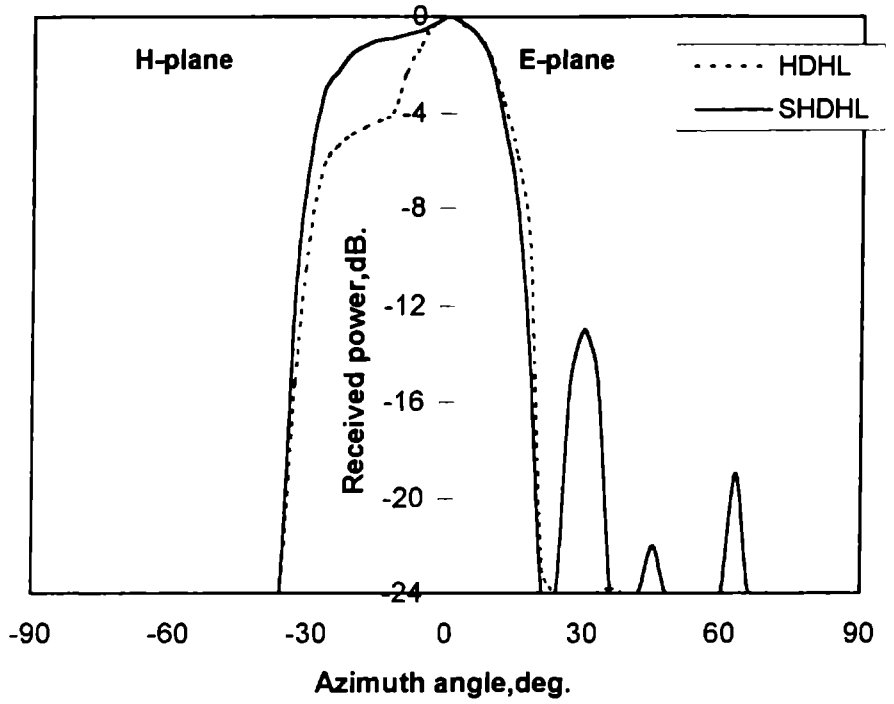

Fig.4.40 E and H-plane radiation patterns of H-plane sectoral HDHL and SHDHL at 10GHz. $\alpha_H = 20°$, $l = 3\lambda_0$.

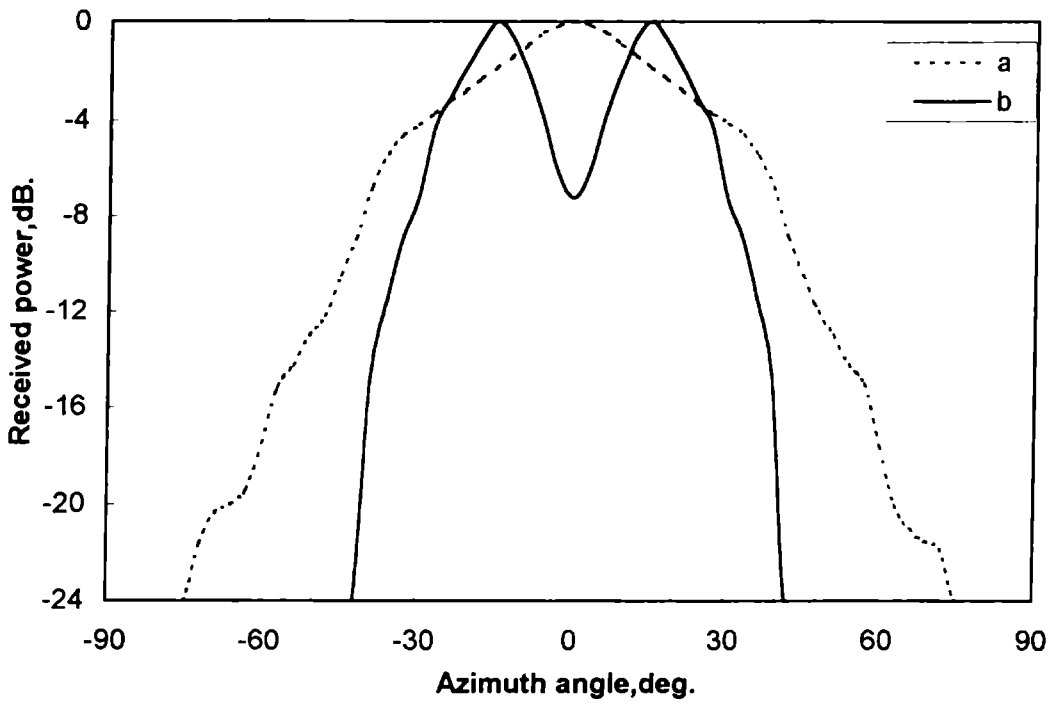

Fig.4.41 H-plane patterns of H-plane sectoral SHDHL, (a) $\alpha_H = 60°$, $l = 2\lambda_0$, f = 9.5GHz. (b) $\alpha_H = 30°$, $l = 1.5\lambda_0$, f = 10.5GHz.

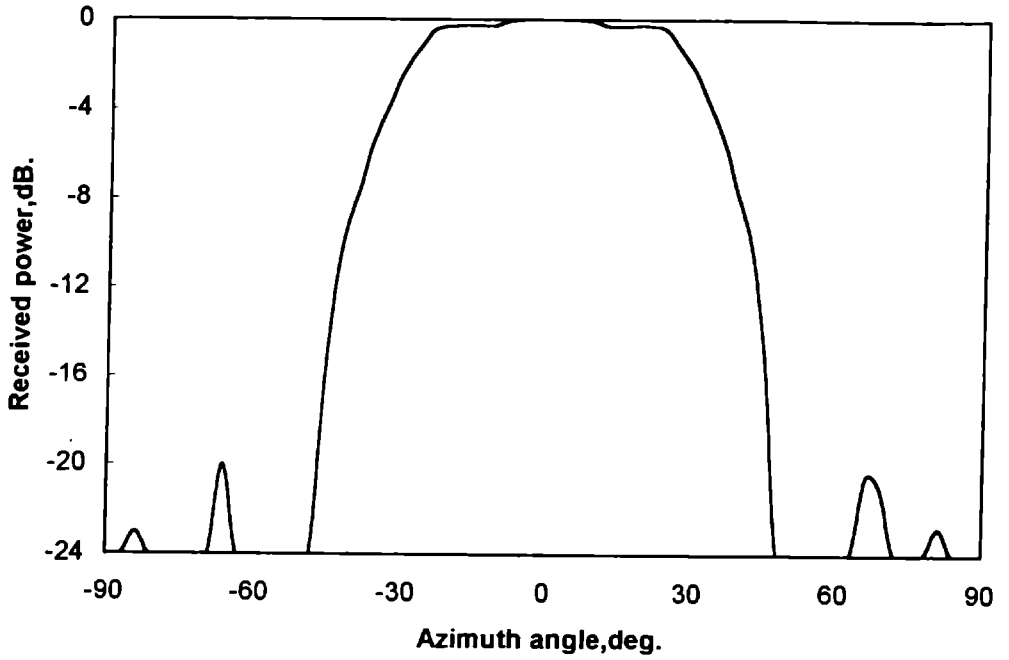

Fig.4.42 Flat-top radiation pattern from H-plane sectoral SHDHL $\alpha_H = 20°, l = 3\lambda_0, f = 10.4GHz$.

The HPBW in the H-plane increases to very high values with increase in strip length for a particular frequency or vice versa. The HPBW in the E-plane is almost independent of strip length, but slightly changes with frequency. The variation of HPBW with frequency for horns of flare angle 10° and 20° are shown in Fig. 4.43.

The side lobe levels of H-plane patterns are very low but that of E-plane patterns are high.(around –12dB). Fig. 4.44 shows the variation of the side lobe level with frequency and strip length for 10° and 20° horns.

Table. 4.12. gives the 3dBbeam width, 10dB beam width and side lobe levels for different experimental H-plane sectoral SHDHL antennas at different frequencies and strip-lengths.

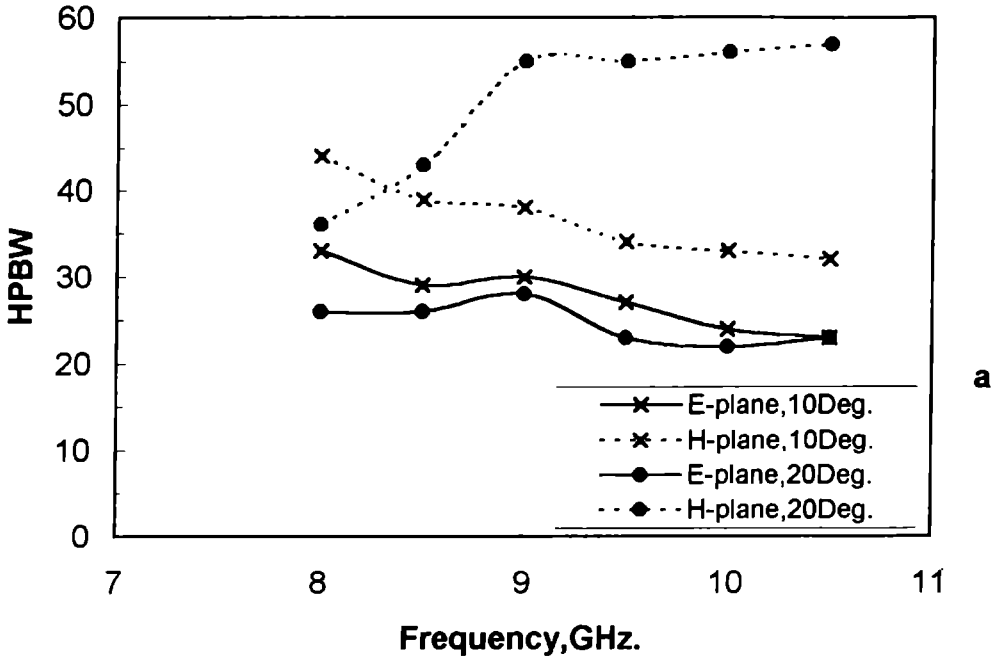

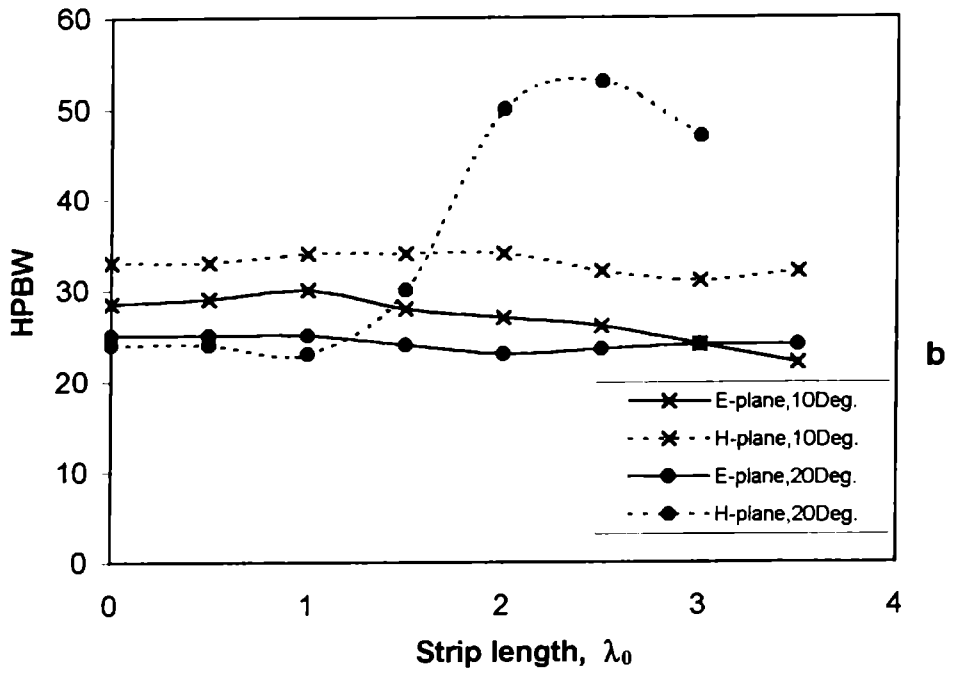

Fig.4.43 E and H-plane HPBW variation with (a) frequency ($l = 2\lambda_0$) and (b) strip length ($f = 9.5$GHz), for H-plane sectoral SHDHL, $\alpha_H = 10°$ and $20°$.

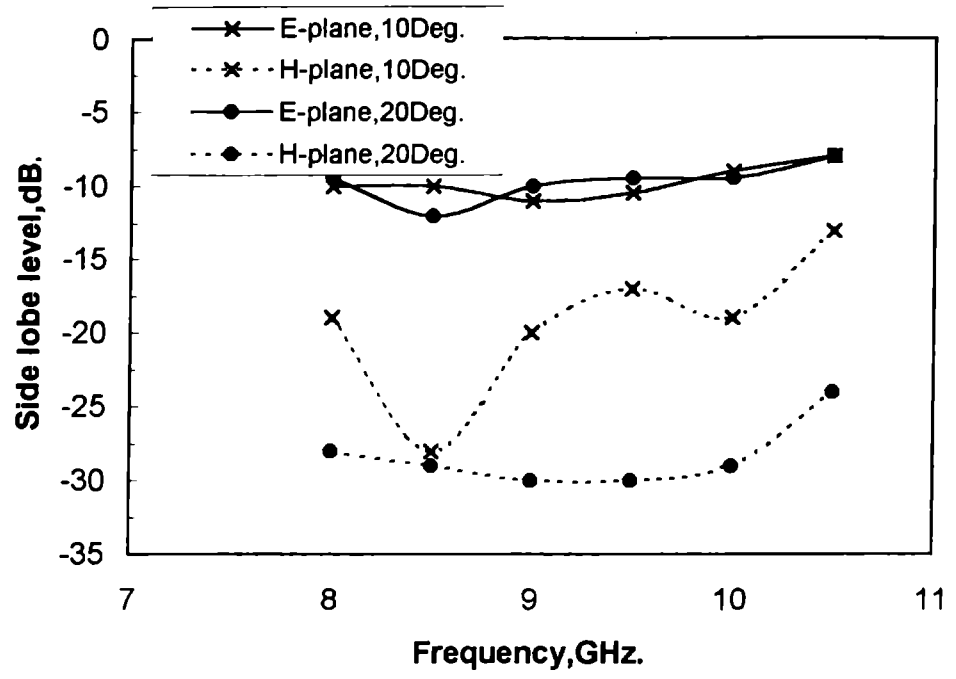

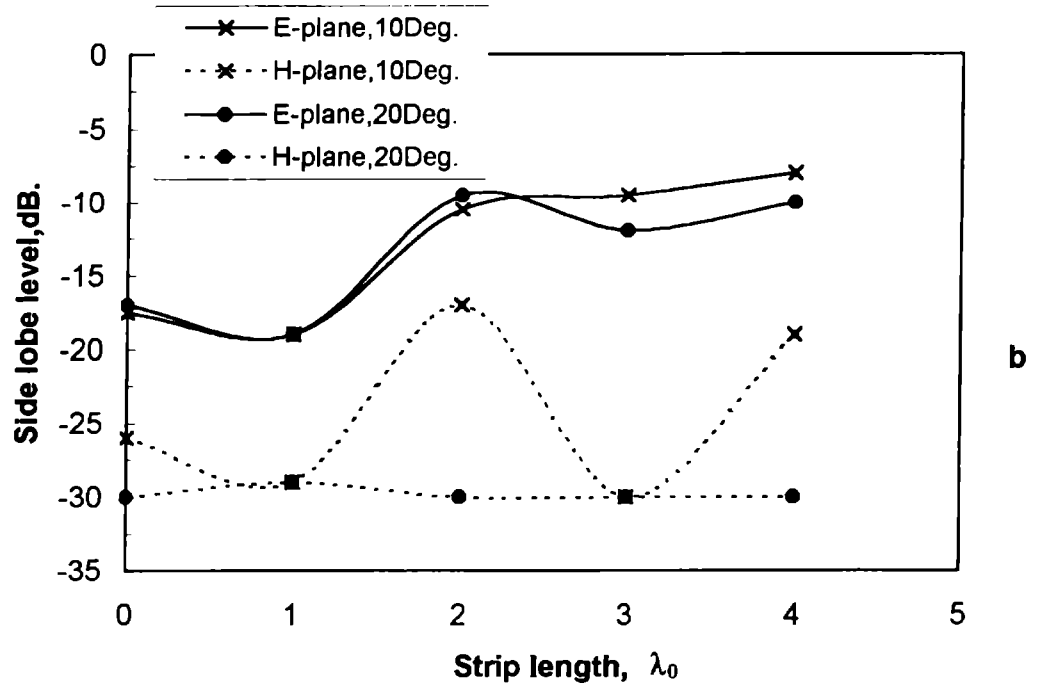

Fig.4.44 Side lobe level variation with (a) frequency ($l = 2\lambda_0$) and (b) strip length (f = 9.5GHz), for E-plane sectoral SHDHL, $\alpha_H = 10°$ and $20°$.

Table 4.11 3dB beam width, 10dB beam width and first side lobe levels for different H-plane sectoral SHDHL horn antennas at different frequencies.

Flare angle (Degree)	Frequency (GHz)	Strip Length λ_0	3dB beam width (Degree)		10dB beam width (Degree)		First side lobe level (dB)	
			H	E	H	E	H	E
10	8.5	1	40.5	31.0	105.0	51.0	-24.0	-16.0
		2	39.0	29.0	99.0	46.0	-28.0	-10.0
		3	36.0	27.0	108.0	45.0	-24.0	-10.0
	9.5	1	34.0	30.0	85.0	46.5	-29.0	-19.0
		2	34.0	27.0	105.0	42.0	-17.0	-10.5
		3	31.0	24.0	95.0	40.0	-30.0	-9.5
	10.5	1	33.0	26.0	98.0	40.0	-18.0	-16.5
		2	34.0	23.0	100.0	37.0	-13.0	-8.0
		3	68.0	18.0	90.0	31.0	-20.0	-6.5
20	8.5	1	32.0	28.0	76.0	45.0	-36.0	-15.5
		2	43.0	26.0	79.0	39.0	-30.0	-12.0
		3	45.0	25.5	76.0	42.0	-34.0	-9.5
	9.5	1	25.0	25.0	64.0	40.5	-29.0	-19.0
		2	50.0	23.0	74.0	37.0	-30.0	-9.5
		3	53.0	24.0	69.0	37.0	-30.0	-12.0
	10.5	1	24.0	24.0	66.0	37.5	-28.0	-20.0
		2	57.0	23.0	62.0	33.0	-24.0	-8.0
		3	51.0	22.5	61.0	34.5	-28.0	-10.0
30	8.5	1	65.0	22.5	89.0	40.5	-35.0	-11.5
		2	59.0	22.0	82.0	39.0	-35.0	-7.5
		3	57.0	22.0	81.0	45.0	-32.0	-6.5
	9.5	1	57.0	21.0	78.0	33.0	-32.0	-13.0
		2	**	--	71.0	--	-32.0	--
		3	48.0	21.0	72.0	70.0	-32.0	-6.0
	10.5	1	**	--	72.0	--	-29.0	--
		2	**	--	66.0	--	-26.0	--
		3	**	--	65.0	--	-24.0	--
45	8.5	1	70.0	25.0	108.0	54.0	-28.0	-16.0
		2	62.0	28.0	102.0	67.0	-22.0	-14.5
		3	57.0	28.0	108.0	61.0	-22.0	-13.5
	9.5	1	73.0	25.0	100.0	48.0	-20.0	-28.0
		2	58.0	27.0	106.0	51.0	-17.0	-20.0
		3	52.0	27.0	100.0	51.0	-17.5	-18.5
	10.5	1	60.0	27.0	105.0	42.0	-16.0	-27.0
		2	54.0	27.0	108.0	42.0	-15.0	-27.0
		3	53.0	26.0	105.0	42.0	-14.0	-22.0
60	8.5	1	66.0	25.5	111.0	43.0	-24.0	-16.0
		2	47.0	25.5	105.0	45.0	-24.0	-17.0
		3	50.0	24.0	105.0	42.0	-24.0	-18.5
	9.5	1	57.0	21.0	96.0	36.0	-23.0	-18.0
		2	48.0	21.0	90.0	37.0	-24.0	-17.5
		3	42.0	22.0	87.0	34.5	-22.0	-20.0
	10.5	1	58.0	20.0	93.0	33.0	-15.0	-20.0
		2	58.0	21.0	87.0	33.0	-15.0	-20.0
		3	57.0	19.5	85.0	31.5	-15.0	-17.0

** split pattern

4.3.2.2 Cross-polar levels

The maximum cross-polar levels of this SHDHL is found to be slightly less than that for the corresponding HDHL. Fig. 4.45. shows the co-polar and cross-polar radiation patterns of SHDHL of flare angle 20° at 10GHz.

4.3.2.3 VSWR and Impedance

For H-plane sectoral HDHL the VSWR is not much affected by strip-loading. The variation of strip-length also produces very little change on the VSWR. Fig. 4.46. gives a comparative study of the impedance and VSWR of H-plane sectoral HDHL and SHDHL. Fig. 4.47 gives the effect of strip-length variation on VSWR.

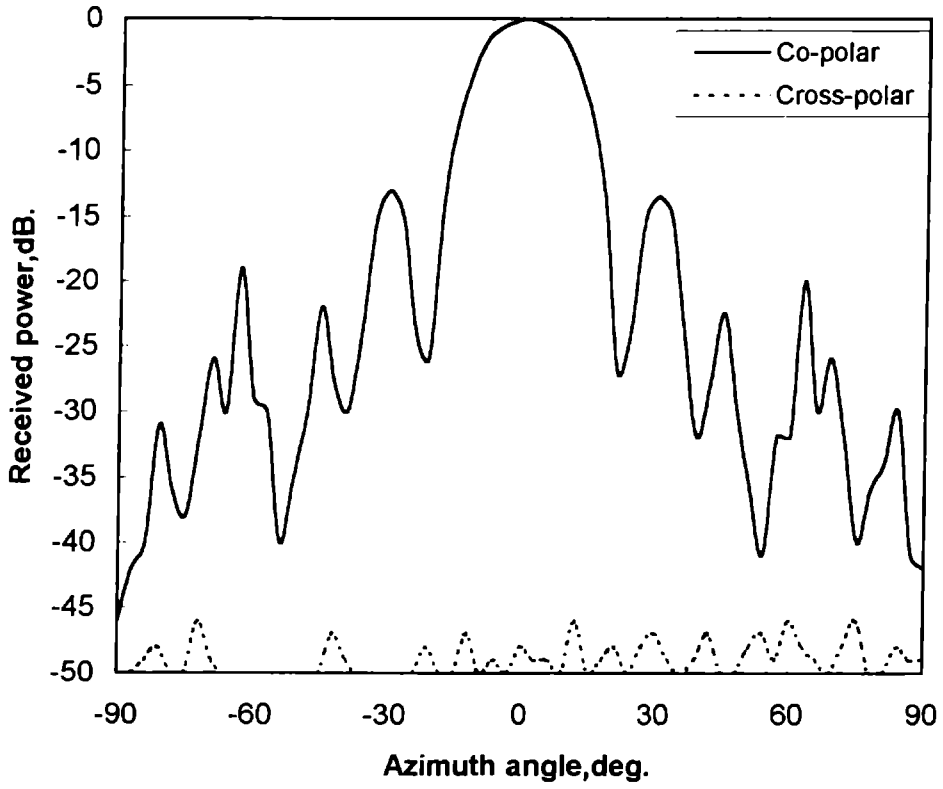

Fig.4.45 Co-polar and cross-polar radiation patterns of H-plane sectoral SHDHL at 10GHz, α_H=20°,l = $2\lambda_0$.

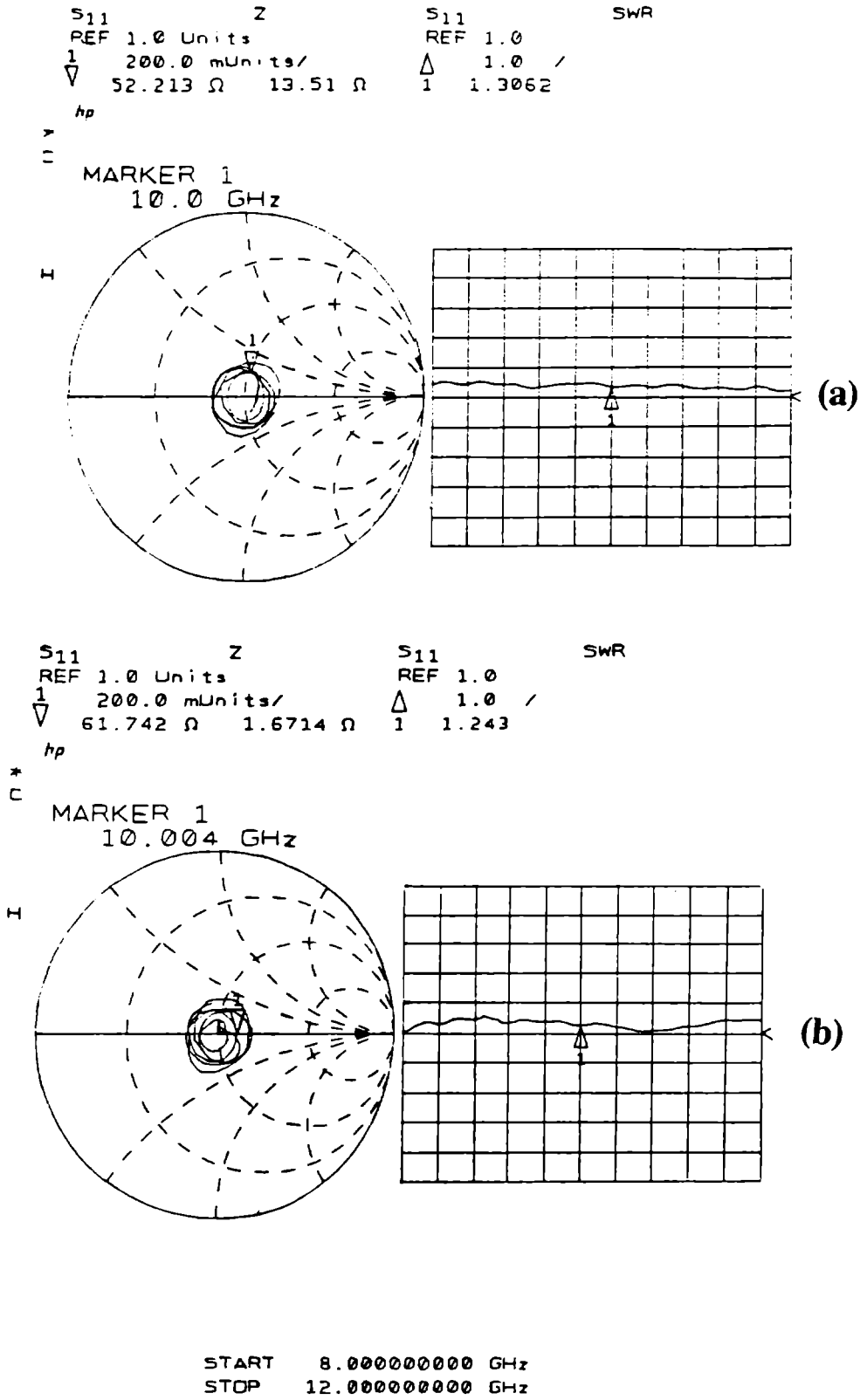

Fig.4.46 VSWR variation with frequency for H-plane sectoral horn. $\alpha_H = 20°$ l = $2\lambda_0$, (a) HDHL, (b) SHDHL.

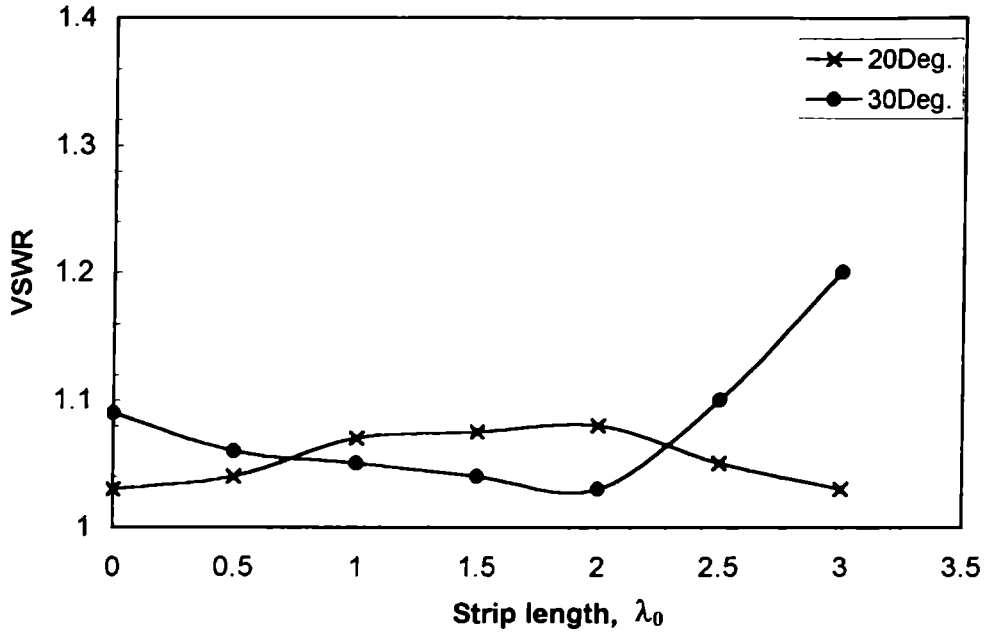

Fig.4.47 VSWR variation with strip length for H-plane sectoral SHDHL at 10.5GHz. for $\alpha_H = 20°$ and 30°.

4.3.2.4 Directive Gain

The axial gain of SHDHL decreases with increase in strip-length or frequency due to flattening of the pattern. In some cases, the axial gain first decreases and then increases with strip-length or frequency because the main beam splits-up into ripples and then merge together to form a single beam, while the parameter is changing. Fig. 4.48. depicts the axial gain variation with frequency for two typical cases, while Fig. 4.49. shows the gain variation with strip-length.

Table. 4.13. gives the values of axial gain for different experimental H-plane sectoral SHDHL at different conditions.

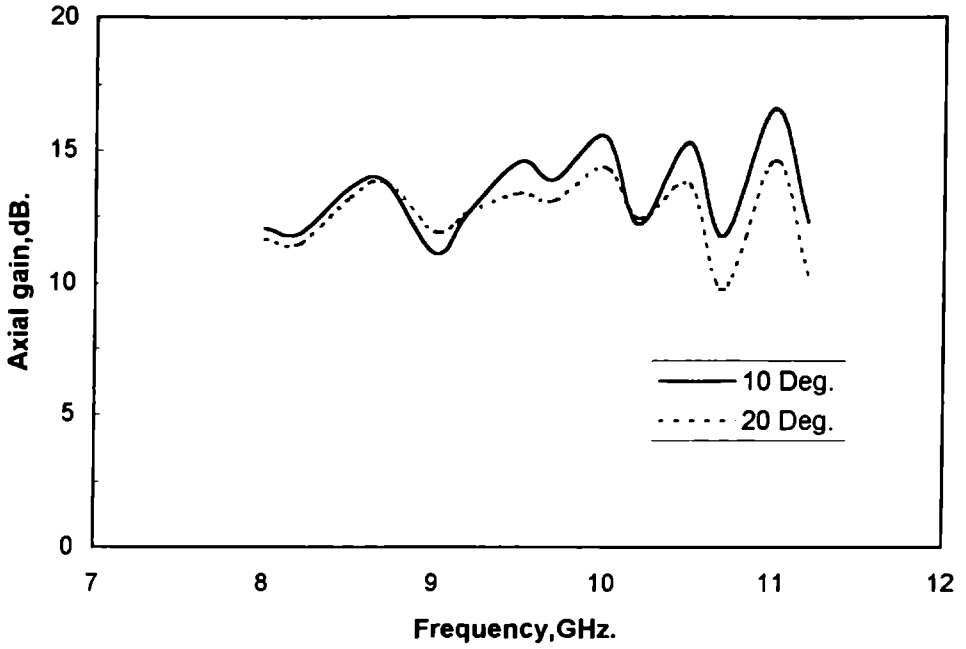

Fig.4.48 Axial gain variation with frequency for H-plane sectoral SHDHL $\alpha_H = 10°$ and 20°, $l = 1\lambda_0$.

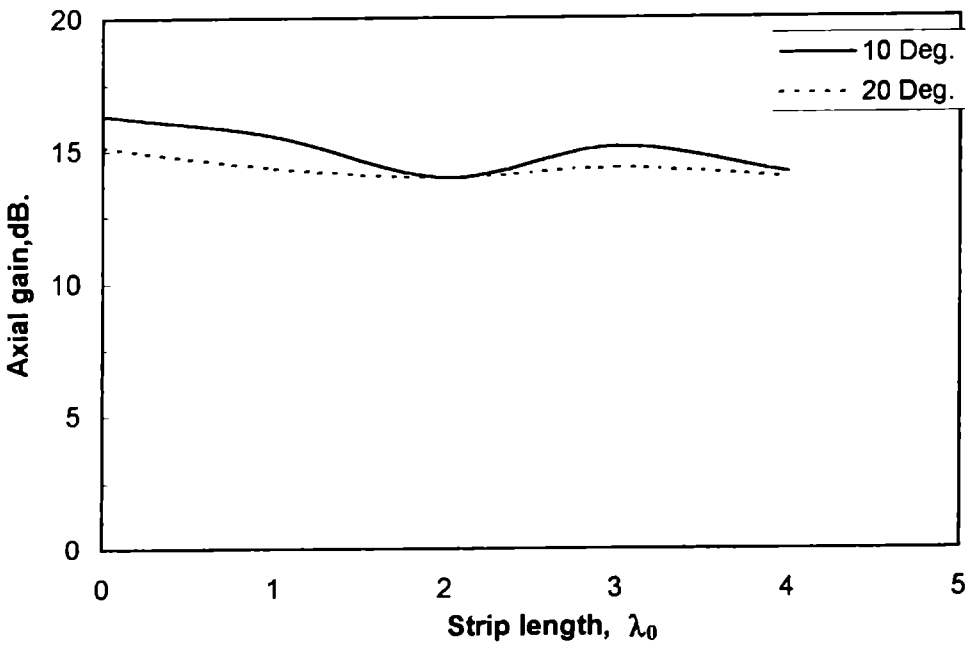

Fig.4.49 Axial gain variation with strip length for H-plane sectoral SHDHL at 10GHz. $\alpha_H = 10°$ and 20°.

Table 4.13 Axial gain of different H-plane sectoral SHDHL antennas.

Frequency (GHz)	Axial Gain (dB)							
	$\alpha_H = 10°$				$\alpha_H = 20°$			
	Strip length(λ)				Strip length(λ)			
	0	1	2	3	0	1	2	3
8.00	12.8	12.0	11.2	11.6	12.4	11.6	10.3	11.2
8.25	12.6	11.8	11.0	11.4	12.2	11.4	10.2	11.0
8.50	14.4	13.6	12.8	13.2	14.0	13.2	12.4	12.4
8.75	14.6	13.8	13.0	13.4	14.2	13.8	13.4	13.0
9.00	11.5	11.1	9.10	9.92	11.9	11.9	11.1	10.7
9.25	14.2	12.6	11.8	13.0	13.8	12.6	11.4	11.8
9.50	14.9	14.5	13.3	14.1	14.9	13.3	12.1	12.5
9.75	14.2	13.8	11.8	13.0	13.4	13.0	11.8	12.2
10.00	16.3	15.5	13.9	15.1	15.1	14.3	13.9	14.3
10.25	14.4	12.2	11.2	12.0	12.8	12.4	11.6	12.0
10.50	17.2	15.2	13.2	14.8	16.0	13.6	12.4	13.2
10.75	14.1	11.7	8.15	10.5	12.7	9.75	7.75	7.75
11.00	17.6	16.6	13.8	14.6	17.0	14.6	13.4	13.8
	$\alpha_H = 30°$				$\alpha_H = 45°$			
8.00	12.0	10.4	9.65	9.65	10.0	9.10	8.80	8.80
8.25	11.4	9.83	9.03	9.43	9.83	9.00	8.60	8.70
8.50	13.2	11.6	12.4	10.8	11.4	10.8	9.60	10.0
8.75	13.0	11.8	11.8	11.4	11.4	10.6	9.80	9.80
9.00	9.93	9.94	9.13	8.73	7.90	6.50	6.20	7.00
9.25	12.2	11.0	9.45	10.2	11.0	10.2	9.90	9.90
9.50	12.9	11.3	10.9	10.5	11.7	10.3	9.50	9.80
9.75	11.8	10.2	10.2	10.2	11.4	10.5	9.60	6.70
10.00	13.5	11.1	11.9	12.3	13.5	12.5	11.9	11.9
10.25	11.6	8.80	9.60	10.0	11.6	10.6	10.4	10.4
10.50	14.4	8.88	10.4	12.0	14.0	13.6	12.9	12.6
10.75	10.9	**	4.5	7.35	10.1	9.80	8.90	8.90
11.00	14.2	10.6	11.8	13.0	15.4	13.8	12.9	12.8

4.3.3 Pyramidal SHDHL

The schematic diagram of strip-loaded pyramidal hollow dielectric horn antenna with the launcher (SHDHL) is shown in Fig. 4.50. Similar strips used for E-plane sectoral SHDHL are used in this case.

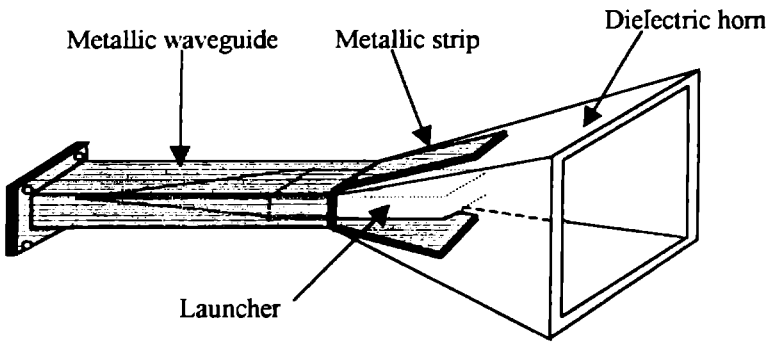

Fig.4.50 Schematic diagram of the pyramidal SHDHL antenna.

4.3.3.1 Radiation pattern

The radiation pattern of pyramidal SHDHL in the E-plane is very narrow for certain cases with low side lobe levels. The H-plane patterns are narrow only for horns of small flare angle in H-plane (α_H). As α_H increases, for any value of α_E, the side lobes increases and becomes ripples on the main beam. For certain cases the beam exactly splits up into a twin beam with sharp null at the axis. For such cases, the E-plane pattern maximum deviates from the horn axis. So the highlights from the study of pyramidal SHDHL reveals the possibility of getting narrow E-plane patterns and split H-plane patterns. Fig. 4.51. shows the E and H-plane patterns of pyramidal SHDHL of α_H=10° and α_E=20°, along with the corresponding patterns for the equivalent HDHL. Fig. 4.52. shows the H-plane patterns with ripples at the top and Fig. 4.53. shows a case of clear splitting.

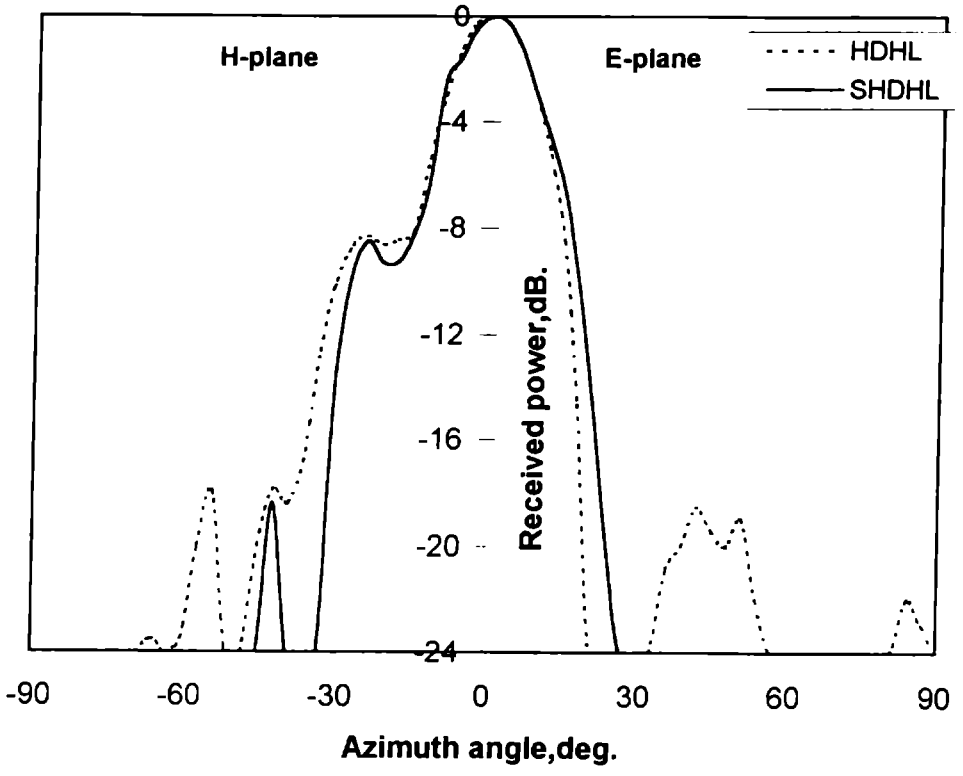

Fig.4.51 E and H-plane radiation patterns of pyramidal HDHL and SHDHL at 9GHz. $\alpha_E = 20°$, $\alpha_H = 10°$, $l = 2\lambda_0$.

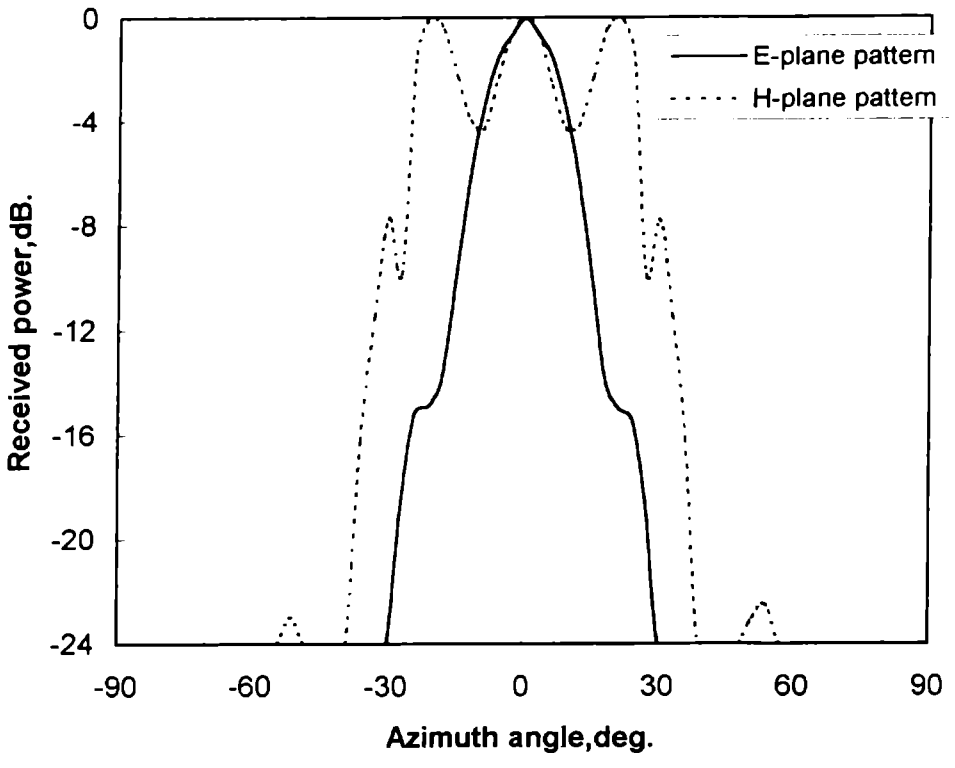

Fig.4.52 E and H-plane radiation patterns of pyramidal SHDHL at 9GHz. $\alpha_E = 20°$, $\alpha_H = 20°$, $l = 2\lambda_0$.

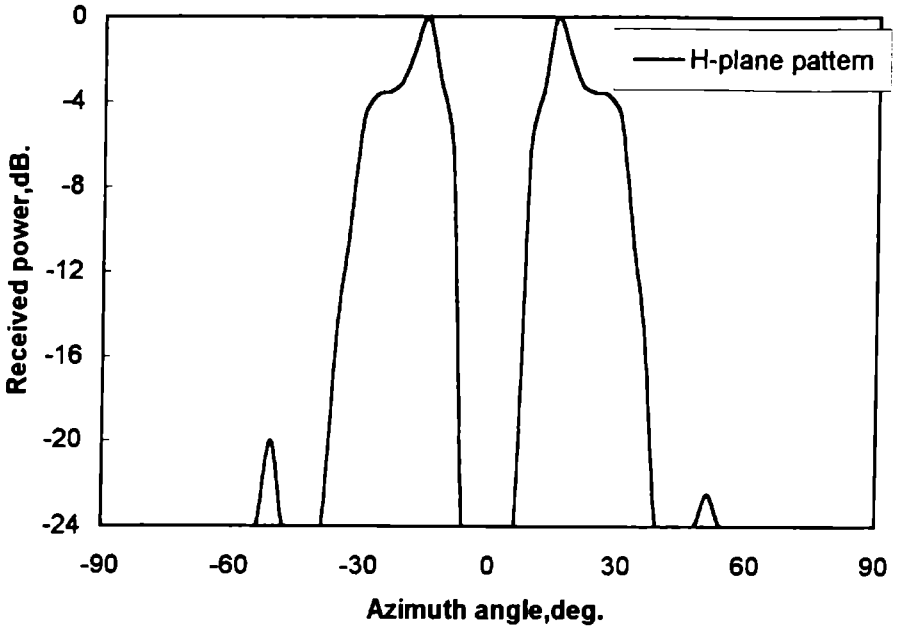

Fig.4.53 H-plane radiation pattern of pyramidal SHDHL at 10GHz. $\alpha_E = 20°$, $\alpha_H = 30°$, $l = 2\lambda_0$ (split pattern).

The HPBW of the H-plane patterns of horns of small H-plane flaring are small. As α_H increases, the measurement of the HPBW becomes difficult due to ripples. For the case of split patterns the HPBW of both beams are very small. The HPBW of E-plane patterns of horns with axial H-plane beams are small. Fig. 4.54. depicts the HPBW variation with frequency and strip-length for two typical horns.

The H-plane side lobe levels of horns of small H-plane flaring are high. For the case of ripples on the main beam, the side lobes are very low. For split patterns also the other lobes are of very low magnitude. The side lobes in the E-plane are very low for the case of axial beam formation. Fig. 4.55. gives a plot of the side lobe level variation with frequency and strip-length for pyramidal SHDHL of flare angle $\alpha_H=10°$,$\alpha_E=20°$ and $\alpha_H=20°$,$\alpha_E=20°$.

The values of 3dB beam width, 10dB beam width and side lobe level for different experimental pyramidal SHDHL antennas are available from Table. 4.14.

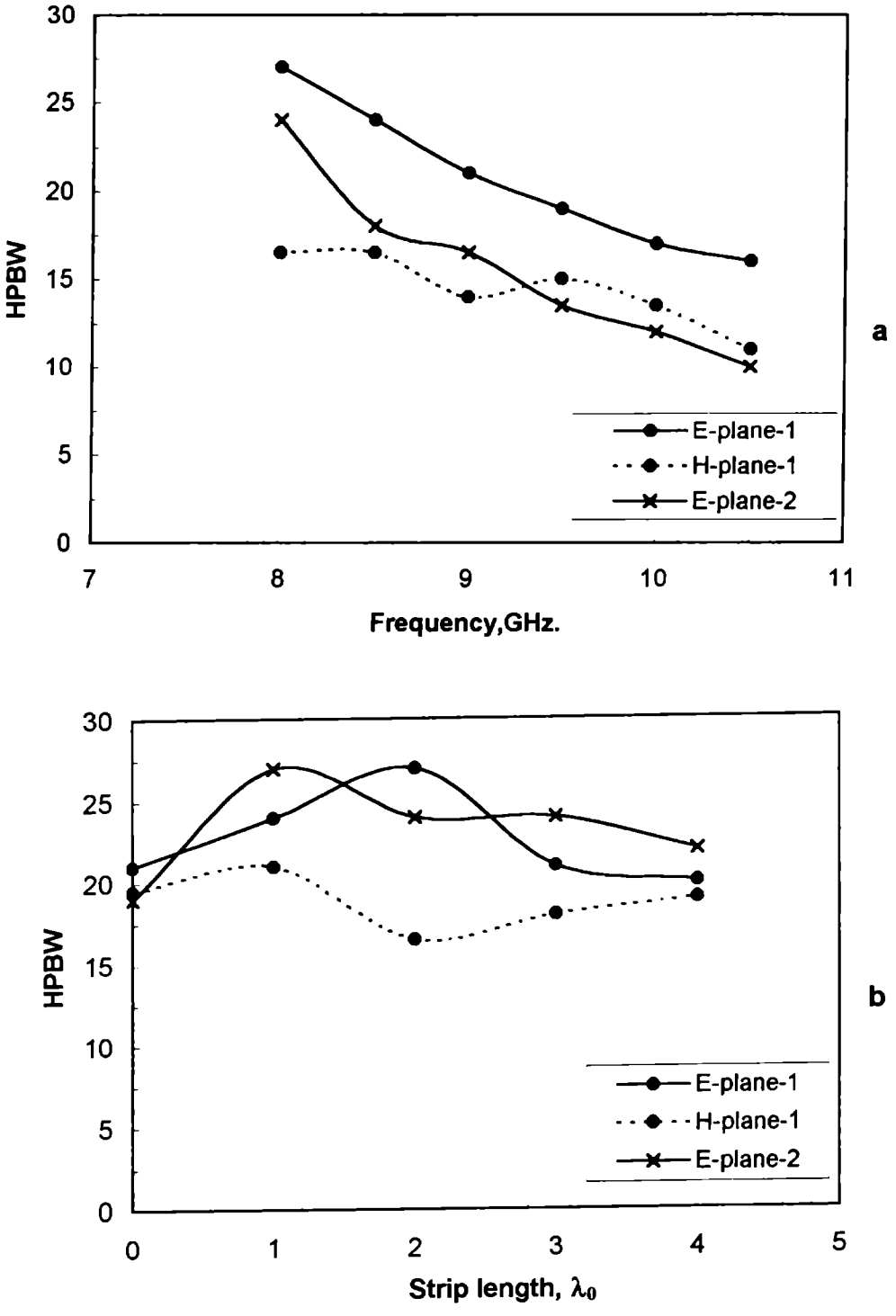

Fig.4.54 E and H-plane HPBW variation with (a) frequency ($l = 2\lambda_0$) and (b) strip length (f = 8GHz), for pyramidal SHDHL, (1) $\alpha_H = 10°, \alpha_E = 20°$ and (2) $\alpha_H = 20°, \alpha_E = 20°$.

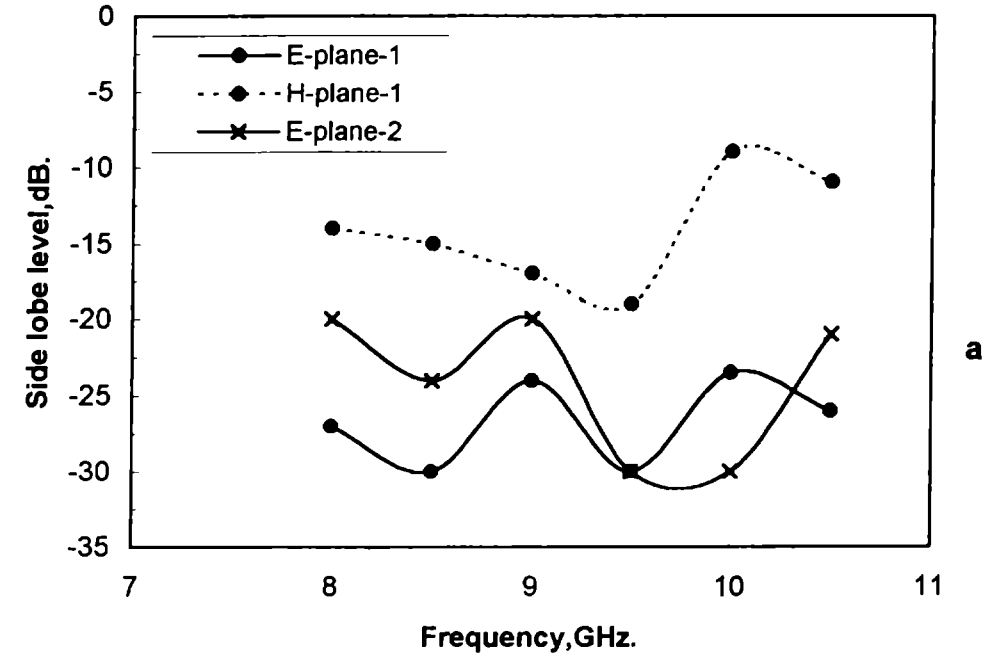

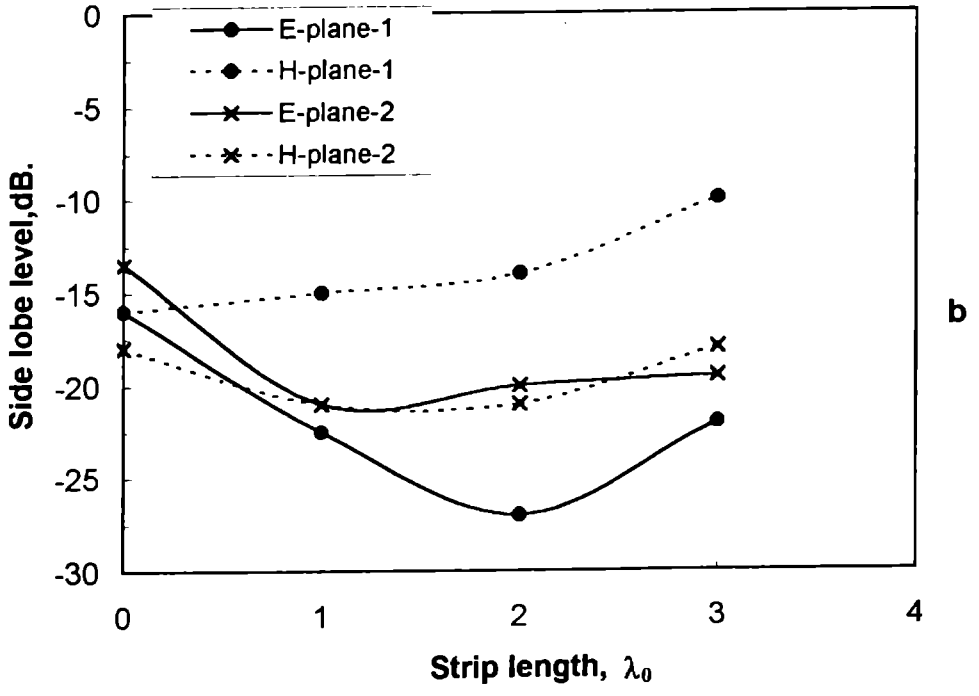

Fig.4.55 Side lobe level variation with (a) frequency ($l = 2\lambda_0$) and (b) strip length (f = 8GHz), for pyramidal SHDHL, (1) $\alpha_H = 10°, \alpha_E = 20°$ and (2) $\alpha_H = 20°, \alpha_E = 20°$.

Table 4.14 3dB beam width, 10dB beam width and first side lobe levels for different pyramidal SHDHL horn antennas at different frequencies.

Flare angle (Degree) α_E α_H	Frequency (GHz)	Strip Length λ_0	3dB beam width (Degree)		10dB beam width (Degree)		First side lobe level (dB)	
			H	E	H	E	H	E
20 10	8.5	1	19.5	19.5	36.0	45.0	-14.0	-21.0
		2	16.5	24.0	45.0	45.0	-15.0	-30.0
		3	18.5	21.0	51.0	37.0	-12.0	-18.0
	9.5	1	16.5	16.5	28.5	31.0	-18.0	-29.5
		2	15.0	19.0	27.0	35.0	-19.0	-30.0
		3	15.0	16.5	34.0	28.5	-16.0	-22.5
	10.5	1	13.5	15.0	22.5	27.0	-11.0	-26.0
		2	11.0	16.0	21.0	28.5	-11.0	-26.0
		3	11.5	14.0	21.0	26.0	-11.0	-22.0
20 20	8.5	1	*	18.0	--	45.0	--	-24.0
		2	*	18.0	--	45.0	--	-24.0
		3	*	20.0	--	42.0	--	-14.5
	9.5	1	*	14.0	--	25.0	--	-18.0
		2	*	13.5	--	25.0	--	-30.0
		3	*	16.5	--	30.0	--	-19.0
	10.5	1	*	12.0	--	19.0	--	-13.0
		2	*	10.0	--	15.5	--	-21.0
		3	*	13.0	--	24.0	--	-15.5
20 30	8.5	1	**	--	--	--	--	--
		2	**	--	--	--	--	--
		3	**	--	--	--	--	--
	9.5	1	**	--	--	--	--	--
		2	**	--	--	--	--	--
		3	**	--	--	--	--	--
	10.5	1	**	--	--	--	--	--
		2	**	--	--	--	--	--
		3	**	--	--	--	--	--
10 20	8.5	1	*	19.5	--	36.0	--	-14.0
		2	*	23.0	--	42.0	--	-16.0
		3	*	24.0	--	45.0	--	-13.0
	9.5	1	*	16.5	--	26.0	--	-14.0
		2	*	18.0	--	29.0	--	-17.0
		3	*	18.0	--	31.5	--	-15.0
	10.5	1	*	12.0	--	21.0	--	-6.0
		2	*	12.0	--	21.0	--	-9.0
		3	*	12.0	--	21.0	--	-16.0
30 20	8.5	1	*	16.0	--	48.0	--	-30.0
		2	*	16.5	--	45.0	--	-18.5
		3	*	16.5	--	40.5	--	-24.0
	9.5	1	*	13.0	--	25.0	--	-32.0
		2	*	12.0	--	22.0	--	-19.0
		3	*	13.0	--	30.0	--	-35.0
	10.5	1	*	10.5	--	27.0	--	-25.0
		2	*	10.0	--	27.0	--	-30.0
		3	*	12.0	--	37.0	--	-27.5

* ripple pattern ** split pattern

4.3.3.2 Cross-polar levels

The cross-polar levels of pyramidal SHDHL are high. Fig. 4.56. is a typical cross-polar plot for SHDHL of flare angles α_H=10° and α_E=20°. The co-polar pattern also is shown The maximum cross-polar levels observed for this case is −19 dB. For split patterns, the maximum cross-polar levels increases up to −16 dB.

4.3.3.3 VSWR and Impedance

Fig. 4.57. gives a comparative study of the impedance and VSWR variation with frequency for pyramidal HDHL and SHDHL. The VSWR of HDHL increases at certain frequencies and decreases at certain other frequencies due to strip-loading. For any horn at fixed frequency, the strip-length variation changes the VSWR .It is shown in Fig. 4.58.

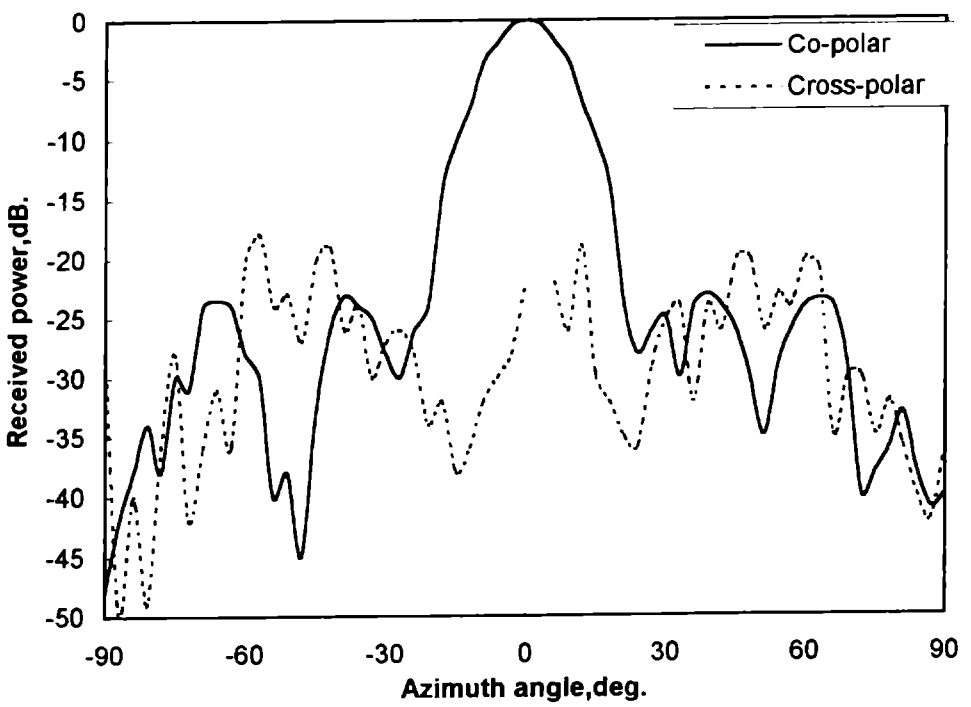

Fig.4.56 Co-polar and cross-polar radiation patterns of pyramidal SHDHL at 10GHz, α_H=10° ,α_E = 20°,l = $2\lambda_0$.

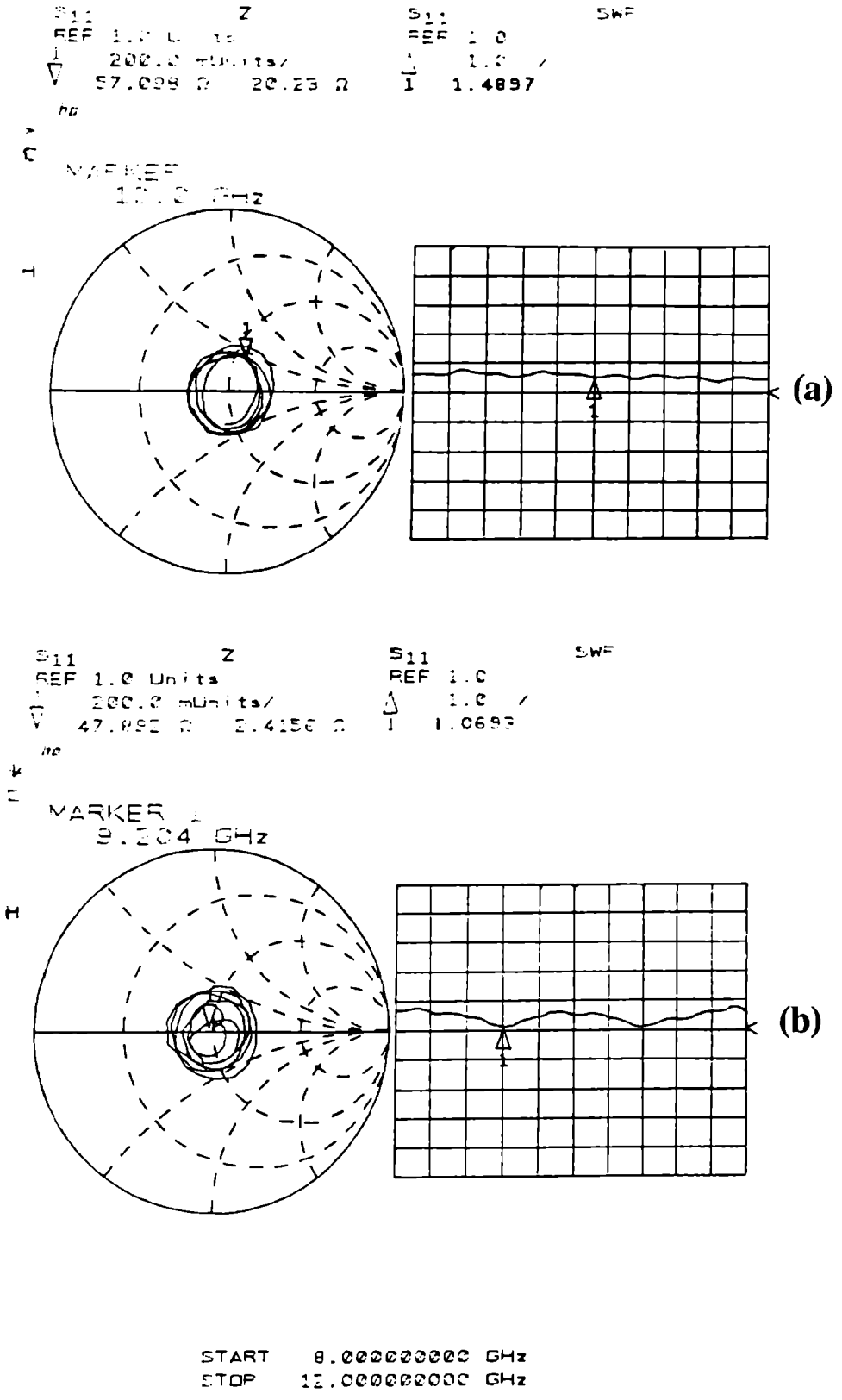

Fig.4.57 VSWR variation with frequency for pyramidal horn.
α_H=10° ,α_E = 20°, l = $2\lambda_0$, (a) HDHL, (b) SHDHL.

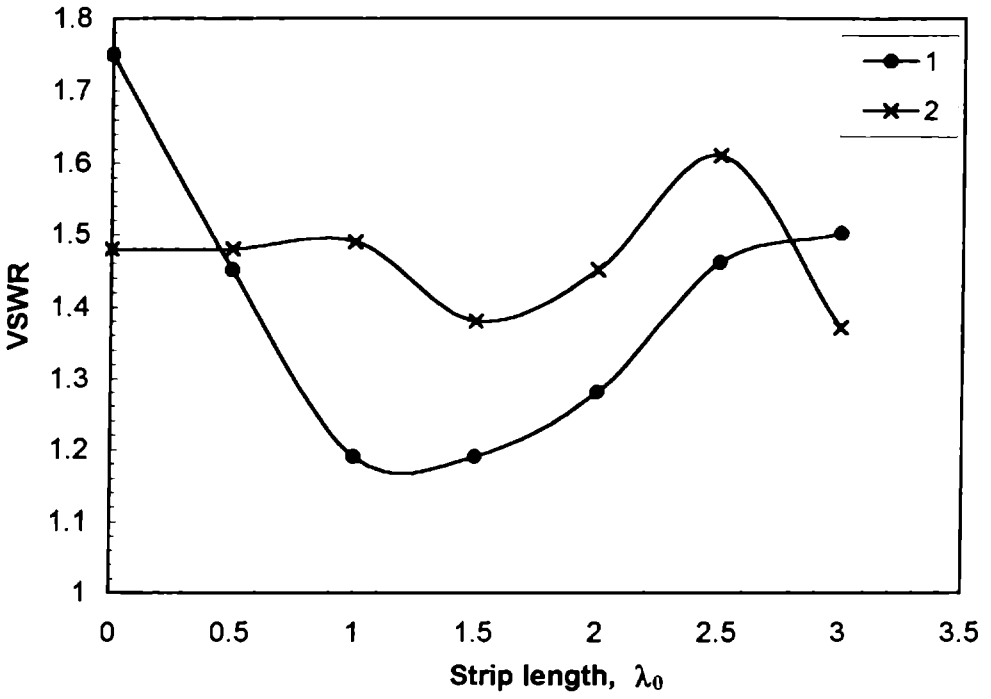

Fig.4.58 VSWR variation with strip length for pyramidal SHDHL at 9.5GHz. for (1) $\alpha_H = 10°, \alpha_E = 20°$ and (2) $\alpha_H = 20°, \alpha_E = 10°$.

4.3.3.4 Directive Gain

The axial gain of horns with small α_H values are high. As α_H increases the gain decreases as for the case of H-plane sectoral SHDHL. Gain variation for two typical horns with frequency is shown in Fig. 4.59. The variation with strip-length is also shown in Fig. 4.60.

Table. 4.15. shows the axial gain for different pyramidal SHDHL antennas for different conditions.

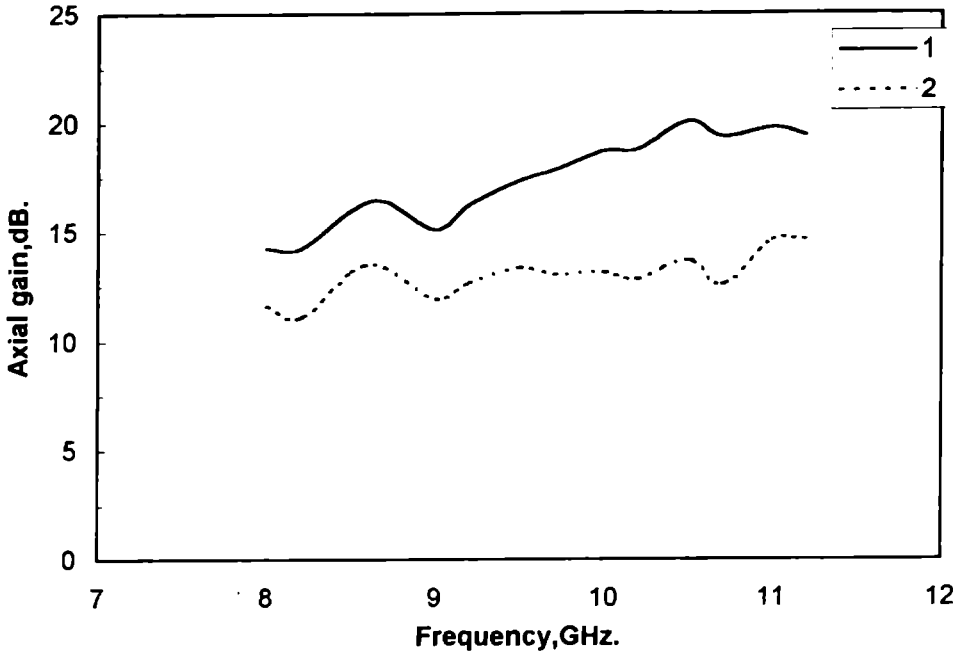

Fig.4.59 Axial gain variation with frequency for pyramidal SHDHL , (1) $\alpha_H = 10°, \alpha_E = 20°$ and (2)$\alpha_H = 20°, \alpha_E = 20°$, $l = 1\lambda_0$.

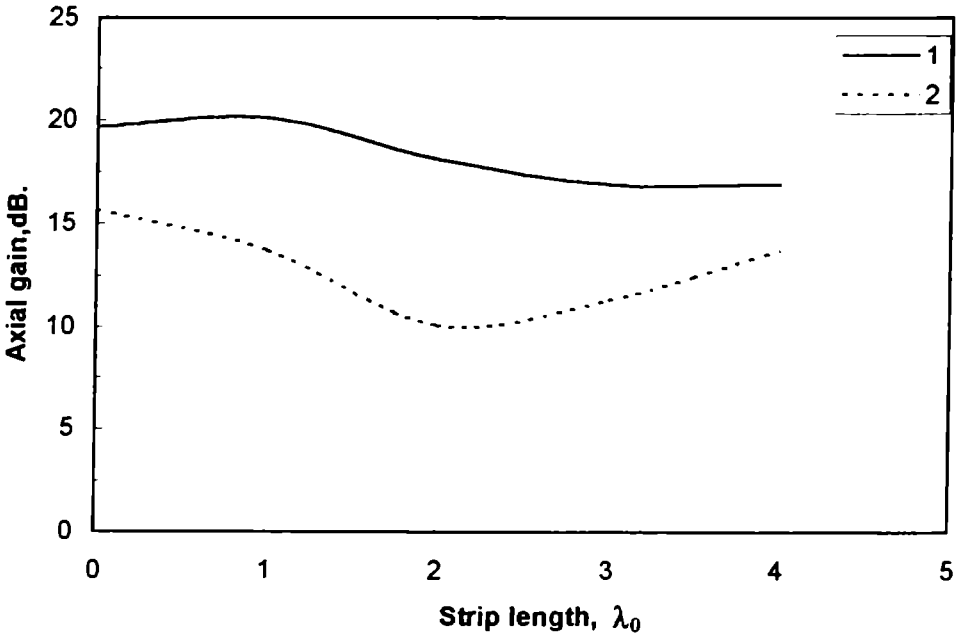

Fig.4.60 Axial gain variation with strip length for pyramidal SHDHL at 10.5GHz.,(1) $\alpha_H = 10°, \alpha_E = 20°$and (2) $\alpha_H = 20°, \alpha_E = 20°$, $l = 1\lambda_0$.

Table 4.15 Axial gain of different pyramidal SHDHL antennas.

Frequency (GHz)	Axial Gain (dB)							
	$\alpha_H = 10°$, $\alpha_E = 20°$				$\alpha_H = 20°$, $\alpha_E = 20°$			
	Strip length(λ_g)				Strip length(λ_g)			
	0	1	2	3	0	1	2	3
8.0	15.2	14.2	13.6	13.2	12.8	11.6	10.0	9.6
8.25	15.0	14.2	13.4	12.2	12.2	11.0	9.8	9.8
8.5	16.6	16.0	16.0	15.2	14.0	13.2	12.4	12.8
8.75	16.8	16.4	15.8	15.4	14.2	13.4	11.4	12.2
9.0	14.7	15.2	13.9	12.9	11.9	11.9	9.1	9.5
9.25	16.8	16.2	15.1	14.2	13.8	12.6	10.2	10.6
9.5	17.9	17.3	16.1	14.9	14.5	13.3	11.3	11.3
9.75	17.3	17.8	16.4	15.4	13.8	13.0	11.4	11.4
10.0	18.7	18.7	17.5	16.3	14.7	13.1	10.7	11.5
10.25	17.6	18.8	16.8	15.6	13.2	12.8	9.6	10.0
10.5	19.6	20.0	18.0	16.8	15.6	13.6	10.0	11.2
10.75	18.2	19.3	17.3	16.3	13.3	12.5	9.7	10.1
11.0	20.4	19.8	17.2	16.2	15.8	14.6	11.0	12.6
	$\alpha_H = 20°$, $\alpha_E = 30°$				$\alpha_H = 20°$, $\alpha_E = 10°$			
8.0	12.8	12.4	10.8	11.6	13.0	12.6	12.4	12.4
8.25	12.2	11.8	11.0	11.4	12.6	12.3	11.5	11.6
8.5	14.0	14.0	13.6	13.6	14.4	13.8	12.9	12.8
8.75	13.8	13.8	13.0	17.0	14.2	13.7	13.0	13.2
9.0	11.5	11.9	9.9	10.3	11.5	11.1	10.5	11.2
9.25	11.0	12.6	11.0	11.4	13.6	13.1	12.5	12.9
9.5	13.3	13.7	11.7	12.9	14.3	13.9	12.9	12.9
9.75	12.6	13.0	11.4	11.4	13.0	12.2	11.5	12.0
10.0	13.9	14.3	13.1	12.7	14.3	13.5	12.8	12.9
10.25	13.2	14.0	13.1	11.6	12.0	11.2	10.9	10.9
10.5	15.6	15.6	13.6	14.0	15.2	14.2	13.9	13.8
10.75	14.1	15.7	14.5	13.7	12.5	11.8	11.5	11.9
11.0	15.0	15.0	13.4	13.4	15.3	14.6	13.9	13.9

4.4 COMPARISON WITH METALLIC HORN ANTENNAS

In order to understand the performance of the test horns it is essential to compare it with standard metallic horn antennas.

4.4.1 E-PLANE SECTORAL HORN

The metallic sectoral horn antennas provides a narrow radiation pattern in the flared plane and a broad pattern in the other plane. In the case of metallic E-plane sectoral horns, the E-plane patterns are narrow and H-plane patterns are broad. But for HDHL and SHDHL we have narrow patterns in both planes. For SHDHL the additional merit of getting identical E and H-plane patterns are also there. Fig. 4.61 gives a comparison of the radiation patterns of three identical HDHL, SHDHL and metallic E-plane sectoral horn antennas.

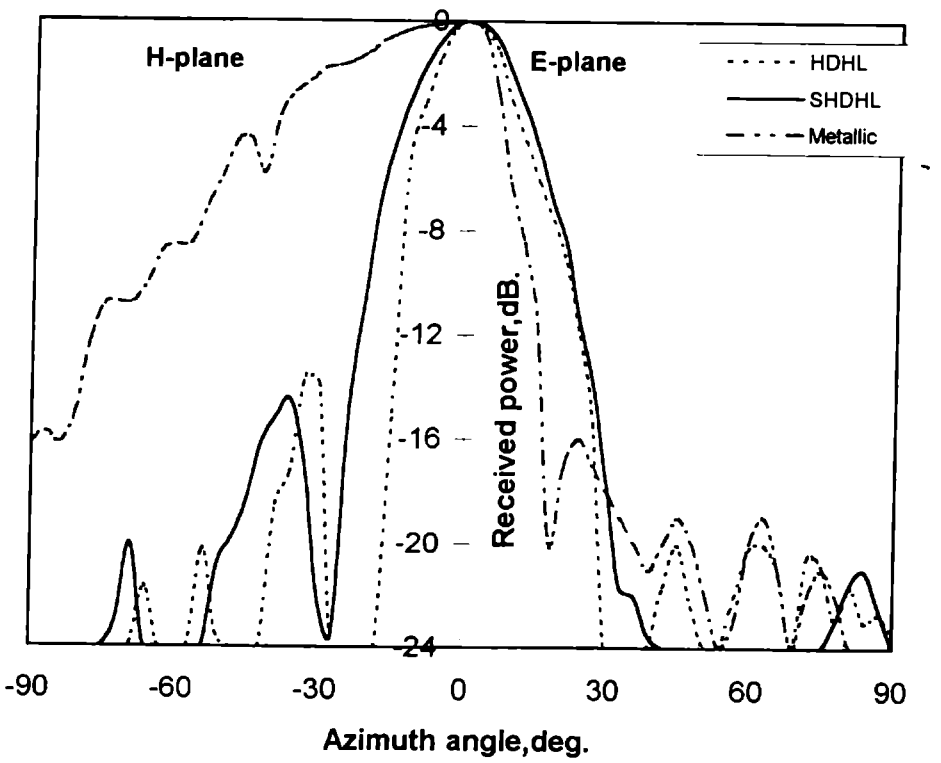

Fig.4.61 Radiation patterns of E-plane sectoral HDHL, SHDHL ($l = 2\lambda_0$) and equivalent metallic horn at 10 GHz, $\alpha_E = 20°$.

HDHL and SHDHL give high gain due to the narrow E and H-plane patterns and low VSWR. It is always greater than the gain of an equivalent metallic horn. Fig. 4.62. gives the axial gain variation with frequency for the test horn and its metallic counterpart.

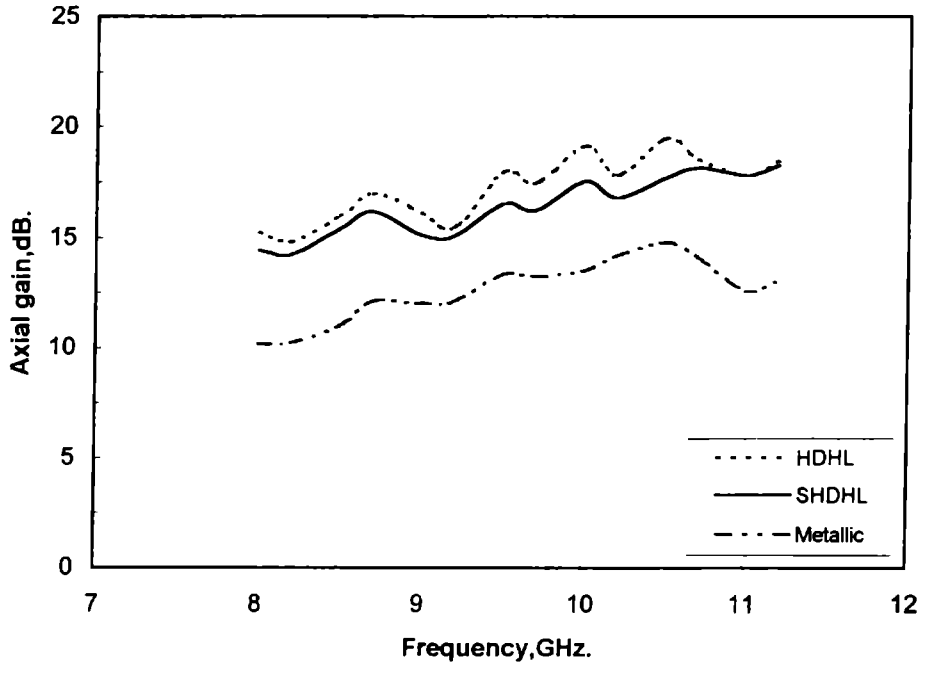

Fig.4.62 Axial gain variation with frequency for E-plane sectoral HDHL, SHDHL ($l = 1\lambda_0$) and equivalent metallic horn, $\alpha_E = 20°$.

4.4.2 H-PLANE SECTORAL HORN

The radiation patterns of metallic H-plane sectoral horns are narrow in the H-plane and broad in the E-plane. The patterns for the corresponding HDHL and SHDHL are in the other way. i.e., narrow E-plane pattern and broad H-plane pattern. For small flared horns, the H-plane HPBW also is small and as the flare angle increases, the pattern becomes broad or split. A plot of radiation patterns of H-plane sectoral dielectric and metallic antennas are shown in Fig. 4.63.

The axial gains of dielectric H-plane sectoral horns are slightly greater than that of equivalent metallic horns. Fig. 4.64. shows the gain variation with frequency for the metallic and experimental antennas of the same dimensions.

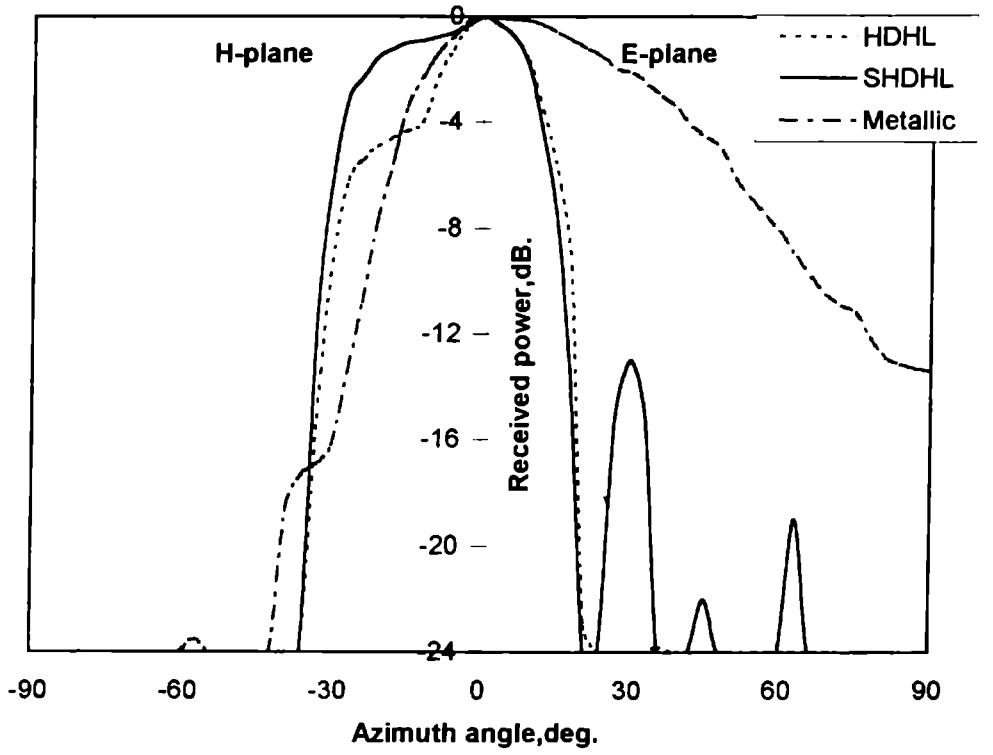

Fig.4.63 Radiation patterns of H-plane sectoral HDHL, SHDHL ($l = 3\lambda_0$) and equivalent metallic horn at 10GHz, $\alpha_H = 20°$.

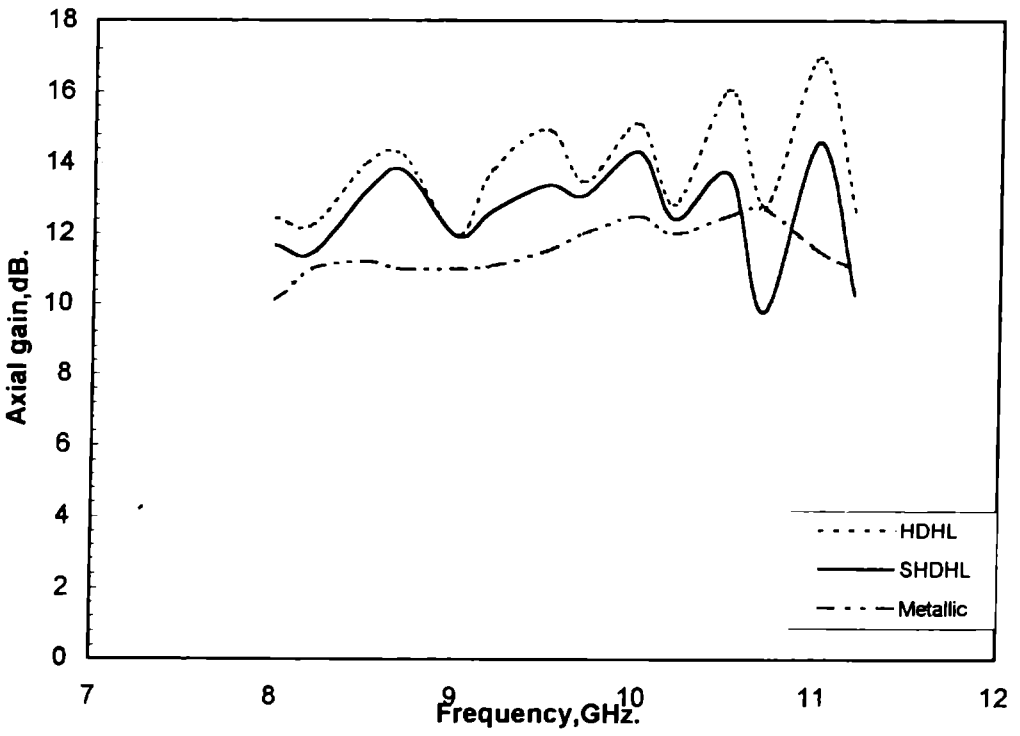

Fig.4.64 Axial gain variation with frequency for H-plane sectoral HDHL, SHDHL ($l = 1\lambda_0$) and equivalent metallic horn, $\alpha_H = 20°$.

4.4.3 PYRAMIDAL HORN

Metallic pyramidal antennas have narrow radiation patterns in both planes. The patterns of pyramidal dielectric test antennas are almost similar to that of metallic, for small values of α_H. It is shown in fig. 4.65. As αH increases the H-plane patterns deviates from that of the metallic horns.

The gain of pyramidal HDHL and SHDHL are less than that of equivalent metallic horns for almost all frequencies, as shown by Fig. 4.66.

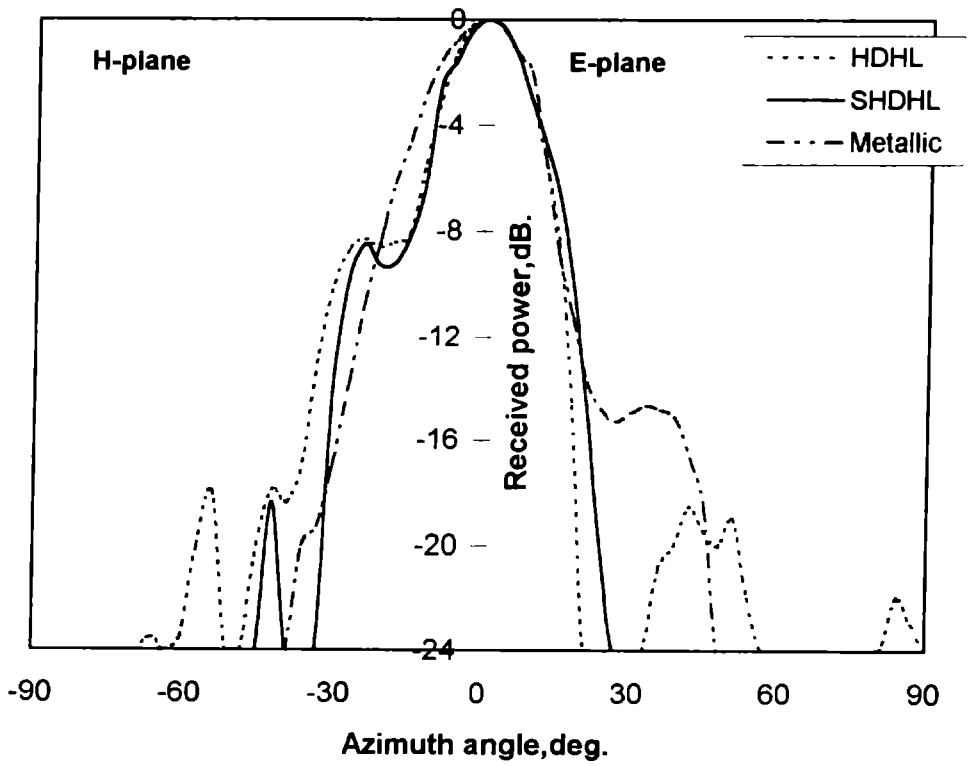

Fig.4.65 Radiation patterns of pyramidal HDHL, SHDHL ($l = 2\lambda_0$) and equivalent metallic horn at 9GHz, $\alpha_H = 10°$, $\alpha_E = 20°$.

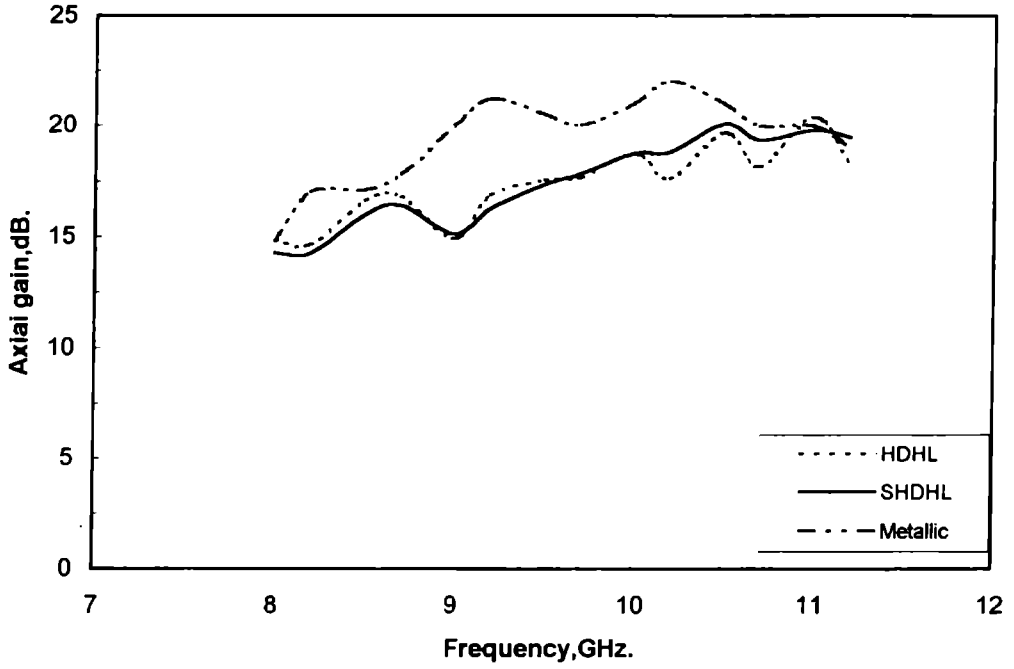

Fig.4.66 Axial gain variation with frequency for pyramidal HDHL, SHDHL ($l = 1\lambda_0$) and equivalent metallic horn, $\alpha_H = 10°$, $\alpha_E = 20°$

Chapter 5

THEORETICAL CONSIDERATIONS

Theoretical analysis of the new hollow dielectric horn antennas is presented in this chapter. The hollow dielectric horn is considered as a solid horn of effective dielectric constant and the aperture field distribution is analyzed based on Marcatili's principle. The feed end of the horn suffers a sudden discontinuity and so the radiation from both feed-end and free-end is considered. The far field radiation pattern is analyzed using 'two-aperture theory' and the effect of strip loading is explained using diffraction theory and image theory.

5.1 RADIATION FROM HOLLOW DIELECTRIC HORN ANTENNAS (HDHL)

Radiation from dielectric rod and horn antennas have been theoretically analyzed by several workers using different methods [26,28,32-44]. The hollow dielectric horn is excited by an open metallic waveguide. The feed-end (open waveguide) of the horn offers a sudden discontinuity for the electromagnetic energy. So the radiation from both feed-end and free-end is taken into consideration. The radiation from the flared sides is neglected. So the most suitable model for the analysis of the HDH antennas is the 'two-aperture' theory.

To find radiation from the hollow dielectric horn antenna, knowledge of the electromagnetic field distribution in and around the horn is essential. The horn structure offers a lot of complications to the boundary conditions and so we need some simplifying assumptions to proceed with the analysis. For reducing the number of existing boundaries, the HDH is assumed to be a solid dielectric horn of effective dielectric constant ε_{eff}. The aperture field distribution and the propagation constants can be computed using Marcatili's principle taking TE to y hybrid mode into considerations.

Knowing the aperture field, the far field radiation due to the free end can be analyzed using scalar diffraction integral. The feed-end radiation is calculated from the aperture field of the open waveguide. The resultant radiation pattern in the far field is the vector sum of the radiation from the feed-end and the free-end.

5.1.1 HDH as a solid horn of effective dielectric constant

For applying Marcatili's principle to the HDH antenna, it is assumed to be a solid horn of effective dielectric constant ε_{eff}. Fig.5.1 shows the E-plane sectoral HDH and its equivalent solid horn.

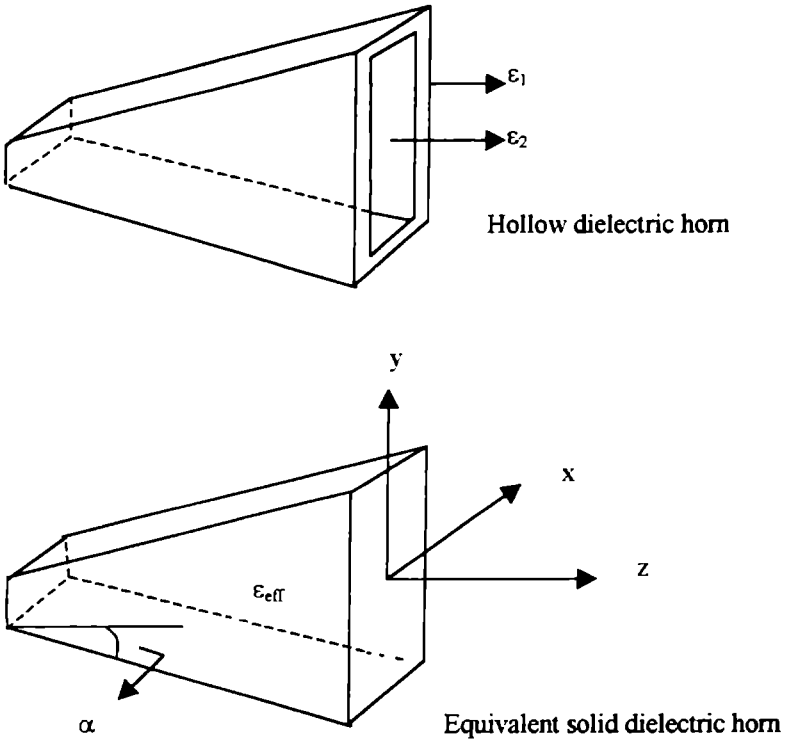

Fig.5.1 HDH and its equivalent solid horn.

For calculating the effective dielectric constant of the sectoral horn, the following formula can be used [128].

$$\varepsilon_{eff} = \frac{2\varepsilon_1(V_1 + V_2) + \varepsilon_2 V_3}{V} \qquad \text{——— (1)}$$

Where, ε_{eff} = Effective dielectric constant

ε_1 = Dielectric constant of the material of the horn

ε_2 = Dielectric constant of air

V_1&V_2 = Volume consumed by E and H walls

V_3 = Volume of air enclosed by the horn

$V = 2(V_1+V_2)+V_3$; Total volume

Using Eqn.(1), for E-plane sectoral horns,

$$\varepsilon_{eff} = \frac{\left[2\varepsilon_1 t\left(\frac{a}{\cos\alpha} + L\tan\alpha + b\right) + \varepsilon_2 a\left(L\tan\alpha + b\right)\right]}{\left[2t\left(\frac{a}{\cos\alpha} + L\tan\alpha + b\right) + a\left(L\tan\alpha + b\right)\right]} \quad \text{—— (2)}$$

Where a = broader dimension of the waveguide (a_0)

b = smaller dimension of the waveguide (b_0)

L = axial length of the horn

t = thickness of the dielectric sheet

and α = semi flare angle of the E-plane sectoral horn

For H-plane sectoral horns, the effective dielectric constant is given by [129],

$$\varepsilon_{eff} = \frac{\left[\varepsilon_2(2ab + bL\tan\alpha) + \varepsilon_1\left(\left(\frac{2bt}{\cos\alpha}\right) + 2Lt\tan\alpha + 4at\right)\right]}{\left[2ab + bL\tan\alpha + \left(\frac{2bt}{\cos\alpha}\right) + 2Lt\tan\alpha + 4at\right]} \quad \text{—— (3)}$$

where, α = semi flare angle of the H-plane sectoral horn.

Using equations (2) and (3), ε_{eff} can be calculated. It is a function of axial length and so it varies as L changes. For t = 2mm, the variation of ε_{eff} with length L for different E-plane sectoral horns is shown in Fig.5.2. It shows that the effective dielectric constant is not a constant throughout the horn for a given length [130]. While calculating the propagation constant inside the horn, we have to take this point also into consideration.

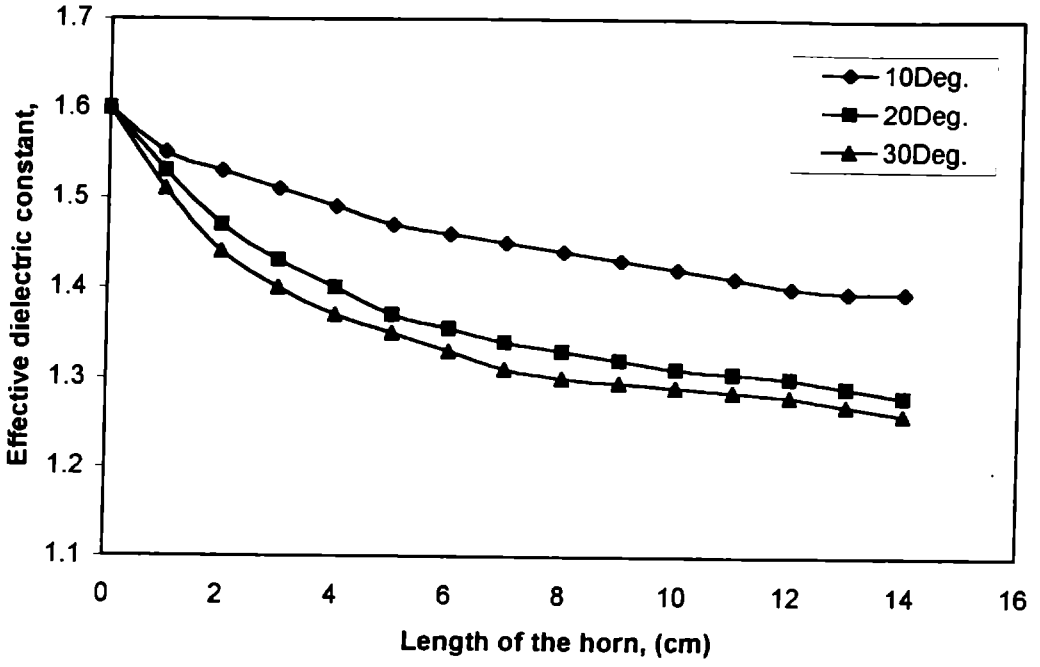

Fig.5.2 Variation of ε_{eff} with horn length for E-plane sectoral horns of different flare angles.

5.1.2 Aperture fields and characteristic equation

The propagating modes in rectangular dielectric guides belong to either E_{pq}^{y} or E_{pq}^{x} or both the hybrid mode configurations. But the fields propagating through the guides are also governed by the field configurations at the feed point (launcher). In the present study the HDH is excited by rectangular metallic waveguide carrying TE_{10} mode. So the fields inside the horn are also assumed to be TE_{10} mode with E-vector in the y direction.

For the evaluation of the aperture fields and propagation constants for the HDH using Marcatili's principle, certain assumptions are made. The theory is applicable

to cases where the difference in refractive index between the guide and the surrounding medium is very small. In the case of HDH also we assume that,

$$\frac{\varepsilon_{eff} - \varepsilon_2}{\varepsilon_{eff}} << 1$$

Marcatili's principle, which is actually suggested for dielectric rods, can be extended to horns by considering the horn structure as a collection of dielectric rods of gradually increasing dimensions as shown in Fig.5.3. For each section (step) of the uniform rectangular dielectric guides, the propagation constants and field components are assumed to be the same as that for an infinitely long guide. The propagation constants depend on the dimensions of the aperture plane. For each rod the aperture area is different and so the propagation constants will be different. The change in the value of ε_{eff}, while moving from one section to another, will also affect the propagation constant.

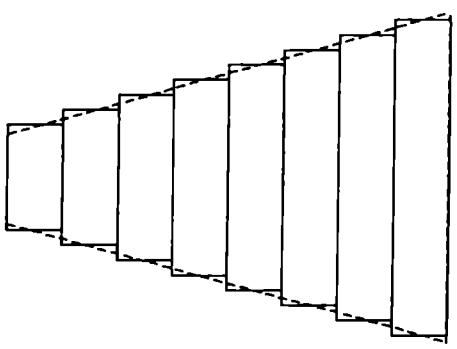

Fig.5.3 Horn structure as a collection of uniform rods of gradually increasing dimensions.

The dielectric horn of permittivity ε_{eff} and permeability μ_1 is assumed to be immersed in a medium (air) of permittivity ε_2 and permeability μ_2, as shown in Fig.5.4. The field variations are assumed to be sinusoidal inside the cross-section of the guide. The fields along the corner regions are neglected.

Assuming the presence of TE_{pq}^{y} hybrid modes inside the guide, the field components and hence the characteristic equation for wave propagation can be analyzed from the Hertz potential π_e, given by[17,51],

$$\overline{\pi}_e = \hat{a}_y \overline{\pi}_{ey} \qquad \text{(4)}$$

a_y is the unit vector in the y direction.

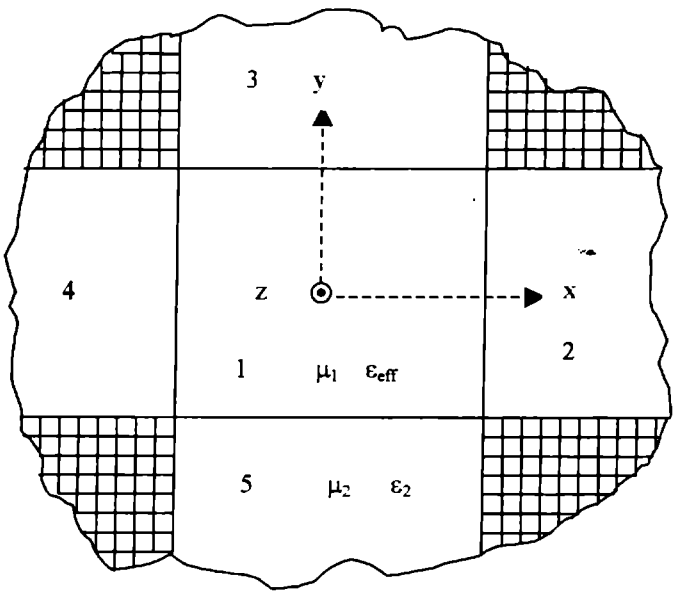

Fig.5.4 Cross-section of the horn divided into different regions.

The scalar wave equation is,

$$\nabla^2 \pi_{ey} = k_\upsilon^2 \pi_{ey} \qquad \text{(5)}$$

where, $k = (2\pi/\lambda)$, is the propagation constant

$\upsilon = 1, 2, 3\ldots$ for different medium.

The solution of the wave equation in different regions 1 through 5 are assumed to be as follows.

For region 1,

$$\pi_{ey_1} = C_1 \cos(k_{x1}x)\cos\left(k_{y1}y\right)\exp[-jk_{z1}z] \qquad \text{(6)}$$

For region 2 and 4,

$$\pi_{ey2(4)} = C_{2(4)} \exp[\pm k_{x2(4)}x]\cos(k_{y2(4)}y)\exp\left[-jk_{z2(4)}z\right] \qquad \text{(7)}$$

For region 3 and 5,

$$\pi_{ey3(5)} = C_{3(5)} \cos(k_{x3(5)}x)\exp[\pm k_{y3(5)}y]\exp[-jk_{z3(5)}z] \qquad \text{(8)}$$

k_x, k_y and k_z are the propagation constants x y and z directions respectively. Solving for the field components, for region 1 we get,

$$\begin{aligned}
E_{x1} &= C_1(k_x k_y)\sin(k_x x)\sin(k_y y)\exp[-jk_z z] \\
E_{y1} &= C_1(k_x^2 + k_z^2)\cos(k_x x)\cos(k_y y)\exp[-jk_z z] \\
E_{z1} &= C_1(jk_z)\cos(k_x x)\sin(k_y y)\exp[-jk_z z] \\
H_{x1} &= C_1(-\omega\varepsilon_1 k_z)\cos(k_x x)\cos(k_y y)\exp[-jk_z z] \\
H_{y1} &= 0 \\
H_{z1} &= C_1(-\omega\varepsilon_1 k_x)\sin(k_x x)\cos(k_y y)\exp[-jk_z z]
\end{aligned} \qquad \text{(9)}$$

The field components for other regions can also be derived in a similar manner. Applying the boundary conditions, for the uniform rod, we get the characteristic equation as[17],

$$\begin{aligned}
k_x \tan\left(k_x \frac{a}{2}\right) &= \left(k_1^2 - k_0^2 - k_x^2\right)^{1/2} \\
k_y \tan\left(k_y \frac{b}{2}\right) &= \frac{\varepsilon_1}{\varepsilon_2}\left(k_1^2 - k_0^2 - k_y^2\right)^{1/2}
\end{aligned} \qquad \text{(10)}$$

For the case of horns, the aperture dimensions are functions of length L. So for an E-plane sectoral horn, the equation changes to,

$$k_x \tan\left(k_x \frac{a}{2}\right) = \left(k_1^2 - k_0^2 - k_x^2\right)^{1/2}$$
$$k_y \tan\left(k_y\left(\frac{b}{2} + L\tan\alpha\right)\right) = \frac{\varepsilon_{eff}}{\varepsilon_2}\left(k_1^2 - k_0^2 - k_y^2\right)^{1/2} \qquad \text{——————} \quad (11)$$

For H-plane sectoral horns, we get

$$k_x \tan\left(k_x\left(\frac{a}{2} + L\tan\alpha\right)\right) = \left(k_1^2 - k_0^2 - k_x^2\right)^{1/2}$$
$$k_y \tan\left(k_y \frac{b}{2}\right) = \frac{\varepsilon_{eff}}{\varepsilon_2}\left(k_1^2 - k_0^2 - k_y^2\right)^{1/2} \qquad \text{——————} \quad (12)$$

k_0 is the free space propagation constant.

Solving (11) we get the value of k_x and k_y for E-plane sectoral horns. From (12), k_x and k_y for H-plane sectoral horns can be calculated.

$$k_x^2 + k_y^2 + k_z^2 = k_1^2$$
$$k_1^2 = \varepsilon_r k_0^2 = \varepsilon_{eff} k_0^2 \qquad \text{——————} \quad (13)$$

$\therefore k_z$, the longitudinal propagation constant can be calculated.

For solving the characteristics equation we have to use Newton Raphson's iteration procedure. The propagation constants k_x, k_y and k_z change with length of the horn because of two reasons. Initially as the length of the horn changes, the cross sectional area of the assumed uniform guide changes and is accounted by the term 'Ltanα' in the expression for characteristics equation. Secondly, the effective dielectric constant of the equivalent solid horn changes with the length of the horn. The variation of kx, ky and kz with length for different E-plane and H-plane sectoral horns are shown in Fig.5.5 and Fig.5.6. From these plots we can find the values of k_x, k_y and k_z for any selected length of the horn which can be substituted in the expression for the aperture electric field for computing the far field pattern.

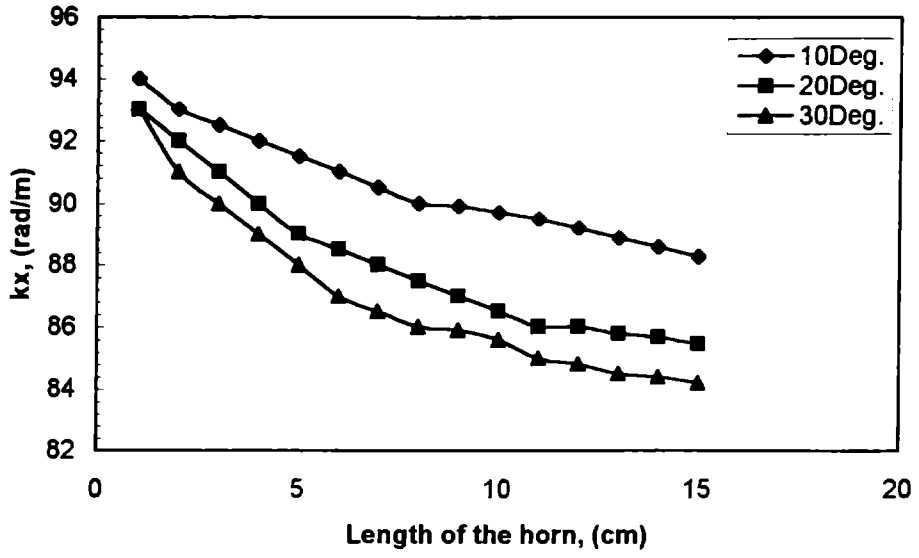

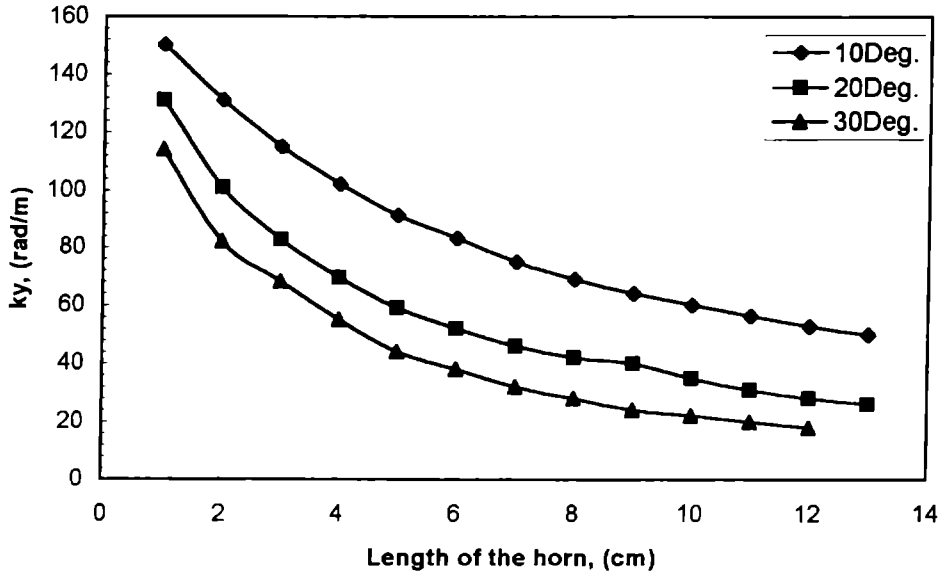

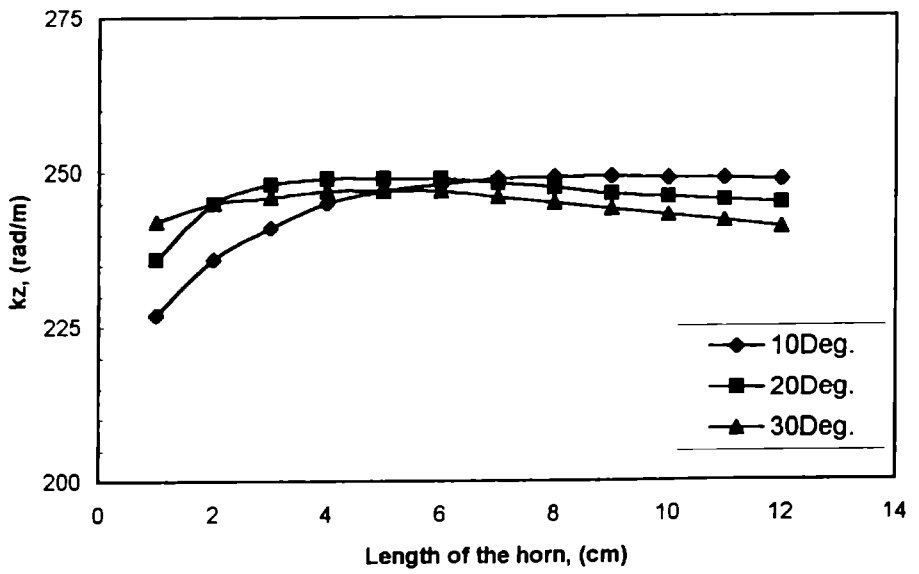

Fig.5.5 Variation of k_x, k_y and k_z with axial length for E-plane sectoral horn.

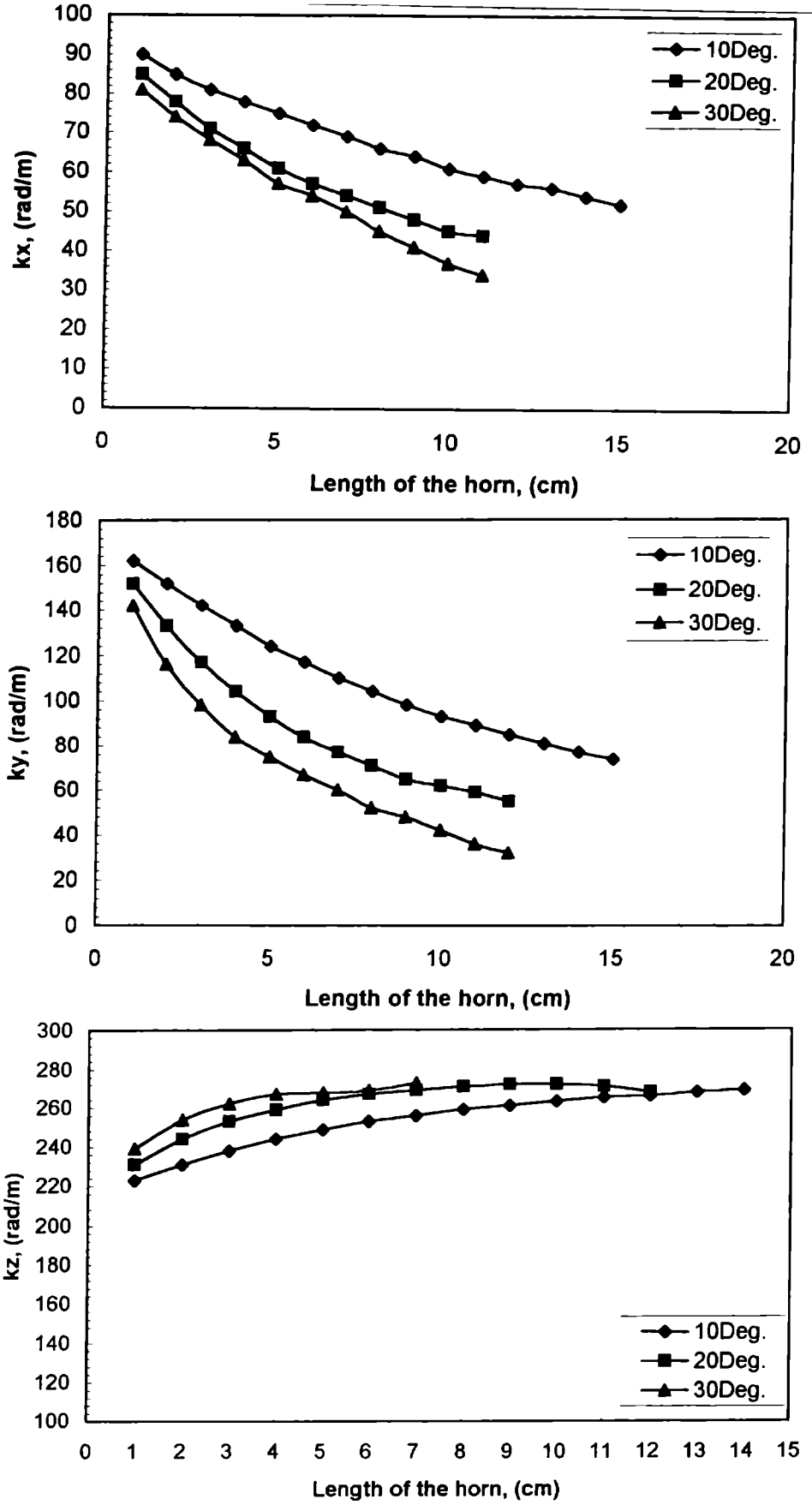

Fig.5.6 Variation of k_x, k_y and k_z with axial length for H-plane sectoral horn .

5.1.3 Role of the launcher

The role of the launcher is to provide good launching. The presence of the launcher increases the launching efficiency and hence reduces the feed-end discontinuity, which in turn will decreases the leakage of power radiated from the feed-end. As the role of the launcher is in increasing the launching efficiency, it is assumed that the launcher is not contributing to the effective dielectric constant of the horn. So the presence of the launcher is not taken into account for evaluating the effective dielectric constant of the hollow horn. Therefore the analysis of HDH and HDHL differs only on the value of the constant C_1 of equation (9).

5.1.4 Radiation patterns of HDHL

As mentioned in the previous section 5.1.2, the rectangular horn is approximated by a cascading uniform guides (Fig.5.3). While moving from the feed end to the free end, we can see that the aperture dimensions of each guide increase gradually. The radiation from the aperture of the first guide is emerging into the second guide and that from the second is into the third and so on. So the radiation from all the uniform guides will finally pass through the free end. i.e., through the aperture of the last section. Neglecting the radiation from the sides of each guides, we can assume that the horn radiates only from its free-end. Due to the discontinuity at the launching section, the feed-end also contributes to the radiated power. Therefore we can apply 'two-aperture theory' by considering the radiation from the free-end and the feed-end.

5.1.4.1 Free-end radiation

Knowing the aperture field distribution at the free-end of the horn, the far field pattern can be evaluated using scalar diffraction integral [36]. The diffracted field U_P at any point P due to the aperture field $F_{(x,y)}$ over the aperture A is given by,

$$U_P = \frac{1}{4\pi}\int_A F_{(x,y)} \frac{e^{(-jk_0 r)}}{r}\left[\left(jk_0 + \frac{1}{r}\right)\bar{i}_z.\bar{r}_1 + jk_0\bar{i}_z.\bar{s}\right]dxdy \quad \text{——— (14)}$$

where,

U_P = diffracted field at P

$F_{(x,y)} = A_{(x,y)} \exp[-j\Psi_{(x,y)}]$

$A_{(x,y)}$ = amplitude distribution of field over A

$\Psi_{(x,y)}$ = phase distribution of field over A

r = distance to point P from any point (x,y) on the aperture

r = unit vector in the direction of the field

s = unit vector normal to the wave front at the aperture plane

The co-ordinate system used for evaluating the far field is shown in Fig.5.7. For the far field region this equation reduces to,

$$U_P = \frac{j}{2\lambda}\frac{e^{(-jk_0 R)}}{R}\int_A F_{(x,y)}\left(\cos\theta + \bar{i}_z.\bar{s}\right)e^{(jk_0 \sin\theta(x\cos\phi + y\sin\phi))}dxdy \quad \text{——— (15)}$$

where R = distance of P from the origin

If the phase error over the aperture (deviation from constant phase) is small, the expression changes to [36],

$$U_P = \frac{-j}{2\lambda}\frac{e(jk_0 R)}{R}\left(1+\cos\theta\right)\int_A F_{(x,y)}e^{(jk_0 \sin\theta(x\cos\phi + y\sin\phi))}dxdy \quad \text{——— (16)}$$

The assumption of constant phase over the aperture is valid only for small apertures. However for horns of moderate flare angle this assumption is found to be correct. Substituting the value of aperture field in the above expression, the far field radiation pattern from the free-end can be calculated. The contributions to the far field due to the field distributions over the outer regions 2, 3, 4 and 5 can also be calculated using the same expression. In the present study, though the horn is considered as a solid

horn of effective dielectric constant ε_{eff}, the actual situation is that of a hollow horn and so the walls of the horns help the power to concentrate well inside the horn. Because of this reason, we can make a reasonable assumption that the field distributions in the outer regions are negligibly small. So for calculating the far field radiation pattern, the aperture field on the region 1 alone is considered.

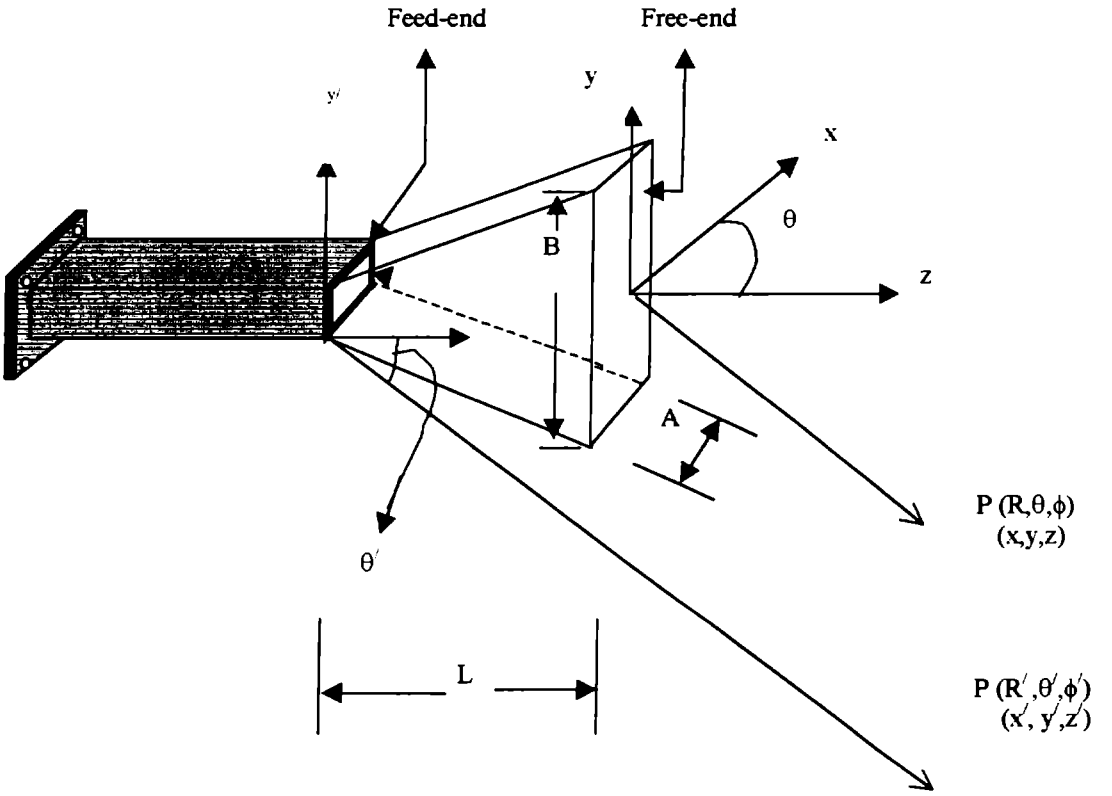

Fig.5.7 Co ordinate system to evaluate the free-end and feed-end radiation.

We have Eqn.(16) for free-end as an equi-phase plane. Hence $\Psi_{(x,y)}$=constant.

$\therefore F_{(x,y)} = A_{(x,y)} = E_{y(x,y)}$; as given by Eqn.(9) for region 1.

$$\therefore U_P = \frac{-j}{2\lambda R}\frac{e^{(-jk_0R)}}{R}(1+\cos\theta)\int_{-\frac{B}{2}}^{+\frac{B}{2}}\int_{-\frac{A}{2}}^{+\frac{A}{2}}|Ey|e^{(jk_0\sin\theta(x\cos\phi+y\sin\phi))}dxdy \quad \text{——— (17)}$$

we have,

$$E_{y1} = C_1(k_x^2 + k_z^2)\cos(k_x x)\cos(k_y y)$$

$$\therefore U_P = \frac{j}{\lambda}\left\{\left(\frac{1+\cos\theta}{2}\right)\left(\frac{e^{(-jk_0R)}}{R}\right)\int_{-\frac{B}{2}}^{+\frac{B}{2}}\int_{-\frac{A}{2}}^{+\frac{A}{2}}C_1(k_x^2+k_y^2)\cos(k_x x)\cos(k_y y)e^{(jk_0\sin\theta(x\cos\phi+y\sin\phi))}dxdy\right\}$$

——(1 8)

E (ϕ =90°) plane and H (ϕ =0°) plane pattern can be evaluated from this equation by changing the value of θ from -90° to +90°.

5.1.4.2 Feed-end radiation

The feed-end is an open waveguide. The feed-end radiation term is to account for the direct (unperturbed) radiation from the feed aperture.

Using the co-ordinate system shown in Fig.5.7, the far field radiation pattern of an open waveguide aperture carrying TE_{10} mode is given by [7,36,41],

$$U'_{P\theta'} = -C_2\left(\frac{\mu_0}{\varepsilon_0}\right)^{1/2}\frac{\pi a_0^2 b_0}{2\lambda^2 R'}\sin\phi'\left[1+\frac{\beta_{10}}{k_0}+\Gamma\left(1-\frac{\beta_{10}}{k_0}\cos\theta'\right)\right]\times$$
$$\left[\frac{\cos\left(\frac{\pi a_0}{\lambda}\sin\theta'\cos\phi'\right)}{\left(\frac{\pi a_0}{\lambda}\sin\theta'\cos\phi'\right)^2-\left(\frac{\pi}{2}\right)^2}\right]\left[\frac{\sin\left(\frac{\pi b_0}{\lambda}\sin\theta'\sin\phi'\right)}{\frac{\pi b_0}{\lambda}\sin\theta'\sin\phi'}\right]\times \quad \text{———} \quad \text{(19.a)}$$
$$e^{-j\left[k_0R'-\frac{\pi}{\lambda}\sin\theta'(a_0\cos\phi'+b_0\sin\phi')\right]}$$

$$U'_{P\phi'} = -C_2\left(\frac{\mu_0}{\varepsilon_0}\right)^{1/2}\frac{\pi a_0^2 b_0}{2\lambda^2 R'}\cos\phi'\left[\cos\phi' + \frac{\beta_{10}}{k_0} + \Gamma\left(\cos\theta' - \frac{\beta_{10}}{k_0}\right)\right]\times$$

$$\left[\frac{\cos\left(\frac{\pi a_0}{\lambda}\sin\theta'\cos\phi'\right)}{\left(\frac{\pi a_0}{\lambda}\sin\theta'\cos\phi'\right)^2 - \left(\frac{\pi}{2}\right)^2}\right]\left[\frac{\sin\left(\frac{\pi b_0}{\lambda}\sin\theta'\sin\phi'\right)}{\frac{\pi b_0}{\lambda}\sin\theta'\sin\phi'}\right]\times \quad \text{——} \quad (19.b)$$

$$e^{-j\left[k_0 R' - \frac{\pi}{\lambda}\sin\theta'(a_0\cos\phi' + b_0\sin\phi')\right]}$$

where $\beta_{10} = k_0^2 - \left(\frac{\pi}{b_0}\right)^2$

Γ = reflection coefficient

$$U'_P = U'_{P\theta'}\cos\theta'\sin\phi' + U'_{P\phi'}\cos\theta' \quad \text{——————} \quad (20)$$

This expression gives the radiation pattern with respect to one corner of the waveguide. So it is necessary to transform the expression to a co-ordinate system with origin at the center of the aperture, so that the feed end radiation can be vectorially added. The required transformation equations are,

$$R' = \left[(x')^2 + (y')^2 + (z')^2\right]^{1/2}$$

$$\theta' = \tan^{-1}\left\{\left[(x')^2 + (y')^2\right]^{1/2} / z'\right\} \quad \text{——————} \quad (21)$$

$$\phi' = \tan^{-1}\left(y'/x'\right)$$

and

$$x' = R\sin\theta\cos\phi + a_0/2$$

$$y' = R\sin\theta\sin\phi + b_0/2 \quad \text{——————} \quad (22)$$

$$z' = R\cos\theta + L$$

5.1.4.3 Superposition of radiations from feed-end and free-end

To get the total radiated field in the far field, the radiations from the feed-end and free-end are vectorially added.

$$U_T = U_P + U'_P \qquad \text{(23)}$$

The interference between the radiations from the two sources produces sharp nulls in the resultant patterns. This effect is very significant from the experimental patterns also. Before adding the two components, we have to know the fraction of power radiated from the feed end. The constant C_2 included along with the amplitude term of the expression for radiation from the feed-end is to account for this. A change of the ratio C_1/C_2, changes the depth of the minima of the theoretical radiation patterns. So the ratio C_1/C_2 is adjusted by iteration, for the nulls of the theoretical patterns coincides well with the experimental patterns. The role of the launcher is to change the value of this ratio, so that the component radiated from the feed-end decreases.

5.1.5 Results

The theoretical radiation patterns in the E and H planes are plotted for different horns. The theoretical patterns agrees well with the experimental patterns for E-plane sectoral HDHL antennas. Fig.5.8 shows a typical plot for a horn of flare angle 20° at 10 GHz. In the H-plane the side lobe levels are found to be greater for the theoretical patterns than that of the experimental patterns for all cases. The value of HPBW and the position of the nulls of the theoretical patterns well agree with that of the experimental results.

For H-plane sectoral horns, the theoretical patterns in the E-plane almost agree with the experimental plot as shown in Fig.5.9. The positions of the minima are the same, but the HPBW and side lobe levels for the theoretical patterns are found to be slightly greater than that for the experimental patterns. In the H-plane the theory agrees

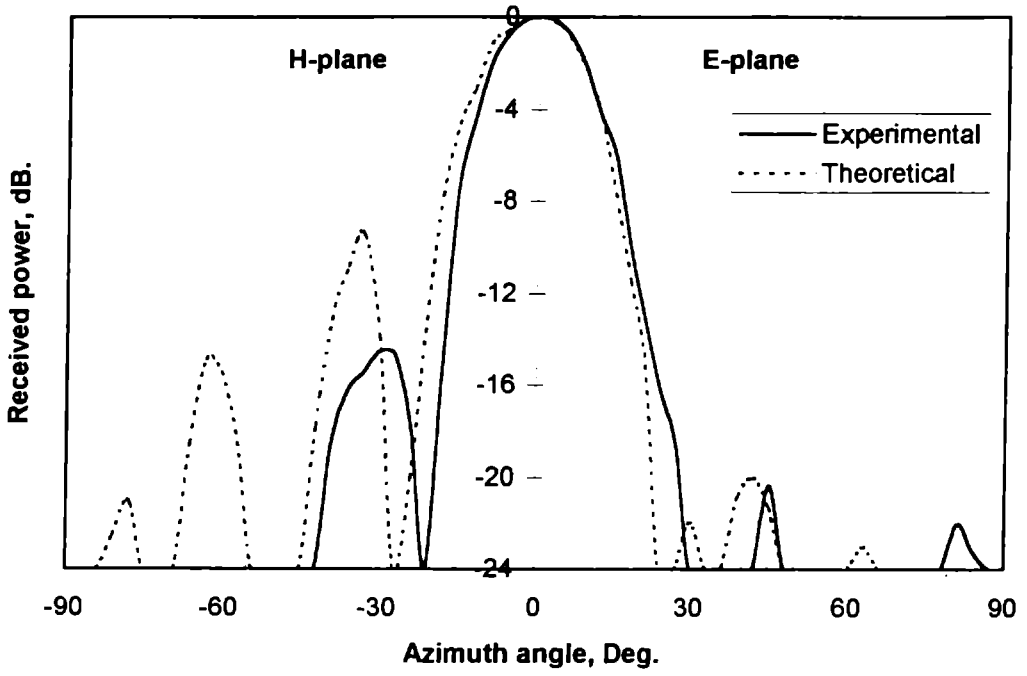

Fig.5.8 Theoretical and experimental radiation patterns for E-plane sectoral HDHL at 10 GHz., $\alpha_E = 20°$.

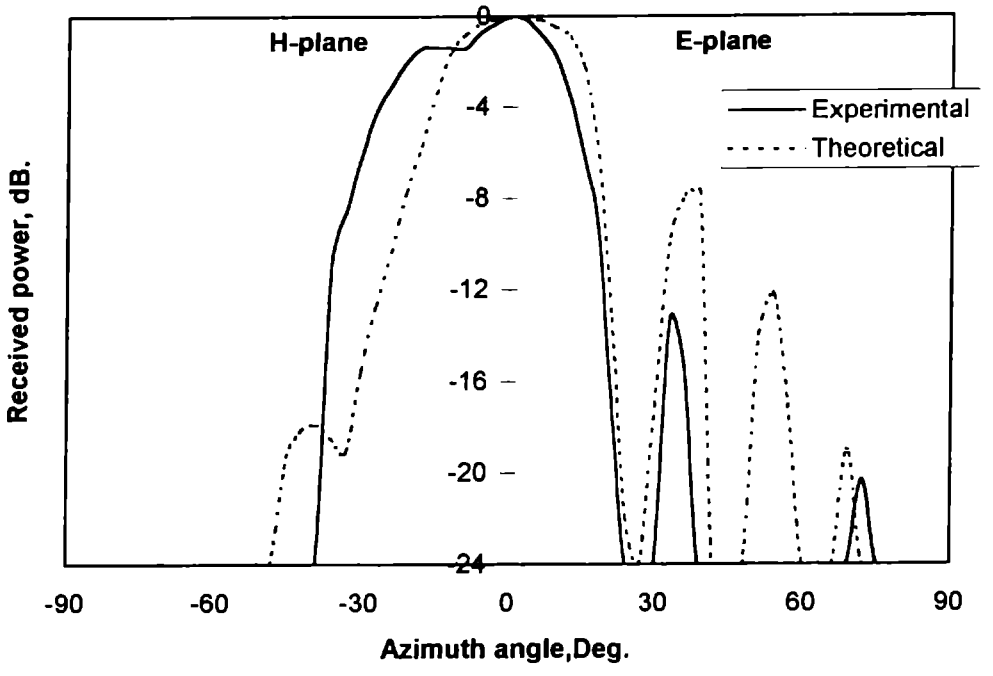

Fig.5.9 Theoretical and experimental radiation patterns for H-plane sectoral HDHL at 9 GHz., $\alpha_H = 30°$.

with the experimental patterns only for horns of small flare angles. As the flare angle increases the theoretical H-plane patterns become narrow and narrow, but the experimental patterns become broader or flat or split. So this theory is not sufficient to explain the radiation pattern in the H-plane of the H-plane sectoral horn. Another approach based on the image theory gives very good agreement between the theoretical and experimental patterns.

5.1.6 Image theory

A close examination of the radiation patterns in the H-plane of the H-plane sectoral horn or pyramidal horn reveals the similarity between these patterns with the H-plane patterns of Corner Reflector (CR) antenna. The H-plane walls of the horns act as reflecting elements and the free-end of the launcher acts as a linearly polarized point source. So the far field radiation will be the vector sum of the feed-end radiation and the radiation from the CR system.

The radiation from the point source is nothing but the radiation from a dielectric rod of aperture dimensions a_0 and b_0. We can use Eqn.(18) to calculate the free-end radiation from this point source. k_x, k_y and k_z should be evaluated using Eqn.(10), for uniform rods.

The field radiated by the source in the presence of the corner reflector of included angle α can be analyzed by considering the sources and the images (Image theory). The treatment is simple for $\alpha = \pi/n$, where n is an integer. The total number of sources for these corner reflectors will be $2\pi/\alpha$. Fig.5.10 shows the number and position of images for a 45° corner reflector.

Total electric field in the far field region can be obtained by summing the contributions from the feed and its images. The far field is given by [143],

$$U(r,\theta,\phi) = E_1(r_1,\theta_1,\phi_1) + E_2(r_2,\theta_2,\phi_2) + \ldots\ldots\ldots + E_n(r_n,\theta_n,\phi_n) \quad \text{——} \quad (24)$$

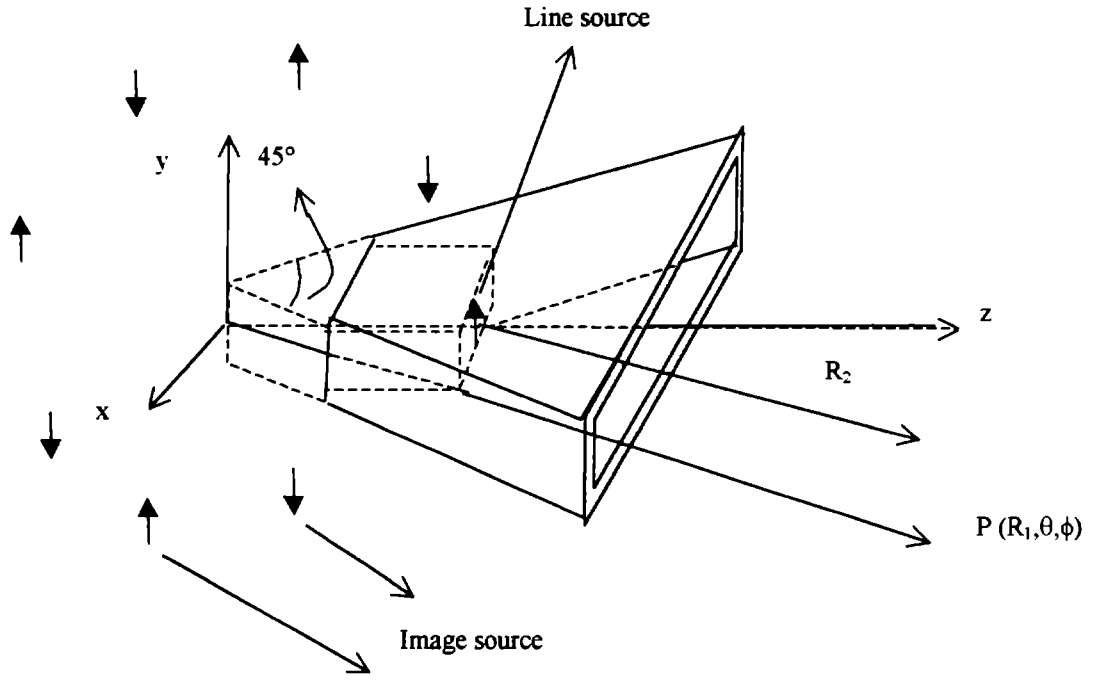

Fig.5.10 Position of images for a H-plane sectoral HDHL of flare angle 45°

for $2\alpha = 30°$,

$$U_{P1} = 2U_{P0}\left[\cos X - 2\cos\left(\frac{\sqrt{3}}{2}X\right)\cos\left(\frac{Y}{2}\right) - \cos Y + 2\cos\left(\frac{X}{2}\right)\cos\left(\frac{\sqrt{3}}{2}Y\right)\right]\frac{e^{(-jk_0R_1)}}{R_1} \quad \text{—— (25)}$$

for $2\alpha = 60°$,

$$U_{P1} = 4U_{P0}\sin\left(\frac{X}{2}\right)\left[\cos\left(\frac{X}{2}\right) - \cos\left(\sqrt{3}\frac{Y}{2}\right)\right]\frac{e^{(-jk_0R_1)}}{R_1} \quad \text{———} \quad (26)$$

where,

U_{P0} is the radiation from the end of the launcher. It can be obtained by modifying equation (18) for uniform rods, given by,

$$\therefore U_{P0} = \frac{j}{\lambda}\left\{\left(\frac{1+\cos\theta}{2}\right)\left(\frac{e^{(-jk_0R_2)}}{R_2}\right)\int_{-\frac{b_0}{2}}^{+\frac{b_0}{2}}\int_{-\frac{a_0}{2}}^{+\frac{a_0}{2}} C_3\left(k_x^2+k_y^2\right)\cos(k_x x)\cos(k_y y)e^{(jk_0\sin\theta(x\cos\phi+y\sin\phi))}dxdy\right\}$$

——— (27)

$$X = k_0 s\sin\theta\cos\phi$$
$$Y = k_0 s\sin\theta\sin\phi$$

The feed-corner spacing 's' may not be a multiple of λ or λ/2. The length of projection 'p' of the launcher is optimized as 3 cm. So 's' will be different for different corner angles. Also, since the experiment is performed in the entire X-band, as frequency changes the value of 's' in terms of λ changes.

The far field pattern in the H-plane will be the sum of the radiations from the feed end and the CR system.

i.e., $U_{TI} = U_P' + U_{PI}$. ——————— (28)

Here also the amplitude constants (C_2 and C_3) are adjusted for getting good agreement with the experimental patterns. A typical radiation pattern plotted using the image theory is shown in Fig.5.11. It is very close to the experimental pattern. Equation (25) and (26) are derived under the assumption that the field amplitudes of all signal elements are the same. The reflector elements are dielectric sheets and so there may be partial reflection only. There fore the above expression may not be that much correct. Also the height of the reflector elements 'h' is equal to breadth a_0 of the launcher (dielectric rod) for H-plane horns, which is less than sufficient for perfect functioning of the CR [144]. The parallel E-plane walls are also another constraint which contributes to the slight deviation of the experimental patterns from the theoretical ones. For pyramidal horns there is flaring in the E-plane also and so the limitation due to the small value of 'h'

and the effect due to E walls are considerably minimized. Fig.5.11 shows the H-plane pattern of a pyramidal horn of flare angle α_H=30°.

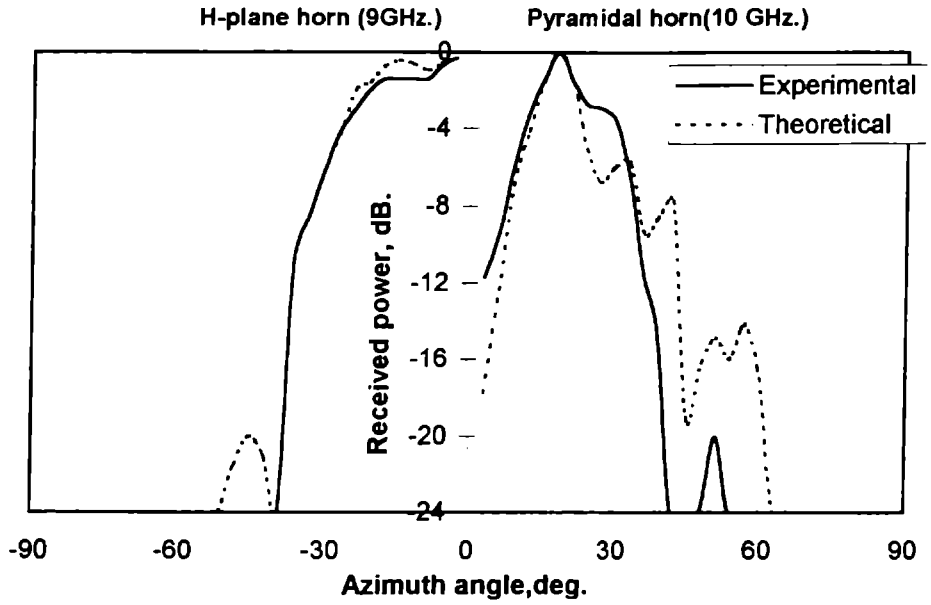

Fig. 5.11 Theoretical (Image theory) and experimental H-plane radiation patterns of H-plane sectoral and Pyramidal HDHL, α_H = 30°.

Because of the optimized position of the launcher, for a particular horn, the value of 's' and hence the radiation pattern changes with frequency. For small values of α_H (<10°), the hollow horn resembles a solid horn. As α_H increases the behavior deviates from solid rod concept and image theory becomes predominant. An increase in α_H changes the value of 's' also. For the optimized condition the 'multiplied patterns' of the feed and the CR give a broad, flat or split pattern. As α_H increases to 20° the radiation pattern show a flattening at the top. As α_H increases above 20° to 30°, the flatness at the top of the radiation pattern gives way to ripples or a split. Further increase of α_H changes the pattern to a broad one. For any α_H it is possible to attain pattern modifications by changing the feed point and frequency.

5.2 EFFECT OF STRIP LOADING

5.2.1 Strip loading on E-plane walls

Strip loading includes additional radiation terms to that of HDHL and that modifies the patterns further. The line source theory can be used for explaining the effect of strip loading on the E-walls of the horn. In this case the diffraction from the ends of the strips also is considered. The open end of the launcher acts as a primary source (point source) and the ends of the strips act as secondary sources (Fig.5.12). The component due to this diffraction term is given by[131],

$$U_{P2} = C_4\left\{1 + K\left[e^{(j\varphi_1)} + e^{(j\varphi_2)}\right]\right\}\frac{e^{(jk_0R_2)}}{R_2}$$

$$R_2 = R + (L-d)\cos\theta \qquad \text{——————} \quad (29)$$

$$\varphi_1 = k_0 d_1 \cos(\beta - \theta)$$

$$\varphi_2 = k_0 d_1 \cos(\beta + \theta)$$

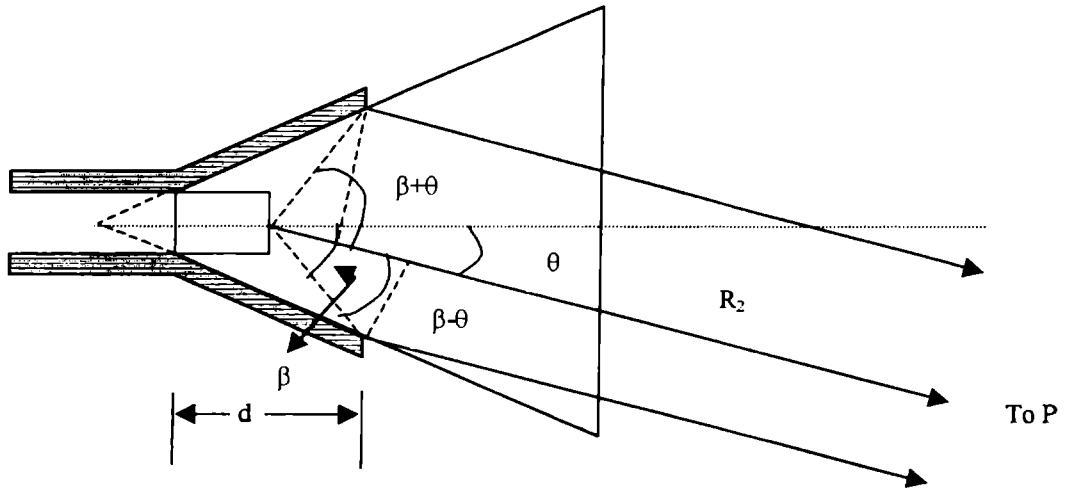

Fig.5.12 Co ordinate system used to evaluate the edge diffraction term of the E-plane sectoral SHDHL

So the far field radiation in the E-plane of SHDHL is the sum of the radiation terms from the feed end, free end and the term due to diffraction.

$$\text{i.e., } U_{T2} = U_P + U_P' + U_{P2} \qquad \text{——————} \quad (30)$$

. The effect of U_{P2} is not much appreciable in the H-plane, as proved by the experiment. Fig.5.13 shows a typical radiation pattern of the E-plane sectoral SHDHL of flare angle 20° at 10 GHz.

5.2.2 Strip loading on H-plane walls

The strip loading on the H-plane walls increases the conductivity of the reflector elements and the assumption of constant field amplitude for feed and image sources becomes more correct. So the use of image theory is more justified here. As the length of the strips increases, the component of the reflected power from different parts of the reflector changes, which in turn will modify the radiation pattern.

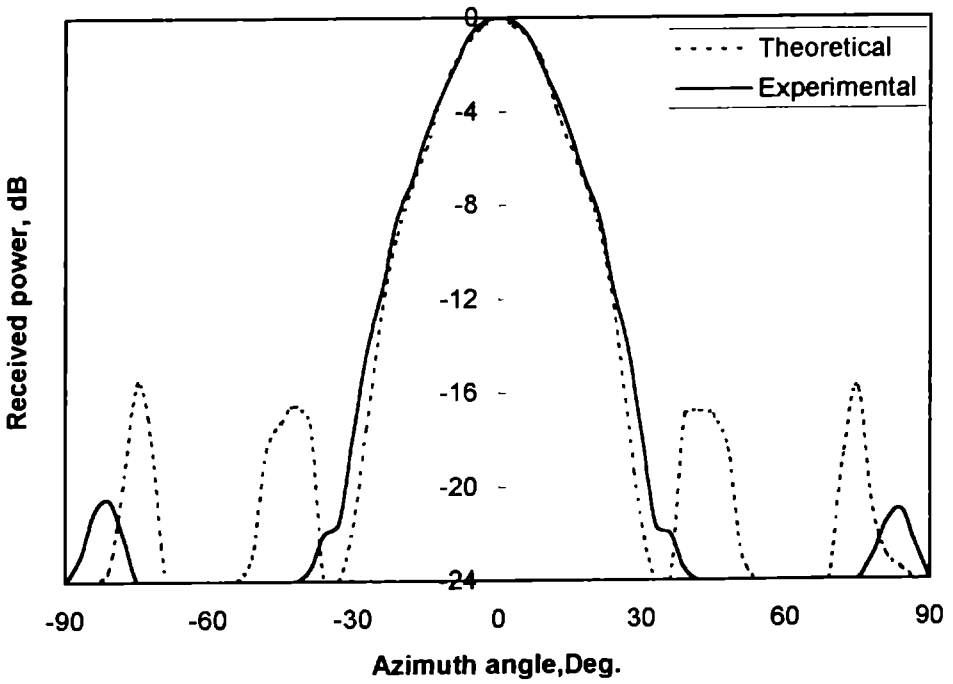

Fig.5.13 Theoretical and experimental E-plane radiation pattern of E-plane Sectoral SHDHL at 10 GHz., $\alpha_E = 20°$.

Chapter 6

CONCLUSIONS

Investigations on the radiation characteristics of the new hollow dielectric horn antennas shows that these novel antennas possess a number of interesting properties. The HDH with the launcher (HDHL) and the strip loaded HDHL (SHDHL) have lot of attractive features when compared with metallic horn antennas. The main highlights of the study and possible applications are discussed in the following sections.

6.1 HIGHLIGHTS OF RESULTS

1. The new antenna developed by introducing the new launching technique (HDHL) is capable of modifying radiation patterns in both E and H-planes with enhanced gain and reduced side lobe levels.

   a). The radiation patterns of E-plane sectoral HDHL is narrow in both E and H-planes, with low side lobe levels. The axial gain of HDHL is always greater than that of the corresponding HDH by up-to 3dB.

   b). The radiation pattern of H-plane sectoral HDHL is narrow in the E-plane and broad or split in the H-plane. In this case the axial gain is less, when compared with E-plane sectoral HDHL, but greater by up-to 4dB than ordinary H-plane sectoral HDH.

   c). For pyramidal HDHL, E and H-plane patterns are narrow for horns having small H-plane flaring(α_H). When α_H increases, the H-plane patterns becomes broad or split as in the case of H-plane sectoral HDHL. The axial gain of pyramidal HDHL is greater than equivalent HDH for small values of α_H.

   d). The VSWR of pyramidal and sectoral HDHL are low ($1.02<VSWR<1.7$) for the entire X-band.

   e). The cross-polar levels of all HDHL antennas are very low (between –35dB and -40dB).

   f). The study shows that the new launching technique is very successful for getting modified patterns with enhanced gain and reduced side lobe levels. It reduces the feed-end (waveguide-horn interface) discontinuity and effectively transfers the electromagnetic energy from the waveguide to the horn structure.

2. The SHDHL antenna constructed by applying strip loading on HDHL are also capable of beam shaping with gain enhancement and side lobe level reduction.

a). The study on E-plane sectoral SHDHL clearly shows that the new horns are capable of producing symmetric and identical radiation patterns in both E and H-planes, a result that a metallic horn does not give. Also it has high gain and low side lobe levels compared to the corresponding metallic horn antennas.

b). The H-plane SHDHL antenna is capable of producing flat-topped radiation patterns with high HPBW in the H-plane of the horn. This type of radiation is not available from any metallic horn antenna.

c). The pyramidal SHDHL antenna can give narrow E-plane patterns with low side lobe levels, split twin-beam with sharp axial null or narrow single beam in the H-plane, under different conditions. The radiation pattern with two lobes having sharp axial null in the H-plane is also a result that any metallic horn fails to give.

d). For E and H-plane sectoral horns, the axial gain is greater than the corresponding metallic horn antennas. For pyramidal SHDHL the axial gain is slightly less than that for equivalent metallic horns.

e). The VSWR of SHDHL antennas are also low, but slightly greater than that for HDHL.

f). The cross-polar levels of E and H-plane sectoral SHDHL are very low. But for pyramidal SHDHL, the cross-polar levels increases up to –16dB.

3. The theoretical treatment is carried out under a lot of simplifying assumptions. The theoretical patterns are found to be in very good agreement with experimental results.

a). Analysis is based on the assumption that, the hollow dielectric horn is equivalent to a solid dielectric horn of effective dielectric constant ε_{eff}. The use of Macarteli's principle agrees well with experimental results in the E-plane for all α_E values and in the H-plane when α_H is small.

b). The effect of strip loading on E-plane walls is explained using diffraction theory and the strip loading on H-plane walls are accounted using image theory.

4. The main draw backs of the new HDH antennas are

a). To explain the radiation characteristics of the antenna a single theory is not sufficient.

b). The launcher should be optimized for each frequency for getting maximum performance.

c). As mentioned by the earlier workers [41,128], the theoretical results obtained using Marcatili's method deviates from the experimental results for large flared horns.

5. The study shows that this new HDH is a good substitute for small metallic horns with easy beam shaping facility and has all the added advantages of dielectric group of antennas.

6.2 IMPORTANCE OF THE STUDY

The design and development of this new dielectric horn antenna is important because of the following reasons.

1. Horn antennas are very important and are widely used. So the development of its dielectric counterpart also is important.

2. Dielectric class of antennas possess lot of advantages like light weight, low cost, low loss, ease of fabrication etc. The new HDH possess all these added advantages.

3. The new HDH can be designed to have different types of radiation patterns such as, rotationally symmetric narrow pencil beam, fan-shaped beam, square patterns or split patterns. Such beam shaping facility is not possible with metallic horns.

6.3 POSSIBLE APPLICATIONS

The new hollow dielectric horn antennas may find applications in different situations due to its capability for producing different types of radiation patterns. The E-plane sectoral HDH or pyramidal HDH with small α_H , can be used in the place of pyramidal metallic horns. The identical narrow E and H patterns with sharp first nulls is an attractive feature of the antenna for using it as the primary feed for parabolic reflectors. H-plane sectoral horns with square patterns may be an ideal feed for cylindrical reflector antennas. H-plane sectoral horns or pyramidal horns with split patterns can be used to feed two separate receivers simultaneously.

6.4 SCOPE FOR FUTURE WORK

The radiation characteristics of the new hollow dielectric horn antennas are found to be attractive in the X-band. So the performance of this model in other possible frequency bands are to be studied. For the present study, the launcher is optimised first. So the free-end of the launcher inside the horn is in a fixed position. The effect of change of this feed point is another important proposal for the future study. The thickness of the dielectric sheet is an important parameter for changing the characteristics of the antenna. For the present study, the thickness of the dielectric sheets are kept constant. So the results of variation of wall thickness is another area to be investigated.

6.5 CONCLUDING REMARKS

The design and development of a new class of hollow dielectric horn antennas have been carried out. The dependence of the radiation characteristics on the antenna parameters has been investigated. It is observed that the new antenna has the added advantage of easy beam shaping facility together with the attractive features of the dielectric antennas. This versatile antenna may find application as an ideal substitute for small metallic horn antennas.

APPENDIX A

RADIATION CHARACTERISTICS OF A DUAL CORNER RELECTOR ANTENNA

The radiation characteristics of a dual corner reflector (DCR) antenna consisting of two corner angles and three reflector elements are presented in this appendix. A DCR antenna is formed by fixing a third element to one of the reflector elements of an ordinary corner reflector (CR). It has been observed that the DCR antenna is more efficient than an ordinary CR as far as the high directivity and easy beam tilting facility are concerned.

A.1 INTRODUCTION

Corner reflector (CR) antennas are widely used in telecommunication engineering because of their simplicity and high performance. The theories and experiments on different types of CRs are available in literature[132-137,140,144]. Mathew et.al. [131,138] reported another method of beam tilting by making the reflector elements asymmetric. The radiation characteristics of a new type of with two corner angles and three reflector elements, called Dual Corner Reflector (DCR) are presented here.

A.2 ANTENNA DESIGN AND EXPERIMENTAL SET-UP

The DCR is constructed by attaching an additional conducting sheet C to one side of the CR of length L>2S. S is the corner-to-dipole spacing. The schematic representation of the DCR is shown in Fig. A.1. An optimum width (d) of 1λ for the sheet C is selected.

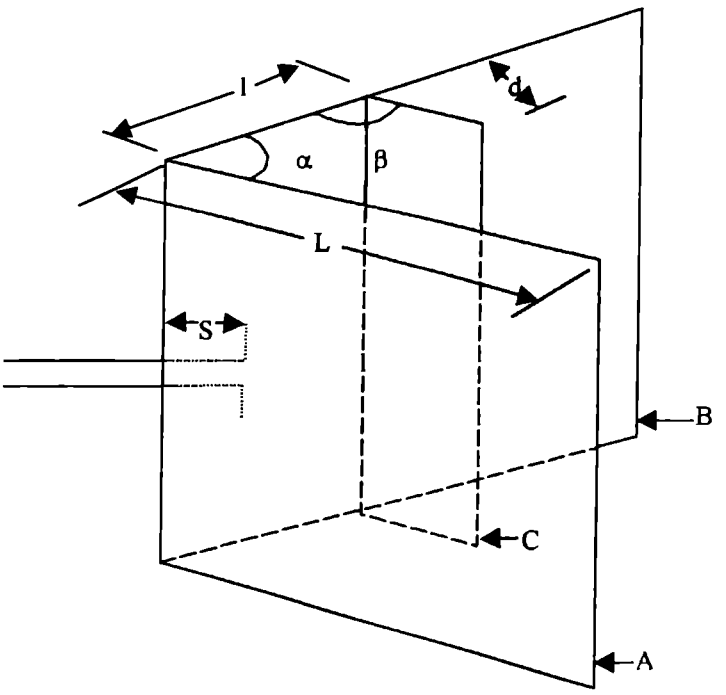

Fig.A.1 Schematic representation of the DCR antenna.

The experiment was performed with a Gunn source followed by a test bench at X-band for various corner angles.the test antenna was used as the transmitter and a standard pyramidal horn as the receiver.

A.3 EXPERIMENTAL RESULTS

The experiment is carried out by changing two parameters, viz. Corner-to-corner spacing 'l' and second corner angle 'β'. Two cases are shown bellow.

A.3.1 Change of 'l' from λ/2 to 4λ (α=β=90°)

Dipole at S=λ/2

The dipole is placed symmetrically at the appex of the first corner (α). The third element C is kept parallel to the element A. the corner-to corner spacing 'l' is varied by moving C along B. In all cases the on-axis power varies almost sinusoidally as shown in Fig.A.2. The positions at witch the on-axis power is maximum is turned as optimum

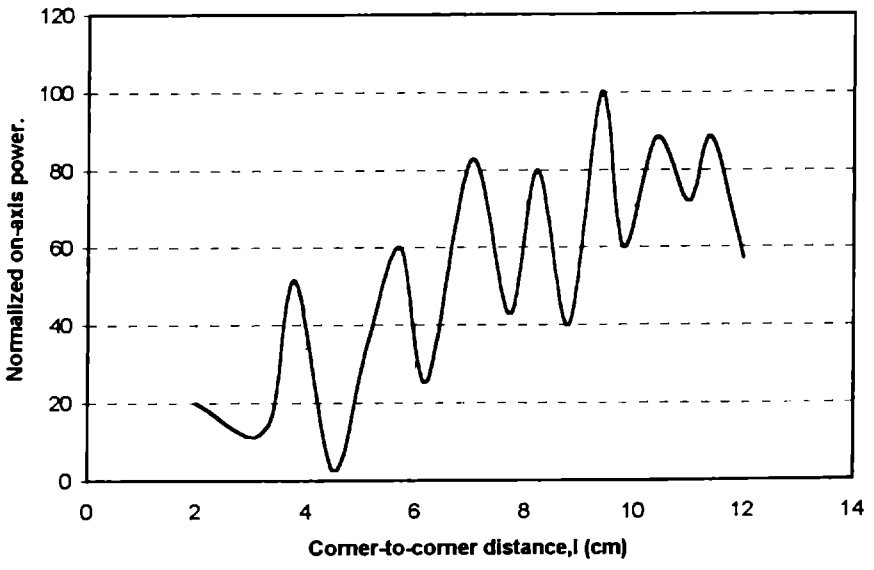

Fig. A.2 Variation of on-axis power of DCR for different values of 'l'.

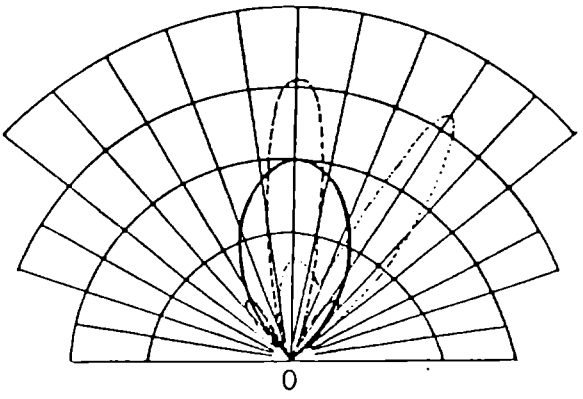

Fig.A.3 Radiation patterns for S=λ/2 for ordinary CR(—), DCR at O position (---) and DCR at M position (····)

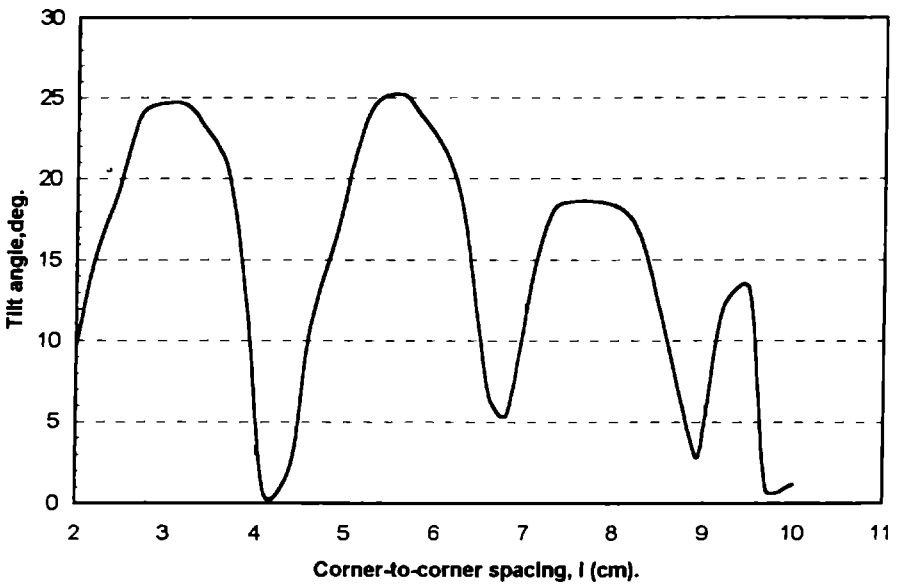

Fig. A.4 Tilt angle versus 'l' for β=90°

positions or O positions and positions of minimum power as minimum positions or M positions. The HPBW is minimum at these positions. At all M positions the beams are found to be either tilted or split. Radiation patterns at different positions of element C are shown in Fig.A.3. The beam tilt for various M positions are shown in Fig. A.4.

Dipole at S= λ

For ordinary CR, we know that the beam is split into two when dipole is at S=λ. Study of the radiation patterns of the DCR at these positions of the dipole shows that the lobes are swinging for these values of 'l' and as one lobe increases the other decreases. This phenomenon is clearly under stood from Fig.A.5.

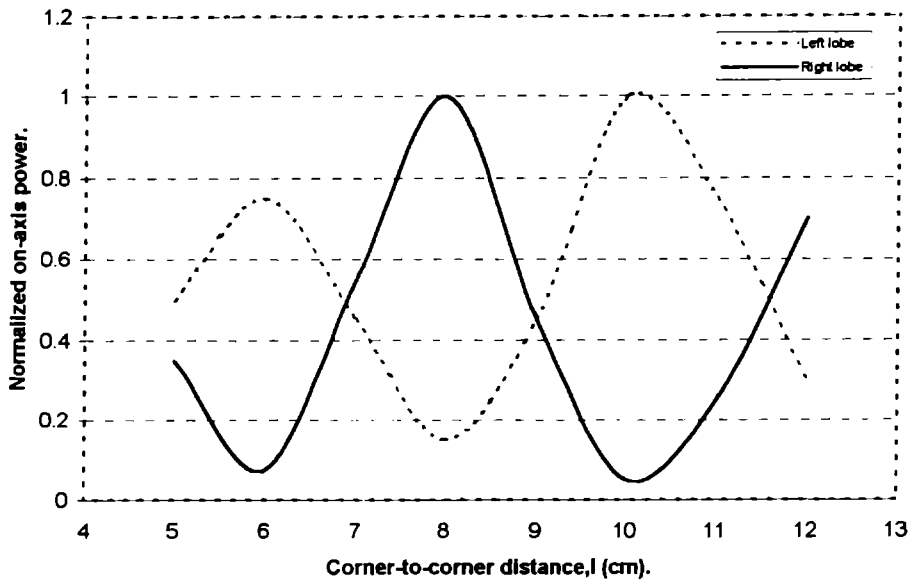

Fig.A.5 Distributon of on-axis power between two lobes for S=λ as a function of 'l'

A.3.2 Change of β (α=90°,l-constant)

Radiation patterns are studied for various 'β' values, keeping C at any arbitrary position.

Dipole at S=λ/2

For any fixed value of 'l', when β is varied from 0 to 180° the axis power varies almost sinusoidaly (Fig. A.6), as for the case of change of 'l'. Here the optimum positions are turmed as O' positions and minimum positions as M' positions. The radiation patterns corresponding to O' and M' positions are shown in Fig.A.7. The beam tilt for different values of 'β' are plotted in Fig. A.8.

Dipole at S=λ

The results for various values of 'β' for a dipole spacing S=λ are not as prominent asfor S = λ/2. This is mainly due to the blocking of one of the lobes by the element C.

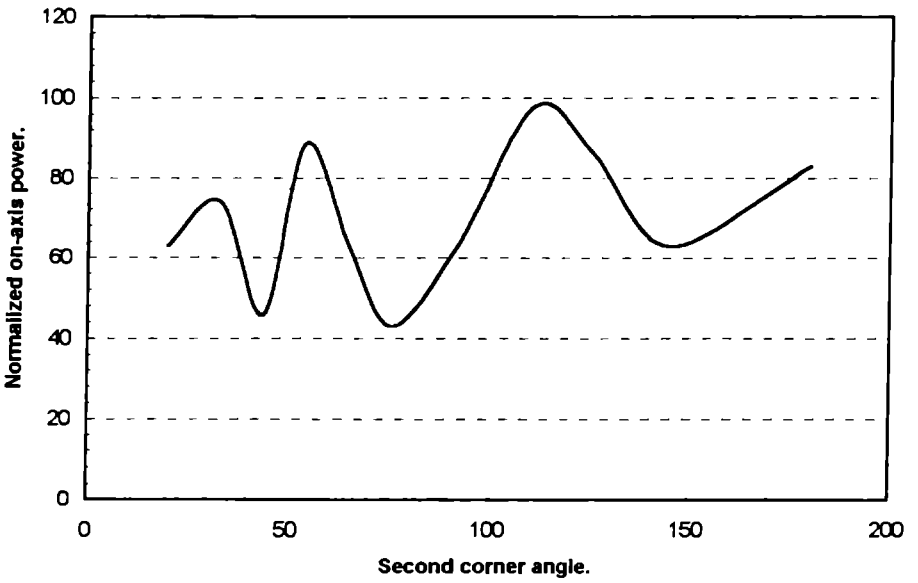

Fig.A.6 Variation of on-axis power of DCR for different values of 'β'.

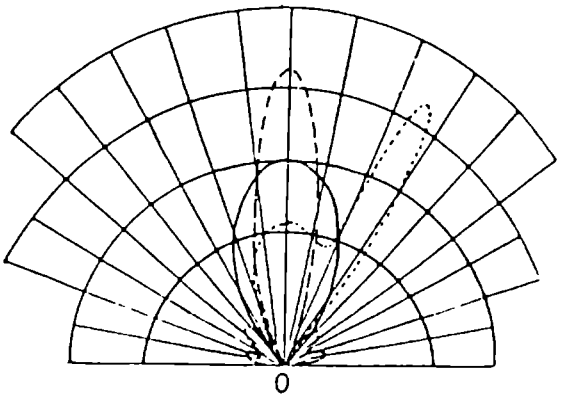

Fig.A.7 Radiation patterns for S = λ/2 for ordinary CR (—), DCR at O′ position (---) and DCR at M′ position (····)

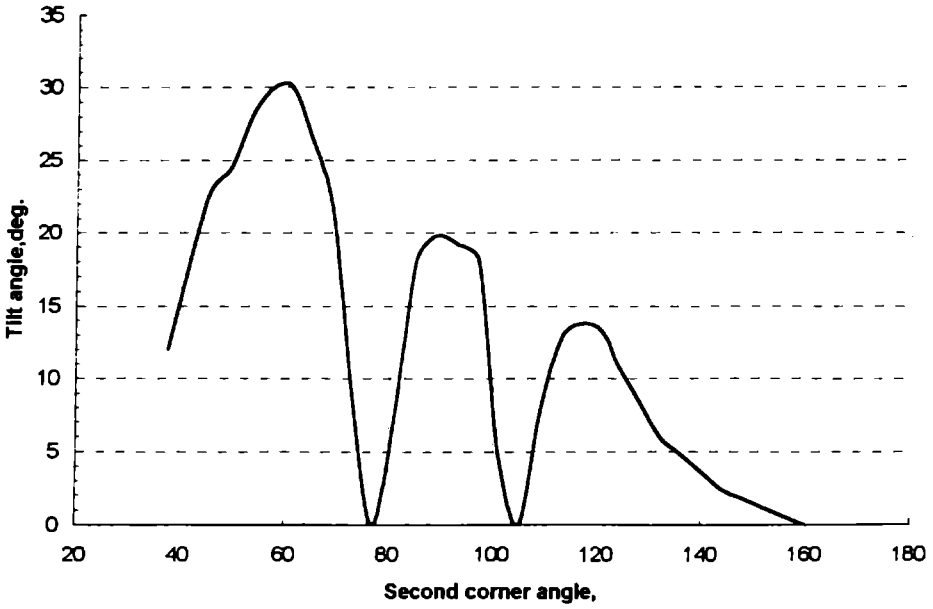

Fig.A.8 Tilt angle verses β for 'l'=6cm.

A.4 CONCLUSIONS

From the study of DCR antenna, the following conclusions can be drawn. The DCR is more efficient than an ordinary CR as far as the directivity and beam tilting facility are concerned. In order to tilt the beam in ordinary CR, either the dipole should be displaced from the axis or element asymmetry should be introduced. But the beam tilt in DCR is easily achieved either by sliding the third element over one of the two elements, or by changing the second corner angle. Beam modification is very prominent when 'l' is between 1.5λ and 3.5λ. It is also found that for 'β' variation, the element C should be placed in this 'active region' for better performance. Almost similar behaviours have been observed for 'l' and 'β' variations.

APPENDIX B

PERIODIC STRIPS ATTACHED CORNER REFLECTOR ANTENNA FOR ENHANCED PERFORMANCE

The design and development of a new corner reflector (CR) antenna are presented in this appendix. The design involves the addition of planar parallel periodic strips to the two sides of a CR antenna. The position, angular orientation, and number of strips have a notable effect on the H-plane radiation characteristics of the antenna. Certain configurations of the new antenna are capable of producing very sharp axial beams with gain of the order of 6dB over the square corner antenna.

B.1 INTRODUCTION

CR antennas are widely used, where a moderate gain is required, due to the simplicity of its design. A modification of the DCR antenna (Appendix A) was presented by Mathew et.al.[139] by adding another supplementary reflector to the DCR. This study presents the design of a CR antenna with periodic planar metallic strips attached to the two reflecting sides and the resulting improvement in the radiation characteristics. It is seen that the gain of the antenna increases and the HPBW decreases. The performance of the antenna for different dimensions of the strip structure is analyzed. There are configurations that can provide axial gains of the order of 6dB over the square corner reflector antenna.

B.2 ANTENNA DESIGN AND EXPERIMENTAL SET-UP

The schematic diagram of the new CR antenna is given in Fig.B.1. It is constructed by attaching two metallic strip structures S_1 and S_2 to the two sides of the CR

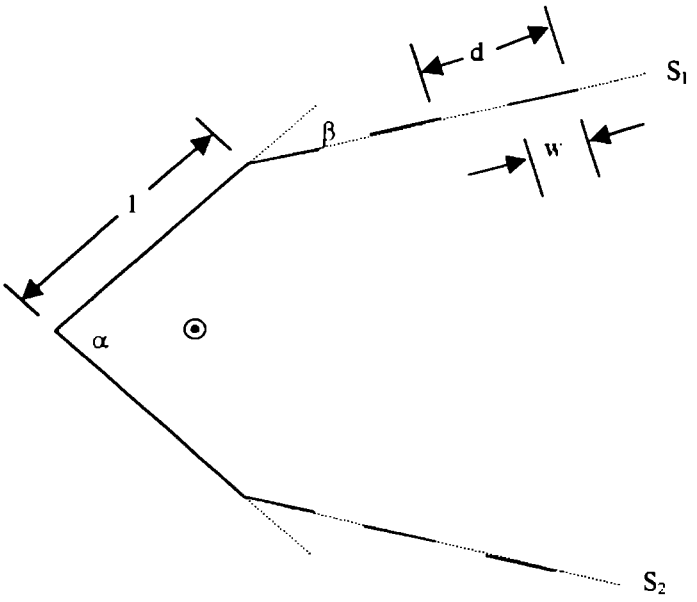

Fig.B.1 Schematic diagram of the new CR antenna.

at a distance *l* from the apex. The structure consists of *n* metallic strips of width *w* and height *h* kept at a periodicity of *d*. α and β are the primary and secondary corner angles respectively. The distance *l*, angle β and the number of strips *n* can be varied. An HP 8350B sweep oscillator, together with an HP 8410B network analyzer were used for studying the radiation characteristics. The AUT was used as the receiver and a standard pyramidal horn as the transmitter.

B.3 EXPERIMENTAL DETAILS AND RESULTS

For a fixed value of α, the radiation patterns are plotted for different values of β, *n*, *l*, *w*, and *d*. The width *w* and the periodicity *d* are optimized as 0.3λ and 1λ for maximum gain. The gain of the antenna is found to be increasing with the number of strips. In all cases, it is seen that when the axial gain increases, the HPBW decreases. A typical radiation pattern of the configuration ($\alpha = 120°$, $\beta = 45°$, $n = 5$ and $l = 1\lambda$) is given in Fig.B.2 in comparison to that of a square corner reflector of equivalent dimensions.

No appreciable change in the VSWR could be observed due to the strip attachment of the CR antenna when *l* is small. But for large *l*, the VSWR goes high. It is seen that the cross-polar levels are bellow –18dB and the side lobe levels are bellow –13dB in most cases.

B.4 CONCLUSIONS

The design and analysis of a new type of corner reflector antenna are carried out. The configurations of the antenna offering enhanced performance are studied, and the characteristics are compared with those of a square corner reflector antenna. An axial gain enhancement of the order of 6 dB and hence a reduction in the HPBW, are observed.

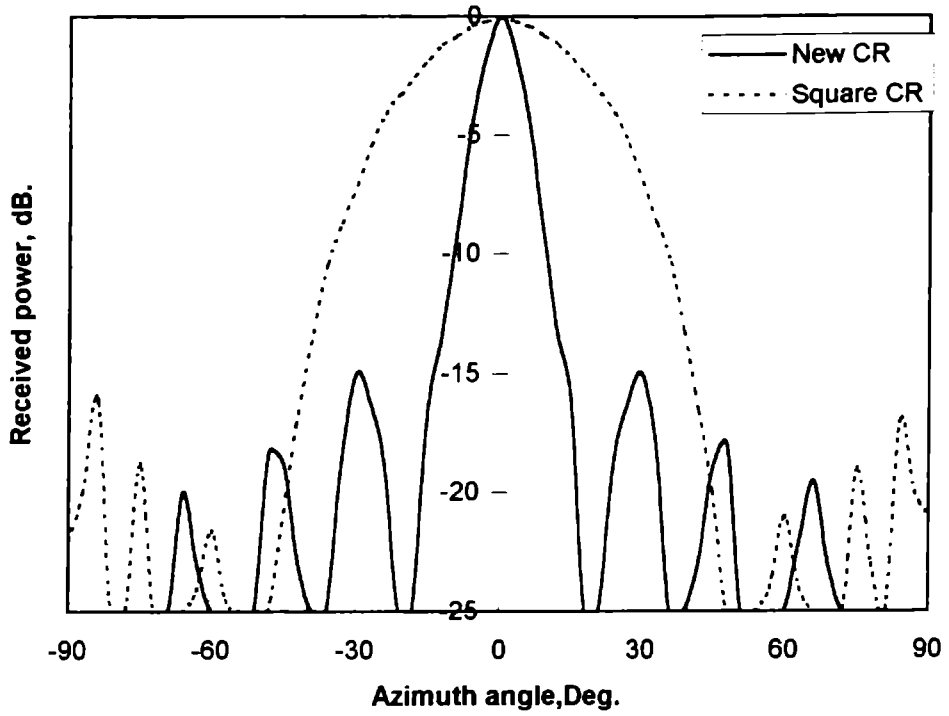

Fig. B.2 Normalized H-plane radiation pattern of a typical configuration ($\alpha = 120°$, $\beta = 45°$, $n = 5$ and $l = 1\lambda$) at 8.5GHz., along with that of a square corner reflector.

APPENDIX C

EFFECT OF SLOTTED HORN ON RADIATION PATTERN

The radiation characteristics of H-plane sectoral horn antenna with periodic slots on one of the broad sides are presented. It is found to be a simple and effective method of beam tilting. By changing the slot width and number of slots the tilt can be conveniently changed.

C.1 INTRODUCTION

Horn antennas are very good radiators of microwave power. They are widely used for lot of applications in different fields. There are many techniques like structural modifications, flanges, corrugations, dielectric loading etc. to modify the radiation pattern of horn antennas[91-123]. Slotted waveguide also have some interesting radiation characteristics[141]. The present work describes the effect of slotted horns on radiation patterns. The H-plane sectoral horn with periodic slots on one of the broad sides provides an easy method for beam tilting. The width of the slots and periodicity changes the radiation characteristics.

C.2 METHODOLOGY

Fig. C.1. shows the schematic representation of the experimental horn. The antenna is constructed by grooving slots of width 'w' on one of the broad sides of the H-plane sectoral horn. Different experimental horns with slot width and spacing equal to $\lambda/2$, $\lambda/3$, $\lambda/4$ etc. are constructed and the radiation pattern and VSWR are measured for each horn at different frequencies. The experimental set-up consists of a Gunn oscillator set-up with the AUT in the receiving mode.

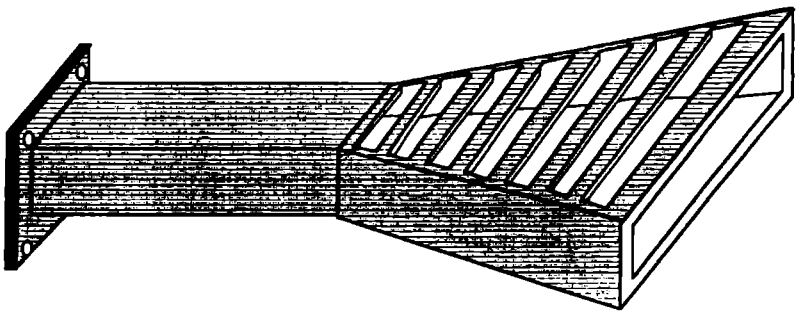

Fig. C.1 Schematic representation of the experimental slotted horn antenna.

C.3 EXPERIMENTAL RESULTS

Radiation characteristics of slotted H-plane sectoral horns of different flare angles and slot widths were studied. The radiation patterns are found to be tilted from the axis of the horn. The beam tilt varies with the width of slots. For a horn of flare angle 25°, the axial beam is tilted through 25° due to slots of width λ/2. A decrease in slot width increases the tilting up-to a maximum value. For slot widths equal to λ/3 and λ/4, the tilts are 35° and 38° respectively. No further reasonable tilt is observed for smaller values of slot widths. Fig.C.2 shows a typical radiation pattern for a horn of flare angle 25° and slot width λ/4 at 10GHz. The corresponding radiation pattern for ordinary metallic horn also is shown for comparison.

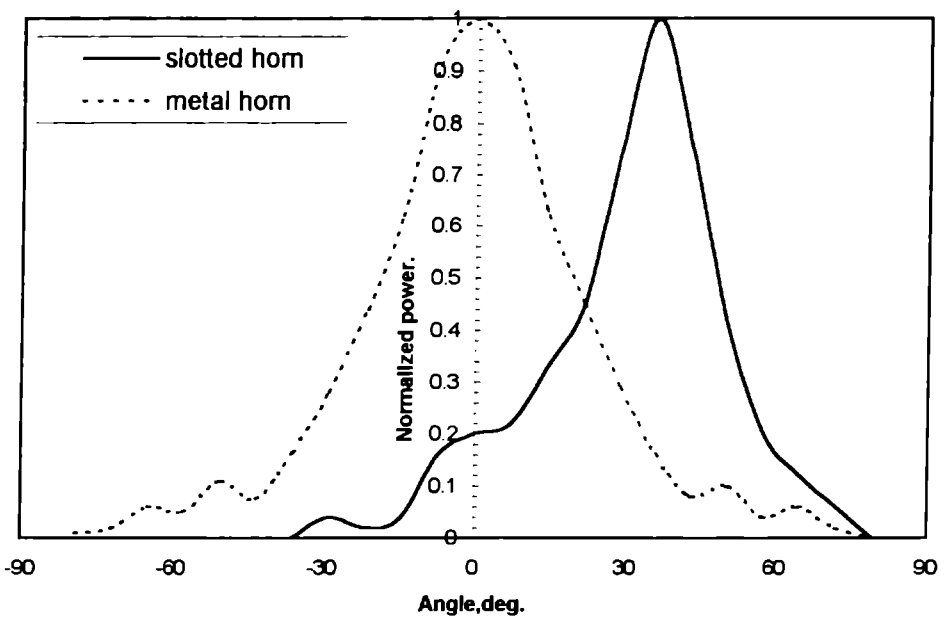

Fig.C.2 Radiation pattern of the experimental horn .

In all cases the tilt is invariably from the side of slots, i.e., towards the side of the flat element. The VSWR of the slotted horn are found to be slightly greater than the ordinary horn antenna.

C.4 CONCLUSIONS

A new effective and simple method of beam tilting using slotted horns is presented. By changing the slot widths and hence the number of slots, the tilt angle can be conveniently changed. These types of horns are practically useful when used as primary feeds for reflector antennas. The primary feed need not necessarily be at the apex of the reflector antenna.

APPENDIX D

MODIFIED RADIATION PATTERN OF AN ASYMMETRIC HOLLOW DIELECTRIC SECTORAL HORN ANTENNA

A method for tilting the axial beam of a symmetric hollow dielectric E-plane sectoral horn antenna by replacing one side of the horn by a metal sheet is presented. Another method for shifting the tilted beam between two angles, using a narrow metal strip of optimum length, arranged on the dielectric side of the horn also is presented.

D.1 INTRODUCTION

The importance and advantages of dielectric antennas are discussed in chapter 1 and 2 of this thesis. This appendix describes an easy method of tilting the axial beam of a hollow dielectric symmetric E-plane sectoral horn by making it asymmetric with a metal element on one side. By arranging a narrow metal strip of optimum length on the dielectric side, it is again possible to shift the power between two angles.

D.2 EXPERIMENTAL SET-UP AND ANTENNA DESIGN

The experimental set-up is a microwave test-bench at X-band with Gunn oscillator as the source. The test horn is used as the transmitter and a pyramidal horn as the receiver. The receiver is connected to a crystal detector which in turn is connected to a sensitive current meter.

The symmetry of the hollow dielectric horn is changed by replacing one side of the horn by a metal sheet. This asymmetry changes the current distribution on both sides of the horn, resulting in a change in the radiation pattern. A narrow metal strip of optimum length is arranged on the dielectric side of the horn using a micrometer screw arrangement. The movement of the strip parallel to the axis changes the radiation pattern completely. Fig.D.1. shows the schematic representation of the test horn.

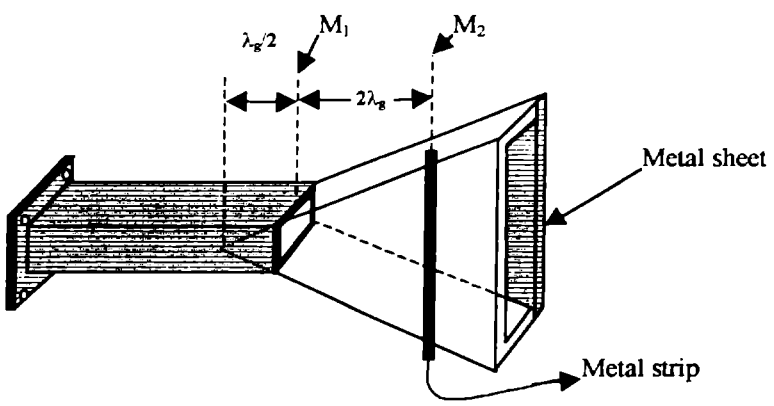

Fig.D.1 Schematic diagram of the test horn.

D.3 EXPERIMENTAL RESULTS

The radiation pattern of the hollow dielectric horn is shown in Fig.D.2. When one side of the horn is replaced by a metal sheet, the axial power is tilted to 45° with a side lobe at 20° as shown in the figure. The peak at 20° is denoted as P_1 and the peak at 45° as peak P_2.

By moving the narrow conducting strip of length 'l' along the dielectric side, it is possible to shift the power from the peak P_1 to peak P_2 and vice versa. For a distance $\lambda_g/2$ from the apex, there is only one peak at 20°. This position of the strip is marked as M_1. The strip at another position $2\lambda_g/2$ from the apex shifts the power to 45°. This position of the strip is marked as M_2.

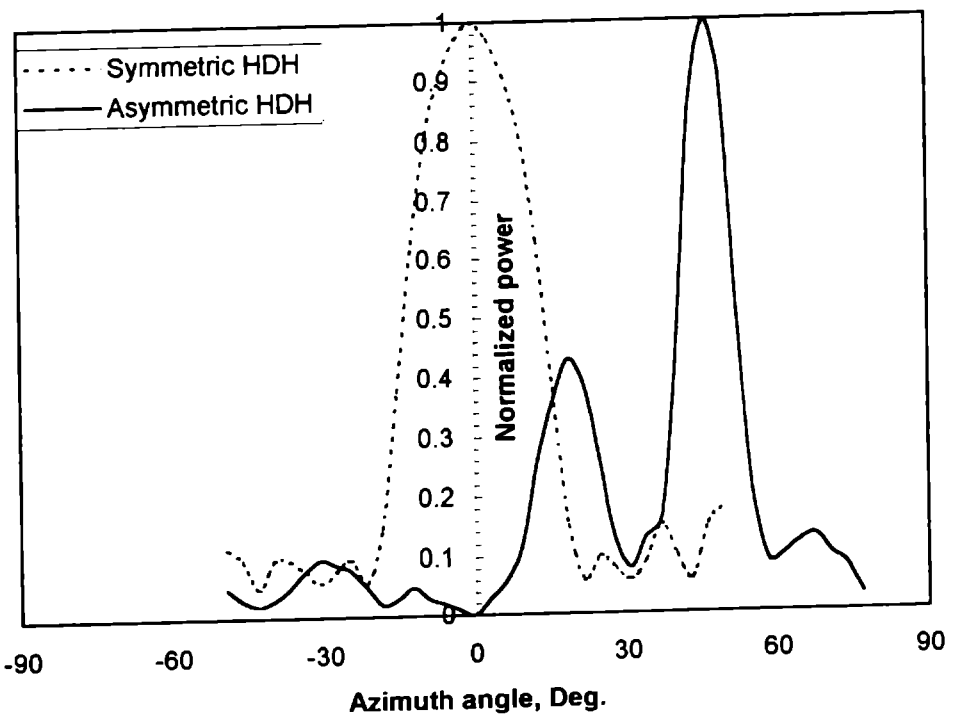

Fig.D.2 Radiation pattern of the asymmetric hollow dielectric sectoral horn antenna.

It is also observed that the extent of power shift depends upon the length of the strip used. The distribution of power between the two peaks, for different strip lengths at M_1 and M_2 is plotted in Fig.D.3. From the figure it is observed that the power is maximum for the first peak P_1 and minimum for the second peak P_2 for 'l'=3λ/2. Also it is evident from the figure that, for the same length of the strip, the second peak P_2 is almost maximum and the first is a minimum. So this length 'l'=3λ/2 is selected as the optimum length of the strip for a most effective shifting of the beam between two angles. The radiation patterns with optimum strip length at M1 and M2 positions are plotted in Fig.D.4.

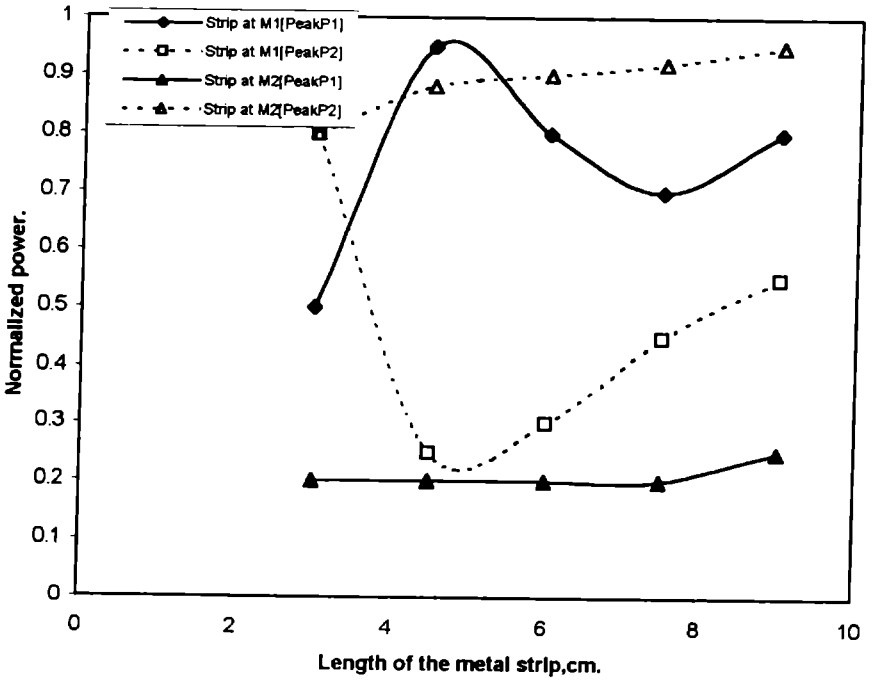

Fig.D.3 Variation of power with strip length for peak P_1 and peak P_2.

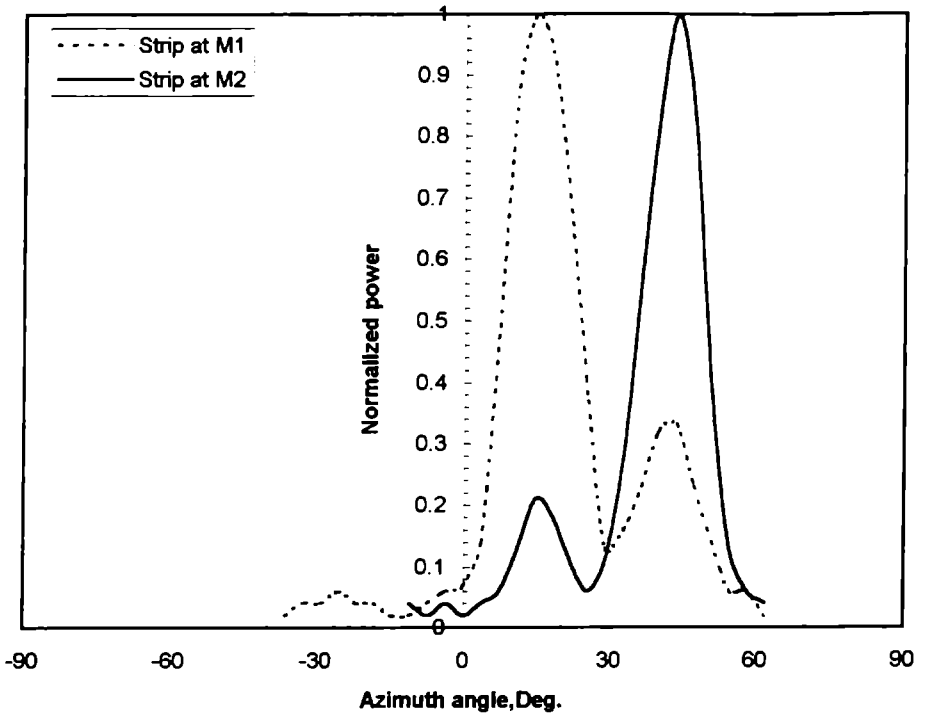

Fig.D.4 Radiation patterns with strips at M_1 and M_2 positions.

D.4 CONCLUSIONS

This beam shifting technique makes the hollow dielectric horn a better choice than the metal horn, for being used as the feed horn of an offset parabolic reflector antenna. It has the added advantage that it can be used alternatively as the feed horn for two offset parabolic reflectors of different look angles, by changing the position of the metal strip with a screw mechanism.

1. J.F. Ramsay, "Microwave antenna and waveguide technique before 1900", Proc. IRE, Vol.46, pp.405-415, Feb. 1958.

2. W.L. Barrow and F.M. Greena, "Rectangular hollow pipe radiators", Proc. IRE, Vol.26, pp.1448-1519, Dec. 1938.

3. W.L. Barrow and L.J. Chu, "Theory of electromagnetic horn", Proc. IRE, Vol.27, pp.51-64, Jan. 1939.

4. W.L. Barrow and F.D. Lewis, "The sectoral electromagnetic horn", Proc. IRE, Vol.27, pp.41-50, Jan. 1939.

5. L.J. Chu and W.L. Barrow, "Electromagnetic horn design", Trans. AIEE, Vol.58, pp.333-338, July 1939.

6. G.S. Southworth and A.P. King, "Metal horns as directive receivers of ultra short waves", Proc. IRE,pp.95-102, Feb. 1939.

7. L.J. Chu, "Calculation of the radiation properties of pipes and horns", J. Appl. Phys., Vol.2, pp.603-610, 1940. 1940.

8. G.A. Woonton, D.R. Hay and E.L. Vogan, "An experimental investigation of formulas for the prediction of horn radiation patterns" J. Appl. Phys.,Vol.20, pp.71-78, Jan.1949.

9. D.R. Rhodes, "An experimental investigation of the radiation patterns of electromagnetic horn antennas", Proc. IRE, Vol.36, pp.1101-1105, Sept. 1948.

10. Herbert S. Bennett, "Transmission line characteristics of the sectoral horn", Proc. IRE, Vol.37, pp.738-749, July 1949.

11. C.W. Horton, "On the theory of the radiation patterns of electromagnetic horns of moderate flare angle", Proc. IRE, Vol.37, pp.744-749, July 1949.

12. A.P. King, "The radiation characteristics of conical horn antennas", Proc. IRE, Vol. 38, pp.249-251, March 1950.

13. Marvin G. Schorr and Fred J. Beck Jr., "Electromagnetic field of conical horn", J. Appl. Phys., Vol.21, pp. 795-801, Aug. 1950.

14. W. C. Jakes, "Gain of electromagnetic horns", Proc. IRE, Vol.39, pp.1160-162, Feb. 1951.

15. E.H. Braun, "Gain of electromagnetic horns", Proc. IRE, Vol.41, pp.109-115, Jan. 1953.

16. A.W. Love, "Electromagnetic horn antennas", IEEE Press, New York, 1976.

17. Rajeswari Chatterjee, "Dielectric and dielectric loaded antennas", Research studies press, John Wiley & Sons, 1985.

18. D. Hondors and P. Debye, "Electromagnetische wellen an Dielektrischen Drahten", Ann. Der Physik, Vol.32(8), pp.465-476, 1910.

19. H. Zahn, "Uber den Nachweis Elektromagneticschen Wellen an Dielectrischen Drahten", Ann. Dre Physik, Vol. 49, pp.907-935, 1916.

20. O. Schriever , "Electromagnetische wellwn an dielektrische drahten", Ann der Physik, Vol. 63, pp. 645-673, 1920.

21. G.C. southworth, "Hyper-frequency waveguides-General considerations and experimental results", Bell. Syst. Tech. J., Vol.15, pp.284-309, 1936.

22. J.R. Carson, S.P. Mead and S. A. Schelkunoff, "Hyper-frequency waveguides – Mathematical theory", Bell. Syst. Tech. J., Vol.15, pp.301-333, 1936.

23. W.M. Elsasser, "Attenuation in a dielectric rod", J. Appl. Phys., Vol.20, pp.1193-1196, 1949.

24. R.B. Watson and C.W. Horton, "The radiation pattern of dielectric rods – Experiment and theory", J. Appl. Phys., pp. 661-670, 1949.

25. R.B. Watson and C.W. Horton, On the calculation of radiation patterns of dielectric rods", J. Appl. Phys., Vol.19, pp.836-837, 1948.

26. D.F. Halliday and D.G. Kiely, "Dielectric rod aerials" , J.I.E.E., Vol.94, pp.610-618, 1947.

27. C.W. Horton F.C. Karal and C.M.. McKinney, "On the radiation patterns of dielectric rods of circular cross-section, the TM_{01} mode", J. Appl. Phys., Vol. 21, pp. 1279-1283, 1950.

28. S.A. Schelkunoff, "Some equivalence theorems of electromagnetics and their applications to radiation problems", Bell. Syst. Tech. J., Vol.15, pp. 92-112, 1936.

29. D.G. Kiely, "Dielectric aerials", Methuen and Co. Ltd. London, 1953.

30. R.E. Collin and F.J. Zucker, "Antenna theory-Part 2", McGraw-Hill Book Co. New York, 1969.

31. R.E. Collin, "Field theory of guided waves", McGraw-Hill Book Co. New York, 1960.

32. J. Larmor, "On the mathematical expression of the principle of Huyghens", Lond. Math. Soc. Proc. (2), Vol.1, pp.1-5, 1903

33. F. Kotter, 'Elektromagnetische theorie der beugung an schwarzen schirmen", Ann. Der Phys., Vol.71, pp475-508, 1923.

34. A.E.H. Love, "The integration of the equation of propagation of electric waves", Phil. Trans. A., Vol.197, pp.1-45, 1901.

35. J.A. Stratton and L.J. Chu, "Diffraction theory of electromagnetic waves", Phys. Rev., Vol.56, pp.99-107, 1939.

36. S. Silver, "Microwave antenna theory and design", McGraw-Hill Book Co. New York, 1949.

37. J.R. James, "Theoretical investigations on cylindrical dielectric rod antennas", Proc. I.E.E.,Vol.104, pp.309-319, 1967.

38. J.R. James, "Radiation from surface wave antennas", electronics Letters, Vol.3, pp.344, 1967.

39. J. Dilli, R. Chatterjee and S.K. Chatterjee, "Gain characteristics of overmoded dielectric rods", J. Indian Inst. of Sci., Vol.59, pp.431-473, 1977.

40. J. Dilli, "Surface-wave and radiation characteristics of over-moded circular cylindrical dielectric rods", Ph.D. Thesis, Indian Institute of science, Bangalore, 1976.

41. K.G. Narayanan, "Radiation characteristics of rectangular dielectric horn antennas", Ph.D. Thesis, Indian Institute of science, Bangalore, 1984.

42. J.B. Andersen, "Radiation from surface wave antennas", Electronics Letters, Vol.3, pp.251-252, 1967.

43. J.R. Blakey, "A scattering theory approach to the prediction of dielectric rod antenna radiation patterns : The TM_{01} mode", IEEE Trans. AP, Vol.23, pp.577-579, 1975

44. G. Wilkes, "Wavelength lenses", Proc. IRE, Vol.36, pp.206-212, 1948.

45. R. Chatterjee and S.K. Chatterjee, "Some investigations on dielectric rod aerials – Part1", J. Indian Inst. of Sci. Vol.38. pp.93-103, 1956.

46. R. Chatterjee and S.K. Chatterjee, "Some investigations on dielectric rod aerials – Part 2", J. Indian Inst. of Sci. Vol.39. pp.134-140, 1957.

47. R. Chatterjee and S.K. Chatterjee, "Some investigations on dielectric rod aerials", J.I.T.E. (India) Vol.3. pp.230-234, 1958.

48. R. Chatterjee and H.R. Ramanujam, "Some investigations on dielectric rod aerials – Part 5", J. Indian Inst. of Sci. Vol.44. pp.164-202, 1962.

49. R. Chatterjee and H.R. Ramanujam, "Some investigations on dielectric rod aerials – Part 6", J. Indian Inst. of Sci. Vol.44. pp.203-218, 1962.

50. S.K. Chatterjee and V. Subramanyam, "Circular cylindrical rod waveguide", J. Indian Inst. of Sci. Vol.50. pp.258-493, 1968.

51. E.A.J. Marcateli, "Dielectric rectangular waveguide and directional coupler for integrated optics", Bell. Sys. Tech. J., Vol.48, pp.2071-2102, 1969.

52. W. Schlosser and H.G. Unger, "Partially filled waveguides and waveguides of rectangular cross-section, Advances in microwaves", Academic Press, New York, pp.319-387, 1966.

53. E. Schweig and W.B. Bridges, "Computer analysis of rectangular waveguides for millimeter waves", Conf. Digest of 6^{th} Int. Conf. (IEEE) on infrared and millimeter waves, pp. W-4, Dec. 1981.

54. J.E. Goell, "A circular harmonic computer analysis of rectangular dielectric waveguides", Bell. Sys. Tec. J., Vol. 48, pp.2133-2160,1969.

55. A.L. Cullen O.Ozkan and L.A. Jackson, "Point matching technique for rectangular cross-section of dielectric rod", Electronics Letters, Vol.7, No.17, pp. 497-499, 1971.

56. R. Pregla, "Analysis of open rectangular waveguides required in integrated optics by use of a variational method", Proc. European microwave conference, pp.B-52, 1973.

57. R. Mittra, Y. Hou and V. Jamnojad, "Analysis of open dielectric waveguides using mode matching technique and variational methodes", IEEE Trans. MTT, Vol.28, No.1, pp.36-43, 1980.

58. C.B. Shaw, B.T. French and C. Warner, "Further research on optical transmission lenses", Sci. Rep. No.2 Contract AF 449(638)-1504, AD 625501, Autonetics report No.C-7929/501,pp 133-44.

59. K. Ogusu, "Numerical analysis of rectangular dielectric waveguide and its modifications", IEEE Trans., MTT. Vol.25, No. 11, pp.874-885, 1977.

60. K. Ogusu, "Measurement of dispersion characteristics and field distributions in rectangular dielectric waveguide and its modifications", IEEE Trans., MTT, Vol.26, No.3, pp. 169-171, 1978.

61. L.A. Pitale, "Propagation in a dielectric waveguide using the Green's function method", Ph.D. Thesis, Drexel Uty., 1980.

62. Huen-Tae-Ha and Jung-Woong Ra, "Edge diffraction by an arbitrary-angled wedge composed of metal and lossless dielectric", MOT Lett., Vol.16, No.2, 1997, pp. 89-93.

63. J.A.G. Malherbe, "Radiation from an open ended nonradiative dielectric waveguide", MOT Lett., Vol.14, No.5, 1997, pp. 266-268.

64. J.A.G. Malherbe, "Corporate feed in nonradiative dielectric waveguide", Electron. Lett., Vol.33, No.3, 1997, pp. 170-171.

65. F.J. Zucker, "Surface and leaky wave antennas", Chap. 16 , Antenna Engineering handbook, McGraw-Hill Book Co. New York, 1961.

66. J.R. James, "Engineering approach to the design of tapered dielectric rod and horn antennas", Radio Elec. Eng. Vol.42, pp.251-259, 1972.

67. D. Marcuse, "Radiation losses of the dominant mode in round dielectric waveguides", Bell. Sys. Tech. J. Vol. 49, pp.1665-1693, 1970.

68. Hiroshi Kubo, "Leakage characteristics of the cylindrical dielectric waveguide with a periodically varying radius", MOT Lett., Vol.5, No.14, 1992, pp. 718-721.

69. A. Kumar and R. Chatterjee, "Radiation from tapered dielectric rod aerials", J. Indian Inst. of Sci. Vol.50(b), pp. 374-392, 1968.

70. A. Kumar and R. Chatterjee, "Tapered dielectric rod aerials", Proc. Nat. Inst. Sci. (India), Vol. 34A, pp. 1-27, 1968.

71. A. Kumar, "Tapered dielectric rod aerials", Ph.D. Thesis Indian Inst. of Sci., Bangalore, India, 1965.

72. L.B. Felsen, "Radiation from a tapered surface wave antenna", IRE Trans., AP, Vol.8, pp.577-586, 1960.

73. Y. Shiau, "Dielectric rod antennas for millimeter wave integrated circuits", IEEE Trans., MTT,Vol.24, pp.869-872, 1976.

74. S. Kobayashi, R. Mittra and R. Lampe, "Dielectric tapered rod antennas for millimeter wave applications", IEEE Trans., AP, Vol.31, No.1, pp.54-58,1982.

75. S. Kobayashi, R. Lampe, N. Deo and R. Mittra, "Dielectric antennas for millimeter wave applications", IEEE MTT-S Int. Symp. Digest, Orlando, USA, pp.566-568, 1979.

76. C. Yao and S.E. Schwarz, "Monolithic integration of a dielectric millimeter wave antenna and mixer diode: An embryonic millimeter wave IC", IEEE Trans., MTT, Vol.30, pp.241-246, 1982.

77. T.K. Sen and R. Chatterjee, "Rectangular dielectric rod at microwave frequencies – Part 1, Theoretical and experimental determination of launching efficiency", J. Indian Inst of Sci. Vol. 60, pp.193-210, 1978.

78. T.K. Sen and R. Chatterjee, "Rectangular dielectric rod at microwave frequencies – Part 2, Radiation characteristics", J. Indian Inst of Sci. Vol. 60, pp.211-225, 1978.

79. S.K. Paulit, "Radiation characteristics of the tapered rectangular dielectric rod antenna at microwave frequencies", Ph.D. Thesis, Indian Inst. of Sci., Bangalore, India, 1982.

80. S.K. Paulit and R. Chatterjee, "Radiation characteristics of the tapered rectangular dielectric rod antenna at microwave frequencies", Proc. URSI Symp. on Electromagnetic theory, Santiago de Compostela (Spain), pp.401-404, 1983.

81. D.G. Kiely, "Factors governing the radiation characteristics of dielectric tube aerials", Proc. IEE, Vol.97, pp.311-321, 1950.

82. I.N.L. Gallet, "Radiation patterns of tubular dielectric structure", European microwave conference, London, pp.367-370, 1969.

83. M.S. Narasimhan and M.S. Sheshadri, "Radiation characteristics of dielectric tube antennas", IEEE Trans. AP, Vol.27. pp. 126-128, 1979.

84. J.R. James, "Theoretical investigations of cylindrical dielectric rod antennas", Proc. IEE, Vol.114, pp.309-319, 1967.

85. H.M. Barlow and J. Brown, "Radio surface waves", Clarendon Press, Oxford, 1962.

86. M.H.N. Potok, J.R. James and I.N.L. Gallet, "Dielectric antennas", Second annual research report, R.M.C.C.,1970.

87. H.C. Booker and P.C. Clemmow, "The concept of an angular spectrum of plane waves and its relation to polar diagram", Proc. IEE, Vol.97, pp.11-17, 1950.

88. J.R. Blakey, "Calculation of dielectric aerial radiation patterns", Electron Letters, pp46-47,1968.

89. G.A. Deschamps, "Determination of reflection coefficient and insertion loss of a waveguide junction", J. Appl. Phys., Vol.28, pp.1046-1050, 1953.

90. T.N. Trinh, J.A.G. Malherbe and R. Mittra, "A metal to waveguide transition with application to millimeter wave integrated circuits", IEEE MTT-5, Int. Symp. Digest, pp.205-207, 1980.

91. H.E. Bartlet and R.E. Moseley, "Deliguides - highly efficient low noise antenna feeds", Microwave J., Vol.9, pp53-58,1966.

92. G.N. Tsandowlas and W.D. Fitzgerald, "Aperture efficiency enhancement in dielectrically loaded horns", IEEE Trans., AP, Vol.42, pp.69-74, 1972.

93. R. Ashton and R. Baldwin, "Rectangular horn with dielectric slab insert", Electron Lett., Vol.9, No.2, pp.26-27, 1973.

94. R. Baldwin and P.A. McInnes, "Radiation patterns of dielectric loaded rectangular horns", IEEE Trans., AP, pp.375-376, 1973.

95. K.K. Sabnani and R.K. Arora, "Radiation characteristics of a rectangular aperture centrally loaded with a dielectric slab in the H-plane", J. Inst. of Electron and Telecom. Engrs., (India), Vol.24 (7), pp. 302-304, 1978.

96. M.A.K. Hamid, S.J. Towaij and G.O. Martens, "A dielectric loaded circular waveguide antenna", IEEE Trans., AP, Vol.20, pp.96-97, 1972.

97. T. Satoh, "Dielectric loaded horn antenna", IEEE Trans., AP, Vol.20, pp.199-201, 1972.

98. V.J. Vokurka, "Dual-frequency-band feed with partially dielectric loaded grooves", Electron Let., Vol. 11, No. 16, pp.376-378, 1975.

99. A.G. Martin, "Radiation from dielectric sphere loaded horns", Electron Let., Vol.14, No.1, pp.17-18, 1976.

100.A. Kumar, "Experimental investigation of the duel-band feed", Int. J. Electronics, Vol. 47, pp.279-284, 1979.

101.A. Kumar, "Dielectric lined waveguide feed", IEEE Trans., AP, Vol. 27, pp279-282, 1979.

102.P. Balling, F. Jacobsen and P.G. Gudmandsen, "Aperture efficiency enhancement in dielectric lined conical horns with low cross polarization", Proc. of European Microwave conference, Netherlands, pp.740-744, 1981.

103.R.A. Nair A.K. Kamal and S.C. Gupta, "A high gain multi-mode dielectric coated rectangular horn antenna", Radio Elec. Eng., Vol.48, pp439-443, 1978.

104.R.A. Nair A.K. Kamal and S.C. Gupta, "Radiation characteristics of dielectric coated conical horn", J. Inst. of Elec. and Tel. Eng. (IETE), Vol.24, pp.331-333, 1978.

105.R.A. Nair and S.C. Gupta, "Double flare multi-mode dielectric loaded horn antennas", Proc. of Int. Symp. on Electromagnetic waves, Munich, West Germany, 1980.

106.R.A. Nair, A.K. Kamal and S.C. Gupta, "A high gain dielectric loaded bicoical horn for circular polarization", IEEE Trans., AP, Vol.27, pp.860-861, 1979.

107.M.S. Aly and S.F. Mahmoud, "Propagation and radiation behavior of a longitudinally slotted horn with dielectric filled slots", Proc. IEE, Vol.132, pp.477-479, 1985.

108.E. Lier, "A dielectric hybrid mode antenna feed : A simple alternative to the corrugated horn", IEEE Trans., AP, Vol.34. No.1, pp.21-29, 1986.

109.E. Lier, "Analysis of soft and hard strip loaded horns using a circular cylindrical mode", IEEE Trans., AP, Vol. 38, No.6, pp. 783-793, 1990.

110.M.S. Narasimhan and M.S. Seshadri, "Propagation and radiation characteristics of dielectric loaded corrugated dual-frequency circular waveguide horn feeds", IEEE Trans. AP, Vol. 27, pp.858-860,

111.K. Raghavan, A.D. Olver and P.J.B. Clarricoats, "Compact dual-mode dielectric loaded horn", Electron Let., Vol.22, pp. 1131-1132, 1986.

112.C.M. Knop, Y.B. Cheng and E.L. Ostertag, "Performance of corrugated and dielectric loaded metallic conical horns", Electron. Let., Vol.22, No. 23, pp.1253-1254, 1986.

113.C.M. Knopp, "On the performance of metallic wall conical horns with centrally loaded dielectric material", Proc.IEE, H-1, Vol.138, pp.23-31, 1991.

114.E. Lier and T.S. Pettersen, "The strip loaded hybrid mode feed horn", IEEE Trans., AP, Vol.36, No.9, pp.1086-1088, 1987.

115.A.D. Olver, P.J.B. Clarricoats and K. Raghavan, "Dielectric cone loaded horn antennas", Proc. IEE, Vol.135, H-3, pp.158-162, 1988.

116.C.S. Lee, S.W. Lee and D.W. Justice, "A simple circular polarized antenna : Circular waveguide horn coated with lossy magnetic materials", IEEE Trans., AP, Vol.36, No.2, pp.279-300, 1988.

117.J.J.H. Wang, V.K. Tripp and R.P. Zimmer, "Magnetically coated horn for low side lobes and low cross-polarization", Proc. IEE, H-2, Vol.136, pp.132-138, 1989.

118.S.I. Ghobrial and H.R. Sharolim, "Radiation patterns of paraboloidal reflector fed by a pyramidal horn with lossy walls", IEEE Trans. AP, Vol.37, No.10 , pp.1316-1317, 1989.

119.R.A. Nair and Robetrt J. Herickhoff, "Gain enhancement of a circularly apertured plural mode diel-core H-plane sectoral horn", Proc. of APSYM, Kochi, India, pp.217-226, 1990.

120.J. Jacob, U. Ravindranath, V.P. Joseph and K.T. Mathew, "Modified radiation pattern of an asymmetric hollow sectoral dielectric horn", Proc. of APSYM, Kochi, India,pp.227-230, 1990

121.R. Cahill, "Design of core support mechanism for mm wave dielectrically loaded horn", Electron. Let. Vol.25, No.18, pp. 1248-1249, 1989.

122.Stephen Rodrigues, P. Mohanan and K.G. Nair, "A new scalar feed with low side lobe levels", Proc. APSYM , Kochi, India, 1990.

123. Stephen Rodrigues, P. Mohanan and K.G. Nair, "Simulated corrugated feed horn antenna", Proc. IEEE AP-S, Int. Symp. Texas, USA, pp.984-987, 1990.

124.Stephen Rodrigues, "Development of a new type of simulated scalar feed", Ph.D. Thesis, CUSAT, Kochi, India, 1992.

125.P.J.B. Clarricoats and C.E.R.E. Salema, "Antenna employing conical dielectric horns: Part 1- propagation and radiation characteristics of dielectric cones ",Proc. Inst. Elec. Eng., Vol. 120, pp.741-756, 1973.

126. P.J.B. Clarricoats and C.E.R.E. Salema, "Antenna employing conical dielectric horns: Part 2- The cassegrain antenna ",Proc. Inst. Elec. Eng., Vol. 120, pp.741-756, 1973.

127.N. Brooking, P.J.B. Clarricoats and Olver, "Radiation patterns of pyramidal dielectric waveguides" Electron. Lett.,Vol.10, pp.33-34, 1974.

128.A.K. Singh, B. Jha and R.K. Jha, "E-plane sectoral hollow dielectric horn antennas", IETE Technical review, Vol. 6, No. 6, pp.457-461, 1989.

129.Anil. K .Singh, B. Jha and R.K. Jha, "Near field analysis of H-plane hollow sectoral dielectric horn antennas", Int. J. Elec., Vol. 68, No.6, pp.1055-1061, 1990.

130.V.P. Joseph and K.T. Mathew, "Strip loaded hollow dielectric sectoral horn antennas", J. Inst. Electron and Telecom. Engrs., India, Vol.38, No.5, pp. 266-270, 1992.

131.K.T. Mathew, "Beam shaping of sectoral electromagnetic horn antennas using corner reflector technique", Ph.D. Thesis, CUSAT, Cochin, India, 1978.

132.J.R. Wait, "On the theory of an antenna with an infinite corner reflector", Can J. Phys.,Vol.32, pp.365-371, 1954.

133.A.C. Wilson and H.V. Cottony, "Radiation pattern of finite size corner reflector antenna", IRE Trans. AP, Vol.8, pp.144-157, 1960.

134.D. Proctor, "Graphs simplify corner reflector antenna design", Microwave J. Vol.14, pp.48-52, 1975.

135.K. Vasudevan and K.G. Nair, "A corrugated corner reflector system", IEEE Trans. AP, Vol.30, pp.524-526, 1982.

136.T.S. Ng and K.F. Lee, "Theory of corner reflector antennas with tilted dipole", Proc. IEE, Vol.129, H-1, 1982.

137.Edward. F. Harris, "An experimental investigation of the corner reflector antenna with tilted dipole", Proc. IRE, pp.645-651, 1953.

138.K.T.. Mathew and K.G. Nair, 'An analysis of the behavior of flanged sectoral horn antennas and corner reflector system", Indian J. of Radio and Space Phys., Vol.10,pp.25-30, 1981.

139.K.T. Mathew, J. Jacob, S. Mathew and U. Ravindranath, "Triple corner reflector and its performance in the H-plane", Electron. Let. ,Vol.32. pp1432, 1996.

140.U.O. Sterr, A.D. Olver and P.J.B. Clarricoats, "Variable beam width corner reflector antenna", Electron Lett., Vol.34, No.11, pp.1050-1051, 1998.

141.Larse Jose-fesson, "Resonant length of longitudinal slots in rectangular waveguids", IEEE Trans. AP, Vol. 8, 1984.

142.E.V. Jull, "Aperture Antennas and Diffraction Theory", Peter Peregrinus Ltd., Stevenage, UK, and New York, 1981.

143.C.A. Balanis, "Antenna Theory, Analysis and Design", John Wiley & Sons., New York, 1982.

144.John D Kraus, "Antennas", McGraw-Hill Book Co., 1988.

INDEX